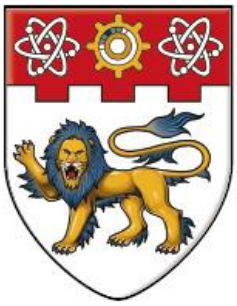

NANYANG TECHNOLOGICAL UNIVERSITY

ROLE OF OSMOTIC PRESSURE IN THE REGULATION OF CYTOSKELETON DURING MITOSIS

Ishani Dasgupta

School of Biological Sciences

2016

ROLE OF OSMOTIC PRESSURE IN THE REGULATION OF CYTOSKELETON DURING MITOSIS

ISHANI DASGUPTA

SCHOOL OF BIOLOGICAL SCIENCES

NANYANG TECHNOLOGICAL UNIVERSITY

SINGAPORE

A thesis submitted to the Nanyang Technological University in partial fulfillment of the requirement for the degree of Doctor of Philosophy

2016

ACKNOWLEDGEMENT

‘Alone we can do so little; together we can do so much’. As I envision the final hardcopy of my thesis with my name resplendent on the cover page, I cannot help but be reminded of the above quote by Helen Keller. Needless to say this entire journey of PhD has been one of the landmarks of my life, which is finally coming to fruition with the submission of this thesis. But all those sleepless nights, the never ending hours of frustration followed by a sudden gleam of hope, the train of informed thoughts sometimes interrupted by an unexpected desperation only to be brought back on track, the grueling months of trial and errors; none of them would have culminated into this hour of fulfillment without the plethora of the well-wishers who have made this journey even more enriching. While I would hardly mince a word in bragging about my PhD degree to others a few years down the line, even then a part of me would whisk a silent thank you to all these people because of whom I dared to wake up and fulfill the dream that I nourished since long. Thus I feel this is a perfect opportunity to express my gratitude to them as well as revisit the treasured moments I have lived with these people during my graduate experience.

None other than my supervisor Dr. Koh Cheng Gee implanted the germinal seed of this thesis. Her vast horizon of knowledge is infectious and spurred the researcher in me to push the envelope every time I seemed to have hit a dead end. Her stoic patience during my incessant tribulations and her continual encouragement cemented my determination and kept me afloat through the recurrent tides of my journey. The unmistakable ability to troubleshoot any given problem at any point of time cushioned me at times when I doubted myself. Furthermore, apart from shaping my academic being, Dr. Koh even took interest in my personal well-being and has lent unforgettable support during my personal crises which helped me sail through my obstacles like a breeze. Her insightful comments and invaluable feedback will be with me throughout my life and will continue to direct my thoughts to the wonders of science.

I am equally thankful to the members of my thesis advisory committee, Dr. Li Hoi Yeung and Dr. Esther Wong, Nanyang Technological University, for their unwavering support and augmenting my thesis with their discerning inputs. Their passion for research is exemplary and commands utmost respect of any biologist, budding or established. It was an honour for me to be associated with such stalwarts of the field.

My journey as a biologist had actually begun in IISC, Bangalore, India under the able guidance of my professor Dr. Dipshikha Chakraborty and my mentor Dr. Sandhya Marathe. Over there I grew to be an independent thinker and researcher under the umbrella of the care and support of these two personalities. Their constant encouragement have triggered my passion and kept me ongoing at the initial stages of this remarkable journey. The researcher in me owes her roots to these towering figures whose inspiration has not left me till date.

I also owe thanks to Dr. Lim Chwee Teck, National University of Singapore, whose insights in the field of mechanobiology are unparalleled. I thank him for allowing me to carry out the micropipette assay under Rosemary and Xiaopeng's assistance with great ease. I express my heartfelt gratitude to Yen Ling for the modeling work. Her valuable inputs in this project have been very beneficial to me.

This thesis would never have seen the light of the day without the two people who forms the centre of my existence; my parents. My father Mr Ajoy Sankar Dasgupta has been instrumental in the maintenance of my sanity throughout this odyssey of mine. He has been the one who taught me never to lose faith in myself and keeping the flag of self-belief flying high at times when I was at my lowest ebb. He put up with my ever changing moods and those fluctuations with a smile of reassurance and a calm confidence. My mother Mrs Indra Dasgupta has been my pillar of strength throughout this endeavor. If there is one person on earth who would digest mood swings and constant naggings, it would be her. Besides their parental role and perhaps lending the most effective scaffold in building my dream, my mother is the very reason for me embarking on this colossal journey. She has been the one who instilled the seed of questioning in me, which later rose to the crescendo of research and finally culminated into the person I am today.

I am blessed to have a bunch of genuine friends in my life who form an integral part of this crucial turn-around of my life. To begin with, Bibek Ray Chaudhuri who has been one of the strongest support systems in my life. Perhaps he has lived this whole thesis writing experience as much as I have. From giving me wake up calls at the wee hours of the morning to uplifting my mood in my darkest hours, he has done it all without an iota of complaint. I can never thank him enough for lending a patient ear to my ever-fluctuating mood and its accompanying tantrums. Thank you Bharat Vaidyanathan for always rekindling my belief in myself when my self-confidence was relegated to a forgotten corner of my subconscious. Your constant reminders have been a lesson to me

in staying focused in my pursuit for excellence. I am eternally grateful to Moumita Rakshit for lending undying support over the years and her constant reminders to eat on time and maintain my composure no matter what. I express my heartfelt gratitude to Manish Muhuri for taking out time to proofread my thesis and chip in his meticulous inputs and his continuous support throughout this endeavor. Thank you Alolika Amrita, Reelina and Manisha for being a constant source of entertainment when it was needed the most. To Abhishek, Raja, Kaushik, Nishanth and Vissu for being there for me whenever needed, for boosting my morale and for being the people I can always count on.

My heartfelt thanks to Nanyang Technological University for the generous scholarship support throughout the four years and for providing excellent learning and research facilities. Many thanks to past and present lab members: Anna, Bakhait, Elynn, Jing Ling, Kim, Kunning, Mei Hua, Sirong, Soak Kuan, Swealing, Song Jing, Weng Ting, Yen Ling, and Yi Wen. They helped to create a joyful and enjoyable working environment. Particularly, I would like to thank Sirong for his immense guidance and assistance during my project.

Finally, I would like to extend my gratitude to my uncle Sujoy Dasgupta who was a great source of strength to me and whom I lost during the course of my thesis.

Above all, I thank the Almighty for His kind blessings and for instilling in me the motivation to strive harder each day with equal zeal and enthusiasm.

CONTENTS

LIST OF FIGURES

LIST OF TABLES

ABSTRACT

The dynamic actin cytoskeleton plays a pivotal role towards the regulation of various cellular functions, including cell motility and division. Adherent cells, which are usually flat during interphase assume a spherical shape at the onset of mitosis. This rounding primarily involves de-adhesion from the substrate and cortical retraction. The mitotic cell rounding is essential for the proper positioning and stabilization of the mitotic spindle and ensures correct chromosome segregation. The actin filaments, present at the cell periphery during interphase, undergo realignment and distribution to the spherical cortex during mitosis. The interaction of the cortical actin with the astral microtubules that radiate towards the cell cortex from the spindle poles generates tensile forces, thus favoring the rounded morphology. In addition to this inward contraction of the actomyosin network, an outward osmotic pressure also governs the mitotic cell rounding. Cells experience an increase in the hydrostatic pressure at the onset of mitosis. A rise in the intracellular osmotic pressure results in an increased cell volume and rounding pressure. A balance between the outward directed osmotic pressure and the inward actomyosin contraction is instrumental in driving the mitotic cell rounding. Earlier work from our lab has shown that an intact actin cytoskeleton is required for proper spindle assembly at the early stage of mitosis. Perturbation of the actin cytoskeleton resulted in a less-defined mitotic spindle with an aberrant increase in astral microtubules emanating from the spindle pole towards the cortex. Cells treated with inhibitors of Rho GTPase pathway to perturb the actin cytoskeleton showed centrosome defocusing and spindle misorientation, thereby suggesting that actin cytoskeleton plays an essential role in mitotic spindle assembly. Perturbation of the osmotic gradient also led to changes in rounding pressure and volume. Failure of the cells to round up is associated with defects

in spindle assembly, pole splitting and a delay in progression. Since reduction of the osmotic pressure is associated with decrease in rounding pressure and volume and defects in cell rounding, we hypothesized that hypertonic stress could have adverse effects on the establishment of a bipolar spindle.

Aim of this thesis was to investigate the effect of osmotic stress on cell cycle progression. More precisely, we examined the role of osmotic stress on the mitotic progression and metaphase spindle assembly.

Our results show an arrest at the G_2/M phase and a decreased expression of cyclin B1 and cyclinD1 protein levels under conditions of hypertonic stress. Further, we observed a delay in the mitotic progression of cells upon hypertonic stimulation. Besides possible defects in cytokinesis, cells displayed a prolonged metaphase arrest when subjected to hypertonic shock. Thus, our results imply the existence of a possible link between the osmotic pressure and cell cycle progression.

We observed an arrest during metaphase, as shown by time-lapse microscopy and therefore we proceeded to study the effects of osmotic imbalance on metaphase spindle assembly. We observed defects in the astral microtubule arrangement and in misorientation of the mitotic spindle upon hypertonic challenge. The increase in the astral microtubule intensity was proportional to the duration of the hyperosmotic shock and the impaired astral microtubule arrangement was restored to normal when the cells were recovered in an isotonic medium, following a hypertonic shock.

The ERM (Ezrin, Radixin, Moesin) family of proteins, known to cross-link the plasma membrane with the underlying actin cortex, are essential for mitotic cell rounding. Previous reports suggest the ERM proteins, upon phosphorylation and activation during mitosis redistribute towards the cell cortex, thereby contributing to cortical rigidity. Our studies have shown that hypertonic stress upregulates phospho-ERM protein levels with a

concomitant increase in the cortical rigidity of mitotic cells. Hyperactivation of moesin also results in an aberrant increase in astral microtubule arrangement and spindle misorientation. Thus, our work suggests that hypertonicity-induced ERM phosphorylation might be responsible for the observed defects in metaphase assembly.

In order to further elucidate the mechanistic details behind the observed phenotypic defects in the spindle assembly, we designed a model based on the fact that hypertonic stress results in a higher diffusion rate. The model predicts that a perturbation of the RanGTP gradient under hypertonic stress owing to the higher diffusion rate. As a result, the cortical recruitment of the proteins required for spindle assembly, namely Gα, LGN, NuMA and dynein/dynactin will be impaired. This atypical localization of the proteins is responsible for the spindle angle defects. Our experimental results corroborate the model as we observe a reduced cortical distribution of these proteins under conditions of hypertonic stress, thereby providing a possible explanation for the defects in mitotic spindle orientation.

In conclusion, our study shows that osmotic balance is required for timely progression through the cell cycle and disruption of the osmotic gradient is responsible for delay in mitotic progression due to defects in the bipolar metaphase spindle assembly, characterized by an aberrant increase in astral microtubules and defects in spindle orientation. One possible reason behind these phenotypic defects might be the hyper activation of ERM proteins since moesin phosphorylation is implicated in the defects observed in mitotic spindle apparatus. Besides, we propose a second mechanism wherein the hypertonicity-induced aberrant cortical localization of several proteins associated with spindle orientation explains the observed impairment in astral microtubules and spindle assembly induced by hypertonic stress.

Abbreviations

ADP	Adenosine diphosphate
APC	Adenomatous polyposis coli protein
APS	Ammonium persulfate
AP-1	Activator protein-1
Arp2/3	Actin-related proteins 2 and 3
ATM	Ataxia telangiectasia mutated
ATP	Adenosine triphosphate
AQP	Aquaporin
BAX	Bcl 2-like protein 4
Bcl2	B cell lymphoma 2
BSA	Bovine serum albumin
CAK	Cyclin-dependent kinase activating kinase
COX2	Cyclooxygenase 2
CDC25	M-phase inducer phosphatase
Cdc42	Cell division control protein 42 homolog
CDK	Cyclin-dependent kinase
Chk2	Checkpoint protein kinase 2
CIK	CDK inhibitors
Cip/Kip	CDK interacting protein/Kinase inhibitory protein
CKI	Cyclin-dependent kinase inhibitor
CLIP170	Cytoplasmic linker proteins
DAPI	4',6-Diamidino-2-phenylindole
DMSO	Dimethyl sulfoxide
DSB	Double stranded breaks
DYNC1I	Cytoplasmic dynein 1 intermediate chain
DYNC1LI1	Cytoplasmic dynein 1 light intermediate chain 1
DTT	Dithiothreitol
EB1	Microtubule plus end binding protein 1
EDTA	Ethylenediaminetetraacetic acid
EIPA	5-(N-Ethyl-N-isopropyl) amiloride
eIF	Eukaryotic Initiation factor

ERK	Extracellular signal-regulated kinase
ERM	Ezrin, Radixin, Moesin
FACS	Fluorescence-activated cell sorting
F-actin	Filamentous actin
FBS	Fetal bovine serum
FRET	Fluorescence resonance energy transfer
G_1-phase	Gap 1 phase
G_2-phase	Gap 2 phase
Gadd	Growth arrest and DNA damage
GAP	GTPase activating protein
GDI	Guanine nucleotide dissociation inhibitor
GDP	Guanosine diphosphate
GFP	Green fluorescent protein
GTP	Guanosine -5'-triphosphate
GST	Glutathione S-transferase
HCl	Hydrochloric acid
HMOX	Heme oxygenase
HSP	Heat shock proteins
H2AX	H2A histone family member X
ICAM	Intercellular adhesion molecules
INK4	Inhibitors of CDK4
JNK	c-Jun N-terminal kinase
KIF	Kinesin superfamily proteins
KIN	Kinesin-related proteins
KCC	Potassium-Chloride (K^+-Cl^-) symporter
LGN	G-protein-signaling modulator 2
LIMK	LIM motif containing protein kinase
M-phase	Mitotic phase
MAP	Microtubule-associated protein
MAPK	Mitogen-activated protein kinase
MEF	Mouse embryonic fibroblasts
MEM	Minimum essential medium
MDCK	Madin Darby canine kidney
mDia	Protein diaphanous homolog

MLC	Myosin light chain
MPF	Mitosis promoting factor
MTOC	Microtubule organizing center
Myt1	Myelin transcription factor
NAC	N-acetyl-L-cysteine
NEBD	Nuclear envelope breakdown
NuMA	Nuclear mitotic apparatus protein
NFAT5	Nuclear factor of activated T-cells 5
NHE1	Sodium Hydrogen (Na^+/H^+) exchanger 1
NKCC	Sodium Potassium Chloride (Na^+-K^+-$2Cl^-$) symporter
NLS	Nuclear localization signal
NPPB	5-Nitro-2- (3-phenylpropylamino) benzoic acid
PAGE	Polyacrylamide gel electrophoresis
PAK	p21-activated kinase
PBS	Phosphate buffered saline
PCM	Pericentriolar material
PIP_2	Phosphatidylionsitol 4,5-bisphosphate
PIP5K	Phosphatidylionsitol phosphate 5-kinase
pERM	Phosphorylated ezrin, radixin, moesin
PKC	Protein kinase C
PLK	Polo-like kinase
PRDX	Peroxiredoxin
βPIX	Paxillin interacting proteins
Rac1	Ras-related C3 botulinum toxin substrate 1
Ran	Ras-related nuclear protein
Rango	Ran-regulated importin β cargo
Rap1	Ras-related protein 1
Rb	Retinoblastoma protein
RhoA	Ras homolog gene family, member A
ROK	Rho-associated coiled coil containing kinase
ROS	Reactive oxygen species
RBD	RhoA binding domain
RCC1	Regulator of chromosome condensation 1
RPE	Retinal pigmented epithelium

RVD	Regulatory volume decrease
RVI	Regulatory volume increase
S-phase	Synthesis phase
SAC	Spindle assembly checkpoint
SDS	Sodium dodecyl sulfate
Ser	Serine
siRNA	Small interfering ribonucleic acid
Slik	Sterile 20 like kinase
SNARE	Soluble N-ethylmaleimide sensitive factor attachment protein receptor
TEMED	N,N,N',N'-Tetraethylethylenediamine
TonE	Tonicity-responsive enhancer
TBS	Tris buffered saline
Thr	Threonine
TNF	Tumor necrosis factor
Tyr	Tyrosine
γ-TURC	γ -Tubulin ring complex
VEGF	Vascular endothelial growth factor

Chapter 1

INTRODUCTION

1.1 The cell cycle

1.1.1 Stages of cell cycle

The orderly sequence of events in which a cell duplicates its cellular contents and divides into two daughter cells is termed as the 'cell cycle'. In eukaryotic cells, a network of regulatory proteins governs the cell cycle progression. The ability to maintain genomic integrity is essential for cell proliferation and survival. The replication of the genome and their proper segregation into the daughter cells during cell division are the key events of the cell cycle. Lack of fidelity in DNA replication and maintenance may result in mutations and accumulation of damages, which eventually lead to cancer or cell death in multicellular organisms.

The eukaryotic cell cycle is divided into four sequential phases, namely, G_1 (G for Gap), S (S for Synthesis), G_2 and M phase (M for Mitosis). G_1, S and G_2 are collectively termed as the Interphase, during which the cell undergoes DNA duplication and synthesizes factors necessary for growth and division. Cells in the G_1 phase prepare for DNA replication, followed by S phase where DNA synthesis takes place. In the second Gap-phase G_2, the cell prepares for the division process. Cells in G_1 not committed for DNA replication can pause their progression through the cell cycle and enter a resting state termed as G_0. Cells can remain in this quiescent, non-proliferating state for days, weeks, or even years before resuming proliferation. Finally, the cell cycle culminates with the M phase, where, chromosome segregation and cell division, both nuclear and cytoplasmic takes place.

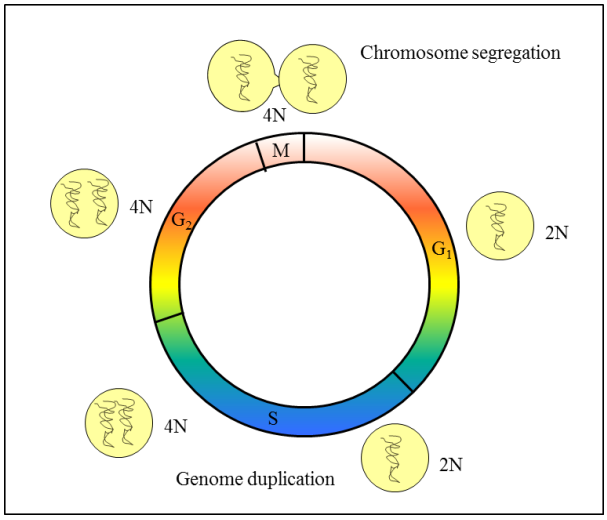

Figure 1.1 Mammalian cell cycle. A typical cell cycle consists of Gap1 (G1), Synthesis (S), Gap2 (G2) phases. During these phases, the cell prepares the proteins needed for entry and progression into the Mitotic (M) phase. During M phase, the genomic material is divided, giving rise to two daughter cells.

The fundamental characteristic of the M phase is a progressive condensation of the chromatin into compact chromosomes. This condensation is the prelude to the segregation of chromosomes, followed by division of the nucleus and finally splitting of the cell into two daughter cells.

The M phase of the cell cycle consists of mitosis (nuclear division) and cytokinesis (cytoplasmic division). At the onset of mitosis, the actin filaments undergo extensive rearrangement and enable the cells to round up Sanger [1]. Mitosis is categorized into five distinct stages, each of which is characterized by changes in the appearance of the chromosomes. The five stages of mitosis include prophase, prometaphase, metaphase, anaphase and telophase. During prophase, the interphase chromatin condenses to form compact chromosome [2]. A constriction called kinetochore is present in each of the chromosome that serves as the point of attachment of the chromosome to the spindle. In parallel, the motor proteins function to separate the centrosomes in order to establish the mitotic spindle. Motor proteins are molecular motors that utilize the energy from ATP hydrolysis to move along the microtubules. Microtubule-based motor proteins of the mitotic apparatus is involved in chromosome segregation and organization of mitotic

apparatus [3]. Mitotic motors include members of the dynein and kinesin family, which generates force in the spindle by sliding along the microtubules [4]. During spindle morphogenesis, the replicated chromosomes are separated to form spindle poles. The spindle poles nucleate astral arrays of microtubules radiating towards the cell cortex. The minus-end of the microtubules are proximal to the centrosome, and the plus-ends are distal. Plus-end directed kinesins contribute to chromosome attachment and movement to the metaphase plate whereas the minus-end directed cytoplasmic dynein focus microtubule minus-ends to poles and also exerts cortical pulling forces on the astral microtubules to ensure spindle bipolarity [3, 5, 6]. The breakdown of the nuclear envelope defines the transition between prophase and prometaphase. Following this, the chromosomes become free to interact with the spindle. A random and dynamic movement of the chromosomes is observed wherein they move towards or away from the spindle poles. Finally, the chromosomes begin to align themselves at the spindle equator, with the kinetochores of each member of the chromatid pair oriented towards the opposite spindle poles. During metaphase, all the chromosomes are present at the spindle equator, also known as the metaphase plate [7]. Anaphase onset is triggered once all the chromosomes are properly aligned to the equatorial plane [8]. The cohesion between the sister chromatids is lost, allowing them to separate. The poleward movement of the new daughter chromosomes leads to a shortening of the kinetochore microtubules [9]. Telophase marks the end of mitosis where further separation of the chromosomes towards the opposite poles takes place. The chromosomes undergo decondensation and the nuclear envelope is reformed around the daughter nuclei [10]. The cells then progress towards cytokinesis, where the cytoplasm of the parent cell is physically partitioned into two daughter cells [11].

Besides the contribution of tubulin and actin, signaling from the anaphase spindle is of critical importance in the assembly and constriction of an equatorial contractile ring

during cytokinesis. Actin and myosin II accumulate at the cell equator and results in the formation of the contractile filaments. ATP hydrolysis driven by myosin II contributes to the constriction of the contractile ring. Besides myosin II, polymerization of actin by formins or Arp2/3 complex also functions to aid the constriction of the contractile ring [12]. As the contractile ring constricts, the midzone of the anaphase spindle forms the midbody. A class of GTP-binding proteins, called Septins are involved in cell division, cytoskeletal arrangement and membrane-remodeling. Septins assemble at the cell cortex on either side of the contractile ring and help to stabilize and restrict the position of the actomyosin contractile ring thus enabling furrow ingression to take place at a site between the separated chromosomes. [13, 14]. The final step of cytokinesis is abscission, which takes place after the complete ingression of the contractile ring. This step involves membrane fusion events to bridge the remaining space following furrow ingression. SNARE (soluble N-ethylmaleimide sensitive factor attachment protein receptor) membrane fusion proteins along with a network of vesicle coat proteins are required for the successful completion of this process [15, 16].

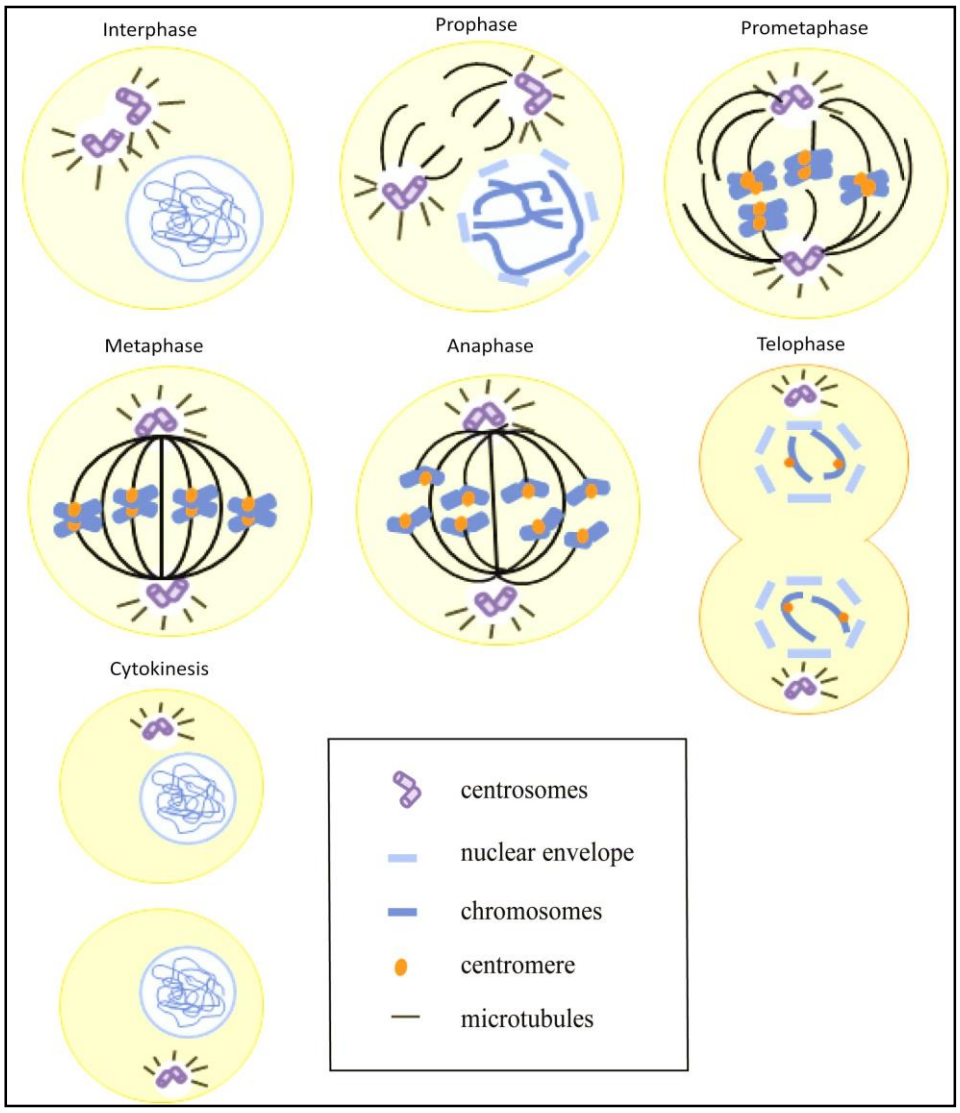

Figure 1.2 Different stages of mitosis. Mitosis is divided into five distinct stages namely, prophase, prometaphase, metaphase, anaphase and telophase. Prophase is characterized by a breakdown of the nuclear envelope and chromosome condensation. The centrioles divide and move apart. During prometaphase, the centrioles and asters migrate towards the opposite poles. The nuclear membrane is completely disintegrated and the spindle begins to interact with the chromosomes. The chromosomes, each with two sister chromatids align at the center of the cell during metaphase. Anaphase is marked by a separation of the sister chromatids and poleward movement to the opposite ends of the spindle. Following this, telophase sets in where the cell membrane constricts at the centre to divide the cell into two daughter cells, nuclear membrane forms around each of the two sets of chromosomes. The chromosomes begin to decondense and become diffused. Cytokinesis defines the successful completion of mitosis whereby the cell is physically separated into two identical daughter cells.

1.1.2 Cell cycle regulation

The cells utilize numerous mechanisms to control their progression through the cell cycle. The transition from one phase of the cell cycle to another takes place in an orderly manner and is regulated by many cellular proteins. Cyclin dependent kinases (CDKs), a

family of serine/threonine protein kinases are the fundamental regulatory proteins involved in the cell cycle progression in eukaryotic cells. The binding of cyclin with the catalytic subunits of CDK is the key event that controls the activity of these kinases [17]. Each CDK interacts with a specific set of cyclins. Out of nine CDKs discovered so far, five of them are involved in regulation of the cell cycle [18]. CDK protein levels remain stable throughout the cell cycle. On the other hand, the levels of the cyclins oscillate during the cell cycle [19, 20]. Different cyclin-CDK complexes participate in different phases of the cell cycle. Cyclin D interacts with CDK4 and CDK6 and controls entry and progression through G1 [21, 22], cyclin E/CDK2 complex regulates transition from G1 to S phase [23, 24] and cyclin A/CDK2 during S phase [25, 26]. Cyclin A/CDK1 complex enables entry into mitosis during G2/M transition. Mitosis is further governed by cyclin B/CDK1 complex [27, 28]. CDK7 in complex with cyclin H functions as CDK activating kinase (CAK) [29]. These cyclins undergo ubiquitin-mediated proteolysis after completion of the respective cell cycle phase [30]. A list of the different cyclin-CDK complexes involved in the cell cycle is tabulated below (Table 1.1).

Besides the interaction with cyclins, phosphorylation of conserved threonine residues in the T loop by CDK activating kinases (CAKs) also controls CDK activity. CDK is phosphorylated at Thr^{161} by CDK7-cyclin H complex. The Wee1 (Wee1 G_2 checkpoint kinase) and Myt1 (Myelin transcription factor1) kinases phosphorylate CDK1 at Tyr^{15} and Thr^{14}. The phosphorylation leads to conformational changes, thereby increasing the affinity to bind to the cyclins [31]. CDK1 binds to cyclin B during S phase to form an inactive mitosis-promoting complex (MPF). During the G_2/M transition, dephosphorylation at Tyr^{15} and Thr^{14} by Cdc25 phosphatase is required for the activation of the MPF and further progression through the cell cycle [32-34].

A group of cell cycle inhibitory proteins known as CDK inhibitors (CKI) function to counteract CDK activity. Presently, two distinct groups of CKIs are known, namely, the

INK4 (Inhibitors of CDK4) family and Cip/Kip (CDK interacting protein/kinase inhibitory protein) family [35]. The INK4 family consists of p15 (INK4b), p16 (INK4a), p18 (INK4c), p19 (INK4d). These CKIs form a stable complex with CDK4 and CDK6 prior to cyclin binding, thereby inhibiting the association with cyclin D [36]. The Cip/Kip family includes p21 (Cip1), p27 (Cip2), p57 (Kip2) and they inactivate the CDK1-cyclin B complex [37-39].

The intracellular localization of cell-cycle regulating proteins is essential for the proper cell cycle progression. Cyclin B is primarily cytoplasmic during interphase. It contains a nuclear exclusion signal and is exported out of the nucleus till the commencement of prophase [40, 41]. Cyclin B is transported to the nucleus, where it associates with the mitotic apparatus at the end of prophase. Wee1 located in the nucleus inhibits the premature activation of CDK1 before mitosis [42]. Myt1 located in the Golgi complex also blocks the CDK1-cyclin B complex [43]. Additionally, 14-3-3 group of proteins also control the intracellular trafficking of the cell cycle regulatory proteins. Cdc25 is present in the cytoplasm due to its interaction with 14-3-3. Sequestration of the CDK1-cyclin B complex in the cytoplasm after DNA damage also involves 14-3-3 proteins [44, 45].

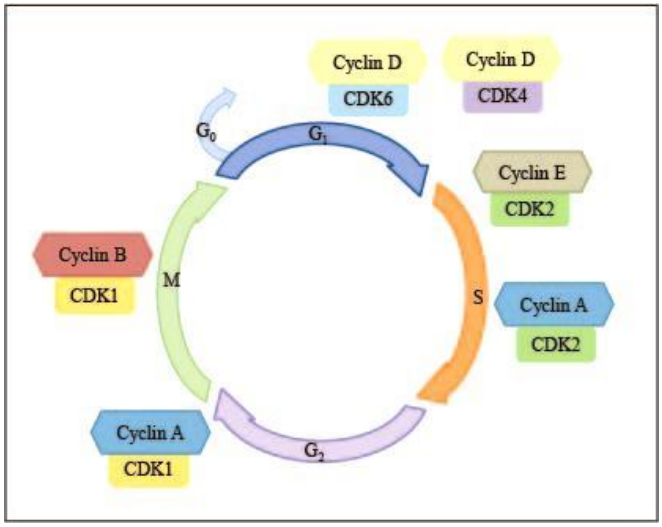

Figure 1.3 CDK-cyclin complexes during cell cycle. Cyclin D-CDK4 and cyclin D-CDK6 stimulate the initiation of G1 phase and the start of the cell cycle. The progression towards the end of G1 phase is characterized by increasing levels of cyclin E-CDK2, which in turn triggers the onset of S phase. The reduction in cyclin E-CDK2 levels by

degradation is important in initiating the S phase. Cyclin A-CDK2 regulates the completion of the S phase and entry into G2 phase, where cyclin A-CDK1 is involved. The level of cyclin B increases during the start of mitosis and diminishes at end of the M phase. The inactivation of CDK1 due to decreasing cyclin B triggers the end of the cell cycle.

Table 1.1 CDK-cyclin complexes in different phases of the cell cycle.

CDK	Cyclin	Cell cycle phase activity
CDK3	Cyclin C	G_0/G_1 phase transition
CDK4	Cyclin D1, D2, D3	G_1 phase
CDK6	Cyclin D1, D2, D3	G_1 phase
CDK2	Cyclin E	G_1/S phase transition
CDK2	Cyclin A	S phase
CDK1	Cyclin A	G_2/M phase transition
CDK1	Cyclin B	Mitosis
CDK7	Cyclin H	All cell cycle phases

1.2 Changes in cell shape during cell division

The maintenance of cell shape plays a key role in various aspects such as organism growth, form and cell division. The adherent cells undergo a series of changes in cell shape at the onset of mitosis till cytokinesis. The cells abandon their flattened morphology and round up to become spherical at mitosis [46, 47]. This process termed as mitotic cell rounding is universal in metazoans and all eukaryotes lacking a cell wall. Extensive research is being carried out to unravel the molecular mechanisms and coordination of signaling pathways underlying this evolutionary conserved process. Earlier studies have shown that a reduction in the cell-surface adhesion and an increased surface tension both contribute to cell rounding [48]. The cell rounding involves de-adhesion from the substrate, thereby disrupting the focal adhesion complexes [49]. This can be also be seen when the cultured cells treated with trypsin are forced to round up by the disassembly of focal adhesions [50] or when interphase cells forcibly round up upon treatment with antibodies against integrin β1 [51]. However, mitotic cells show retraction fibres and not all the focal adhesion complexes are disassembled [52]. Additionally, the force generated for mitotic rounding is higher compared to trypsin-mediated cell rounding

[53], suggesting that the disruption of the focal adhesion complex is not the only factor involved in cell rounding upon mitotic entry. Besides, the cells exhibit a concomitant increase in the intracellular hydrostatic pressure, causing them to swell up [53]. In parallel, the complete reorganization of the actin cytoskeleton is also essential to drive efficient cell rounding [54]. Interphase actin structures, namely stress fibres and lamellae are disassembled at the onset of mitosis and undergo extensive rearrangement and are enriched at the spherical cortex underlying the plasma membrane [54, 55].

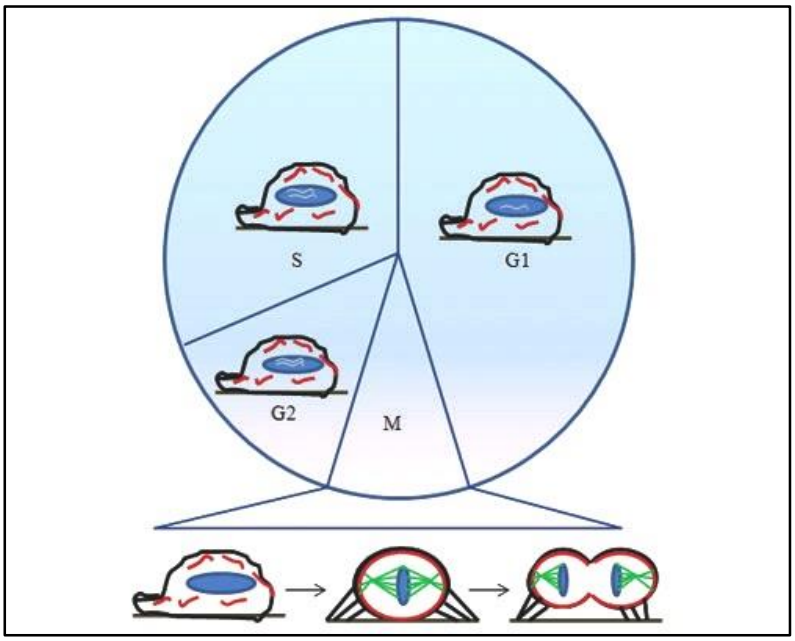

Figure 1.4 Cell shape changes associated with cell cycle. Cells remain attached to the substrate as they grow and replicate the DNA during Interphase. During mitosis, they dissociate from the substrate and undergo transition from the flat shape and round up, a process termed as mitotic cell rounding. Upon mitotic entry, cells round up, leaving the retraction fibers (black) tethering them to substrate adhesion sites. The actomyosin network generates tensile forces in retraction fibres. These tensile forces enable the rearrangement and distribution of actin filaments (red) to the cell cortex. Interaction of the actin filaments with the astral microtubules (green) generates pulling forces on the mitotic spindle, essential for its bipolar alignment.

1.2.1 Importance of mitotic cell rounding

Several studies have been carried out to highlight the significance of mitotic rounding. The primary goal of mitosis is to ensure symmetrical and accurate segregation of chromosomes. It was shown that when HeLa cells with flattened shape induced by

overexpression of adhesion regulator Rap1 or by mechanical confinement which altered the cell geometry entered mitosis, they failed to round up, leading to chromosome segregation errors and aneuploidy [56]. This study showed that perturbation of mitotic rounding led to defects in chromosome capture and bipolar spindle assembly. In order to accomplish segregation of genetic material with high fidelity, all the chromosomes need to be captured by binding of microtubules to kinetochore, thereby forming a bipolar spindle. Any unattached kinetochore results in the activation of the spindle assembly checkpoint (SAC), a cell cycle surveillance pathway that delays chromosome segregation until all the chromosomes are attached [57]. Chromosomes in the flattened cells are scattered over a large area; thus some of the chromosomes are out of reach from the microtubules or can be reached by microtubules emanating only from one pole. In comparison with spherical cells, artificially flattened cells led to a significant delay in anaphase onset due to chromosome capture defects [56]. The spherical geometry of cells enables that all the chromosomes are captured effectively by spindle microtubules in a limited space, thus affirming the significance of cell rounding during mitosis [56, 58].

Flattened interphase-like cell shape decreases cell height and this in turn affects mitotic spindle assembly, characterized by splitting of spindle poles and subsequent formation of ectopic poles resulting in multipolar spindles and aneuploidy [56]. Additionally, rounding plays a crucial role in enabling the spindle to locate the center of the cell. The position of the cleavage furrow during cytokinesis and the distribution of the cellular contents between the daughter cells are determined by the location of the mitotic spindle [11]. The spindle is positioned at the center of a round metaphase cell, which is achieved by the balance of cortical pulling forces on astral microtubules radiating from the spindle poles [58]. On the other hand, in flat cells possessing an elongated axis, astral microtubules fail to establish contact with the cortex, causing spindle-positioning defects.

The mitotic spindle in the flat cells is unable to form at the center and this results in asymmetric division of daughter cells following cytokinesis. As a result, one of the daughter cells is of larger size as compared to other [59]. Since the mechanisms underlying the symmetry of division are precisely regulated, asymmetries in the cell size of the daughter cells might have certain severe consequences that need future exploration. However, there are examples of asymmetric divisions wherein the two daughter cells have different fates [60]. For instance, oocytes undergo asymmetric meiotic divisions to form a large gamete, which inherits all the cellular content and a small polar body [61, 62]. *Caenorhabditis elegans* zygote also divides asymmetrically to give rise to a small germline-precursor cell and a larger anterior somatic cell [63, 64]. Another example is seen in the *Drosophila* neuroblasts when they divide to produce a large self-renewing apical daughter and a small basal daughter cell. Since the mechanism governing off centering of the mitotic spindle mainly depends on a balance of cortical pulling forces, investigating the exact role of the cell dimensions and shape during asymmetrical cell division provides an interesting avenue of future research.

Mitotic rounding has been speculated to play a role in cancer progression. Cancer cells, characterized by chromosomal and centrosome aberrations face more challenges during the establishment of the mitotic spindle. High number of chromosomes forms a large metaphase plate and a subsequent loss of bipolarity [65]. HeLa cells subjected to mechanical confinement are unable to form a bipolar spindle and exhibit severe mitotic defects [56], thereby highlighting the notion that mitotic rounding provides the space required for a functional spindle assembly in aneuploid cancer cells. Moreover, cancer cells possessing a higher number of centrosomes can form a bipolar spindle only if they undergo efficient rounding possibly because a large metaphase plate imparts stronger force on the poles and counteracts clustering forces [66]. However, further studies on the

involvement of the mitotic cell size and shape in physiological milieu, in both normal developing tissue and cancer cells need to be done.

1.3 Actin cytoskeleton: role in mitotic cell rounding

The actin cytoskeleton undergoes profound remodeling upon mitotic entry, which primarily governs cell rounding. Actin filaments in interphase cells are arranged in distinct structures and the spatial organization of these structures determines the structural and functional polarity of the cell. Mitotic entry is achieved by a complete transformation of this arrangement, wherein the network of interphase actin filaments is disrupted and subsequently reformed [67]. The first step involves deconstruction of the adhesion protein complexes, followed by dissolution of stress fibres and enrichment of cortical actin at the cell periphery. The cell margins begin to move inward towards the cell center and remain connected via retraction fibres. These actin-rich fibers are linked to the mitotic cell at their proximal terminal and to the adhesion substrate via their distal end. This retrograde movement along with the reorganization of the cortical actomyosin network allows the cells to assume a spherical and rigid shape.

An intact actin network is necessary to facilitate the onset of mitosis. Reports showing disruption of the actin cytoskeleton causes cell cycle arrest in different adherent mammalian cells further strengthen the aforesaid statement. Treatment of the cells with actin depolymerizing drugs like cytochalasin D and latrunculin B causes delay in mitotic progression [68, 69]. Cell cycle arrest triggered by the dissociation of the actin filaments can be attributed to several mechanisms including p53 activation, down-regulation of cyclin D1, retinoblastoma protein phosphorylation or deregulation of the p42/44 MAPK (Mitogen-activated protein kinase) pathway [70-80]. In addition to depolymerization of the actin network, excessive polymerization is also associated with defects in cell cycle progression. Presence of jasplakinolide, which enhances actin polymerization leads to

multinucleated cells and possible cytokinesis defects [81].

The regulation of actin cytoskeleton dynamics and remodeling is primarily under the control of the Rho family of GTPases, namely RhoA (Ras homolog gene family, member A) Rac1 (Ras-related C3 botulinum toxin substrate 1) and Cdc42 (Cell division control protein 42) [82, 83]. Among these, RhoA (Ras homolog gene family, member A) mediates cortical retraction and rigidity, thereby promoting cell rounding during mitosis [84]. Many RhoA effectors have been implicated to affect actin cytoskeleton remodeling. RhoA-dependent Rho kinase (ROCK) leads to the phosphorylation of the Myosin light chain kinase (MLC) kinase, either by direct phosphorylation [85, 86] or by an inhibitory phosphorylation of MLC phosphatase, thereby elevating MLC phosphorylation [86]. MLC phosphorylation, in turn, promotes actomyosin contractility and contributes to the state of the cortical actin during mitosis [85, 86]. Besides, MLC is also implicated in centrosome separation and mitotic spindle assembly [87]. Besides MLC, other Rho-kinase substrates are also involved in the regulation of the actin cytoskeleton. Rho-kinase phosphorylates LIM kinase (LIM domain kinase), which then phosphorylates and down-regulates the actin-severing protein, cofilin [88]. Cofilin is known to bring about the depolymerization of filamentous (F-) actin. Cofilin levels have been shown to be lower in mitosis as compared to interphase and the levels decrease further during cytokinesis [89]. Thus, high levels of RhoA activity could likely mediate the down-regulation of cofilin during mitosis, thereby stabilizing the actin cytoskeleton and enhancing rigidity in mitotic cells. In addition, Rho-kinase phosphorylates Adducin, which acts as a spectrin-based linker of F-actin to the plasma membrane [90, 91]. This connection of the actin cytoskeleton with the membrane could possibly promote cortical rigidity and mitotic cell rounding.

Previous reports have suggested that the ERM family proteins (Ezrin, Radixin and Moesin) act as linkers between the plasma membrane and actin filaments [92]. ERM

proteins have also been shown to be downstream effectors of RhoA [92, 93]. Recently, some studies have revealed that a positive feedback system governs the ERM protein activation, wherein the activated form of the ERM proteins directly binds to Rho-GDI, which suppresses the GDP-Rho release, concomitantly leading to Rho activation [94]. The role of ERM proteins in the organization of the cortex and mitotic cell rounding is discussed below in detail.

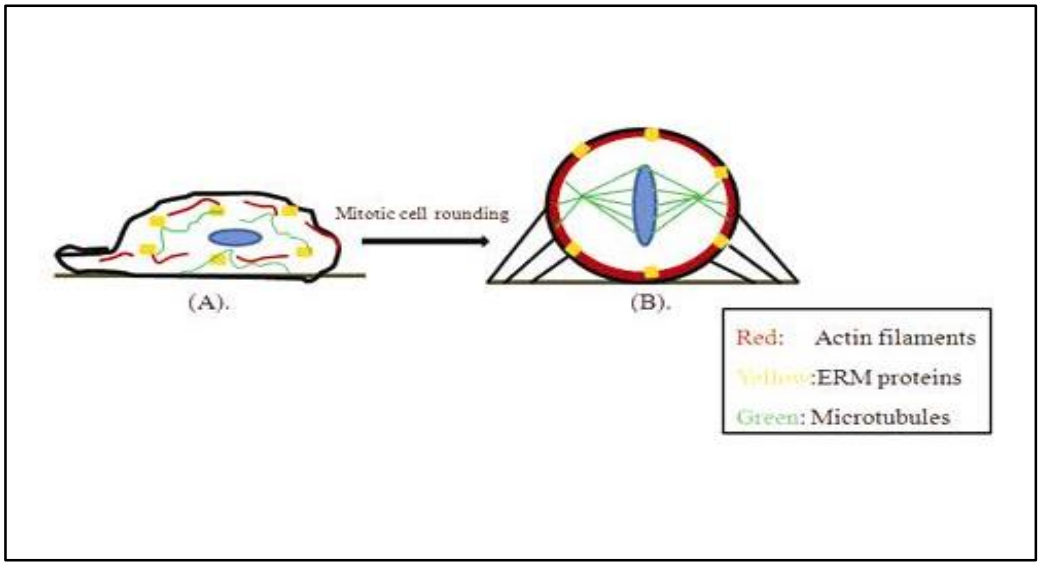

Figure 1.5 Mitotic cell rounding. Flat, adherent interphase cells (A) undergo extensive remodeling of the actin cytoskeleton and assume a rounded shape during mitosis (B). The actin filaments (red), located towards the cell periphery during interphase are enriched in the spherical cortex. The phosphorylation and redistribution of the ERM proteins (yellow) to the cellular cortex favor the realignment of the actin filaments. Interaction between the actin filaments and microtubules (green) generates a pulling force on the mitotic spindle, ensuring proper spindle alignment.

1.3.1 ERM proteins

1.3.1.1 Structural organization of ERM proteins:

The ERM family includes three closely related proteins, ezrin (82kDa), radixin (80kDa) and moesin (75kDa), collectively termed as ERM. The NH_2-terminal halves of the ERM proteins are highly conserved, bearing around 85% identity [95]. The NH_2-terminal domain of the ERM proteins associates with the plasma membrane. Integral membrane proteins and intercellular adhesion molecules (ICAM-2 and ICAM-3) directly bind to the NH_2-terminal of the ERM proteins [96-98]. This is followed by an extended α-helical

region and terminates in a C-terminal domain, which contains the actin-binding site. The co-existence of both the plasma membrane binding and actin-filament binding domains enables the ERM proteins to serve as cross-linkers of the plasma membrane and the actin cytoskeleton [99]. These proteins exist in an inactive, closed conformation, wherein the C-terminal domain is sequestered in a negatively charged pocket, located within the N-terminal domain [100]. Upon activation, this auto-inhibited structure undergoes a conformational change, allowing the ERM proteins to assume an open, active structure that enables membrane-cortical cross-linking.

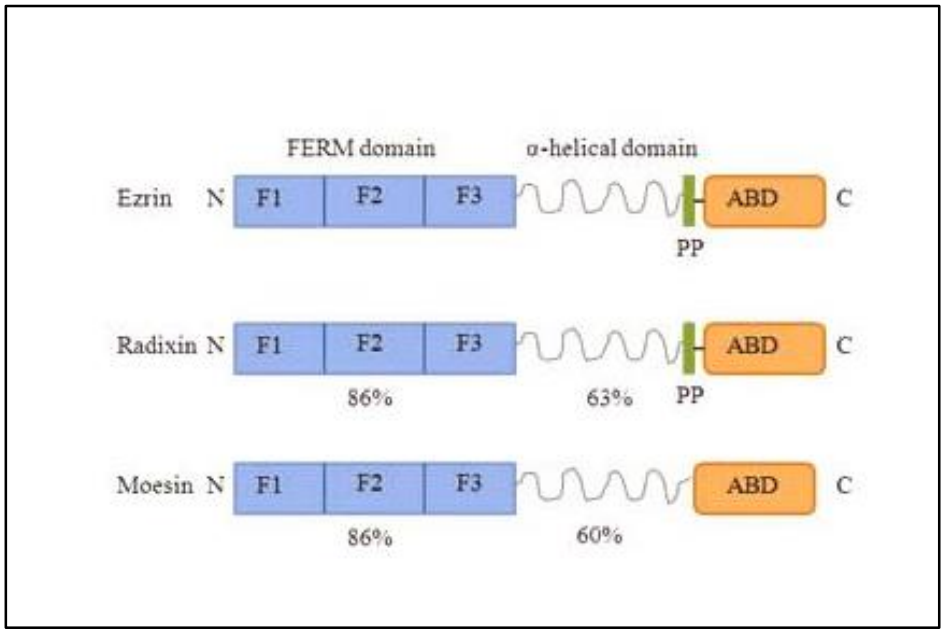

Figure 1.6 ERM family protein structure. Ezrin, radixin and moesin (ERM) proteins contain a highly conserved FERM domain in the amino terminal region (sequence identity to ezrin is shown above). This is followed by α-helical coiled coil domain. The carboxy terminal domain has a filamentous actin-binding site (ABD). Mammalian ezrin and radixin contain a polyproline rich region although the functional significance is unknown.

1.3.1.2 Regulation of ERM proteins:

The fundamental molecular event leading to the activation of ERM proteins is phosphorylation of the C-terminal threonine residue (T576 in ezrin, T564 in radixin and T558 in moesin) [101]. A potential candidate for the activation signal of these proteins is phosphatidylinositol 4,5-bisphosphate (PIP_2). PIP_2-rich membrane regions trigger the

membrane recruitment of the ERM proteins from the cytosolic pool [102]. This PIP_2-mediated recruitment makes the conserved threonine residue accessible to phosphorylation and is a pre-requisite step for the subsequent ERM protein phosphorylation [102-104]. Apart from Rho-kinase, mentioned earlier, a few other kinases have also been reported to bring about this phosphorylation. Studies in *Drosophila melanogaster*, which has a single ERM, namely Moesin (Moe) suggest that Slik kinase (Sterile 20-like kinase) is responsible for the phosphorylation at the conserved Thr (Thr559) residue [105]. Protein kinase Cα (PKCα) and PKCθ are also implicated in the ERM protein phosphorylation on this regulatory Thr residue [106].

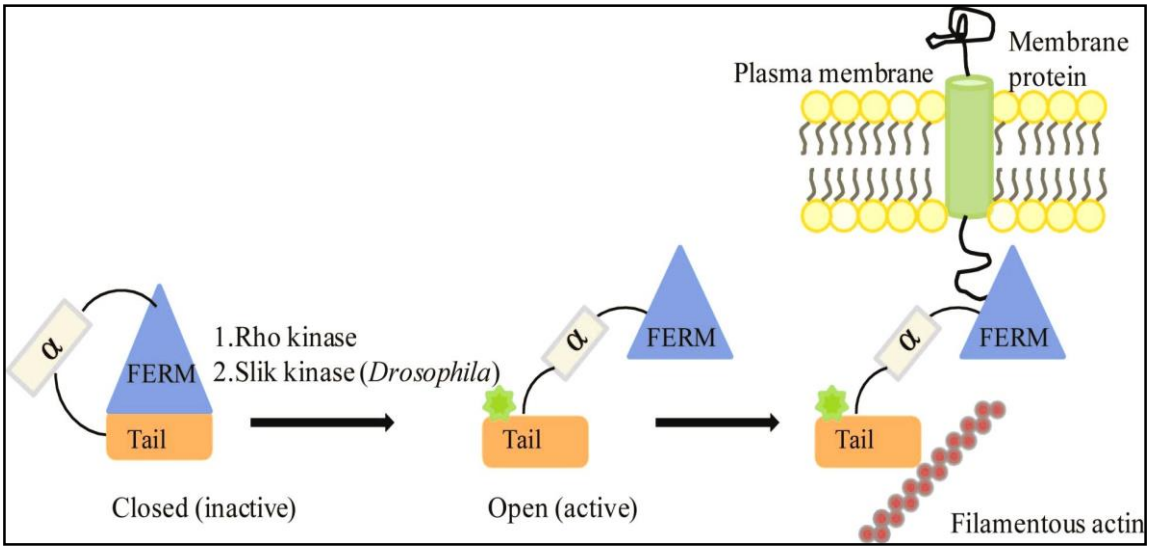

Figure 1.7 ERM protein activation. ERM proteins are present in an inactive, closed conformation by the intramolecular association between the FERM domain and C-terminal domain. PIP2 production enables the recruitment of the ERM proteins from the cytosolic pool to the plasma membrane, rendering a highly conserved threonine residue in the tail domain of ERM proteins more accessible to phosphorylation by kinases. Upon phosphorylation, these proteins undergo a change in the conformation and the open conformation favors the crosslinking of the membrane with the underlying actin filaments.

1.3.2.3 ERM proteins in mitotic cell rounding:

Apart from playing a pivotal role in cell rounding during mitosis, the ERM proteins are involved in a multitude of biological processes like, maintenance of *Drosophila* oocyte polarity, lumen morphogenesis and epithelial integrity [107-109].

Upon mitotic entry, cells encounter increased cortical stiffening, a concomitant loss of stress fibres and an accumulation of actin filaments around the cortical region [103]. Recently, studies in *Drosophila melanogaster* cells have gained insight into the functional role of moesin during cell cycle progression. The Thr 559 phosphorylated form of moesin was observed only at the onset of mitosis, suggesting that functionally active moesin is implicated in mitotic processes. A reduction in the moesin levels by using RNA interference led to abnormalities during mitosis. Cells where moesin is knocked down failed to undergo normal cortical retraction, did not show increased cortical rigidity and remained flat during metaphase. Moreover, they showed defects in spindle morphogenesis and orientation, denoted by asymmetric, elongated spindles generating protrusions, resulting in a deformed cell cortex. [54]. Thus, active moesin is required for the assembly of the metaphase plate, proper chromosome segregation, generation of a well-organized spindle, and the establishment of cortical tension during mitotic cell rounding. The actin filaments, predominantly present in the cellular edges in the interphase cells are oriented perpendicular to the membrane. At the beginning of mitosis, the phosphorylation and distribution of moesin at the cortex, under the regulation of Slik kinase stimulates the alignment of the cortical actin filaments, whereby they assume a parallel orientation with plasma membrane plane. This arrangement promotes cell rigidity and cell rounding [54].

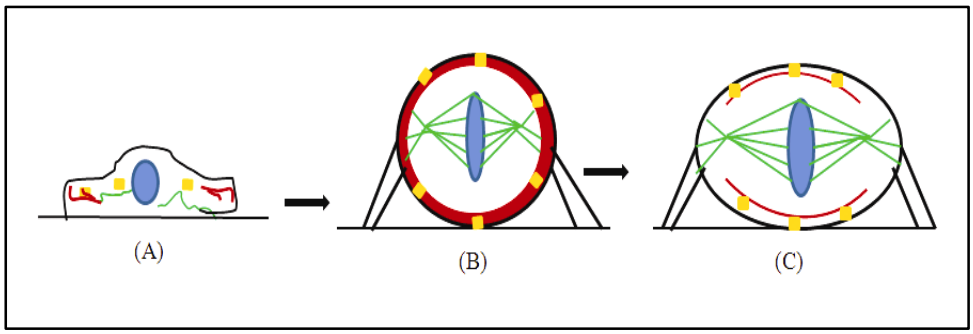

Figure 1.8 ERM proteins in mitotic cell rounding. During interphase, the cells are flat as shown in (A), the actin filaments (red) are concentrated towards the cell edge where they assume a perpendicular orientation relative to the cell membrane. During mitosis,

particularly metaphase (B), phosphorylation of ERM proteins (yellow) facilitated their redistribution to the cortex and induces alignment of the actin filaments, which are enriched in the spherical cortex. The actin filaments now assume an orientation parallel to the plasma membrane and this enhances cortical stiffening, thereby favoring a rounded morphology. During anaphase (C), decrease in the pERM levels at the spindle poles results in elongation of the spindle prior to cytokinesis.

1.4 Osmotic pressure

The pressure applied in order to prevent the inward movement of the solvent in a solution is defined as the 'osmotic pressure'. When a cell is placed in a hypertonic environment, water flows out of the cell, leading to cell shrinkage. Conversely, introduction of a hypotonic environment enables water uptake and consequent volume increase of the cell.

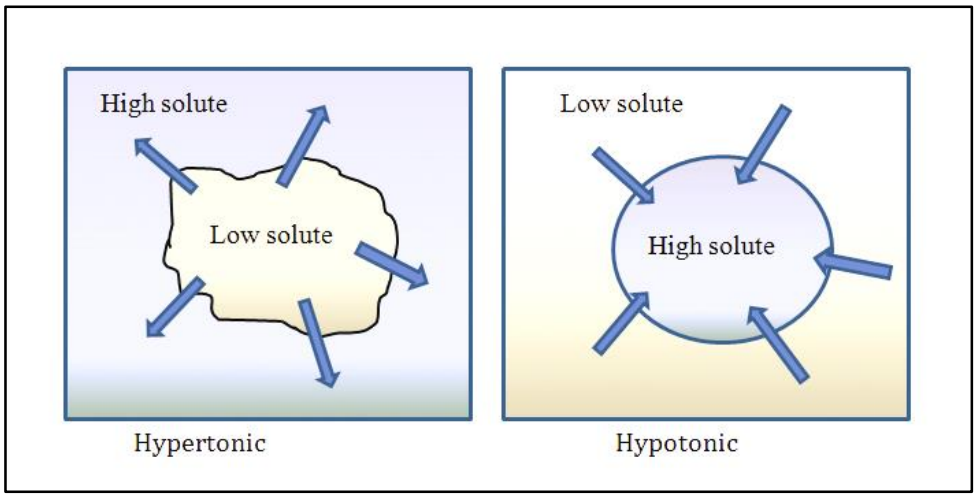

Figure 1.9 Different osmotic environments. When the solute concentration inside the cell is lower compared to environment, the medium is considered hypertonic and results in loss of water from the cells, leading to cell shrinkage. Conversely, a hypotonic medium has lower salt concentration compared to that of the cell. Exposure to hypotonic medium causes water influx and a concomitant cell swelling.

1.4.1 Role of osmotic pressure in cell rounding during mitosis:

In addition to the actomyosin contractility, the regulation of osmolarity is essential to drive cell rounding. Disruption of the osmotic gradient affects cell volume and rounding pressure during mitosis [53]. Exposure to a hypertonic environment, reflecting a drop in the osmotic pressure is accompanied by a decrease in rounding pressure and cell volume. Conversely, an increase in the osmotic pressure is associated with a higher rounding pressure and a concomitant increase in cell volume. During mitotic entry, dissociation

from the substrate aids rounding and simultaneously cells increase their intracellular pressure in order to enable effective rounding in a tissue environment. In order to establish a connecting link between osmotic pressure and actomyosin contraction, experiments showing the inhibition or stimulation of the actomyosin cortex have been done. These studies show that treatment of HeLa cells with blebbistatin, an inhibitor of myosin contraction, followed by latrunculin A, which depolymerizes actin filaments display an increase in cell volume and an abrogation in rounding pressure. On the other hand, stimulation of actomyosin contractility showed a rise in rounding pressure and a reduction in cell volume [53]. These findings reflect that the actomyosin contraction acts against an opposing intracellular pressure and the cross-linkers between the membrane and the underlying cortex couple these two phenomena. Thus, regulation of cortical tension along with an intracellular hydrostatic pressure will provide an impetus to alter cell shape, dynamics and administer the mechanics of mitosis.

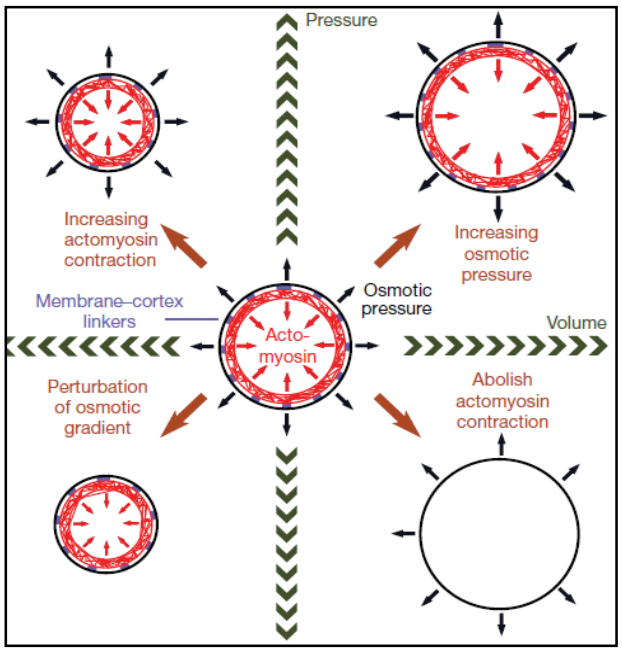

Figure 1.10 Actomyosin contraction is balanced by outward intracellular osmotic pressure. Proteins acting as cross-linkers of the membrane and cortex (purple) coordinate the outward directed intracellular osmotic pressure (black) and the actomyosin contractility (red) to enable cell rounding. Perturbation of the osmotic gradient or abrogation of actomyosin contraction affects cell rounding during mitosis. Modified from [53].

1.4.2 Effects of hypertonic stress:

Primarily, the cells in the renal medulla are exposed to high levels of sodium chloride (NaCl) and urea [110]. Under physiological conditions, the kidney-derived epithelial cells face marked fluctuations in osmolarity [111, 112]. Extensive studies about the consequences of hyperosmotic stress have been studied primarily on renal medullary cells because under physiological conditions, these cells are constantly exposed to high interstitial concentration of NaCl and urea, in comparison to other cells in the body. Since the effects are more pronounced in renal medullary cells, most of the studies have been carried out on these cells. Recent studies have shown that non-kidney-type cell functions are also modulated by hypertonic stress [113]. Several cellular functions other than of kidney cells have been shown to be affected by hypertonic stimulation.

A wide variety of other types, including macrophages [114] endothelial cells [115], chondrocytes [116], astrocytes [117] and retinal pigmented epithelial cells (RPE) [113] are also exposed to hyperosmotic conditions.

1.4.2.1 Cell cycle arrest:

The perturbing effects of hyperosmotic stress include cell cycle arrest associated with DNA damage, high levels of reactive oxygen species and cytoskeletal rearrangement. Studies conducted on RPE cells subjected to 100mM NaCl or 200mM sucrose caused accumulation in the G1/S and G2/M phase pertaining to cell cycle arrest and consequently lower cell proliferation [113]. Cell cycle arrest allows the cells to adapt to the high osmolarity changes by accumulating protective osmolytes and higher expression of heat shock proteins. Arrest at the G1 and S phase depends on p53 activation [118] and G2 arrest in turn depends on p38 activation [119] following hypertonic shock.

1.4.2.2 DNA damage:

DNA damage is one of the causes of cell cycle arrest. High concentration of NaCl induces DNA breaks in cells (ref 73,153 cellular responses to hypertonic stress); however, the underlying mechanism behind this induction and stress response is not well understood. Hypertonic stress activates several signaling cascades, including activation of p38, JNK and Plk3, which in turn trigger the transcription factor activating protein-1 (AP-1) [120-124]. Studies reveal that hypertonic stress shows an upregulation in the Polo like kinase (Plk3)-mediated phosphorylation of H2AX levels at Serine 139 residue, thereby causing changes in cell fate [125]. The nucleosome core histone H2A variant, H2AX serves as a marker for double strand breaks (DSBs) in mammalian cells [126, 127]. Plk3 is implicated in the hypertonicity-induced activation of DNA damage response proteins, like p53 (tumor protein p53), ATM (Ataxia telangiectasia mutated) and Chk2 (Checkpoint kinase 2) [128, 129]. Hyperosmotic shock resulted in a higher population of cells in G_2/M stage and apoptotic stage in corneal epithelial cells as well as mouse embryonic fibroblasts (MEFs) and this altered distribution was restored upon inhibition of Plk3 and H2AX activities [110]. Thus, hypertonicity-induced Plk3 mediated H2AX phosphorylation has essential functional roles in cell fate.

1.4.2.3 Apoptosis:

Cells exposed to extreme hypertonic conditions eventually undergo apoptosis *in vitro* and *in vivo* [110]. The cells subjected to cell death due to harsh hypertonic conditions encounter characteristic apoptotic features like, DNA fragmentation, nuclear condensation, activation of caspases, phosphatidylserine exposure at cell surface and formation of apoptotic bodies. Evidence of the role of an intrinsic pathway stems from the reported mitochondrial depolarization, decrease in the Bcl2/Bax ratio and rise in the ADP/ATP ratio [130] when cells are exposed to extreme levels of osmolality like 700 mosmol/kg. Furthermore, HeLa cells subjected to 900 mosmol/kg resulted in

internalization of tumor necrosis factor-α (TNFα) receptors [123], validating the role of the extrinsic pathway. An osmolality of around 500 mosmol/kg is able to induce apoptosis in macrophages and B-lymphocytes, in association with higher TNF-α production [131]. Hence, both the intrinsic and extrinsic apoptotic pathways are involved in the hypertonicity- induced cell death.

1.4.2.4 Transcription and translation inhibition:

High salt concentration causes a reversible inhibition of DNA, RNA and protein synthesis in cells [132]. RNA synthesis is repressed when HeLa cells are subjected to osmotic shock [133]. Hypertonic stress also abrogates translation due to the accumulation of intracellular inorganic ions and this inhibition might possibly result in cell cycle arrest [134, 135]. But the underlying mechanism is not well established. Previous work suggests that hypertonic stress blocks translation initiation of proteins by activating eIF2α (Eukaryotic translation initiation factor 2). However, although the synthesis of most cellular proteins is repressed during hyperosmotic conditions, the translation of a few heat-shock proteins is increased.

1.4.2.5 Oxidative stress:

The reactive oxygen species (ROS) has the ability to alter DNA bases by the incorporation of 8-oxoguanine [136]. Besides the alteration of DNA bases, ROS is also involved in protein carbonylation. Carbonylated proteins show a compromised stability and function, significantly affecting enzyme activity [137]. Hypertonic treatment results in oxidative stress, with a concomitant rise in the ROS levels and subsequently protein carbonylation. The inner medullary cells of the kidney, experiencing elevated levels of NaCl and urea indeed have a higher proportion of carbonylated proteins [138]. Low level of oxygen tension in the renal medullary cells in turn might prove beneficial to curtail the oxidative stress-induced damage. Though the functional basis of the perturbing effects of

the hypertonicity-induced carbonylation are yet to be unraveled, some observations throw light on the role of ROS in osmoprotective signaling. For example, the antioxidant N-acetyl-L-cysteine (NAC) inhibits the hypertonic stress-induced levels of oxidative stress-regulated transcription factor Gadd153 (Growth arrest and DNA damage inducible gene) [139]. Additionally, NAC also impedes the phosphorylation of ERK1/2 and p38, which play a role in cell cycle delays induced by hyperosmotic conditions [140].

1.4.3 Adaptive response to hypertonic stress:

The maintenance of an appropriate cell volume is necessary for survival. A perturbation of the cell volume as a result of the alteration of the osmotic gradient hampers the plasma membrane integrity and the cytoskeletal architecture. The cells employ several compensatory mechanisms to counteract the hazardous effects of osmotic imbalance and to restore its normal cell volume. The ion transporters at the plasma membrane function effectively in cell volume regulation and serve as the first line of adaptive response against osmotic imbalance [141]. In order to counteract the hypertonicity-induced cell shrinkage, cells activate transporters, resulting in an increased concentration of intracellular ions and a restoration of osmotic balance [110]. The role of the ion transporters in osmoprotective responses will be discussed later in detail.

The cells are likely to encounter an imbalance of the intracellular ion homeostasis as a result of the compensatory ion influx. Therefore, as a second line of adaptive responses, organic compounds known as osmolytes are transported. Examples include creatine, myoinositol, glucose [142]; these compounds either function as osmolytes or aid in their synthesis. An integrated influx of water, ion and osmolyte is required for the establishment of osmotic balance. Aquaporins are a family of water channels, involved in the reabsorption of water in the epithelial cells of the renal medulla [143]. Aquaporin 1 (AQP1) has been shown to be activated by hypertonic stress-mediated ERK, p38 and JNK

(c-Jun N-terminal kinase) kinase in renal medullary cells [143, 144] whereas, AQP4 and AQP9 is triggered by p38 activation in astrocytes [117], suggesting that induction of the AQP isoform is dependent on the cell type. Thus, the hypertonic stress-dependent activation of AQP1 requires all the three kinases of the MAPK pathway and is vital in eliciting an adaptive response against perturbation of the osmotic gradient.

Another osmoprotective response is the activation of Cyclooxygenase 2 (COX2) in the liver, lung and kidney [145, 146]. COX2 plays a role in the production of prostaglandin E, which in turn acts as vasodilator in kidney cells [147]. Moreover, hypertonic stress-mediated COX2 gene upregulation is implicated in the transactivation of the epidermal growth factor receptor (EFGR) and MAPK family members, including ERK, JNK2 and MAPK14 [110, 148].

As mentioned earlier, when the osmotic balance is disturbed, it leads to the production of ROS [149]. In order to negate the harmful effects of oxidative stress, antioxidant enzymes are stimulated. Hypertonic conditions lead to an elevated expression of several proteins with antioxidant properties like, heme oxygenase 1 (HMOX1), peroxiredoxin-2 (PRDX2), PRDX6 and lactate dehydrogenase [150, 151].

Cells protect themselves from harsh hyperosmotic conditions via an increased expression of the osmoprotective genes [134]. The nuclear factor of activated T-cells 5 (NFAT5) aids in the induction of genes involved in osmolyte synthesis and transport, antioxidant response, unfolded protein response and cytoskeletal rearrangement [152, 153] NFAT5 is phosphorylated upon exposure to hypertonicity. Kinases known to phosphorylate NFAT5 include cyclin-dependent kinase 5 (CDK5), ATM Kinase, phosphatidylionositol 3-kinase, protein kinase A and MAPK14 [110, 154, 155]. The phosphorylated form of NFAT5 enters the nucleus and controls gene expression by binding to a conserved sequence in the promoter region of the target gene referred to as tonicity-responsive enhancer (TonE), also known as osmotic response element (ORE) [110]. NFAT5-mediated gene expression

of the osmoprotective genes safeguards the cells from the deleterious effects of hyperosmotic shock.

Hypertonic stress is accompanied by a loss of water from the cells and corresponding cell shrinkage. The water efflux results in macromolecular crowding and as a result, the macromolecules encounter a mechanical stress. In order to counterbalance this stress, the cells show elevated expression of chaperones such as, heat shock proteins, HSP27, HSP70, HSP90 [110, 151]. These protein chaperones stabilize the protein structure and function and also prevent apoptosis, thereby allowing the cells to adjust to the altered cellular milieu [156].

In response to the cell shrinkage, followed by a hypertonic challenge, among the several adaptive and compensatory mechanisms employed by the cell to withstand the osmotic stress, the reorganization of the cytoskeleton plays a prominent role in the adaptive responses and the details are discussed below.

1.4.3.1 Cytoskeletal rearrangements in response to hypertonic stress:

Remodeling of the cytoskeletal architecture is one of key modifications in the compensatory mechanism against extracellular osmolarity. This rearrangement helps in the restoration of normal cell volume and maintains cellular integrity. Studies suggest that hyperosmotic stress activates the small Rho GTPases namely, Rac and Cdc42, leading to the activation of the Arp2/3 (Actin-related proteins 2/3) complex. Consequently, actin nucleation commences and cortactin is recruited at the cell periphery, thereby further promoting F-actin polymerization and branching. Cortactin accumulation serves as the indicator of the F-actin assembly at the periphery and its translocation results in the stabilization of the peripheral actin network [157, 158]. This cortical remodeling may act as a protective response against osmotic stress.

Secondly, hypertonicity induces PIP_2 levels via the dephosphorylation of Phosphatidylionositol phosphate 5-kinase (PIP5K). PIP_2 is synthesized by the phosphorylation of PI4P (phosphatidylionositol 4-phosphate) at the 5^{th} position of the inositol ring to generate PIP_2, catalyzed by PIP5K [159]. Elevated PIP_2 levels stimulate regulatory proteins that mediate actin nucleation and assembly and inhibit filament severing and depolymerizing proteins, thereby reorganizing the actin cytoskeleton.

Cofilin is a F-actin severing protein and is regulated by phosphorylation [160]. The cofilin phosphorylation inhibits its filament severing property and thus stabilizes and brings about a net increase in the F-actin network. Introduction of the hyperosmotic stress activates Rho. The downstream Rho-kinase ROK phosphorylates LIM Kinase, which in turn is responsible for cofilin phosphorylation [161, 162]. This osmoprotective phenomenon has been observed in kidney tubular cells.

Further, hyperosmotic stress also has the ability to induce the Myosin light chain (MLC) phosphorylation via the Rho/ROK pathway [163]. The role of the MLC in the reinforcement of the cytoskeleton has been mentioned earlier.

Finally, osmotic stress triggers ERM protein phosphorylation; the upstream effectors being the elevated levels of PIP_2 and RhoA [164]. The increased level of phosphorylation promotes the translocation of the ERM proteins to the plasma membrane and enables their colocalization with the F-actin in the cortical region.

1.5 Ion channels in cell volume regulation

The cells readjust the perturbations in cell volume, caused by anisotonic conditions through the concerted action of the ion transporters, resulting in the net movement of osmolytes and water [165]

A majority of the animal cell types confront the hypertonicity-induced cell shrinkage via a compensatory mechanism termed regulatory volume increase (RVI). RVI results in the

uptake of ions and organic solutes, thus reviving the intracellular osmolarity. RVI is brought about the combined activation of the Na^+/H^+ exchanger (NHE) and Cl^-/HCO_3^- antiporter and Na^+ -K^+ -2Cl^- symporter (NKCC), depending on the cell type [166-168]. NKCC is activated by protein kinase C (PKC) dependent and MLC kinase mediated phosphorylation [169, 170] H^+ and HCO_3^- ions are extruded by the Na^+/H^+ exchanger (NHE) and Cl^-/HCO_3^- antiporter respectively with the concomitant NaCl entry. Since, these ion transporters restore the cellular volume and increase the intracellular osmotic pressure immediately after hypertonic exposure, they are likely to contribute to mitotic cell rounding.

On the other hand, the hypotonicity-induced cell swelling is counter-balanced by efflux of ions, release of osmolytes and compensatory cell shrinkage, termed as regulatory volume decrease (RVD). The K^+-Cl^- symporter (KCC) is activated by upon cell swelling in many cell types [165] KCC activation leads to KCL efflux from cells. Besides KCC, several K^+ channels are also implicated in RVD in many cell types.

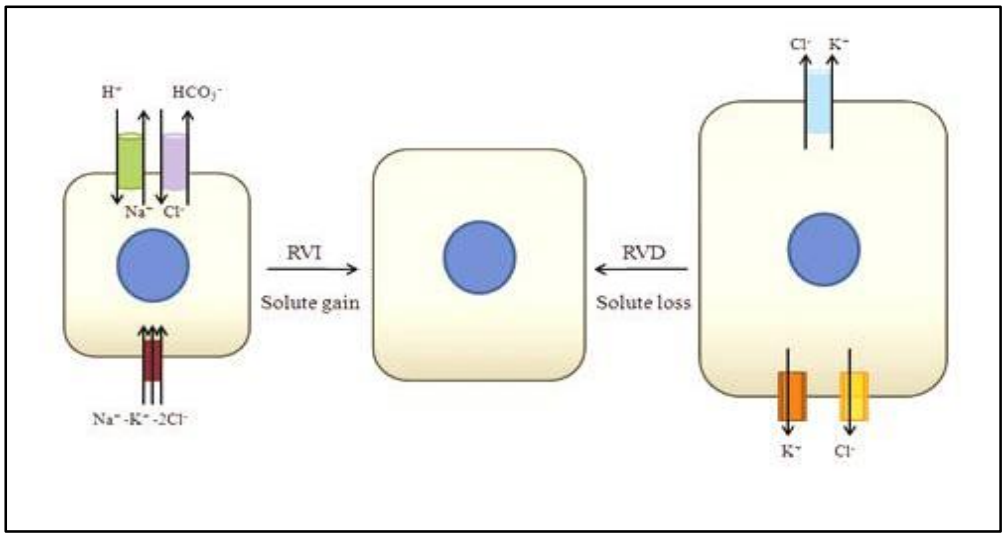

Figure 1.11 Ion channels act as molecular mediators of cell volume regulation following osmotic shock. Ion transporters and channel are actively involved in the homeostatic counter-responses during osmotic gradient disruption. Hypertonicity-induced cell shrinkage is balanced by regulatory volume increase (RVI), promoted by activation of Na+ -K+ -2Cl- symporter (NKCC), Na+/H+ exchanger (NHE) and Cl-/HCO3- antiporter. The net effect is the influx of Na+ and Cl-, thus restoring osmotic balance. On the other hand, cell swelling is balanced by regulatory volume decrease (RVD), carried out by the activation of the K-Cl cotransporters and potassium and chloride channels.

1.5.1 Na^+/H^+ exchanger

1.5.1.1 Regulation:

A wide range of cell-surface receptors, like receptor tyrosine kinases, integrin receptors and G protein-coupled receptors regulate the activity of NHE1 [171]. Ras-mediated activation of NHE1 by ERK signaling cascade is an example of the receptor tyrosine kinase dependent pathway [172]. Among the G protein-coupled receptors, $G\alpha_q$ and $G\alpha_{13}$ stimulate NHE1 activity [173-175] $G\alpha_q$ triggers NHE1 with the help of Protein Kinase C whereas $G\alpha_{13}$ dependent NHE1 activation involves RhoA [176]. The downstream kinase ROK phosphorylates C-terminal serine residues in the cytoplasmic domain of NHE1 [177], enabling actin stress fiber assembly [178]. Thirdly, treating cells with fibronectin or plating cells on a fibronectin coated surface activates integrin, which leads to NHE1 induction [177] . The cytoskeletal action of integrins is controlled by NHE1, which functions in anchoring the cortical cytoskeleton to the membrane. Apart from the above-mentioned processes, NHE1 function can also be governed by hypertonic stress. Hyperosmolarity-induced activity of NHE1 acts as a compensatory response to administer volume restoration against cell shrinkage. An intriguing question is how this exchanger detects changes in the cell size. Regulation of NHE1 antiporter by osmotic stress is independent of NHE1 phosphorylation [168] or MAPK signaling [179]. The dynamic changes in the actin cytoskeleton can be a possible candidate for this activation. A recent study has determined a direct interaction between NHE1 and the ERM proteins [180]. This association is necessary in the rearrangement of cortical actin and also modulates the transporter activity [180]. Other studies showing that serum triggers NHE1 function by a filamentous actin-dependent mechanism [181] and inhibition of myosin light chain kinase abrogates shrinkage-induced stimulation of the antiporter further validate the role of the cytoskeleton-mediated NHE1 induction [182].

1.5.1.2 Cellular functions of NHE1:

Since changes in the intracellular pH exert pleiotropic effects, leading to a wide variety of altered cellular functions, NHE1 has also been shown to regulate cell proliferation, survival, adhesion and migration [171, 183]. The expression of this ion channel conferred an increased proliferative response and the ion translocation function was fundamental in driving the rise in proliferation [180]. However, the underlying mechanistic details remain elusive. A conceivable interpretation could be that since the cell cycle progression is accompanied by increase in cell volume and NHE1 acts to accomplish a critical cell size, this ion transporter is perceived to regulate mitotic entry [184]. The observation showing cells expressing a translocation-defective NHE1 mutant facing a delayed G_2/M transit with a concomitant aberrant expression of G_2/M-checkpoint regulatory genes, namely Wee-1 kinase and 14-3-3 tau/theta further asserts the role of NHE1 in cell cycle [183].

Moreover, the rise in cell proliferation brought about by this exchanger may also be administered by cell survival of prevention of apoptotic cell death [185]. The intracellular acidification and volume decrease, which are characteristic features of apoptosis, are negated by osmoprotective function of NHE1, thereby, exhibiting an anti-apoptotic signal. Studies showing fibroblasts expressing an ion-translocation defective NHE1 mutant are less tolerant to serum deprivation as compared to wild type affirms its role in cell survival [186].

Elucidation of NHE1 functions in controlling actin cytoskeleton and cell migration is an emerging field of research. As mentioned earlier, the anchoring property of NHE1, through its association with ERMs and other effectors downstream of integrin receptors drive many cytoskeletal events, including cell adhesion, regulation of cell shape and actin filament assembly.

The presence of this transporter in lamellipodia suggests a possible role in cell migration [187]. Pharmacological inhibition of NHE1 impedes migration of endothelial [188] and Madin-Darby canine kidney (MDCK) cells [170, 189]. Also, fibroblasts expressing ion transporter defective NHE1 mutant were unable to move in a polarized fashion as observed in wound-healing assays [186]. Thus, if the ion translocation function is necessary for membrane protrusion, the molecular details need to be investigated. The current model governing membrane projection is actin polymerization [190]. In that case, it is possible that the Na^+/H^+-exchanger could control actin nucleation by modulating pH-sensitive proteins, such as cofilin [191]. Changes in the actin network in response to a localized rise in osmotic pressure could be another direct consequence of NHE1 function in driving membrane protrusion [192]. Thus, findings pertaining to the contribution of NHE1 in migratory functions and how actin polymerization might be modulated by changes in osmotic pressure and intracellular pH require additional reevaluation.

1.6 The mitotic spindle

The mitotic spindle is a macromolecular machine, which plays an instrumental role in chromosome segregation during mitosis. Improper segregation of chromosomes results in aneuploidy thereby causing genomic instability and cancer [193]. Hence, it is essential to understand the function of the mitotic spindle.

1.6.1 Components of the bipolar mitotic spindle:

1.6.1.1 Microtubules

The primary structural and dynamic components of the spindle are the microtubule polymers, whose innate polarity and dynamicity are imperative for bipolar spindle assembly. These polarized filaments grow and shrink by the addition and loss of tubulin dimers at the polymer ends [194]. A group of proteins, called the microtubule-associated proteins (MAPs), improve the stability of microtubules and are subjected to spatial and

temporal regulation within the spindle [195]. The microtubules are arranged in a bipolar array; each half consisting of uniformly oriented structures, with the minus ends at the poles and the plus ends towards the central spindle. The first stage of mitosis, prophase, is characterized by a cascade of steps, which include nuclear envelope breakdown, chromosome condensation and centrosome duplication and separation. Additionally, a high rate of catastrophes, resembling microtubule shrinkage and lower levels of growth disassembles the interphase array of microtubules, promoting interaction between the dynamic plus ends and chromosomes [196, 197]. Prometaphase marks the attachment of the microtubules radiating from one centrosome to the kinetochore of the duplicated chromosomes, followed by attachment of the sister kinetochore to the microtubules emanating from the other centrosome. Finally during metaphase, all the chromosomes are aligned at the equatorial plate. There are three subsets of microtubules present at the spindle during this phase. Firstly, the kinetochore microtubules which extend to the kinetochores of the paired chromatids with the minus ends at the poles, secondly the interpolar microtubules which extend towards the central spindle, forming an overlapping antiparallel network and the third subset includes the astral microtubules which emanate from the poles towards the cell cortex away from the spindle and are engaged in anchoring and positioning the spindle in the cell [10, 198, 199]. The dynamic polarity and antiparallel organization of the microtubules is pivotal for mitotic spindle assembly.

1.6.1.2 Centrosomes

The centrosomes act as the major site of microtubule nucleation and define the spindle poles [200]. It is the fundamental microtubule-organizing centre (MTOC) in mammalian cells, enabling the polymerization of microtubules and acting as an anchor to the astral microtubule filaments, which extend towards the cell periphery. The centrosome consists of a pair or centrioles surrounded by periocentriolar material (PCM), where nucleation occurs thereby producing polarized microtubule filaments with their plus ends radiating

outwards. γ-tubulin and pericentrin are the major components of PCM, which assembles to form a multi-subunit γ-tubulin ring complex (γ-TURC) [201]. During mitosis, more -TURC and other additional components are recruited to the centrosome, resulting in an elevated nucleation capacity of the centrosomes [202, 203]. This aids in the attachment of the microtubules with the chromosomes and leads to the establishment of a stable spindle structure.

1.6.1.3 Chromosomes

The chromosomes are active players of the mitotic process and contribute significantly to the nucleation and stabilization of microtubules during mitotic spindle assembly. Each sister chromatid of a replicated chromosome contains a kinetochore. This macromolecular complex is the site of end-on attachments with a subset of spindle microtubules and is crucial for chromosome segregation [204]. The kinetochore further regulates the spindle assembly checkpoint (SAC), which administers the proper attachment of chromosomes to the spindle and pauses mitosis until the attachment is accomplished with the sister chromatids oriented towards opposite spindle poles [205]. Hence, the kinetochore serves as an important component of the spindle machinery.

1.6.1.4 Motor proteins

The motor proteins are an integral component of the mitotic spindle. Motor proteins belonging to the kinesin and dynein superfamilies both participate in several aspects of spindle formation [3]. Kinesin family members have the ability to drive transport along spindle fibers [3, 6]. The motor domain of the kinesin-related proteins is highly conserved. KIN-N has the N-terminal motor domain and migrates towards plus end of the microtubules whereas, KIN-C containing C-terminal motor domain move towards minus end, KIN-I motors contain intrinsically located motor domains that seemingly destabilizes microtubule ends [194, 206]. Cytoplasmic dynein moves towards the minus end of the

microtubules using energy from ATP hydrolysis. Both motors have been implicated in participation of spindle assembly. Separation of the duplicated chromosomes is one of the early events in spindle assembly. The cytoplasmic dynein present at the cell cortex functions to pull the centrosomes apart and kinesin C and kinesin N cross link microtubules emanating from the two centrosomes, forming strong bundles to conserve centrosome separation and spindle bipolarity [207, 208].

The spindle pole is the site of origin for most of the spindle microtubules. The integrity of the spindle pole is essential for the stability of the spindle structure and chromosome segregation. Cytoplasmic dynein is localized to the spindle poles and kinetochores in higher eukaryotes [207]. Disruption of dynein resulted in abnormal spindles in frog egg extracts [209] and impaired the formation of astral microtubules in mammalian cell extracts [210, 211]. Further, the centrosome dissociates from the spindle body upon perturbation of dynein [210]. These observations reveal that the minus-end directed motor activity governs the convergence of microtubule minus ends at the spindle poles. Additionally, dynein helps in the recruitment of structural proteins, which are engaged in spindle architecture. One of the key proteins recruited by dynein include NuMA (nuclear mitotic apparatus). It is sequestered in the nucleus during interphase and upon nuclear envelope breakdown at the onset of mitosis; NuMA interacts with microtubules of the mitotic spindle and eventually becomes concentrated at the spindle poles [212]. The globular head region of NuMA interacts with dynein and the C-terminal tail domain contains microtubule and LGN binding sites [213]. During metaphase, NuMA is present at the cortical region above the spindle poles, where it forms a ternary complex with LGN and G-α and this cortical distribution increases as the cell progresses to anaphase [213-215]. This complex is essential to anchor the dynein at the cortex and the cortical enrichment of NuMA and dynein is vital for proper spindle elongation [58, 216]. The

cortically anchored dynein exerts a pulling force on the plus ends of astral microtubules, thereby regulating spindle positioning [216].

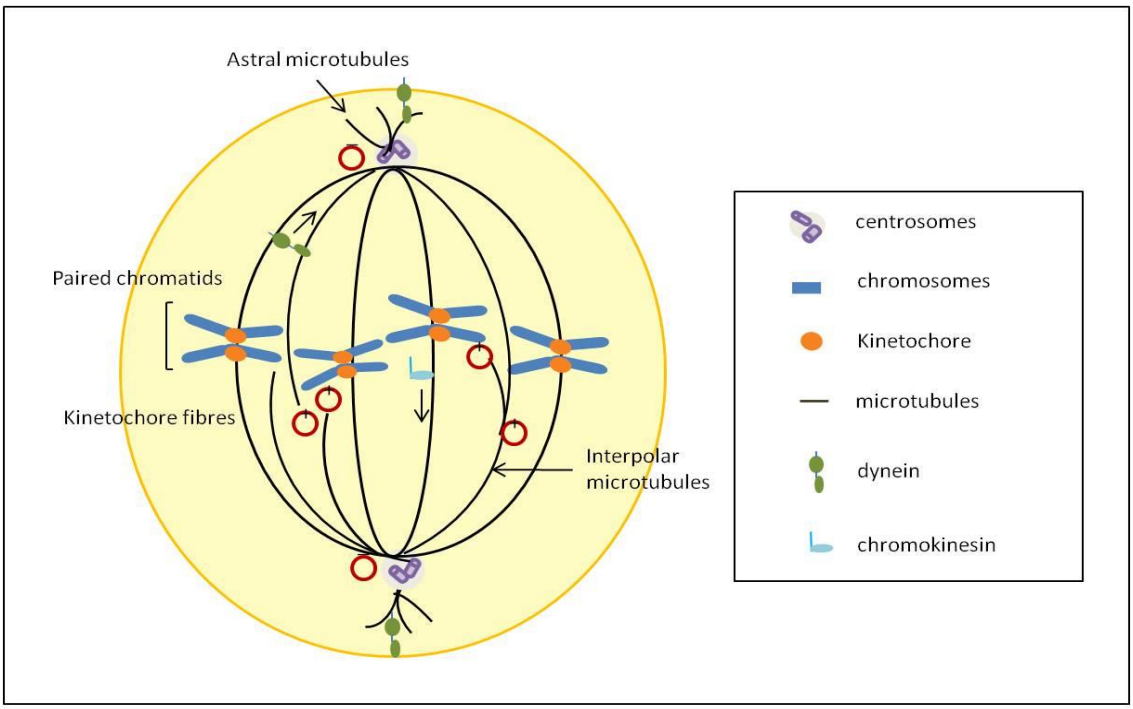

Figure 1.12 Mitotic spindle architecture during metaphase. The microtubules emanate from the centrosomes with their minus ends tethered at the spindle poles. Some microtubules attach with the kinetochore of paired chromatids, known as spindle microtubules or kinetochore fibres, some form an overlapping antiparallel array termed as interpolar microtubules and another subset extend from the poles towards to the cell cortex called astral microtubules. Minus-end directed motor proteins like dynein exert pulling forces on the astral microtubules, which help in proper spindle positioning. Another group of motor proteins called chromokinesins promotes the plus-end directed movement.

1.6.2 Mechanisms underlying mitotic spindle assembly

The "search and capture" is the most prevailing model in a majority of vertebrate cells for the correct chromosome attachment and alignment on the spindle [199] According to this model, the dynamic growing and shrinking microtubules that project from the centrosomes search the three-dimensional space between the poles until they are captured by one of the sister kinetochores on a chromosome [217]. The mono-oriented chromosomes then oscillate until a pair of sister chromatids is attached to both poles and thus bi-orientation is accomplished. The probability of kinetochore capture is elevated by enhanced nucleation of centrosomal microtubules. The activity of Aurora A kinase is

triggered during mitosis and is shown to coordinate this increased microtubule growth [218]. However, this model alone is insufficient to align all the chromosomes in the mitotic spindle.

A second possibility is the "self-assembly" model wherein the microtubules in the vicinity of the sister chromatids are arranged into a bipolar network, primarily depending upon the motor proteins [219]. The motor proteins including dynein and kinesin help to organize the microtubules into two antiparallel arrays, in which the plus ends of the arrays overlap in the center and the minus ends form a pair of spindle poles. As the microtubules grow, some plus ends are attached to the kinetochores, thereby linking chromatids to the poles. This mechanism of spindle assembly is usually seen in cells lacking centrosomes.

The GTPase Ran mediates another mode of regulation that has been studied mainly in *Xenopus* egg extracts. RanGTP is present in the nucleus and is hydrolyzed to Ran-GDP in the cytoplasm and drives nucleocytoplasmic transport in interphase [220]. The cargoes containing a nuclear localization signal (NLS) bind to import receptors called importin β and are transported through the nuclear pore and in the presence of RanGTP, the cargo is released [221]. Similar functions of Ran have been observed during mitosis. The chromatin association of its guanine nucleotide exchange factor RCC1 and the cytoplasmic localization of RanGAP that promotes hydrolysis of RanGTP establish a RanGTP gradient surrounding the chromosomes. This RanGTP in the vicinity of chromosomes provides a favorable niche for microtubule growth and bipolar spindle organization. The gradient is disrupted as the distance from the chromosomes increases. The presence of this gradient has been observed in *Xenopus* egg extracts [222, 223] and in cells [224]. The RanGTP gradient functions to release cargoes like microtubule-associated proteins (MAPs) and motor proteins [225] that participate in spindle assembly, thus affirming its role in the maintenance of a bipolar spindle.

1.7 Perspectives of the study

Adherent cell types are flat during interphase. The onset of mitosis is characterized by a loss of adhesion from the substrate to form rounded cells with higher cortical rigidity. This process, termed as mitotic cell rounding depends on the extensive remodeling of the actin cytoskeleton and regulation of osmotic pressure. The cells gain a defined geometry and proper orientation of a bipolar mitotic spindle by rounding up. Earlier studies have shown the involvement of RhoGTPases namely RhoA and ROK in the maintenance of mitotic spindle assembly [226] and cell cycle progression. However, not much has been explored about the role of the osmotic pressure during mitotic progression.

During mitotic cell rounding, the cells increase their intracellular osmotic pressure. Exposure of metaphase cells to hypotonic medium leads to an immediate increase in cell volume and rounding pressure; whereas, an opposite effect is seen when cells are subjected to hypertonic shock [53]. The decrease in the rounding pressure is recovered by the influx of osmolytes during regulatory volume increase [185]. The Na^+/H^+ antiporter has also been shown to increase mitotic rounding pressure since ion channels are involved in compensatory volume regulation upon hypertonic challenge [53]. Thus, cells need to maintain a proper osmotic balance for effective rounding during mitosis.

Under physiological conditions, the cells in our renal medulla are constantly exposed to interstitial higher concentration of NaCl [227]. Hyperosmotic conditions are stressful to cells and lead to cell cycle arrest, DNA damage, cytoskeletal rearrangement and even apoptosis [110]. Recent studies have shown that the effects are not restricted to kidney cells alone and the effects of osmotic stress have been examined in many other mammalian cell types. Fluctuations in the osmolarity may lead to several disorders like dehydration, diabetes mellitus, diabetes insipidus, uremia, retinopathy, asthma, cystic fibrosis and cancer [228-231]. For example, hypertonicity has been reported to stimulate vascular endothelial growth factor (VEGF) production in colon cancer cells. The

expression of VEGF is directly correlated with increased metastatic potential [232]. Additionally, prolonged exposure to hypertonic stress also leads to cell death while some cells undergo mitotic slippage to form polyploid cells, which serve as one of the hallmarks of cancer. Defects in proper spindle morphogenesis and positioning account for improper cell division, which in-turn, leads to aneuploidy and eventually cancer [233]. Thus, the association between hypertonic stress and cancer underscores the need for a detailed understanding of the cytoprotective mechanisms in response to this stress, which will enable us to treat and prevent the disease effectively.

As mentioned before, hypertonic stimulation causes a decrease in mitotic rounding pressure. Defects in cell rounding in turn is associated with spindle morphogenesis defects, delay in mitotic progression [56] and eventually aneuploidy. Therefore, it is worthwhile to explore the effects of osmotic stress directly on the assembly and orientation of the mitotic spindle apparatus.

1.8 Hypothesis of the study

Osmostress response has a broad impact on a wide variety of cell type behavior and modulates the expression of several proteins. Among the several adverse effects of hypertonic stress, cells encounter defects in cell cycle progression. RPE (retinal pigmented epithelial) cells subjected to hypertonic conditions accumulated at the G_0/G_1 and G_2/M phases of the cell cycle [113]. Since most of the studies to study the effects of hyperosmotic changes have been carried out in renal medullary cells, this study supported the idea that hypertonic stress also affects cellular functions of non-kidney-type cells. Exposure to hypertonic stress (100mM NaCl or 200mM sucrose) for 4 hours altered the expression of genes involved in transcriptional regulation and cell proliferation. This is presumably because cells induce changes in transcription and cell cycle progression as an early osmoadaptive response. Exposure to hypertonic stress led to an accumulation in

G_1/S and G_2/M phases of the cell cycle in retinal pigmented epithelial (RPE) cells [113]. Since in cancer cells, the cell cycle checkpoints and apoptotic mechanisms are less effective as compared to diploid cells, we intended to examine whether osmotic stress affected cancer cells, such as HeLa. Based on the above-mentioned observation, we hypothesized that hypertonic stress might affect cell cycle progression in non-kidney-type cells, like HeLa. As expected, our results showed a delay in cell cycle progression under hypertonic conditions.

Moreover, it has been shown that cells assume a spherical shape upon mitotic entry [234]. This mitotic cell rounding is important for proper chromosome segregation with high fidelity. Cell rounding during mitosis is primarily driven by actomyosin cytoskeleton and osmotic pressure. Upon mitotic entry, de-adhesion from the substrate enables the cells to round up. Simultaneously, the cells increase their intracellular hydrostatic pressure to facilitate rounding in tissue environment. Disruption of actomyosin activity by using inhibitors of myosin contraction and actin depolymerizing drugs show a reduction in rounding pressure [53]. Earlier work from our lab has shown that an intact actin cytoskeleton is required for proper spindle assembly at the early stage of mitosis. Perturbation of the actin cytoskeleton resulted in a less-defined mitotic spindle with an aberrant increase in astral microtubules emanating from the spindle pole towards the cortex. Cells treated with inhibitors of Rho GTPase pathway to perturb the actin cytoskeleton showed centrosome defocusing and spindle misorientation, thereby suggesting that actin cytoskeleton plays an essential role in mitotic spindle assembly [226]. Perturbation of the osmotic gradient also led to changes in rounding pressure and volume [53]. However, not much has been explored about the role of osmotic pressure in the assembly and maintenance of a bipolar mitotic spindle. On the basis of this study, we hypothesized that since cells exposed to hypertonic stress show defects in mitotic rounding, they might experience defects in mitotic progression upon hypertonic

challenge. After we established that cells indeed show a delayed mitotic progression and metaphase arrest during hypertonic stress, we next examined whether the observed metaphase arrest was due to defects in mitotic spindle assembly and proposed a possible mechanism underlying these defects.

1.9 Aim of the study

Mitotic cell rounding is imperative for proper spindle morphogenesis, assembly and correct segregation of parental chromosomes into daughter cells. This rounding force is controlled by an outward osmotic force and opposed, inward actomyosin contractility [53]. The remodeling of the filamentous actin network is required for effective mitotic cell rounding. Previous studies from our lab have shown that disruption of the actin cytoskeleton is implicated in defects in spindle orientation and centrosome integrity [226]. However, the contribution of the osmotic pressure changes remains elusive. Since cells undergoing mitosis experience fluctuations in osmotic pressure and osmotic stress is implicated in a wide variety of cellular functions, including cell cycle arrest, the emphasis of the project is to study the impact of hyperosmolarity on

(1) the control of different stages of cell cycle, and

(2) assembly and orientation of the mitotic spindle.

Chapter 2

MATERIALS AND METHODS

The materials and methods used in this study are mentioned in this chapter.

2.1 Materials

2.1.1 Chemicals and reagents

Table 2.1 List of chemicals and reagents

Name of chemical and reagents	Company
Acrylamide	Bio-Rad
Agarose	Bio-Rad
Ammonium persulfate (APS)	Bio-Rad
Ampicillin	Calbiochem
Bisacrylamide	Bio-Rad
Bromophenol blue	Sigma Aldrich
C3-Transferase (Rho inhibitor)	Cytoskeleton Inc
Dimethyl sulfoxide (DMSO)	Sigma Aldrich
Dithiothreitol (DTT)	Sigma Aldrich
Ethanol	Merck
Ethidium bromide	Bio-Rad
5-(N-Ethyl-N-isopropyl) amiloride (EIPA)	Sigma Aldrich
Ethylenediaminetetraacetic acid (EDTA)	Bio-Rad
Fibronectin (0.1% solution)	Sigma Aldrich
Glycine	1st Base
Hydrochloric acid	Merck
Kanamycin	Gibco
LipofectAMINE® 2000	Invitrogen
Methanol	Merck
5-Nitro-2-(3-phenylpropylamino)benzoic acid (NPPB)	Sigma Aldrich
N,N,N',N'-Tetramethylethylenediamine (TEMED)	Bio-Rad
Paraformaldehyde	Merck
Phalloidin-Alexa 546	Sigma Aldrich
PhosSTOP phosphatase inhibitor cocktail tablets	Roche
Ponceau S	Sigma Aldrich
Propidium Iodide	Sigma Aldrich
Protease inhibitor cocktail tablet	Roche
Sodium bicarbonate	Merck
Sodium chloride	Merck
Sodium dodecyl sulfate (SDS)	USB
Tris Base	Promega
Triton X-100	Bio-Rad

Trizol	Invitrogen
Tween 20	Bio-Rad
Vectashield® with DAPI	Vector Labs
Xylose	Sigma Aldrich
Y27632 (ROCK inhibitor)	Calbiochem

2.1.2 Primary Antibodies

Table 2.2 List of primary antibodies

Antibody	Species	Clonal	Company
Anti-Actin	mouse	monoclonal	Chemicon International
Anti-BubR1	mouse	monoclonal	Abcam
Anti-Cyclin A	rabbit	polyclonal	Santa Cruz Biotechnology
Anti-Cyclin B1	rabbit	monoclonal	Santa Cruz Biotechnology
Anti-Cyclin D1	mouse	polyclonal	Santa Cruz Biotechnology
Anti-Cyclin E	mouse	polyclonal	Santa Cruz Biotechnology
Anti-EB1	mouse	monoclonal	Santa Cruz Biotechnology
Anti-Ezrin/Radixin/Moesin (ERM)	rabbit	polyclonal	Cell Signaling Technology
Anti-GAPDH	mouse	monoclonal	Ambion
Anti-Gα	mouse	monoclonal	Santa Cruz Biotechnology
Anti-LGN	rabbit	polyclonal	Abcam
Anti-NuMA	rabbit	polyclonal	Cell Signaling Technology
Anti-Mad2	rabbit	polyclonal	Covance
Anti-p150Glued	mouse	monoclonal	BD Transduction laboratories
Anti-Pericentrin	rabbit	polyclonal	Abcam
Anti-phospho-Ezrin(Thr567)/Radixin(Thr564)/Moesin (Thr558) (pERM)	rabbit	polyclonal	Cell Signaling Technology
Anti-phospho-histone H3(Ser10)	rabbit	polyclonal	Santa Cruz Biotechnology

Anti-PLK1	mouse	monoclonal	Abcam
Anti-α-tubulin	mouse	monoclonal	Sigma-Aldich

2.1.3 Secondary Antibodies

Table 2.3 List of secondary antibodies

Antibody	**Company**
Goat anti-mouse IgG, HRP conjugated	Dako Cytomation
Goat anti-rabbit IgG, HRP conjugated	Dako Cytomation
Goat anti-mouse IgG, Alexa Flour 488	Molecular Probes
Goat anti-mouse IgG, Alexa Flour 546	Molecular Probes
Goat anti-rabbit IgG, Alexa Flour 488	Molecular Probes
Goat anti-mouse IgG, Alexa Flour 556	Molecular Probes

2.1.4 Mammalian cell culturing materials

Table 2.4 List of cell culture reagents

Material	**Company**
Dulbecco's modified Eagle's medium (DMEM)	Sigma Aldrich
Fetal Bovine Serum (FBS)	PAA Laboratories Cell Culture company
L-Glutamine	Gibco
Minimum Essential Medium Eagle (MEM)	Sigma Aldrich
Trypsin	Sigma Aldrich

2.1.5 Commercial Kits

Table 2.5 List of commercial kits

Name of commercial kit	**Company**
AxyPrep™ Plasmid Miniprep Kit	Axygen
Novex® ECL Chemiluminescent Substrate Reagent Kit	Invitrogen
QIAquick® Gel Extraction Kit	QIAgen

2.1.6 Bacteria strains and mammalian cell lines

Table 2.6 List of cell lines

Strain/Cell Line	**Description**
DH5α	Chemically competent *Escherichia coli* (Invitrogen)
BL21	Chemically competent *Escherichia coli* (Invitrogen)

HeLa	Human cervix adenocarcinoma epithelial (ATCC-CL-2)

2.1.7 Buffers

Table 2.7 List of buffers

Buffer	Components
Lysogeny Broth (LB)	10 g bacto-tryptone 5 g bacto-yeast extract 10 g NaCl 1000 mL MilliQ water
Lysogeny Broth (LB) Agar	10 g bacto-tryptone 5 g bacto-yeast extract 20 g bacto Agar 10 g NaCl 1000 mL MilliQ water
Mammalian cell lysis buffer	25 mM Hepes, pH 7.5 0.25 M NaCl 1 mM $MgCl_2$ 1 mM EGTA 20 mM p-glycerol phosphate 1 mM sodium vanadate 10 mM NaF 5% glycerol 0.5% Triton X-100 5 mM DTT Protease inhibitor cocktail tablet (Roche) Phosphatase inhibitor cocktail tablet (Roche)
Nitrocellulose transfer buffer, 10x	30.3 g Tris base 144 g glycine 1000 mL water
Nitrocellulose transfer buffer, 1x	100 mL 10X nitrocellulose transfer buffer 100 mL methanol 800 mL MilliQ water
Phosphate Buffered Saline (PBS), 1x	137 mM NaCl 2.7 mM KCl 10 mM Na_2HPO_4 2 mM KH_2PO_4 1000 mL MilliQ water Adjusted to pH 7.4
SDS sample buffer, 6x	5 mL 4X Tris-Cl/SDS pH 6.8 5 mL glycerol 1 g SDS 0.93 g dithiothreitol (DTT) 0.15 mg bromophenol blue
SDS-PAGE electrophoresis buffer,	30.2 g Tris base 144 g glycine

10x	10 g SDS 1000 mL MilliQ water
SDS-PAGE electrophoresis buffer, 1x	100 mL 10X SDS-PAGE electrophoresis buffer 900 mL of MilliQ water
Tris-Cl/SDS pH 6.8, 4x	6.05 g Tris base (0.5 M Tris-Cl) 0.4 g SDS (0.4% SDS) 100 mL of MilliQ water Adjusted to pH 6.8
Tris-Cl/SDS pH 8.8, 4x	91 g Tris base (1.5 M Tris-Cl) 0.4 g SDS (0.4% SDS) 100 mL of MilliQ water Adjusted to pH 8.8
Trypsin-EDTA solution	0.25% (w/v) Trypsin 0.53 mM EDTA

2.1.8 Stealth siRNA

Table 2.8 List of siRNA

siRNA Name	RNA Sequence (5' to 3')
Luciferase siRNA sense	ACAUCACGUACGCGGAAUACUUCGA
Luciferase siRNA antisense	UCGAAGUAUUCCGCGUACGUGAUGU
NHE1 siRNA-1 sense	CCCUGUUAAUCAUUCCGUCACUGAU
NHE1 siRNA-1 antisense	AUCAGUGACGGAAUGAUUAACAGG G
NHE1 siRNA-2 sense	UCAAGAAGGAUCUUUGUACUGUGA U
NHE1 siRNA-2 antisense	AUCACAGUACAAAGAUCCUUCUUGA

2.1.9 Site-directed mutagenesis primers

Table 2.9 List of site-directed mutagenesis primers

Primer name	DNA sequence (5' to 3')-(mismatch sites highlighted in red)
MSN T558D sense	GCC GAG ACA AAT ACA AGG ACC TGC GCC AGA TCC G
MSN T558D antisense	CGG ATC TGG CGC AGG TCC TTG TAT TTG TCT CGG C

MSN T558A sense	GCC GCG ACA AAT ACA AGG CCC TGC GCC AGA TC
MSN T558A antisense	GAT CTG GCG CAG GGC CTT GTA TTT GTC TCG GC

2.1.10 Plasmids

Table 2.10 List of plasmids

Plasmid	Tag	Name	Amino acid	Mutation(s)
pEGFP-MSN	EGFP	Moesin	1 to 577	
pEGFP-MSN T558D	EGFP	Moesin	1 to 577	T558D
pEGFP-MSN T558A	EGFP	Moesin	1 to 577	T558A

2.2 Methods

2.2.1 Tissue culture, cell cycle synchronization and drug treatment

HeLa cells were maintained in Minimum Essential Media (Sigma), supplemented with 10% (v/v) FBS and cultured in a humidified incubator supplemented with 5% CO_2 at 37°C.

For routine sub-culturing, cells were washed once with PBS (137mMNaCl, 2.7mM KCL, 10mM Na_2HPO_4, 2mM KH_2PO_4, pH 7.4) and treated with 2ml of 0.25% (w/v) trypsin in 0.53mM EDTA at 37° C till the cells round up. 8mL of complete MEM was added to inhibit the reaction and cells were gently flushed off the culture dish. Cells were pelleted by centrifugation at 1200 rpm for 2 minutes and re-suspended in fresh complete growth media.

For preparation of frozen stock of cells for preservation, cells were trypsinized and re-suspended in FBS containing 10% DMSO at $1.5x10^6$ cells/mL densities. The cells were then cooled at the rate of 1°C/minute until -80°C and maintained in liquid Nitrogen gaseous phase for long-term storage. During thawing, the frozen vial of cells were kept at 37°C and washed with complete growth media before culturing as mentioned above.

Cell cycle synchronization at the G_1/S border was achieved by double thymidine block. Cells were arrested with freshly prepared 2mM thymidine (Sigma) for 17 hours, released into fresh media (thymidine free media) for 12 hours, followed by a second block with 2mM thymidine for 17 hours. This method helped to obtain a highly synchronized cell population at the G_1/S transition. Cells were arrested at the G_1/S border and also the S phase at the end of the first thymidine block, owing to the inhibition of DNA synthesis. The cells that were arrested at the G_1/S transition progressed to the G_2/M phase during the 12 hour release. The cells that were arrested in the late S phase progressed into G_1 during the first block. During the second thymidine treatment, cells that were in G_2/M phase

progressed into G_1 and were blocked at the G_1/S border. The cells that were already in the G_1 phase will also be arrested at the G_1/S transition, thus enabling a highly synchronized cell population at the G_1/S phase border. Mitotic cells were harvested 10-12 hours post release. The cells were washed thrice with the complete growth media during release from the thymidine block.

In all the experiments performed in the thesis, where osmotic balance was perturbed, three different set of media was used. MEM (Minimum Essential Salts Medium), supplemented with 10% FBS (Foetal bovine serum) and 100% Glutamine was used as an isotonic control. Hypertonic conditions were stimulated by two different sets of media.

i. MEM media supplemented with 0.15M NaCl.

ii. MEM media supplemented with 4% Xylose.

The osmolality of the media was measured using a vapor pressure osmometer (Vapro) before the commencement of the experiments. Earlier studies have also used medium containing 100-150mM NaCl [113] or 3% xylose [53], with a +Δ 200 change in osmolality as hypertonic. We have also used the similar osmolality range in our experiments.

Media	**Osmolality (mOsm/kg)**
Isotonic control (Complete MEM medium)	290-300
Hypertonic MEM (MEM and 0.15M NaCl).	+Δ 200 (~496)
Hypertonic MEM (MEM and 4% xylose).	+Δ 200 (~496)

Unless otherwise stated, cells were treated with 50μM EIPA (5-(N-Ethyl-N-isopropyl) amiloride) (Sigma) and 50μM NPPB (5-Nitro-2- (3-phenylpropylamino) benzoic acid) (Sigma).

2.2.2 Molecular cloning

Total RNA were isolated from cells using Trizol (Invitrogen) and used to synthesize cDNA using Superscript VILO cDNA Synthesis Kit (Invitrogen) according to the manufacturer's protocol. Primers with appropriate restriction enzyme recognition site were designed to amplify desired DNA sequence from synthesized cDNA by polymerase chain reaction (PCR) using TaKaRa Ex TaqTM polymerase (TaKaRa). Amplified products were subjected to agarose gel electrophoresis and purified with QIAquick Gel Extraction Kit (QIAGEN) according to manufacturer's protocol. Plasmid vectors and purified PCR products were incubated with the appropriate restriction enzymes (New England Biolabs) at 37^{o}C for 2 hours. Digested plasmid and PCR products were subjected to agarose gel electrophoresis and purified with QIAquick Gel Extraction Kit (QIAGEN) according to the manufacturer's protocol.

Gel purified plasmid vector and PCR product were mixed at a molar ratio of 1:3 for ligation reaction using T4 DNA ligase (New England Biolabs). Ligation mixtures were then incubated in 16^{o}C for at least 8 hours. After incubation, the ligation reaction were transformed into chemical competent DH5α cells by heat-shock method, plated on Lysogeny Broth (LB) agar plates supplemented with either 100 µg/ml ampicillin or 50 µg/ml kanamycin. The agar plates were then incubated at 37^{o}C for at least 12 hours before checking for colony growth. Colonies were picked, inoculated in LB broth supplemented with appropriate antibiotics selection and plasmids were purified using AxyPrep™ Plasmid Miniprep Kit (Axygen) according to the manufacturer's protocol.

Purified plasmids were subjected to restriction enzyme digestion and agarose gel electrophoresis to screen for plasmids with the appropriate insert size ligated. The identities of the inserts were verified by DNA sequencing and positive constructs were selected for large-scale purification using HiSpeed Plasmid Maxi Kit (QIAGEN) according to manufacturer's protocol.

2.2.3 In-vitro site-directed Mutagenesis

The respective phospho-dead or phospho-mimic mutants were generated using the QuikChange Site-Directed Mutagenesis Kit (Stratagene). Mutagenic oligonucleotide primers were designed using the QuikChange Primer Design Program. Mutagenesis reactions were carried out using the thermal cycling parameters as stated in the manufacturer's protocol. Parental DNA templates were removed by incubating the mutagenesis reaction with *Dpn*I at 37°C for 1 hour. 5 µl of the *Dpn*I-digested mutagenesis reaction was used for transformation into DH5α competent cells using the heat shock method and plated on suitable antibiotic selection agar plates. Agar plates were then incubated at 37°C for at least 12 hours before checking for colony growth. Colonies were picked, incubated in LB broth with suitable antibiotics, and plasmids were purified using AxyPrep™ Plasmid Miniprep Kit (Axygen) as described by manufacturer's protocol. Purified plasmids were then sequenced to verify for mutation and positive constructs were selected for large-scale purification using HiSpeed Plasmid Maxi Kit (QIAGEN) according to manufacturer's protocol.

2.2.4 siRNA and plasmid transfections

For all transfections, cells were seeded onto 35-mm dishes 24 hours prior to transfection. For siRNA transfection, 200 picomole of Stealth siRNA (Invitrogen) were mixed with 3 µl LipofectAMINE-2000 (Invitrogen) and incubated at room temperature for 20 minutes. The siRNA/Lipofectamine mixture was then added to and incubated with the cells for 48 hours. For plasmid transfection, 1 µg of plasmid were mixed with 3 µl LipofectAMINE-2000 and incubated at room temperature for 20 minutes. If two or more plasmid constructs were transfected into cells, the amount of plasmids was adjusted such that the total amount of plasmids transfected would be 1 µg. The DNA/Lipofectamine mixture was then added to and incubated with the cells for 24 or 48 hours as described. For rescue

experiments, cells were first transfected with siRNA for 24 hours and subsequently transfected with respective plasmid constructs. 24 hours after plasmid transfection, cells were processed for subsequent experiments.

2.2.5 Indirect immunofluorescence microscopy

Cells were seeded at a density of 2 x 10^5 cells/ml on glass cover slips. The cells were fixed with 4% PFA (paraformaldehyde) in 0.1 % Triton-X/PBS for 20 minutes and washed once with PBS. The cells were then permeabilized using 0.2% Triton-X/PBS for 10 minutes and blocked with 4% BSA in 0.1% Triton/PBS for 30minutes. After blocking, 100µl of the appropriate primary antibody was added and incubated overnight at 4°C humidified chamber. The coverslips were then incubated with 100µl of Alexa Flour 488- or Alexa Flour 546-labelled secondary antibodies (Invitrogen) and/or phalloidin (Sigma) for 1 hour in dark at 25°C humidified chamber. The coverslips were washed using 0.1% Triton X-100 in PBS. The immuno-stained samples were dried and mounted on a clean glass slide with the Vectashield mounting medium containing DAPI (Vector Laboratories).

The samples were then viewed using the Axio Observer microscope (Carl Zeiss), equipped with Zeiss EC Plan-neofluar 40x/1.3 oil (for interphase cells) or Zeiss EC Plan-neofluar 63x/1.25 oil (for mitotic cells) objective lens coupled to CoolSNAP HQ^2 camera (Photometrics). Immunofluorescence images were analyzed using ImageJ software and processed in red/green/blue (RGB) colour mode.

For centrosome and spindle staining intensity representation, integrated intensity was measured in an area of 50 by 50 pixel box surrounding each individual centrosome and the spindle pole. Intensities were corrected for signal to noise ratio.

For calculation of cell surface area, the cells were then fixed and stained with DAPI and anti-pericentrin to visualize DNA and centrosomes respectively. Brightfield images were

captured to obtain the cell boundary. Boundary of the cells was outlined using the ImageJ tool from the brightfield images and the surface area was measured using the software. The surface area of the cells served as a measure of the cell size.

2.2.6 Astral microtubule measurement

Following fixation, the cells were immuno-stained with α-tubulin antibody (1:100 dilution in 1%Triton-X/PBS). The total fluorescence intensity of the tubulin stain and the fluorescence intensity of the central spindle were measured using ImageJ software. The average background fluorescence was subtracted from the total (i) and the central spindle fluorescence (ii) to obtain the normalized intensity values. The normalized central spindle fluorescence (ii) was subtracted from that of the total fluorescence (i) to obtain the fluorescence contributed by the astral microtubules. The ratio of the normalized astral microtubule fluorescence/normalized total fluorescence was used to compare the astral microtubule changes between the control and treated cells.

2.2.7 Spindle orientation assay

Cells were cultured on coverslips, coated with fibronectin (Sigma-Aldrich) at a density of 3μg/cm^2, prior fixation. Post various treatments, the cells were fixed and immune-stained with anti-pericentrin and DAPI. Z-stack images of metaphase cells at 0.5μm apart were captured. DAPI stained the DNA, which was used as a reference for cell cycle stage. Spindle angle was calculated using inverse trigonometric function, $\alpha=\tan^{-}1$ (A/B), where α denotes the spindle angle during metaphase, in degrees, relative to the substratum. A represents the z axis distance between spindle poles in μm; and B denotes the x-y axis distance between spindle poles in μm. ImageJ software was used for analysis.

2.2.8 Live cell imaging

For fluorescence live cell imaging, HeLa cells were stably transfected with GPF-tagged H2B for viewing the DNA. Cells were cultured in glass-bottom dishes and images were acquired using Axiovert 200 microscope (Carl Zeiss) with Zeiss LD Plan-neofluar 20x/0.6 Corr F objective lens coupled to CoolSNAP HQ camera (Photometrics). Cells were maintained in a humidified chamber at 37°C supplemented with 5% CO_2 during imaging. Temperature was controlled with the help of temp control 37-2 digital (Carl Zeiss) and CO_2 levels are controlled by CO_2-controller (Carl Zeiss) or by suspending the cells in Leibovitz's L-15 media (Gibco) supplemented with 20% FBS. For phase-contrast live imaging, cells were grown in glass-bottom chambers and images were taken using Axiovert 200 microscope (Carl Zeiss) with Zeiss LD Plan-neofluar 40x/0.6 Corr Ph2 objective lens coupled to CoolSNAP HQ camera (Photometrics).

2.2.9 Confocal microscopy

For detecting cortical localization of Gα, NuMA and $p150^{Glued}$, cells were pre-extracted the cells in PHEM buffer containing 25 mM HEPES, 60 mM 1,4-piperazinediethanesulfonic acid, 10 mM ethylene glycol tetraacetic acid, 2 mM $MgCl_2$, pH 6.9 containing 0.2% Triton X-100 and fixed in 4% PFA in 0.1 % Triton-X/PBS for 20 minutes and washed once with PBS. The cells were then permeabilized using 0.2% Triton-X/PBS for 10 minutes and blocked with 4% BSA in 0.1% Triton/PBS for 30minutes. After blocking, 100µl of the appropriate primary antibody was added and incubated overnight at 4°C humidified chamber. The coverslips were then incubated with 100µl of Alexa Flour 488- or Alexa Flour 546-labelled secondary antibodies (Invitrogen) and/or phalloidin (Sigma) for 1 hour in dark at 25°C humidified chamber. The coverslips were washed using 0.1% Triton X-100 in PBS. The immuno-stained samples were dried

and mounted on a clean glass slide with the Vectashield mounting medium containing DAPI (Vector Laboratories).

The cells were then viewed using Zeiss LSM 710 Meta Scanning confocal microscope. Immunofluorescence images were analyzed using ImageJ software and processed in red/green/blue (RGB) colour mode.

2.2.10 SDS-polyacrylamide gel electrophoresis gel electroporation and Western blot

For Western blot analysis, cells were washed once with ice-cold IX PBS and lysed in protein lysis buffer (50mM HEPES, pH 7.5, 300mM NaCl, 1mM $MgCl_2$, 10mM β-Glycerophosphate, 10mM NaF, 1mM Sodium Vanadate, 5% Glycerol, 5mM DTT and 0.5% Triton X-100). The protein lysis buffer was supplemented with 1X Protease inhibitor (Roche) and 1X Phosphatase inhibitor (Roche). The cell lysates were then centrifuged at 14,000 rpm for 10 minutes at 4°C. The supernatant was collected and the protein concentration was determined using Bradford reagent assay (BioRad). 6X SDS sample buffer was added to equal amount of the lysates. Lysates were heated at 100°C for 5 minutes and subjected to sodium dodecyl sulphate-polyacrylamide gel electroporation (SDS-PAGE) and transferred to nitrocellulose membrane 0.45µm (BioRad) at 80V, 4°C for 2 hours. The nitrocellulose membrane was subjected to 1X Ponceau staining and then blocked with 2% BSA in TBS for 1 hour and incubated with primary antibodies at 25°C for 2-3 hours or 4^0C, overnight. The membrane was washed thrice for five minutes each and incubated with horseradish peroxidase (HRP)-conjugated anti-mouse (DakoCytomation) or anti-rabbit (Amersham Biosciences) secondary antibodies at 25°C for 1 hour. All the antibodies were prepared in 2% BSA in TBS. The membrane was washed with 0.05% Tween20 in TBS. Following the secondary antibody incubation, the membrane was subjected to chemiluminiscence detection with the ECL Plus Detection

Kit (Amersham) and exposed to Super RX Fuji medical X-ray film (Fuji) and developed with the Kodak X-OMAT ME-1 processor.

2.2.11 Flow cytometry

Cells were trypsinized and washed with PBS at 1000rpm for 5 minutes. The cell pellet was re-suspended in 1mL PBS at 4°C and fixed in 4mL of ice-cold absolute ethanol, added dropwise while vortexing the cells. The cells were fixed overnight at 4°C. The cells were then washed once with PBS at 1300 rpm for 5 minutes and re-suspended in 500µL 0.05% Triton-X 100 in PBS containing 50µg/mL Propidium Iodide (Sigma), to stain the DNA and 0.1mg/ml RNase Atype IIIA (Sigma). The staining was performed for 2 hours at 25°C. Samples were then transferred to the polystyrene FACS tubes and subjected to flow cytometric analysis using the Fortessa –X. Data was analyzed using the FlowJo software.

2.2.12 Micropipette aspiration assay

Cells were cultured to 70% confluency in 25cm^2 flasks. The mitotic cells were collected by a mechanical shake-off and re-suspended in 500µl complete growth media at 37°C. The cell suspension was placed between a coverglass chamber and subjected to aspiration by the micropipette.

The micropipettes were made with borosilicate glass capillaries (World Precision Instruments, USA) with outer diameter of 1.0mm and inner diameter of 0.75mm. The diameter of the micropipette ranged from 7.8µm to 13.1µm with the help of a micropipette puller and micro forge (ALA Scientific Instruments, Inc., USA). The micropipettes were coated with 1% BSA and stored at 4°C. A gentle suction was applied to bring the mitotic cells in contact with the micropipette. The movement of the micropipette was controlled with the help of a micromanipulator (Eppendorf AG, Germany). The suction pressure was then increased and images were taken at an interval

of 9 seconds using the 100x objective brightfield microscope (Leica). The suction pressure was controlled using a precision pump (Cole-Parmer) with a flow rate between 20 to 60 ml/hr.

MetaMorph software (Molecular Devices) was used to measure the cortical deformation. Young's modulus was calculated using the formula, $\Delta P = (2\pi/3)\ E\ (L_p / R_p)\ \varphi$, where ΔP is the change in pressure, calculated by $\Delta P = \Delta h \rho g$; Δh denotes change in liquid height in mm; ρ represents water density, 1000kg/m^3; g denotes the gravitational force, 9.8m/s^2; φ represents ratio of the pipette wall thickness to lumen radius, approximately 2.1, L_p denotes deformation in length in μm and R_p represents the radius of the pipette in μm.

2.2.13 Statistical analysis

Graphpad Prism software was used for statistical analysis. Unpaired student's t-test was performed for all statistical analysis. A p-value of less than 0.05 was considered to be statistically significant. All results were represented by mean ± standard error of at least three independent experiments.

Chapter 3

Effect of hypertonic stress on temporal control of mitosis

Earlier studies have reported that besides kidney cells, non-kidney-type cellular functions are also affected by hypertonic stress. Exposure to a hypertonic challenge alters cell proliferation and as an early adaptive response, the cells induce changes in transcription, translation and also cell cycle. In this chapter, we describe our study on the effects of hyperosmotic stress on cell cycle progression.

3.1 Results

3.1.1 Hypertonic stress resulted in a higher percentage of cells in G_2/M phase

As disruption of the osmotic balance is associated with changes in cell proliferation, we examined the distribution of cells in different phases of the cell cycle in the presence of hypertonic environment. HeLa cells were chosen for this study since the mitotic events are well documented in this cell line.

Since earlier reports suggest that cells exposed to extreme hypertonicity undergo apoptosis and cell death [235], we selected the optimum concentration of the hypertonic media the cells were able to withstand and measured the osmolality using a vapour pressure osmometer (Vapro) before the commencement of the experiments. Osmolality of the isotonic medium was 290-300 mOsm/kg and the osmolality of the hypertonic media containing 0.15M NaCl and 4% xylose were around 496 mOsm/kg.

In order to study the effects of osmotic stress on the distribution of cell cycle phases, asynchronized HeLa cells were treated with 0.15M NaCl or 4% xylose for 24 hours and subjected to DNA profiling by FACS. Cell cycle analysis revealed a significant decrease in the percentage of cells in G_0/G_1 and a concomitant increase in percent of cells in G_2/M phase (Figure 3.1 A). Compared to the isotonic control which showed about 20 % of cells in G_2/M phase, almost 40 % of cells were present in G_2/M for cells exposed to 0.15M NaCl (Figure 3.1 B).

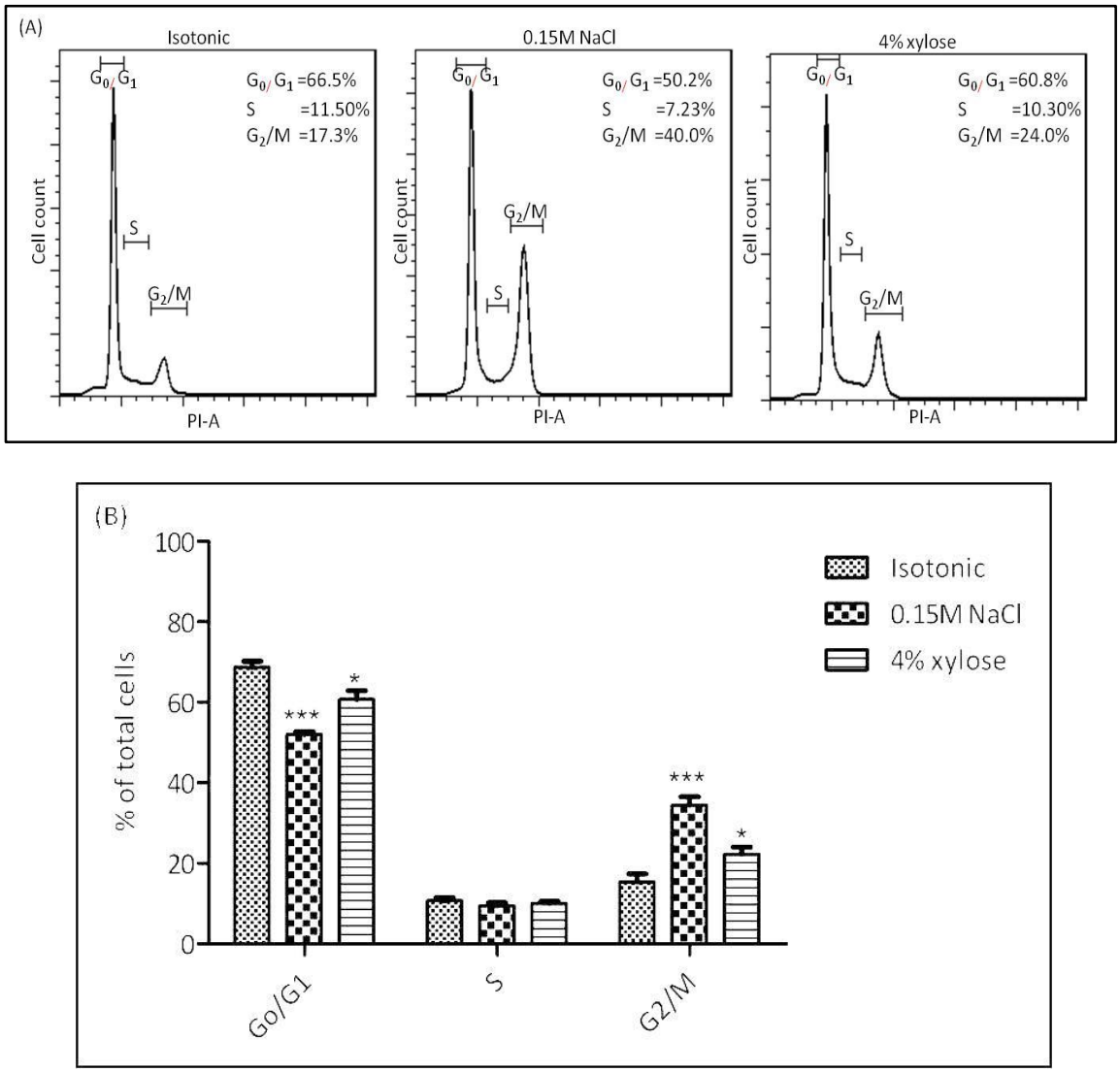

Figure 3.1 Hypertonic stress led to a significant decrease in G_0/G_1 and increase in G_2/M phases. (A) Asynchronized HeLa cells treated with 0.15M NaCl or 4% xylose for 24 hours were subjected to PI (Propidium iodide) staining and analyzed by FACS. The plots are representative DNA content plot for each condition. (B) The percentage of cells present in each cell cycle stage was analyzed using FlowJo software. The mean percentage of cells from four independent experiments was calculated and plotted using Graphpad Prism software. Error bars represent mean (±SEM). *** p=0.0001, * p=0.01.

3.1.2 Synchronisation of cells by double thymidine block

Since quantification of the cell cycle phases showed a higher percentage of cells in G_2/M phase in response to osmotic stress, it could possibly due to an arrest at this stage of the cell cycle or a delay in cell cycle progression. In order to gain insight into this, we first proceeded with synchronization of cells using double thymidine block (Figure 3.2 A). Following the second release from thymidine, cells were harvested for FACS and Western blot analysis every two hours for a period of 18 hours to track the cell cycle progression timings. FACS data showed that the majority of cells were synchronized at the G_1/S boundary post second release from thymidine (Figure 3.2 B). This was further confirmed by the presence of cyclin E (late G_1 and early S phase marker) in the Western blot data during 0-2hours (figure 3.2 C). At 4-6 hours of release, the 2N DNA peak shifted to 4N, indicating entry and progression through S phase. The Western Blot showing an increase in cyclin A (S and G_2 phase marker) levels with a simultaneous drop in cyclin E levels provides additional evidence for entry into S phase. Following this, a G_2/M peak is observed from 8 hours onwards and phosphorylated histone H3 levels (mitosis marker) are also observed during 10-12 hours post release, confirming entry into mitosis. From 14 hours onwards, the synchronized cells re-enter G_1, as shown by the decrease in the G_2/M peak and reappearance of the 2N peak in FACS and cyclin D levels in Western Blot. During 16-18 hours, majority of the cells show the reappearance of the 2N peak, suggesting successful completion of mitosis and entry into mitosis. Since, the cells released after double thymidine block are arrested at G_1/S boundary (0hour) and cells after 18hours of release enter G_1 phase of the next cycle, the 2N DNA peak is observed in both cases. However, the Western Blot data showing high cyclin E level at 0hour and reduced level at 18hours suggests that the cells at 0 hours post release are arrested at G_1/S boundary. Moreover, the high levels of cyclin D1 (G_1 phase marker) observed at 18hours further affirm that entry into G_1 phase of the next cycle. The FACS

and Western Blot data using several cell cycle markers, taken together suggested that synchronization of cells using double thymidine block was successful.

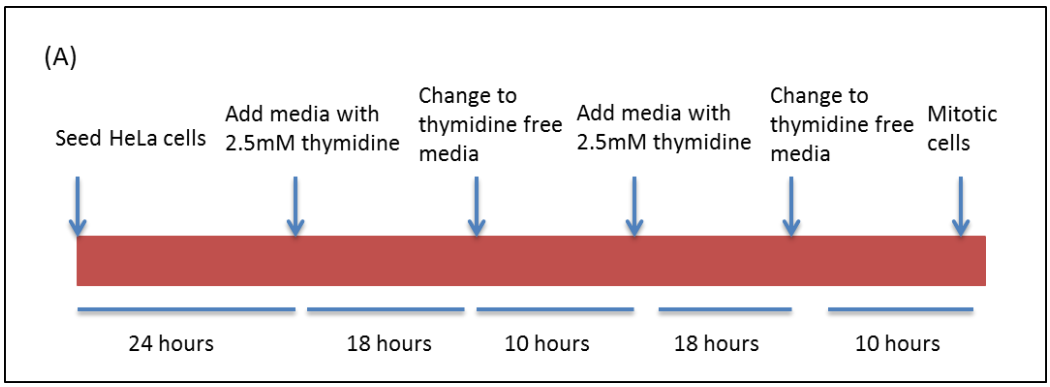

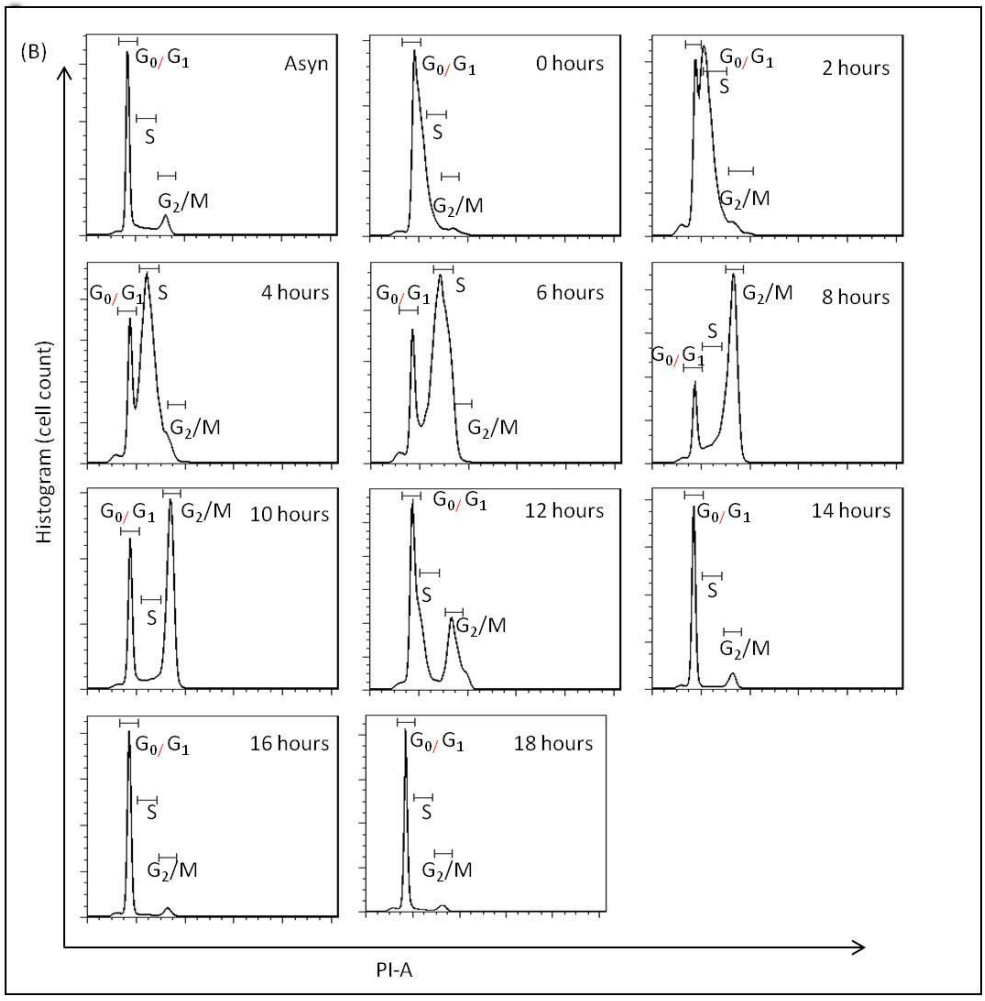

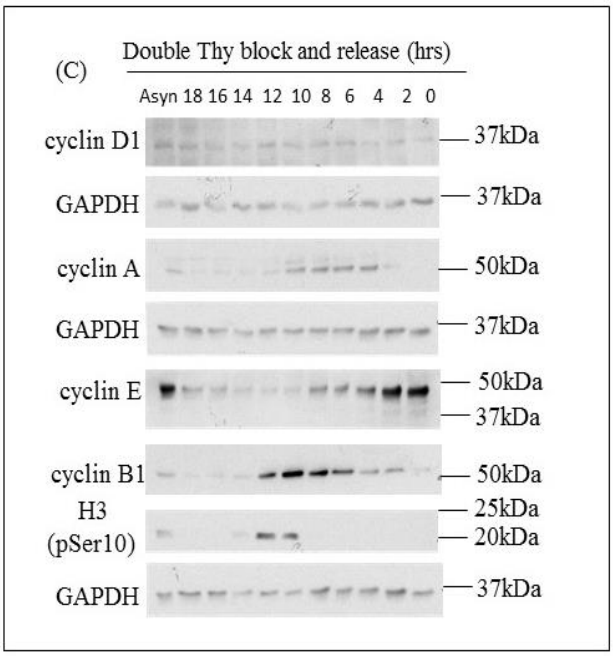

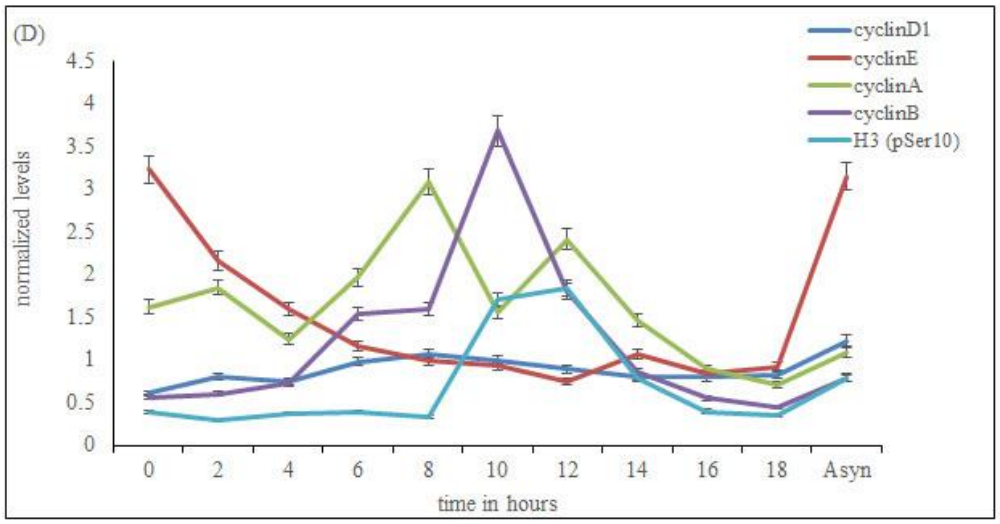

Figure 3.2 Mitotic cells were obtained 8 to 10 hours post release of double thymidine block. (A) Timeline showing the workflow of double thymidine block. (B) HeLa cells were synchronized using double thymidine block and released into fresh media. Cells were harvested after every two hours for a period of 18 hours and subjected to FACS DNA profiling. The plots are representative DNA content plot for each condition. (C) Cells harvested every 2 hours were immunoblotted with various cell cycle markers. Endogenous cyclin-D (G1-phase marker), cyclin-E (G1/S-phase marker), cyclin-A (S- and G2-phase marker), cyclin-B (M-phase marker) and phospho-Ser10 Histone 3 (M-phase marker) levels were probed to track the cell cycle progression after second thymidine release. Asyn denotes asynchronized cells. GAPDH was used as a loading control. (D) Densitometric analysis of the different cyclin levels was performed using ImageJ software and plotted in the graph shown. Values obtained are from two independent experiments. Error bars represent mean (±SEM).

3.1.3 Hypertonic stimulation of cells caused a delay in cell cycle progression

After obtaining the timeline of the cell cycle synchronization using double thymidine block, we next ventured to study the effects of osmotic imbalance on the timing of entry into the various stages of the cell cycle.

As mentioned above, HeLa cells were synchronized using double thymidine block and released into fresh isotonic media. Similar to the control set, synchronized cells were released into media containing 0.15M NaCl or 4% xylose and harvested for tracking the progression through cell cycle. Data from the FACS experiment showed that in control cells the peak shifted from 2N to 4N within 4-10 hours post release (Figue 3.3 A). During 12 to 16 hours, the 4N peak gradually decreased and 2N population returned, denoting that cells proceed to the next cell cycle after successfully completing mitosis (Figure 3.3 A). Contrary to this, when cells were released in media containing 0.15M NaCl, cells failed to progress efficiently through the cell cycle. The DNA content remained 2N for almost 6 hours post-release (Figure 3.3 B). At 8 hoursabout 60% of cells entered S phase, however, the entry into the G_2/M phase could only be observed from 14 hours post-release. About 36.3% cells entred G_2/M phase and about 50% of the population was arrested at this phase till 22 hours post release. Once, the cells entered G_2/M phase, they (34.5% of cells) remain arrested for a period of 24 hours, indicating a delay in mitotic progression. When cells were released in media containing 4% xylose, a distinct 4N DNA peak was observed at 6 hours post-release, indicating that cells undergo proper DNA replication and progress through S phase. However, from 14 hours, the cells began entry into the G_2/M phase. The 2N DNA peak returned from 22 hours post-release, however, a considerable proportion of cells still remained in the G_2/M phase, thus affirming the delay in cell cycle progression (Figure 3.3 C). In comparison to the control cells that entered

G_2/M phase after about 8 hours and took only about 2 to 3 hours to complete the G_2/M phase, the cells treated with hypertonic media exhibited a delayed entry into G_2/M stage and also spent a greater duration of almost 8 to 10 hours, affirming a prolonged delay in the progression of the cell cycle.

Taken together, these results reveal a lag in the cell cycle, corroborating with the observed decrease in G_0/G_1 and increase in the percentage of G_2/M cells upon hyperosmotic challenge.

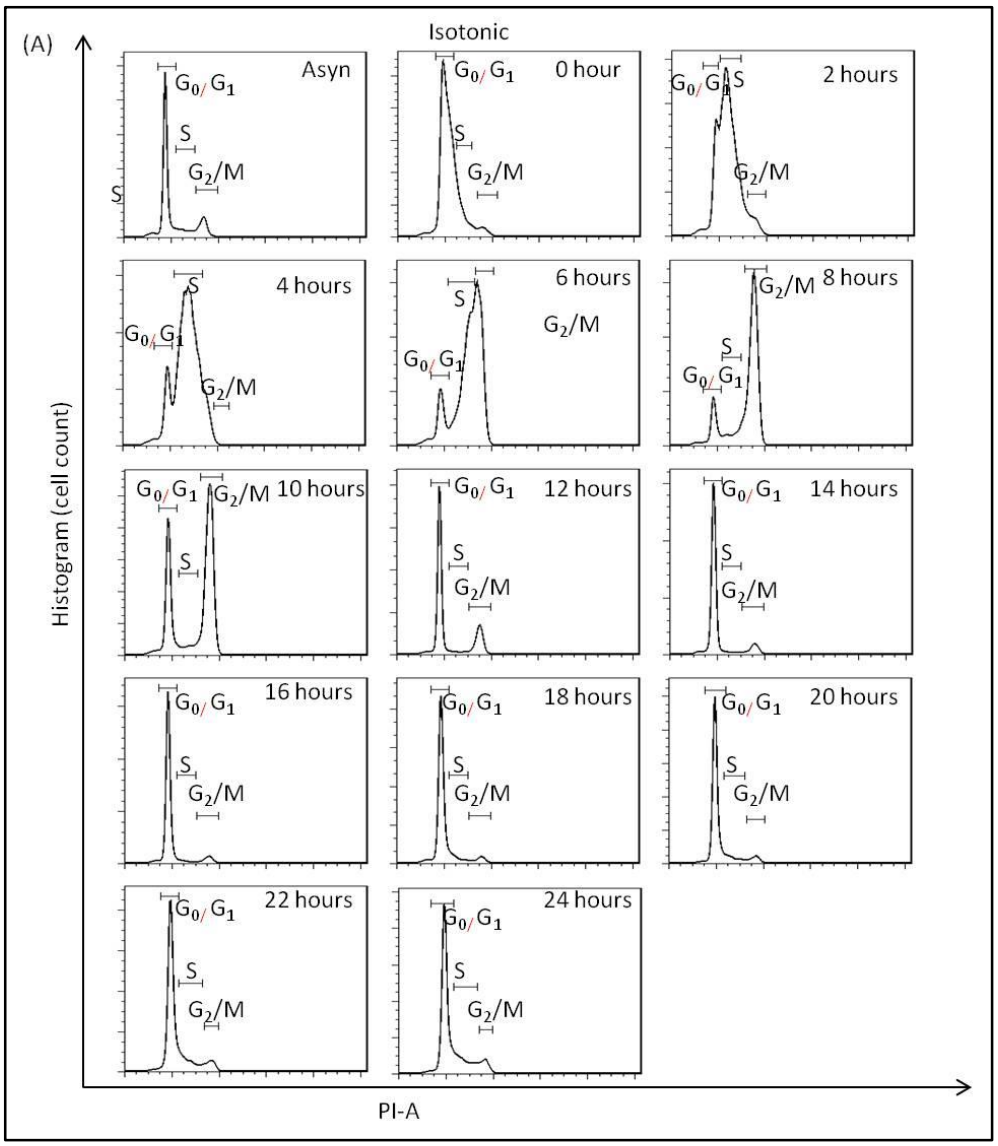

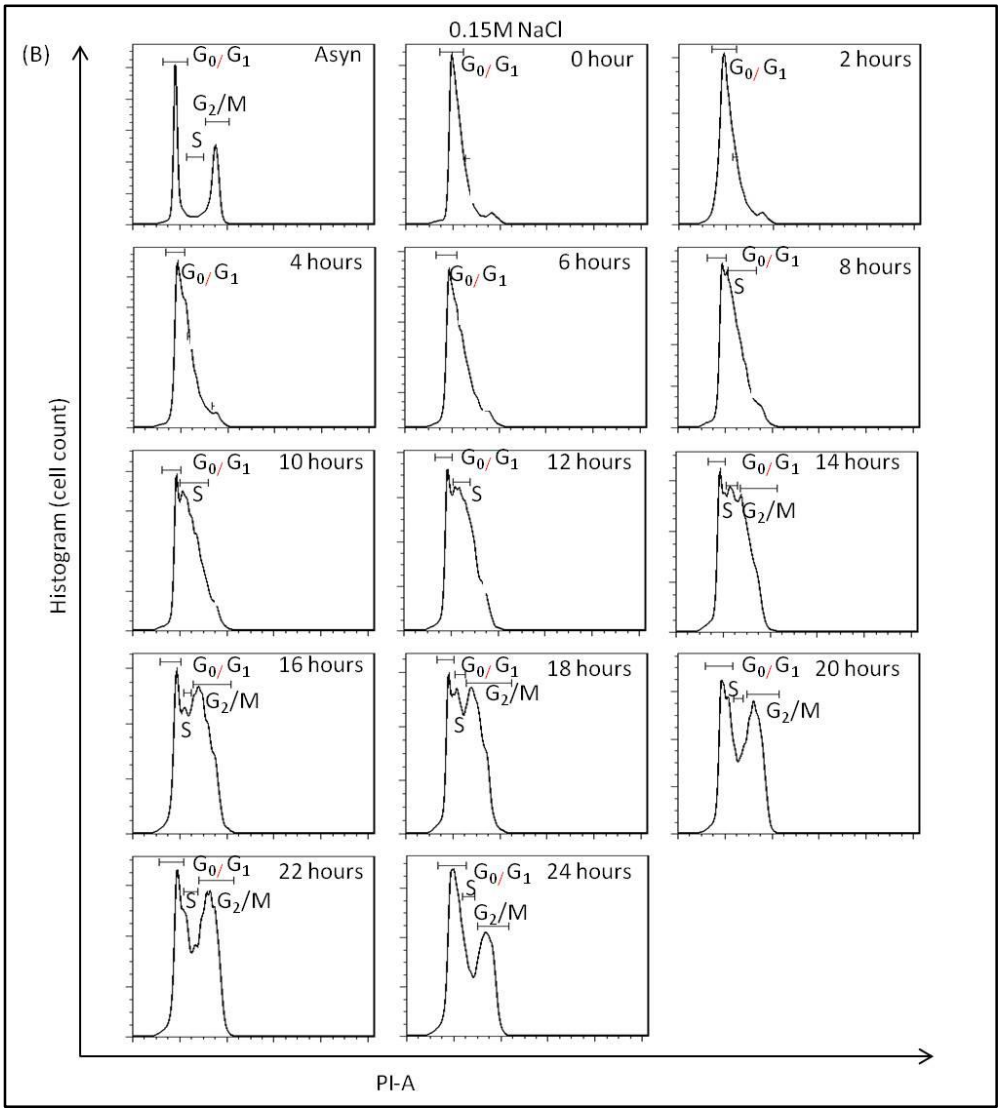
(B)
0.15M NaCl
Asyn
0 hour
2 hours
4 hours
6 hours
8 hours
10 hours
12 hours
14 hours
16 hours
18 hours
20 hours
22 hours
24 hours
G0/G1
G2/M
S
Histogram (cell count)
PI-A

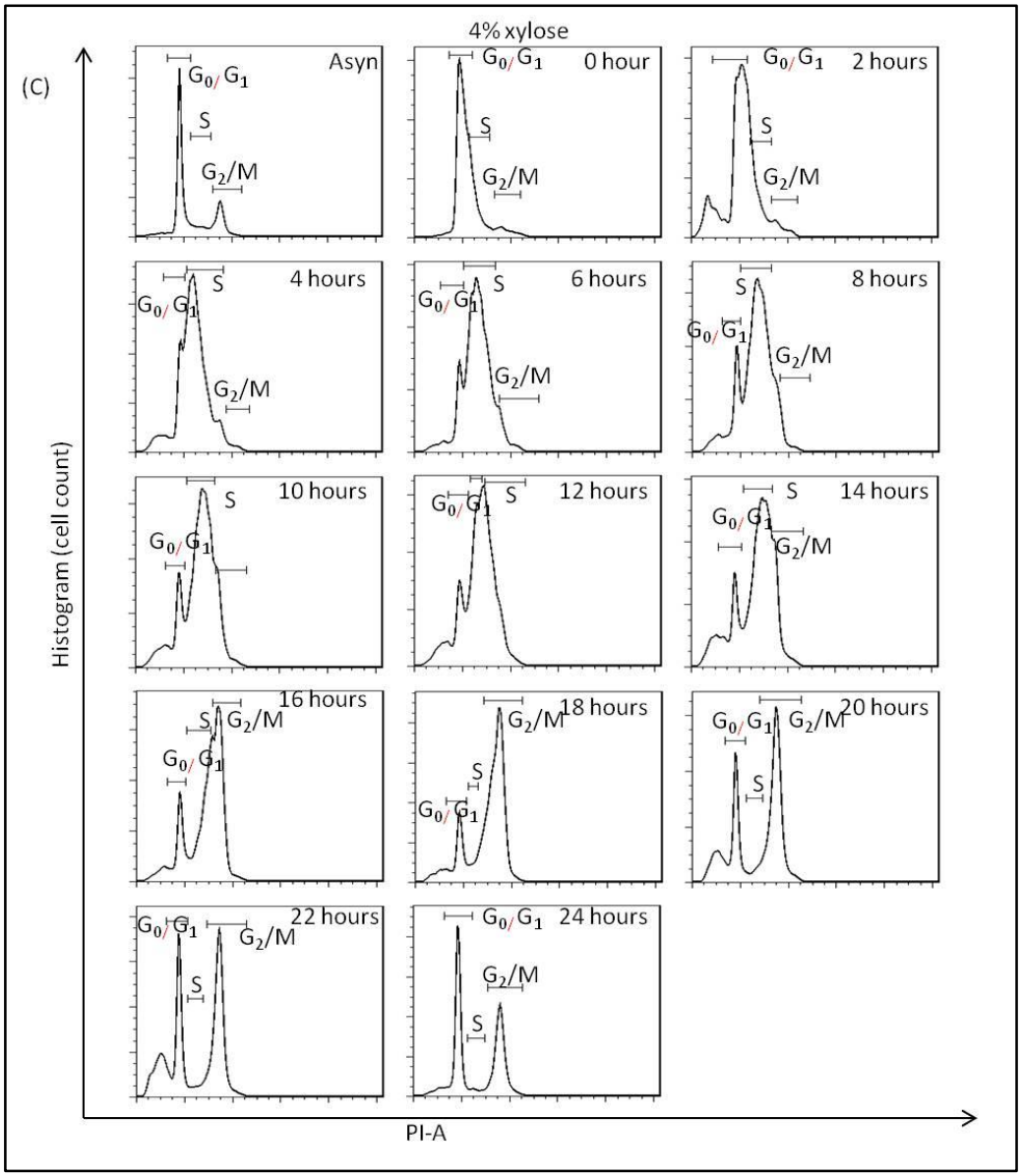

Figure 3.3 Hypertonic stress results in a delay in cell cycle progression. HeLa cells were synchronized using double thymidine block and released into (A) fresh media, media containing (B) 0.15M NaCl or (C) 4% xylose. Cells were harvested after every two hours for 24 hours and FACS DNA profiling was performed. The plots are representative DNA content plot for each condition for each time point. Asyn denotes asynchronized cells. This experiment was performed in triplicates.

3.1.4 Cell cycle proteins show altered expression during hypertonic stress

As shown above, since HeLa cells subjected to hypertonic shock show defects in cell cycle progression, the expression of various cell cycle proteins in response to osmotic stress was studied. It is known that timely progression of the cell cycle depends on the sequential activation of the cyclins and their association with the respective cyclin

dependant kinases (CDKs) [236]. Therefore, studies were done to examine the expression of various cyclins under early and prolonged duration of osmotic stress.

Upon exposure to osmotic stress induced by 0.15M NaCl or 4% xylose, HeLa cells showed a decrease in the cyclin D1 protein levels. The expression of cyclin B1 was also suppressed upon exposure to hypertonic stress for 4 hours (Figure 3.4 A). This decreased expression of cyclin D1 and cyclin B1 further strengthened the previously observed cell cycle delay.

Taken together, these results show lower protein levels of cyclin D1 and cyclinB1 and no apparent changes in the SAC proteins, thereby suggesting that this checkpoint may not be triggered by osmotic stress-activated signaling cascade in HeLa cells.

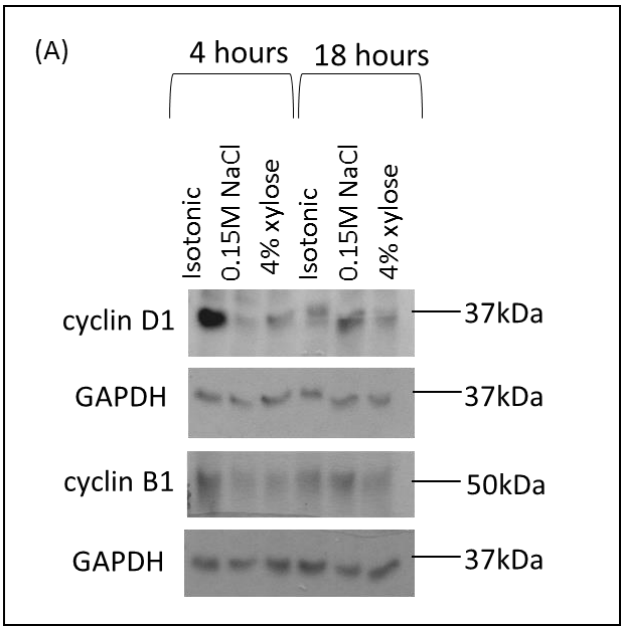

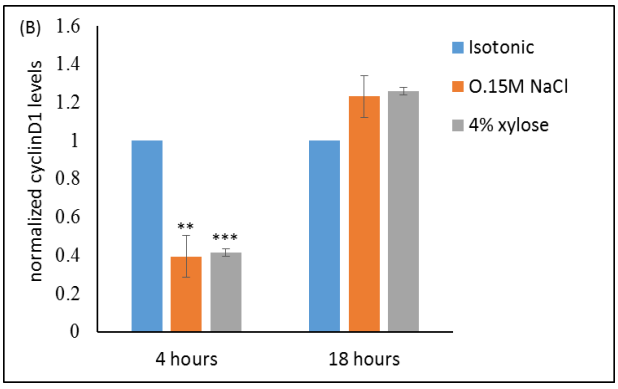

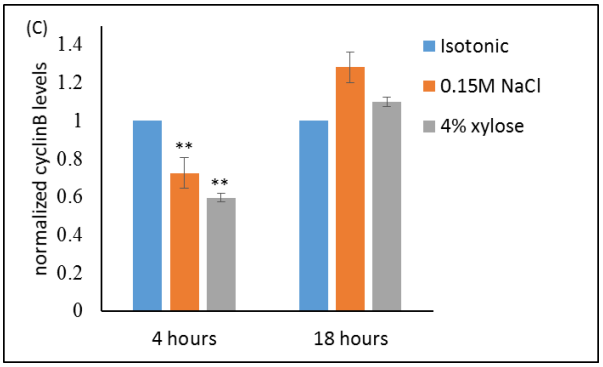

Figure 3.4 Hypertonic stimulation results in downregulation of cyclin D1 and cyclin B1 protein levels. (A) Hela cells were treated with hypertonic 0.15M NaCl or 4 % xylose for 4 hours and 18 hours and subjected to immnuoblotting with cyclin D1 and cyclin B1 antibodies (4 hours). GAPDH was used as a loading control. Densitometric analysis of (B) cyclin D1 and (C) cyclin B1 levels were performed using ImageJ software. The values from three independent experiments were plotted and the graph shows a decrease in cyclin D1 and cyclin B1 protein levels. Error bars represent mean (±SEM). *** p=0.0001, ** p=0.001.

A possible reason for the changes in cell cycle progression upon hyperosmotic exposure may be attributed to osmo-adaptation mechanisms. Hypertonic milieu is responsible for the activation of G_1/S and G_2/M checkpoints [119, 237]. G_1/S checkpoint activation is p53 dependant and G_2/M checkpoint activity is governed by stress-activated MAP kinase signaling cascades [238]. The p38 MAP kinases are involved in early and long-term adaptive responses to osmotic stress [239] and are known to delay progression through G_2 phase [134, 240]. Therefore, in order to determine the involvement of p38 MAP kinase in the osmotic stress response of HeLa cells, we investigated p38 activation in HeLa cells. Activated p38 was detected by a specific antibody which recognizes phosphorylated p38 MAP kinase. Our results show the presence of phosphorylated p38 at 30 minutes, 4hours as well as 18 hours post-hypertonic treatment (Figure 3.5 A), thereby affirming it's role in early as well long-term osmoadaptation in HeLa cells.

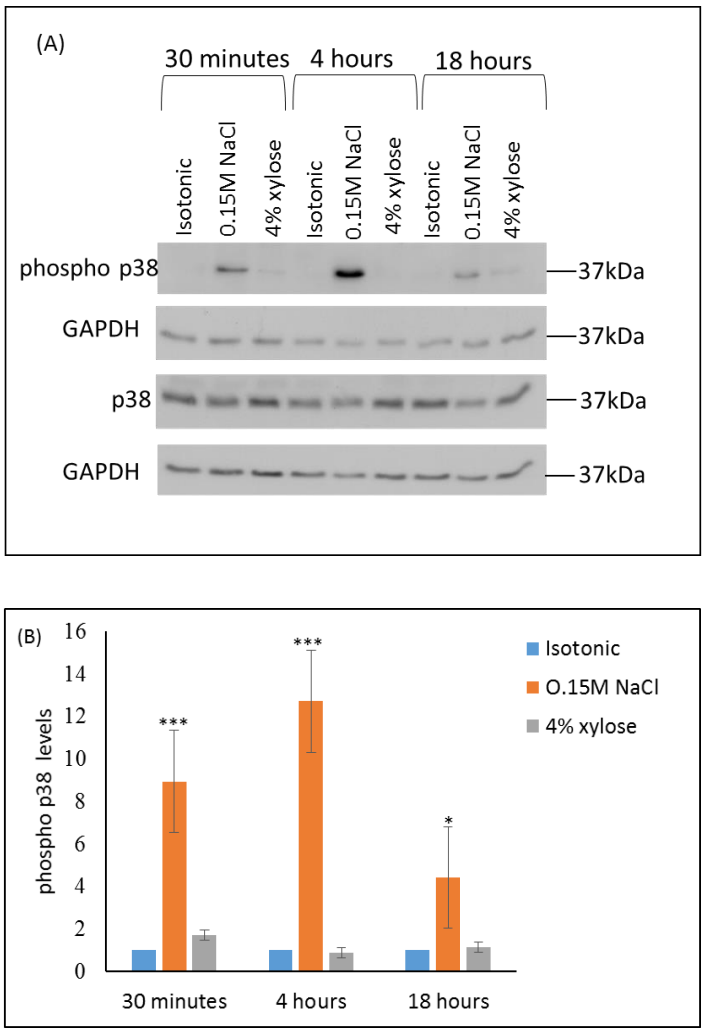

Figure 3.5 Hypertonic stress results in an activation of p38 levels. (A) HeLa cells were subjected to hypertonic media and harvested at different time points for Western Blotting with phoshorylated p38 and p38 antibodies to examine the activation of p38 during early and late osmoprotective response. (B) Densitometric analysis of phospho p38 levels was performed using ImageJ software. Endogenous GAPDH levels was used as a loading control. Phospho p38 and p38 levels were normalized to their respective GAPDH levels and the adjusted phospho 38 was then normalized to adjusted p38 levels. Values are expressed as mean (±SEM) of three independent experiments. *** $p<0.0001$, ** $p<0.001$.

3.1.5 Exposure to hyperosmotic media results in mitotic delay

Since we observed a delay in cell cycle progression and a prolonged duration of cells in G_2/M phase upon hypertonic exposure, we next investigated the effects of the osmotic stress on the progression timing of each mitotic stage.

In order to study this, HeLa cells were synchronized in early mitotic stage using nocodazole. Nocodazole is frequently used to arrest cells during early mitosis,

specifically at prometaphase by depolymerisation of microtubules *in vivo* [241]. The effect of hypertonic stress on the progression timing of each mitotic stage was studied. HeLa cells were synchronized by nocodazole for a period of 12 hours and released into isotonic, 0.15M NaCl or 4% xylose containing media. Since the average time taken by HeLa cell to complete mitosis is about 60-75 minutes, the cells were released from nocodazole and imaged at 30, 60 and 90 minutes post release to study the progression timing through the mitotic stages. Mean percentages of cells in each phase were plotted. During 30 minutes, most of the cells (75%) are stuck in early mitotic stage and gradually progress towards metaphase, as seen by their chromosome structure, suggesting that the cells were synchronized since nocodazole is a well-established drug routinely used to induce arrest at early mitotic stage. The values suggest that by 60 minutes post release, around 30% cells enter metaphase and 15% enter anaphase and by 90 minutes release, 23% enter anaphase and about 31% are in telophase, suggesting recovery from nocodazole arrest and successful completion of mitosis. Our data showed that at 30 minutes post-nocodazole release, there were very few or hardly any cells at metaphase in the hypertonic milieu compared to the control cells (Figure 3.6), suggesting that cells present in hypertonic environment were unable to recover from the nocodazole-induced disruption of mictotubules and mitotic arrest. By 90 minutes post-nocodazole release, most of the control cells were present in anaphase (23%) and progressed to telophase (31%) whereas in 0.15M NaCl treated condition, a large proportion of cells (~60%) were still arrested in prometaphase and cells released in xylose exhibited a slow progression to metaphase.

These data validated the prolonged duration of M phase observed in FACS (Figure 3.3), which could be primarily attributed to prometaphase and metaphase arrest in response to osmotic stress. Our results thus show that the recovery of microtubule structures after nocodazole release, which is essential for alignment of chromosomes at the metaphase

plate and the subsequent chromosome separation during anaphase are impaired under hyperosmotic conditions.

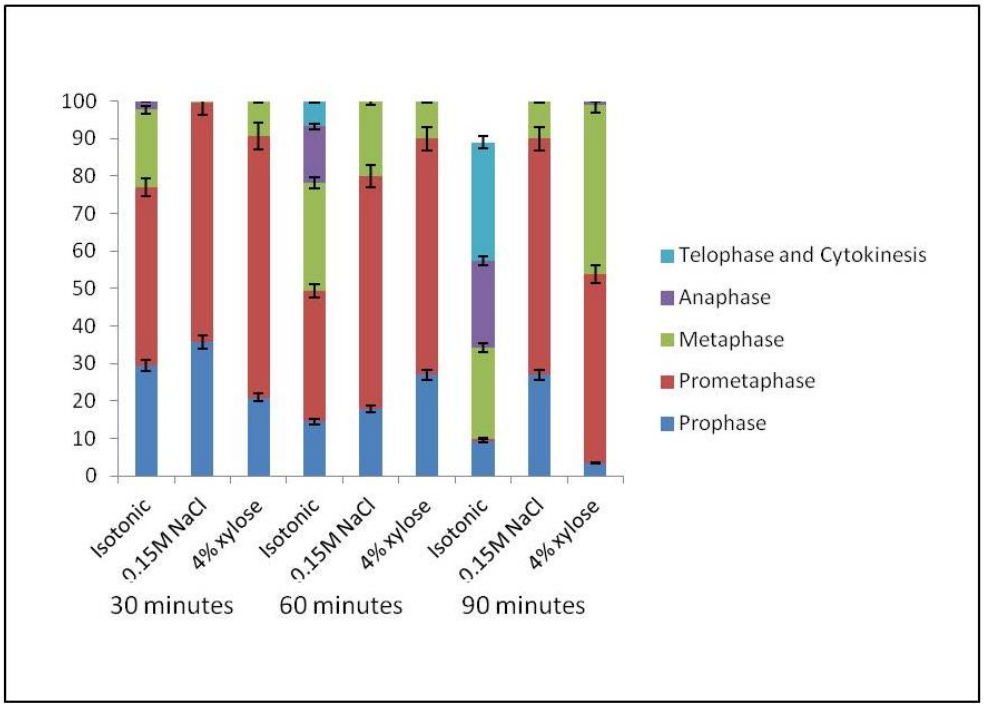

Figure 3.6 Exposure to hypertonic stress delayed recovery from nocodazole arrest. HeLa cells were synchronized by nocodazole for 12 hours and released into isotonic media, media containing 0.15M NaCl or 4% xylose. Cells were imaged at regular intervals of 30, 60 and 90 minutes. Mean percentage of cells in each mitotic phase from two independent experiments were scored and plotted. Error bars represent mean (±SEM). n≥300.

3.1.6 Hypertonic stress perturbed progression through mitosis

So far, the results obtained show hypertonic stress induced arrest at the G_2/M phase and probably during the metaphase stage of mitosis. Confirmatory results can be obtained only by time-lapse microscopy to visaulaize the progression of cells though mitosis.

In order to accomplish this, HeLa cells synchronized by double thymidine block were released into isotonic, 0.15M NaCl or xylose containing media respectively and subjected to time-lapse phase contrast microscopy every 15 minutes for a period of 24 hours.

The cells present in isotonic medium progressed through mitosis normally taking an average time of 70 minutes for its completion (Figure 3.7 A). On an average, within 45 minutes from the start of mitosis, characterized by prophase, the cells progressed to

cytokinesis. In contrast, cells exposed to media containing 0.15M NaCl failed to progress through mitosis (Figure 3.7 B). On the other hand, cells exposed to xylose exhibited two defects. Most of the cells were arrested at metaphase for almost 90 minutes and when they finally progressed to telophase, they showed cytokinetic defects, characterized by the absence of a definite cleavge furrow and cell blebbing (Figure 3.7 C). Another population of cells showed delayed progression and were stuck in metaphase for almost 4 hours before proceeding to anaphase (Figure 3.7 D).

Taken together, the time-lapse microscopy experiment confirmed that the cell cycle delay observed in the FACS analysis (Figure 3.3) was due to mitotic arrest. Our observations suggest that cells need to maintain a proper osmotic balance in order to progress through mitosis effectively.

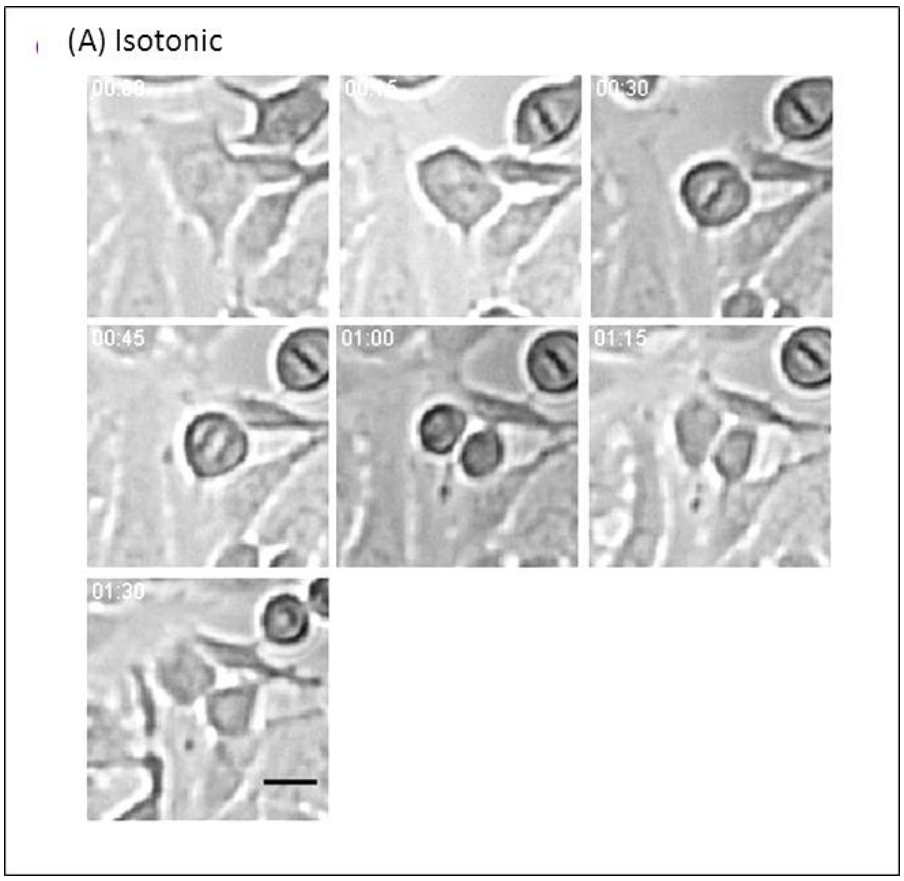

(B) 0.15M NaCl

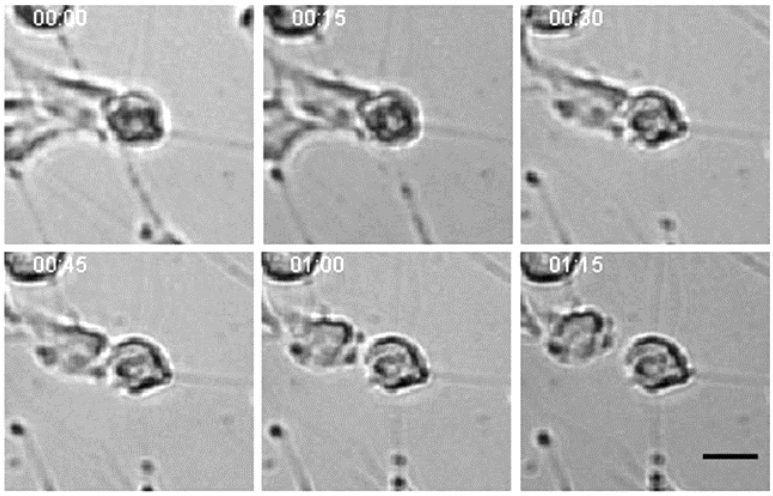

(C) 4% xylose

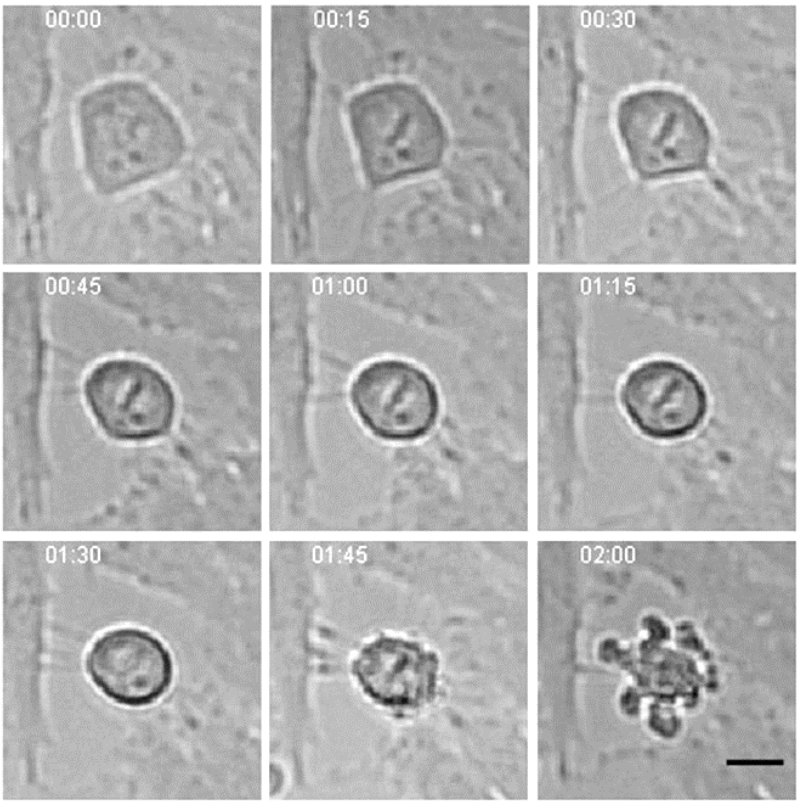

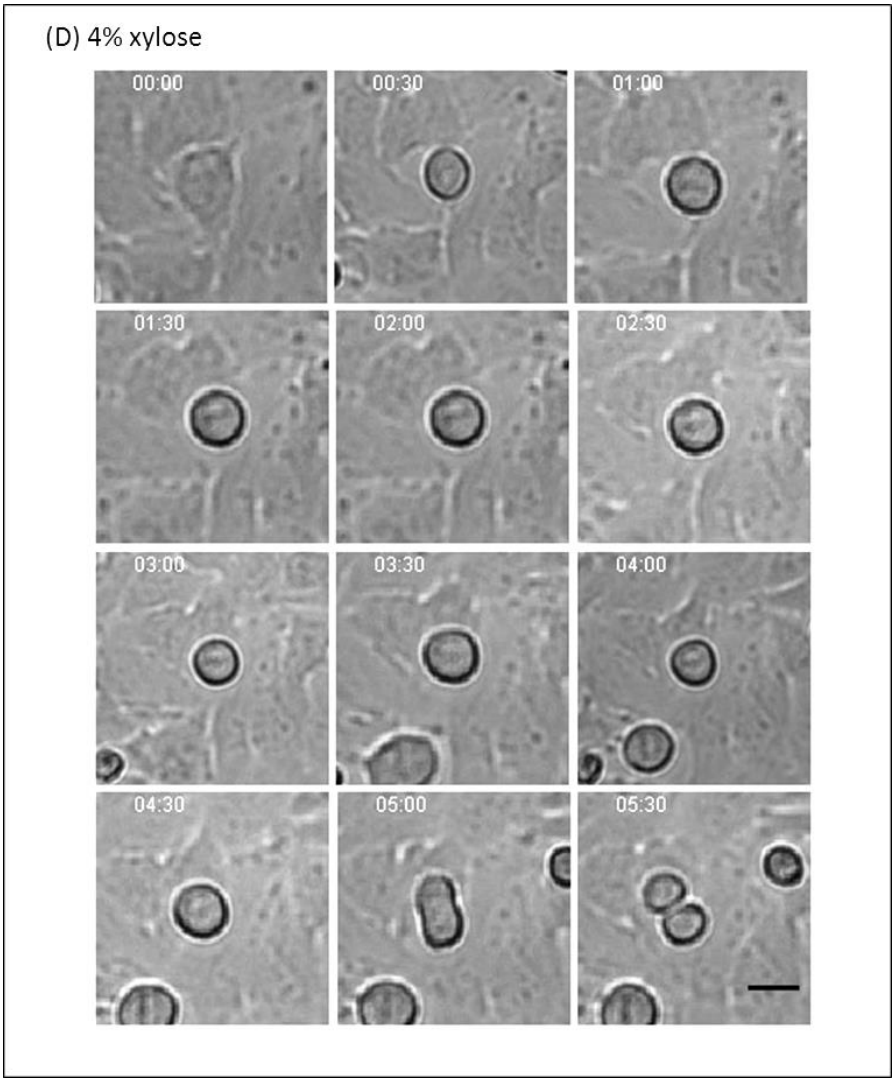

Figure 3.7 Hypertonic stress leads to a delay in mitotic progression in HeLa cells. HeLa cells were synchronized by double thymidine block and released into (A) isotonic media, (B) media supplemented with 0.15M NaCl or (C), (D) media supplemented with 4% xylose at 7 hours post-release. Cells were imaged by phase-contrast live imaging from 8 hours to 24 hours post-release. Images were captured at an interval of 15 minutes and images for (D) are shown after an interval of 30 minutes. Numbers on frames represent elapsed time in minutes. This experiment has been performed in triplicates. On an average, a total of ≤40 cells were counted for every condition during each experiment. Therefore, a total of 120 cells were counted per condition. The time taken by these cells to progress through mitosis was calculated. Scale bar 20μm.

3.1.7 Disruption of the osmotic gradient leads to cytokinetic defects.

We found that cells grown in media containing xylose experienced inhibitory effects on cytokinesis. In contrast to the control cells, which showed the presence of cleavage furrow ingression and midbody, followed by abscission and separation into two daughter cells, cells treated with hypertonic media containing xylose did not show furrow ingression and the cells subsequently fused to form multinucleated cell or underwent

blebbing (Figure 3.7 C). To further examine the effects of osmotic stress on cytokinesis, the localization of polo-like kinase (PLK1), implicated in cleavage furrow formation was examined in HeLa cells.

Immunofluorescent images showed the presence of PLK1 in the midzone and midbody of the separating cells (Figure 3.8) whereas cells exposed to hypertonic environment 30 minutes failed to show the presence of PLK1 at the midbody of the separating cells.

We observed that perturbation of the osmotic gradient caused defects in cytokinesis, characterized by an inability to undergo cleavage furrow ingression (Figure 3.8).

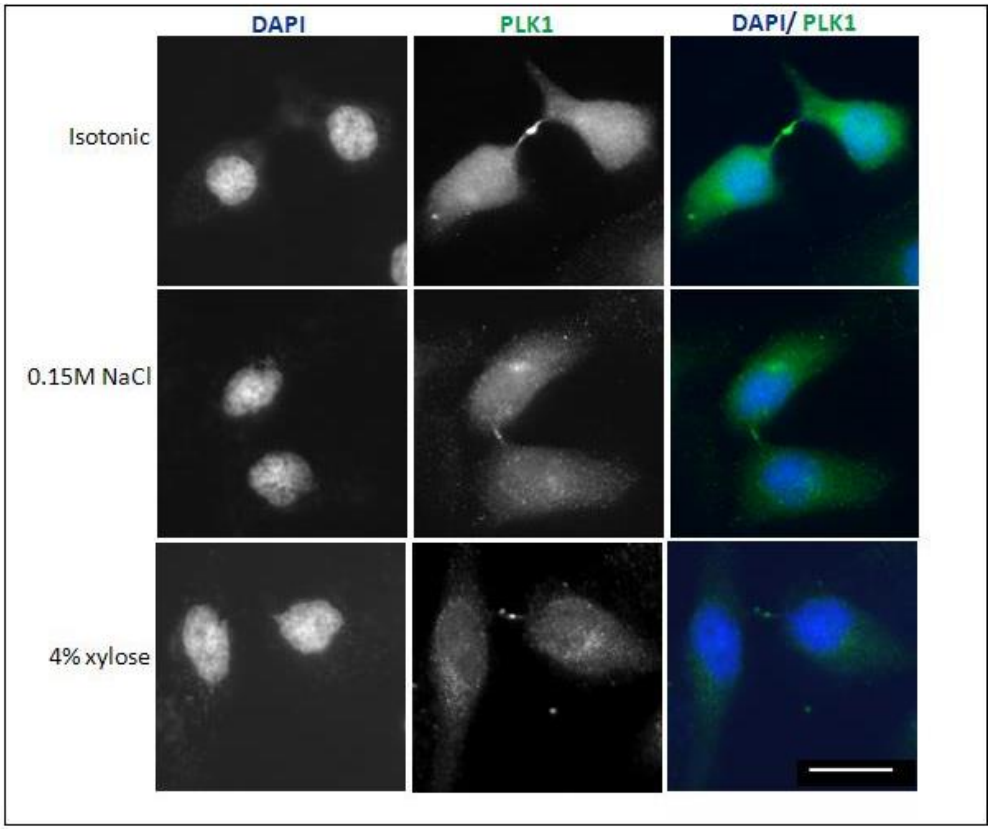

Figure 3.8 Hypertonic stress led to aberrant Polo-like-kinase 1 (PLK1) staining during telophase and cytokinesis. HeLa cells treated with 0.15M NaCl and 4% xylose were stained with PLK1 (green) and DAPI (blue). 90 cells at cleavage furrow stages from three independent biological repeats were imaged. Scale bar 10μm.

3.2 Discussion

In this part of the study, we have shown the link between osmotic stress and cell cycle control. We explored the effects of hyperosmotic stress on cell cycle progression and mitosis. Our results show cell cycle arrest during metaphase upon exposure to hypertonic media. Additionally, the contractile ring formation and cleavage furrow ingression, which ensure proper cytokinesis are also affected by alterations in osmotic balance. Taken together, our results reflect that the ability of the cell to regulate its osmotic pressure is essential for effective progression of the cell cycle. Proper coordinated cell division timing is necessary and any abrogation in the cell division control may lead to severe defects in embryonic growth and development and cancer. Therefore, a detailed understanding of the contribution of the extracellular milieu during mitosis requires further investigation.

Previous studies have reported that renal medullary cells experience fluctuations in osmotic pressure. Prolonged exposure to extreme hypertonic conditions is known to cause DNA double-strand breaks [242] and apoptosis [243, 244]. Despite severe hypertonic conditions, cells employ compensatory adaptive responses, enabling them to surive and function. The cells accumulate organic osmolytes to restore the intracellular osmtic balance and cell volume [128] as a response to hypertonicity. In addition, the cells respond to this increased tonicity by inducing cell cycle arrest [134, 243-245]. Our cell cycle analysis supported this further. HeLa cells exposed to hypertonic conditions accumulate in G_1 and G_2/M phases, evntually leading to decreased cell proliferation. The hypertonicity-induced arrest at the G_1 and S phases is controlled by the activity of the tumor suppressor protein p53. p53 is phosphorylated at Ser 15 residue during S phase of the cell cycle and thereby protects the cells against osmotic imbalance by restricting DNA replication.

On the other hand, cells also encounter arrest at the G_2/M phase and the stress-activated MAPkinase pathway is implicated in this [246]. p38 MAP kinase, a member of the mitogen-activated protein kinase is activated during acute hypertonic challenge and this activation is attributed to the G_2/M arrest in renal inner medullary epithelial cells [119, 247]. Recent studies have shown that the osmotic stress response is solely not restricted to renal medullary cells but can affect a variety of cell types [110, 248, 249]. p38 MAP kinase has been reported to retard the progression through G_2 in kidney cells and this effect can be counteracted by inhibiting this kinase [119]. Our results showing a delay in G_2/M progression during hypertonic stress and the subsequent increase in p38 MAP kinase activation further confirms the role of osmotic pressure during cell cycle progression in non-kidney cells and asserts the contribution of p38 MAP kinase during early and long-term osmo-protective response. During G_2 arrest, p38 acts as a switch, which turns 'on' to activate the process and is turned 'off' after the process has properly started. Our results show that in HeLa cells subjected to hypertonic stress, p38 is indeed activated, as detected by the phospho-p38 antibody. Since, p38 is implicated in early adaptive response, we observe a band within 30 minutes of osmotic stress. Cells tend to accumulate compatible organic solutes to restore the intracellular salt concentration. This process takes several hours. Under these conditions of higher osmosensitivity, p38 activation is prolonged. Therefore, the phospho-38 levels are high at 4 hours. Prolonged hypertonic stress results in cell death. As a result, the phospho-38 levels are lower as compared to the early time-points. Another probable explanation is that many cells tend to adapt to the osmotic imbalance and survive after restoration of normal cell volume and intracellular hydrostatic pressure, which explains the reduction in phospho-38 protein levels at 18 hours (Figure 3.5).

Our cell cycle analysis supported the notion that cells undergo changes in cell cycle progression as a part of osmoadaptive responses. Our results show that a rise in the

numbers of cell in G_2/M phase upon hypertonic stimulation could account for cell cycle arrest, thereby allowing cells to adapt to the osmotic stress. Sequential activation of cyclin-dependent kinases (CDKs) and their association with the cyclins are responsible for driving cell cycle progression [236]. The cyclin D/CDK4 complex drives G_1 phase and cyclin E/CDK2 complex is necessary for G_1/S transition. Progression through the S phase is controlled by cyclin A/CDK2 and cyclin A/CDK1 monitors G_2 phase. Finally, G_2/M transition is driven by cyclinB/CDK1 complex. The results obtained by Western Blotting showed that arrest at the G_1 and G_2/M correlated with the downregulation of cyclin D1 and cyclin B1 protein levels upon hypertonic stress (Figrue 3.1.4 A). The expression of the mitotic CDK1 however did not change during our experimental conditions. Since the activity of CDKs is controlled by the presence or absence of their respective cyclins [250], the decrease in cyclin D1 and cyclin B1 protein levels will likely lead to less activated CDK4 and CDK1 respectively, which restults in the observed cell cycle arrest of HeLa cells.

PCNA (Prolferating cell nuclear antigen), mainly involved in DNA replication and repair [251] is capable of interacting with cyclin/CDK complexes and cell cycle inhibitor p21 [252]. The interaction of p21 with PCNA could thereby inhibit DNA replication activity and also block its binding to to the cyclin/CDK complexes, consequently resulting in cell cycle arrest at the G_1/S and G_2/M phase. Therefore, it would be useful to study the expression profile of these proteins under hypertonic conditions in future.

Cell synchronization experiments using double thymidine block show that cells released from thymidine-induced G_1 arrest were able to recover and proceed to successfully complete the cell cycle. During the synchronization, cells treated with excess thymidine form thymidine dinucleotides, pTpT. These mimic the small DNA fragments released during excision repair [253]. Our experiments show that when cells are released into

media containing 0.15M NaCl or 4% xylose following by G_1 arrest by excess thymidine, they failed to recover completely and the transgression to the subsequent phases was abrogated, suggesting that the cells may adopt a mecahism to delay cell cycle progression as a response to osmotic stress in order to allow the cells to adapt.

Our results show that when cells were released from nocodazole arrest into hypertonic media, they failed to recover and were stuck for prolonged duration in metaphase. (Figure 3.6) The metaphase arrest was further confirmed using time-lapse phase contrast imaging of HeLa cells (Figure 3.7 B, C, D). It is known that cells experience a drastic change in their architecture driven by actin cytoskeleton remodeling and osmotic pressure regulation upon mitotic entry to achieve a spherical shape [52, 53]. The failure of the cells to round up prevents mitotic exit, causes defects in astral microtubule organization and spindle pole function. The contribution of the osmotic pressure in these processes is discussed in details in the next chapter. The metaphase arrest observed upon hypertonic stimulation could be due to these defects in spindle organization.

Apart from the defects in mitotic events, hypertonic stress was shown to cause defects in cytokinesis, particularly during the formation and regression of the cleavage furrow. Time-lapse imaging (Figure 3.7 B, C) and PLK1 (Figure 3.8) immuno-staining reflect these defects. Although the involvement of RhoA, one of the factors in mitotic cell rounding has been well-documented [254, 255], the underlying mechanism of the osmotic stress leading to dexfects in cleavage furrow ingression still requires further investigation.

Chapter 4

Effect of osmotic pressure on mitotic spindle assembly during metaphase

In the previous chapter, we have observed delay in timings of the cell cycle upon disruption of the osmotic balance, particularly an arrest during metaphase. Since a common cause of prolonged metaphase is due to improper bipolar mitotic spindle assembly, we will therefore further investigate the effects of hypertonic stress on mitotic events, such as astral microtubule arrangement and spindle orientation.

4.1 Results

4.1.1 Osmotic balance is necessary for proper astral microtubule arrangement during mitotic spindle formation

In order to examine the effects of the osmotic pressure changes in the modulation of the mitotic spindle assembly, asynchronized HeLa cells were treated with hypertonic media containing 0.15M NaCl or 4% xylose for a period of 30 minutes. The duration of mitosis usually ranges from 60 to 90 minutes and metaphase lasts for about half an hour. Following this osmotic shock, the cells were immuno-stained with anti-α-tubulin to observe the microtubules and DAPI to select the metaphase cells for analysis. Control cells exhibit a well-defined spindle with the microtubules at the metaphase plate and less visible astral microtubules. On the other hand, cells treated with hypertonic media do not show a well-defined crescent-shaped spindle but displayed an aberrant astral microtubule arrangement, emanating from the spindle poles towards the cortex (Figure 4.1 A). We next quantified the amount of astral microtubules through comparison of the fluorescence intensities of cells immuno-stained with anti-tubulin antibodies. The astral microtubules

were measured by subtracting the corrected background intensity of the kinetochore microtubules from the total microtubule fluorescence intensity (Figure 4.1 B). Quantification shows that in comparison to control cells, cells facing a hypertonic challenge show a significant increase in the integrated astral microtubule intensities (Figure 4.1 C).

The EB1 family of proteins localizes to the distal ends of the microtubules and regulates microtubule stability. More pronounced EB1 staining at the growing tip of the astral microtubules was observed in cells exposed to 0.15M NaCl or 4% xylose containing media (Figure 4.1 D).

These findings indicate that perturbation of the osmotic balance can lead to an increase in astral microtubules during metaphase.

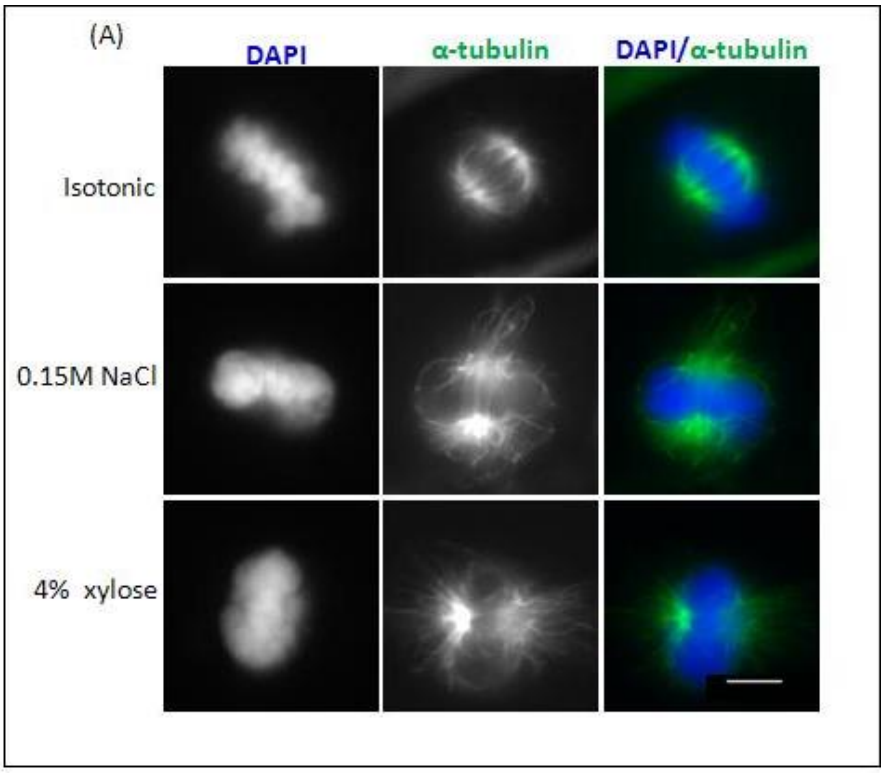

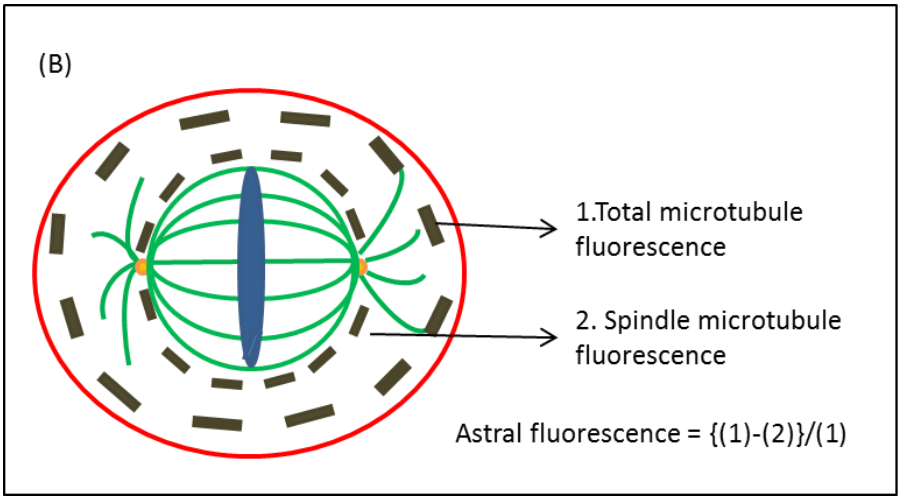
(B)
1.Total microtubule fluorescence
2. Spindle microtubule fluorescence
Astral fluorescence = {(1)-(2)}/(1)

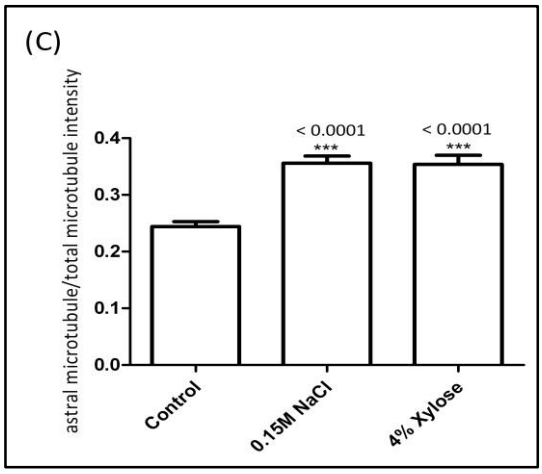
(C)
astral microtubule/total microtubule intensity
0.4
0.3
0.2
0.1
0.0
< 0.0001
***
< 0.0001
***
Control
0.15M NaCl
4% Xylose

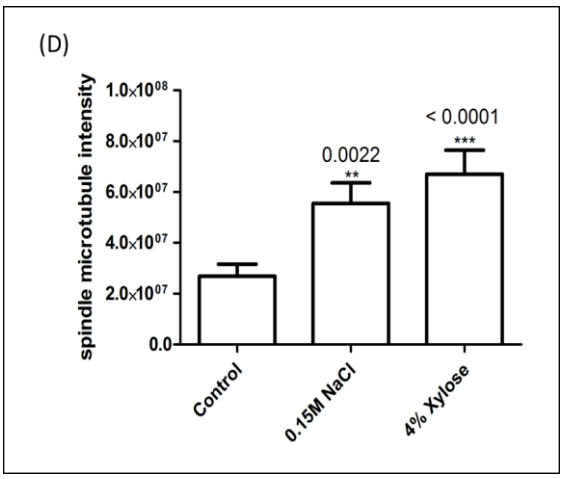
(D)
spindle microtubule intensity
1.0x10^08
8.0x10^07
6.0x10^07
4.0x10^07
2.0x10^07
0.0
0.0022
**
< 0.0001
***
Control
0.15M NaCl
4% Xylose

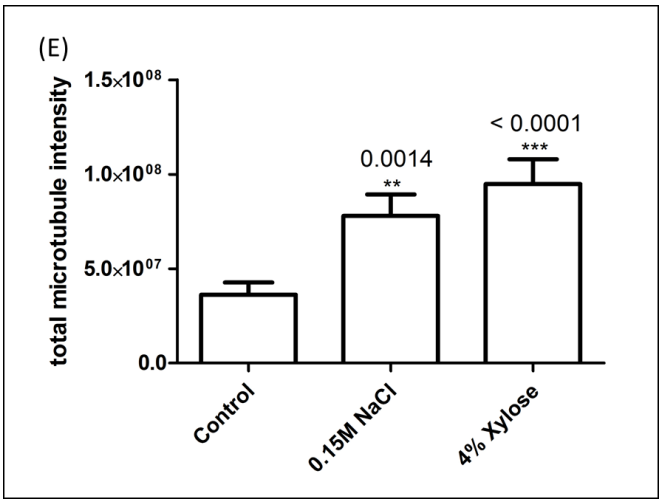
(E)
total microtubule intensity
1.5x10^08
1.0x10^08
5.0x10^07
0.0
0.0014
**
< 0.0001
***
Control
0.15M NaCl
4% Xylose

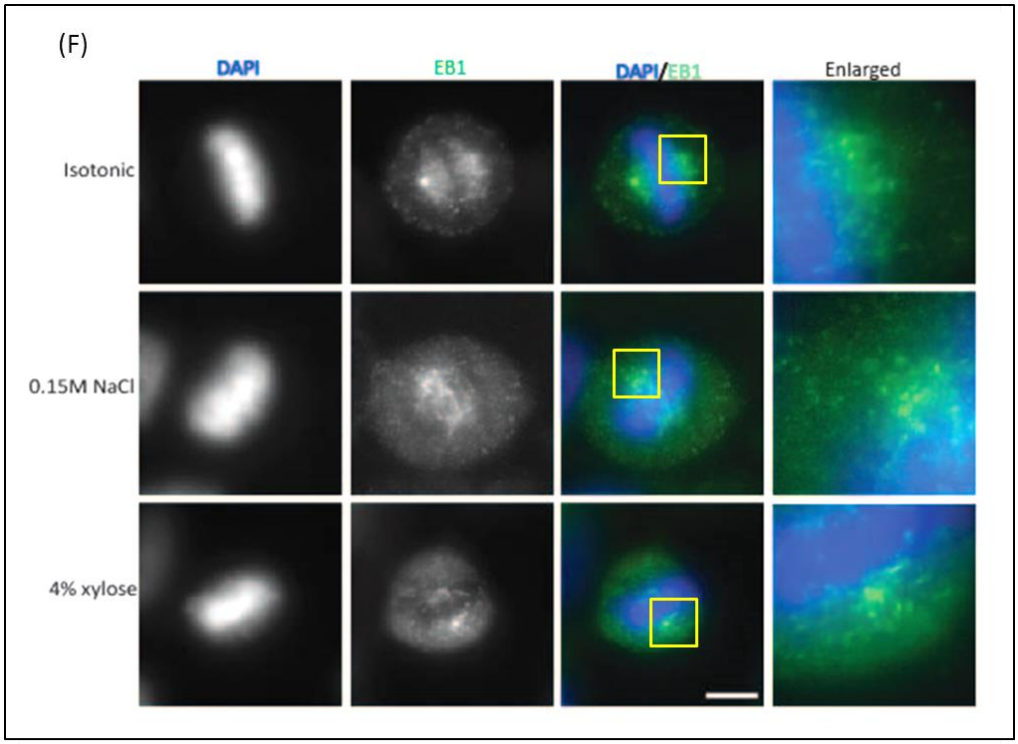

Figure 4.1 Disruption of osmotic balance resulted in increased astral microtubules. (A) HeLa cells were subjected to media containing 0.15M NaCl or 4% xylose for 30 minutes and stained with anti-α-tubulin (green) and DAPI (blue). Scale bar10µm. (B) Diagrammatic representation showing quantification of astral microtubules. The background corrected integrated fluorescence intensities of the kinetochore microtubules and total microtubule were then calculated using Image-J software. The astral microtubule intensity was then calculated by subtracting the intensity of spindle microtubules from the total microtubule intensity. (C) The background-corrected integrated astral microtubule fluorescence was calculated as shown in (B) and ratio of astral to the background-corrected integrated total intensity was plotted. The background corrected integrated (D) spindle microtubule intensity and (E) total microtubule intensity was plotted. 180 cells from four independent biological repeats were imaged, analyzed and plotted for quantification. Unpaired student's t-test was performed for statistical analysis. Error bars represent mean (± SEM) ***p < 0.0001. (F) HeLa cells were exposed to isotonic (control), media containing 0.15M NaCl or 4% xylose for 30 minutes followed by staining with anti-EB1 (green) and DAPI (blue) Scale bar 10µm. Last panel represents enlarged image of boxed region.

4.1.2 Hypertonicity induced changes in the astral microtubules increase with time.

To determine whether the changes induced by hypertonic medium are rapid responses of the cells, they were subjected to hypertonic media for different time points. A short exposure to the 0.15M NaCl or 4% xylose containing media for 5 or 10 minutes was not able to bring out aberrations in the astral microtubules (Figure 4.2 A). However, as the duration of exposure increased, the effects became more pronounced (Figure 4.2 B).

We next intended to examine whether the defects in the astral microtubules was reversible. This was accomplished by treating the cells with hypertonic media for 30 minutes, followed by recovery in the isotonic medium for 3 hours. The cells were then subjected to immuno-staining with anti-α-tubulin and DAPI (Figure 4.2 C). Quantification of the background-corrected integrated intensity of the astral microtubules showed a rescue of the astral microtubule defects upon restoration of the osmotic balance in these cells, suggesting that the effects are transient and reversible (Figure 4.2 D).

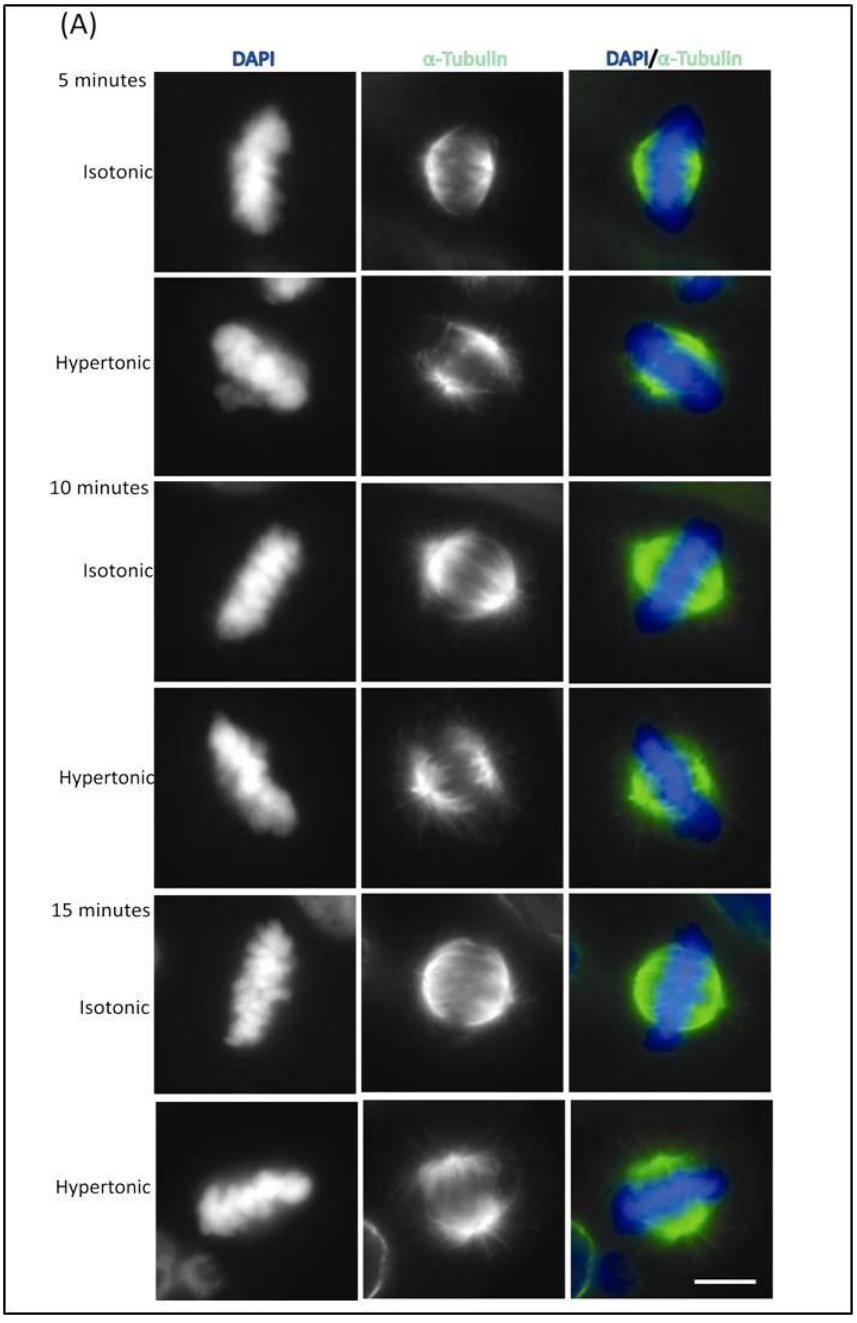

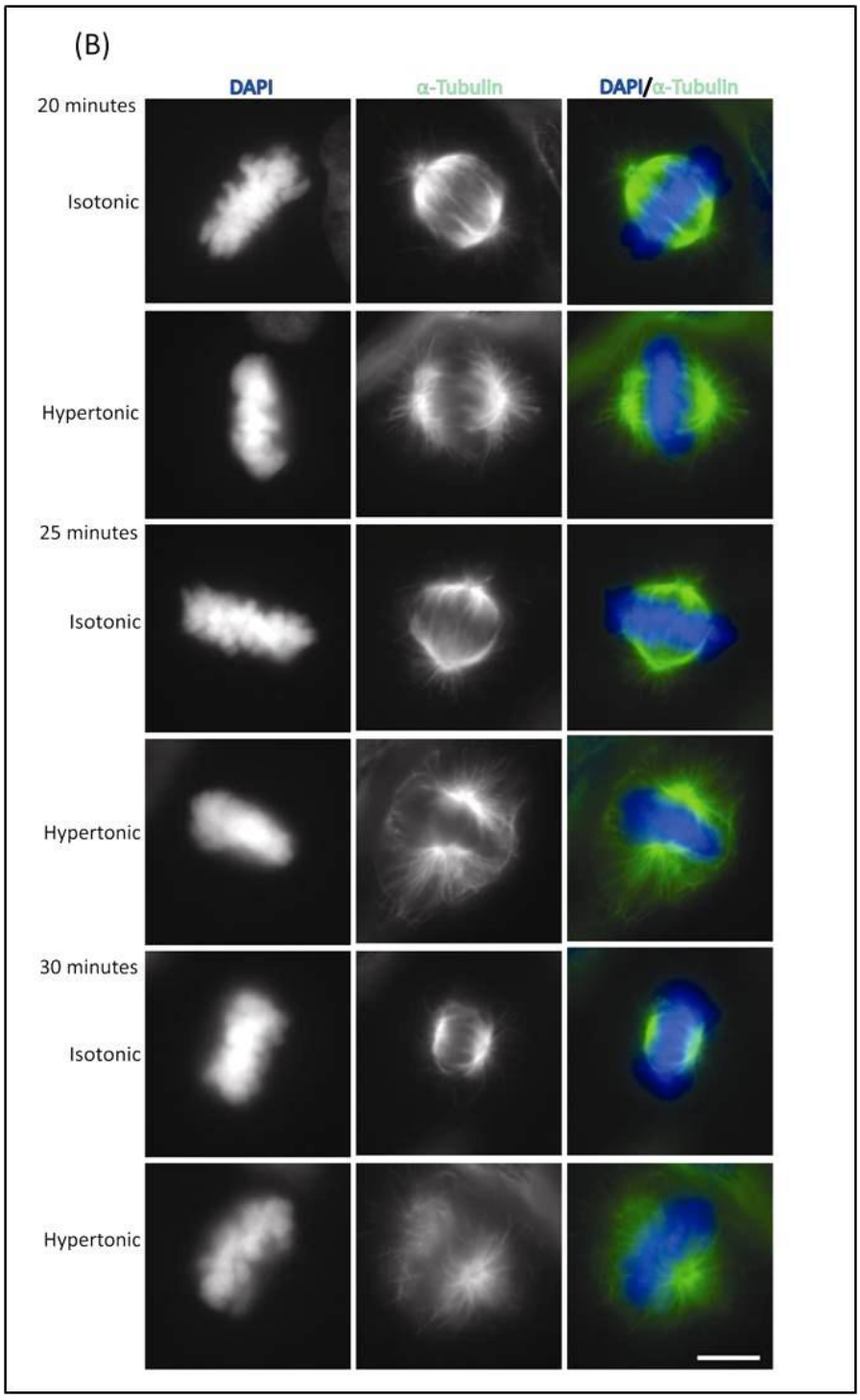
(B)
DAPI
α-Tubulin
DAPI/α-Tubulin
20 minutes
Isotonic
Hypertonic
25 minutes
Isotonic
Hypertonic
30 minutes
Isotonic
Hypertonic

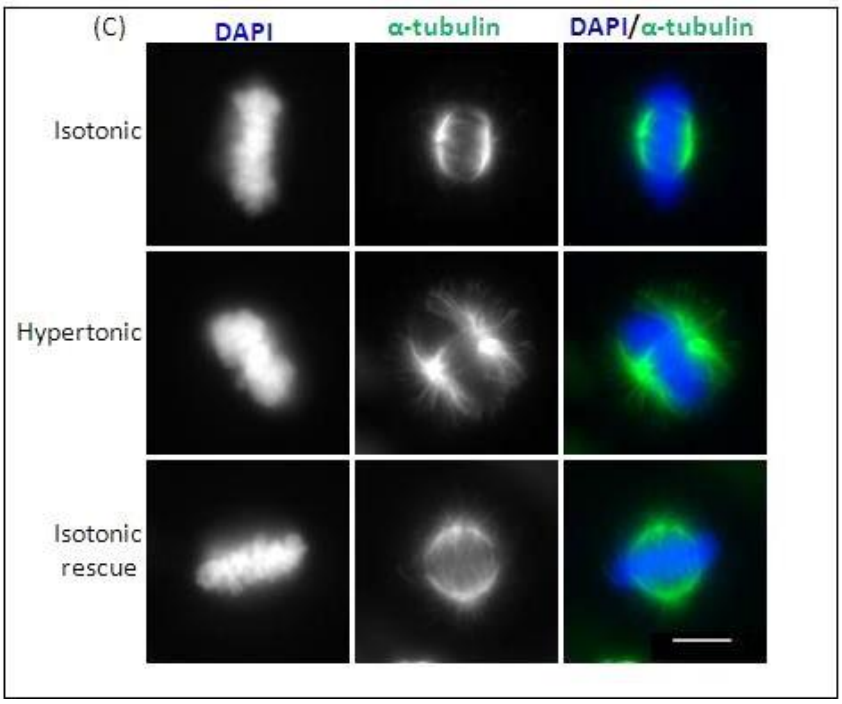

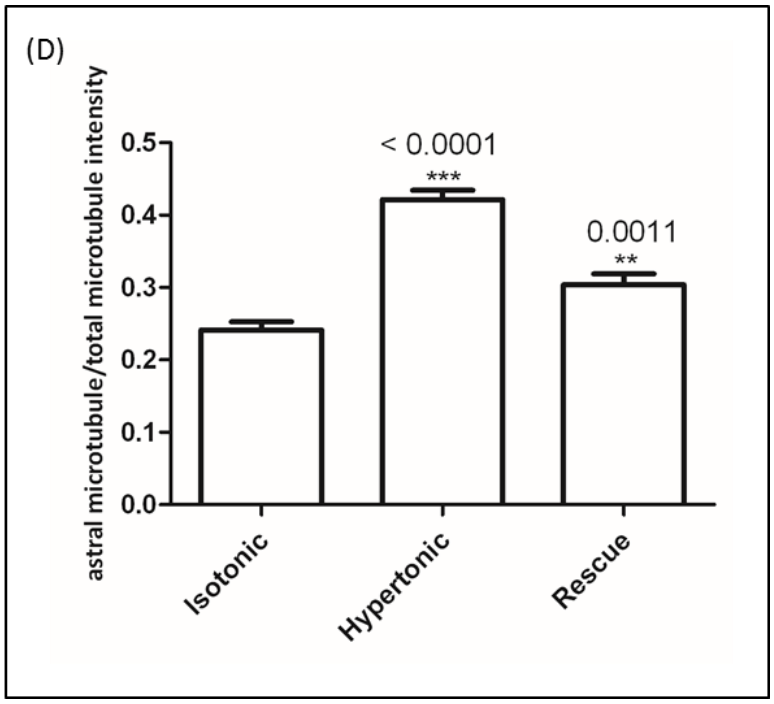

Figure 4.2 Hypertonic stress induced increase in astral microtubule is dependant on the duration of the stress and is reversible. (A), (B) HeLa cells were subjected to osmotic shock for different time points followed by staining with anti-α-tubulin (green) and DAPI (blue). Scale bar 10µm. (C) HeLa cells exposed to hypertonic media for 30 minutes was grown in isotonic media for 3 hours and stained with anti-α-tubulin (green) and DAPI (blue). Scale bar 10µm. (D) Graph showing quantification of astral microtubule intensity suggested rescue upon return to isotonic media. 100 cells from three independent experiments were imaged and analyzed using ImageJ software. Unpaired student's t-test was done and graph showing the adjusted astral microtubule intensity was plotted using Graphpad Prism software. Error bars represent mean (±SEM). *** $p < 0.001$; ** $p = 0.0011$.

4.1.3 Perturbation in the osmotic balance affects the size of the spindle.

Cells exposed to a hypertonic medium encounter loss of water and a concomitant shrinkage in cell size. The maintenance of an appropriate cell size and volume is essential for survival. Since the cell size is the predominant parameter regulating the size of subcellular structures, it was believed that the spindle size was proportional to the cell size [256]. However, this holds good only in the case of small cells and in large cells like, *Xenopus laevi* eggs, spindle size reaches an upper limit [257]. The size of the metaphase spindle is a primary factor that determines the position of the chromosome at the center of the dividing cell. An optimum length of the spindle, denoted as the pole-pole spacing during metaphase enables the proper spacing of the astral microtubules, which in turn facilitates cytokinesis and effective cell division [258]. A given cell type has a constant metaphase spindle length and alterations in this length results in cell division defects [259]. Further, recent simulation studies have suggested that cell size can control the size, oscillation and positioning of the metaphase spindle [260]. The assumptions are based on the fact that a balance between the outward pushing force and the astral microtubule-dependent cortical pulling force involving the molecular motors is required for positioning of the mitotic spindle [261, 262]. This requires control on the position through length-dependent or position-dependent forces, likely governed by cell size [259]. However, such predictions still need to be validated by additional experiments. Moreover, several physical and chemical perturbations alter the spindle size. High hydrostatic pressure or low temperature shortens spindle length [263]. Since our current results (Figure 4.1 A) suggest exposure to hypertonic stress impairs astral microtubule arrangement; the cortical pulling forces are likely to be affected.

Thus, in order to examine the involvement of cell size, the surface area of metaphase cells under hyperosmotic conditions was measured (Figure 4.3 A). The cells were stained with

DAPI and anti-pericentrin to visualize DNA and centrosomes respectively. Brightfield images were captured to obtain the cell boundary. Boundary of the cells was outlined using the ImageJ tool from the brightfield images and the surface area was measured using the software. The surface area of the cells served as a measure of the cell size. Besides cell size, the spindle size was also calculated. The distance between the spindle poles was a measure of the spindle length and the spindle width was determined by the microtubule width at the equatorial plate during metaphase (Figure 4.3 B). HeLa cells were subjected to hypertonic media and stained with anti-pericentrin to detect the spindle poles and DAPI for scoring metaphase cells for calculation of spindle length and width respectively (Figure 4.3 C). Our results do not show any significant change in the cell size (Figure 4.3 D) and spindle length (Figure 4.3 E) however; the width of the spindle is less in comparison to the control cells (Figure 4.3 F).

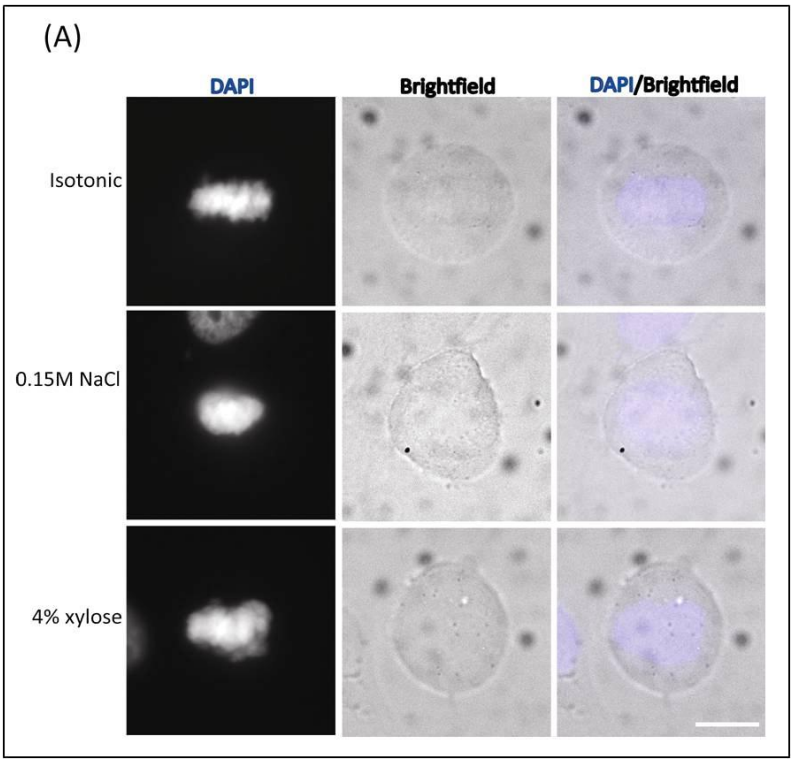

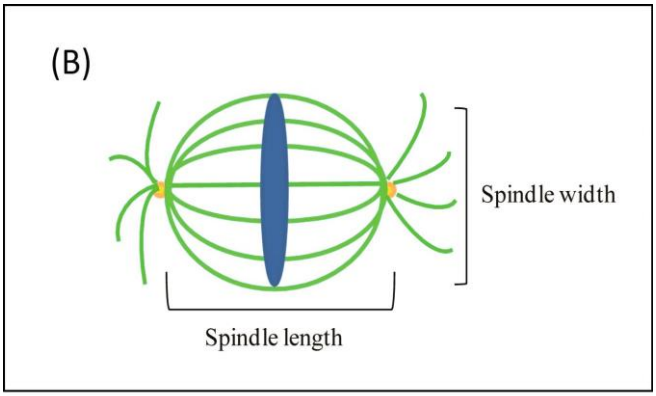
(B)
Spindle width
Spindle length

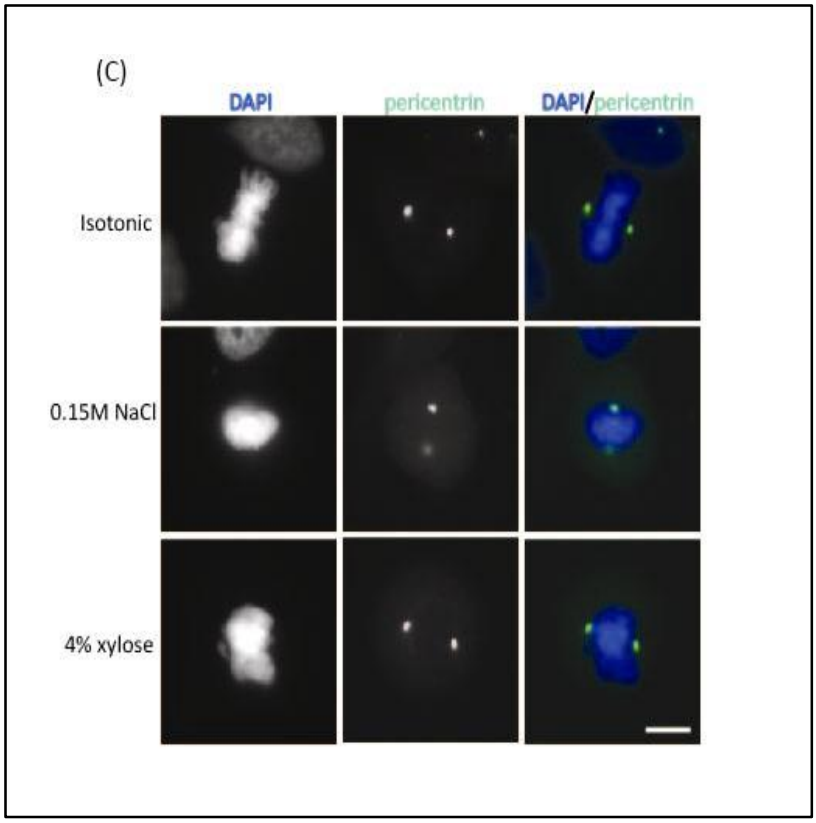
(C)
DAPI
pericentrin
DAPI/pericentrin
Isotonic
0.15M NaCl
4% xylose

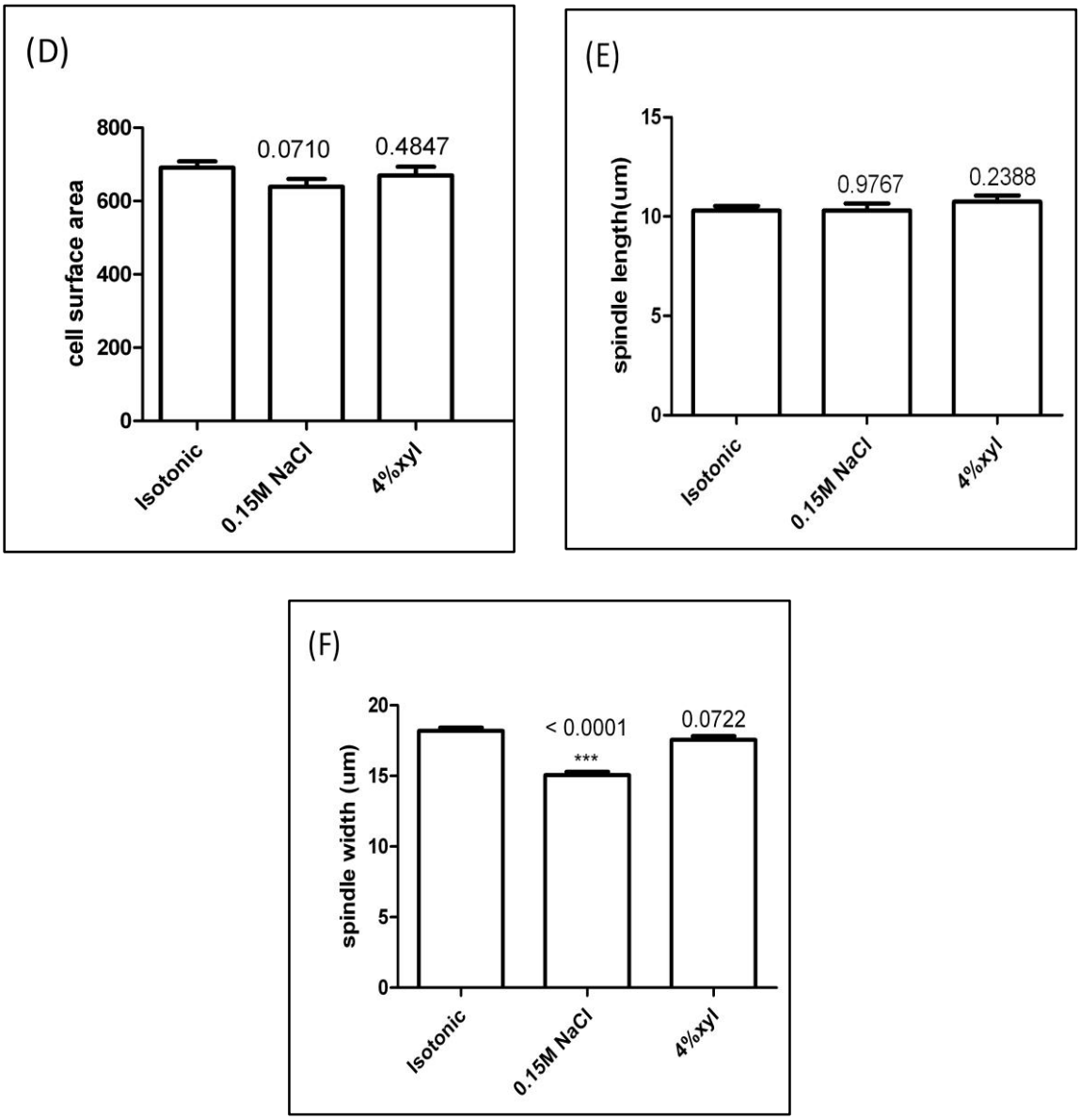

Figure 4.3 Hypertonic stress affects the size of the metaphase spindle. (A) HeLa cells were subjected to media containing 0.15M NaCl or 4% xylose, followed by staining with DAPI. Cells were imaged under brightfield to view the cell boundary. Cells grown in isotonic media served as control. Scale bar 10µm. (B) Schematic representation showing the measurement of spindle length and spindle width. (C) HeLa cells treated with 0.15M NaCl and 4% xylose were stained with anti-pericentrin and DAPI for measuring the spindle length and width. 120 cells from three independent biological repeats were images and analyzed. Unpaired student's t-test was performed using Graphpad Prism software. (D) Surface area of the cells calculated by ImageJ was plotted. P value shown on graph denotes the difference is not significant. (E) Spindle length, calculated by measuring the distance between spindle poles and (F) spindle width measured by the width of the metaphase plate perpendicular to the spindle axis was plotted. Error bars represent mean (±SEM). ***p <0.0001.

4.1.4 Disruption of the osmotic balance results in mitotic spindle misorientation and positioning

Astral microtubules serve as a physical link between the spindle and cortex and hence play an essential role in controlling spindle orientation and positioning in a metaphase cell [264]. In order to study the role of osmotic pressure in mitotic spindle orientation, HeLa cells were exposed to hypertonic challenge and then subjected to immunofluorescence staining with anti-pericentrin. Z-stack images were captured at an interval of 0.5 μm and the angle of spindle relative to the substratum was calculated. Cells grown in isotonic media served as control. Spindle orientation was calculated as illustrated (Figure 4.4 A).

From the images of the z-stacks, we found that in majority of the control cells, both the centrosomes were focused on the same z-plane (Figure 4.4 B). Under normal conditions, the mitotic spindle lies relatively parallel to the substratum. In contrast, in cells treated with hyperosmotic media, the mitotic centrosomes were not focused on the same plane (Figure 4.4 C, D). Measuring the spindle angle further supported this observation. The mean spindle angle (θ) in control cells was close to zero (Figure 4.4 E). The mean spindle angles of cells treated with 0.15M NaCl or 4% xylose were significantly higher than the control cells (Figure 4.4 E). These results suggest that the mitotic spindle apparatus is not parallel to the substratum and thus is mis-oriented.

Taken together, our data shows the when osmotic balance is disturbed it results in misorientation of the mitotic spindle, characterized by an increase in the spindle angle. Additionally, osmotic balance is vital for positioning the spindle in the center of the cell.

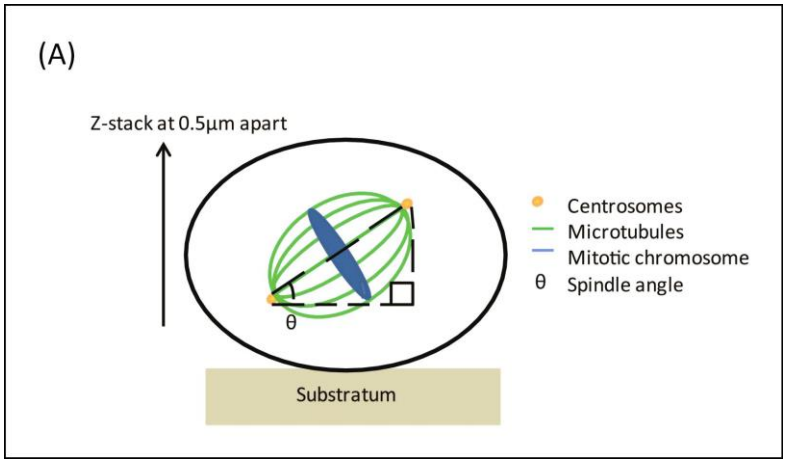
(A)
Z-stack at 0.5µm apart
θ
Substratum
Centrosomes
Microtubules
Mitotic chromosome
θ Spindle angle

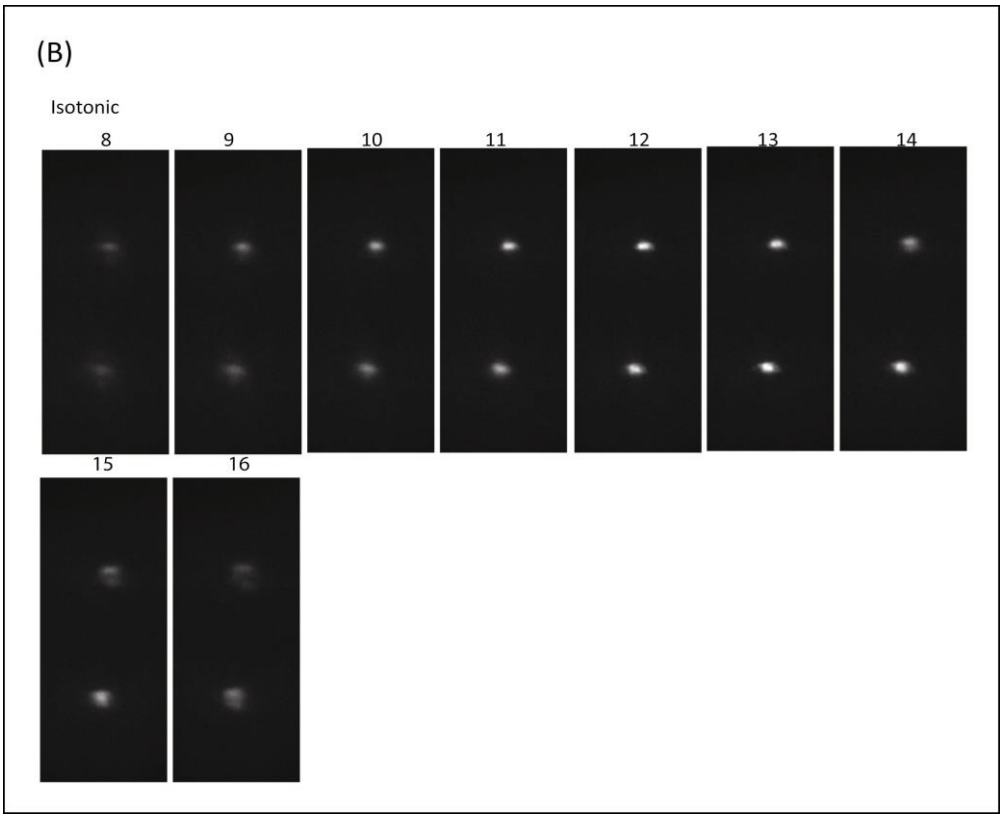
(B)
Isotonic
8
9
10
11
12
13
14
15
16

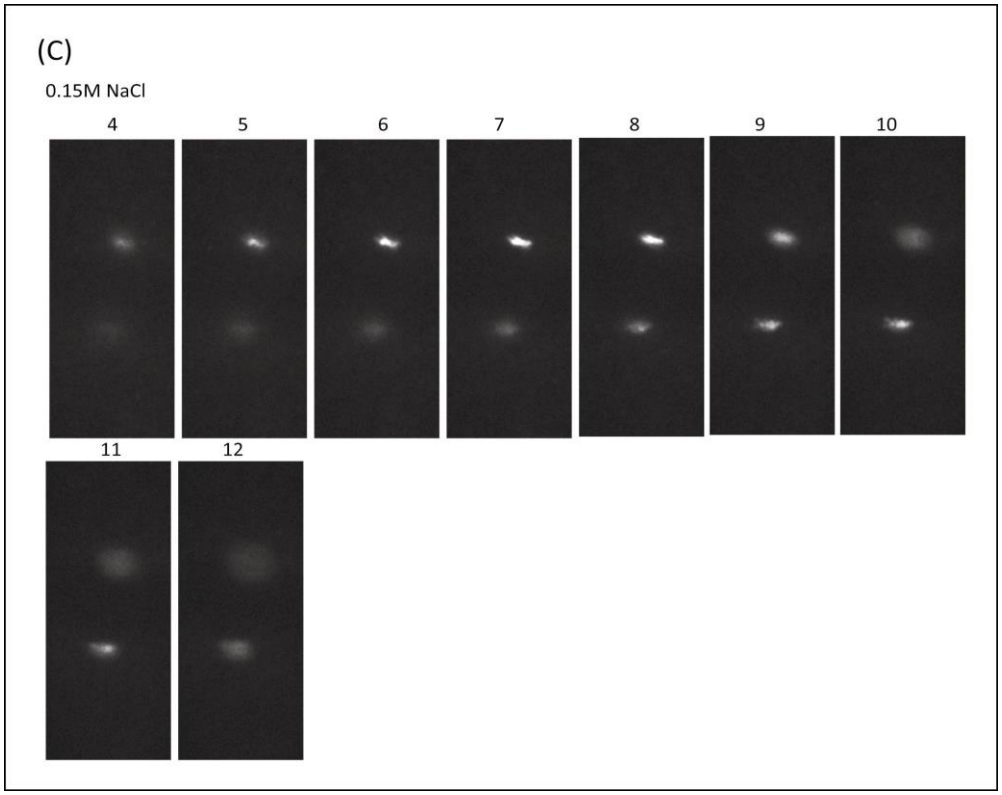
(C)
0.15M NaCl
4
5
6
7
8
9
10
11
12

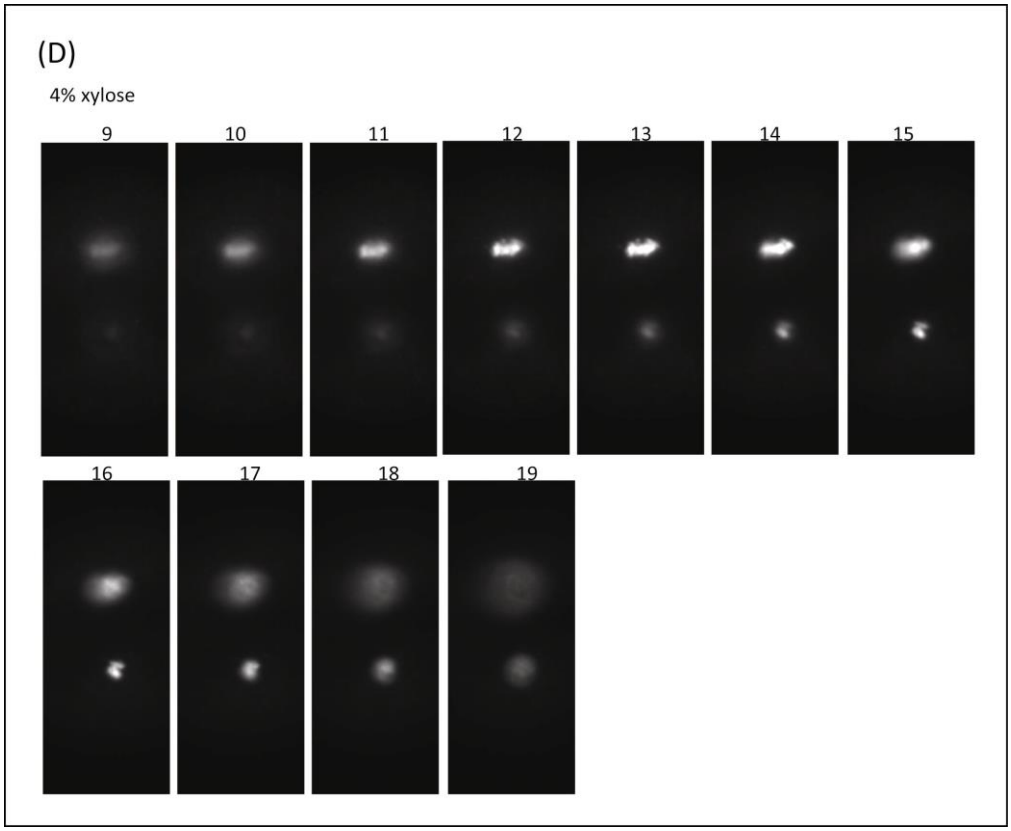
(D)
4% xylose
9
10
11
12
13
14
15
16
17
18
19

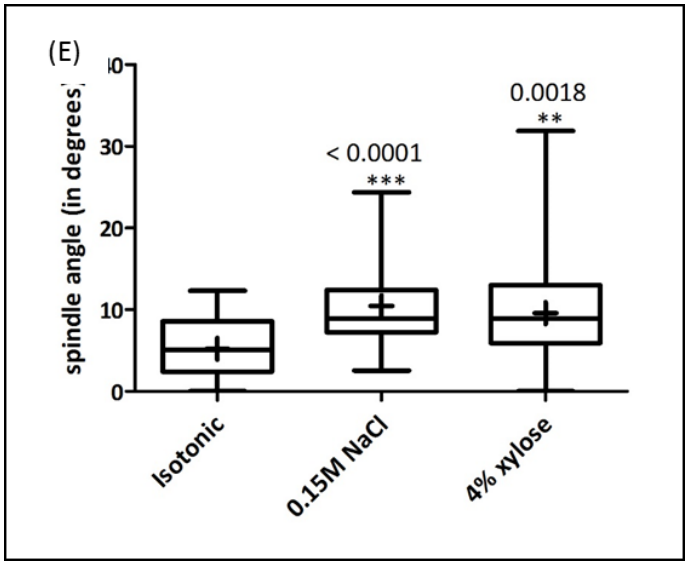

Figure 4.4 Hypertonic stress results in a misorientation of metaphase spindle, characterized by an increase in spindle angle relative to the substratum. (A) Schematic representation showing calculation of spindle angle. Following immuno-staining, cells were imaged for z-stack at a distance of 0.5µm. The orientation of the metaphase spindle, relative to the substratum was measured by calculating the spindle angle (θ) using inverse trigonometric function, θ= sin-1 (A/B), where θ denotes the spindle angle, in degrees, relative to the substratum; A represents the z axis distance between spindle poles in µm; and B denotes x-y axis distance between spindle poles in µm. (B), (C), (D) HeLa cells seeded on fibronectin coated glass coverslips and subjected to isotonic and media containing 0.15M NaCl or 4% xylose respectively. Treated cells were then immune-stained with pericentrin to visualize centrosomes. DAPI staining was carried out to visualize mitotic chromosomes. Numbers above the images indicate the Z-plane of the respective image. All images are taken under 63X objective. (E) Graph displaying the spindle angles under different osmotic conditions. The spindle angles were calculated as described in the Methods section. The mean spindle angle (θ) for each condition were then calculated and plotted. Experiment was performed in quadruplicates; n=160 for each condition. Box-and-whiskers diagram; box lines represent upper quartile, median and lower quartile; whiskers represent 5-95 percentile, + represents the mean spindle angle. Error bars represent mean (±SEM). *** represents $p \leq 0.001$, ** denotes p=0.0018.

4.1.5 Ion channels play an essential role in the maintenance of cortical rigidity in mitotic cells

Ion channels maintain the appropriate cell volume by increasing the intracellular osmotic pressure and restore normal cell volume by compensatory regulatory volume increase after exposure to the hypertonic stress. Our studies suggest that perturbation of the osmotic gradient affects spindle assembly, characterized by an aberrant increase in astral microtubule. Since ion channels are involved in the rescue of the cells following osmotic shock, they might be important in the organization of the cortical cytoskeleton and

spindle morphology. Therefore, we assessed the role of the ion channels implicated in regulatory volume increase by using inhibitors of the respective channels. HeLa cells were treated with 50µM EIPA (Na^+/H^+antiporter inhibitor) or 50µM NPPB (Cl^- exchanger inhibitor) for 1 hour, fixed and then immuno-stained using anti-α-tubulin (green) and DAPI (blue) (Figure 4.5 A). The ratio of the background corrected integrated astral microtubule intensity to total intensity was plotted (Figure 4.5 B). Inhibition of Na/H+ exchanger and the Cl^- ion channels was found to result in a significant increase in astral microtubules radiating towards the cell cortex.

Next, we assayed the role of ion channels in maintenance of cortical rigidity of mitotic cells using the micropipette aspiration assay (Figure 4.5 C). Inhibition of these ion transporters would block regulatory volume increase and might affect cell rounding and rigidity. HeLa cells were treated with 50µM EIPA (Na^+/H^+antiporter inhibitor) and 50µM NPPB (Cl^- exchanger inhibitor**)** for 1 hour as before. The deformation of mitotic cells in response to suction pressure by the micropipette was measured (Figure 4.5 D) and Young's modulus was calculated. Young's modulus is a direct measure of cortical rigidity. As expected, mitotic cells treated with inhibitors of Na^+/H^+antiporter and Cl^- exchanger displayed lower value of Young's modulus and hence less in cortical rigidity compared to untreated control cells (Figure 4.5 E).

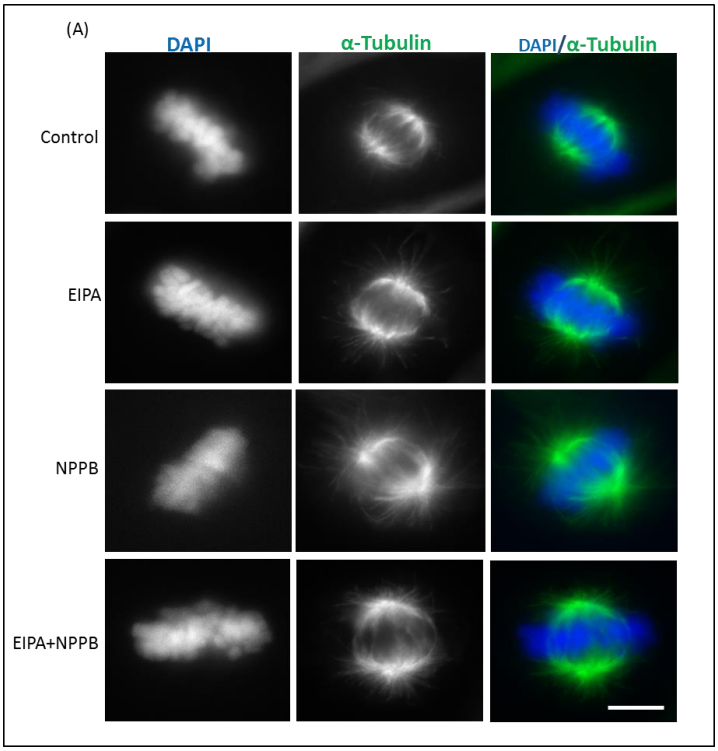
(A)
DAPI
α-Tubulin
DAPI/α-Tubulin
Control
EIPA
NPPB
EIPA+NPPB

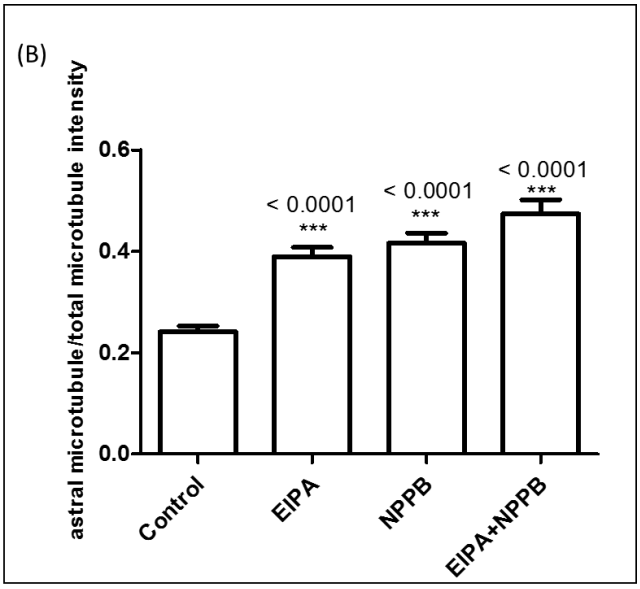
(B)
astral microtubule/total microtubule intensity
0.6
0.4
0.2
0.0
< 0.0001
***
< 0.0001
***
< 0.0001
***
Control
EIPA
NPPB
EIPA+NPPB

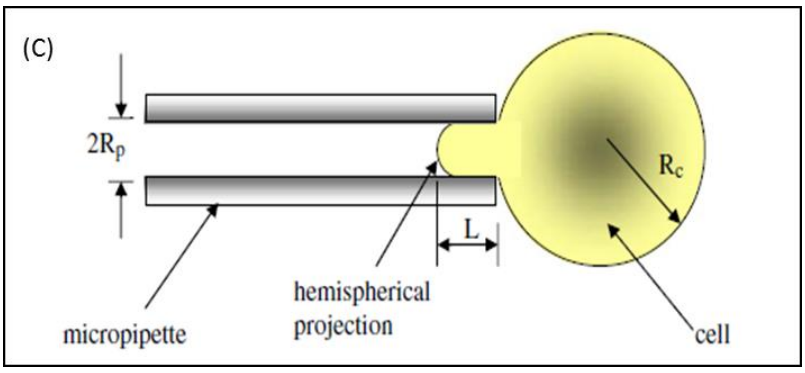
(C)
2Rp
Rc
L
hemispherical
projection
micropipette
cell

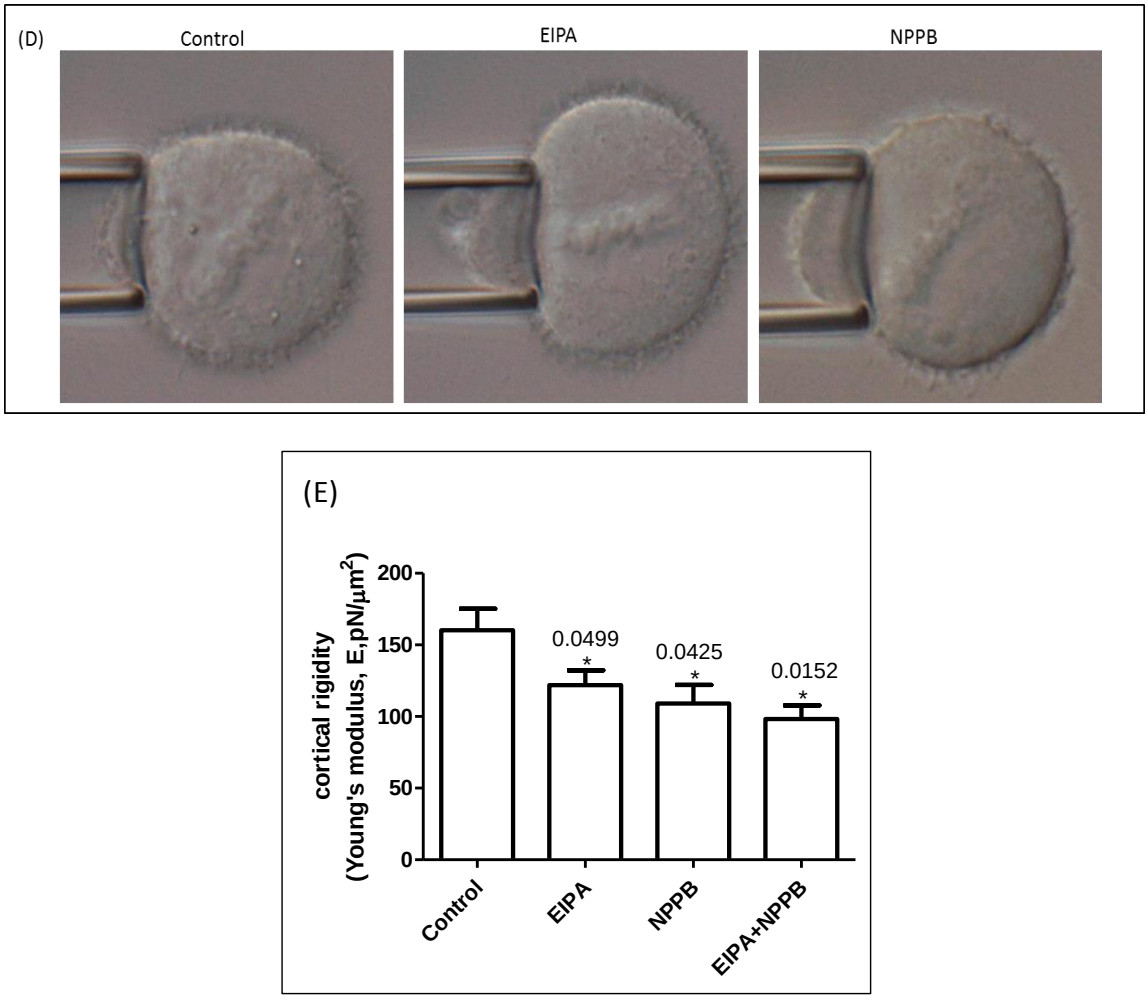

Figure 4.5 Ion channels play a vital role in the proper astral microtubule arrangement and cortical rigidity of mitotic cells. (A) HeLa cells treated with EIPA or NPPB and both for 1 hour was subjected to staining with anti-α-tubulin (green) and DAPI (blue). Untreated cells serve as the negative control. Scale bar 10μm. (B) 150 cells from three independent biological repeats were imaged and analyzed. The corrected astral microtubule intensity was measured as described in the Methods using ImageJ software. Unpaired student's t-test was performed using Graphpad Prism software for statistical analysis. Quantification of the astral microtubule intensity showed a significant increase upon inhibition of ion channels. Error bars represent mean (±SEM). ***p < 0.0001. (C) Graphical representation of micropipette aspiration assay for measurement of cortical rigidity [265]. (D) Mitotic cells treated with the respective ion channel inhibitors were collected by mechanical shake off and subjected to suction by the micropipette. (E) Deformation obtained was used to calculate Young's modulus, which is a direct measure of cortical rigidity. Graph showing the Young's modulus of treated cells show a significant decrease upon perturbation of ion channels. Error bars represent mean (±SEM). Experiment was performed in triplicate. n>20. *p = 0.0499, *p = 0.0425, *p=0.0152.

4.1.6 Ion channels enable the proper orientation of metaphase spindle

As mentioned before, astral microtubules play an important role in spindle orientation by establishing links with the cortex. Since our previous finding shows aberrant increase in

astral microtubules upon inhibition of ion channels, we proceeded to study the effects on the spindle orientation.

In order to determine spindle orientation, HeLa cells were grown on fibronectin-coated coverslips, treated with EIPA and NPPB for one hour and stained with anti-pericentrin. Z-stack images at a distance of 0.5 μm were captured (Figure 4.6 A, B, C) and spindle angle was calculated as described above. We observed an increase in the spindle angle upon treatment with EIPA and NPPB (Figure 4.6 D).

Majority of the cell types confront the hypertonicity-induced cell shrinkage by an adaptive response, termed as regulatory volume increase, brought about by the activation of RVI is brought about the combined activation of the Na^+/H^+ exchanger (NHE) and Cl^-/HCO_3^- antiporter and Na^+ -K^+ -$2Cl^-$ symporter (NKCC), depending on the cell type [166-168]. Na+/H+ exchanger isoform 1 (NHE1) is found in all cells in mammals and is involved in numerous physiological processes, including regulation of intracellular pH, cellular volume, cytoskeletal organization, heart disease and cancer [183, 266, 267]. Since we observed defects in spindle orientation upon inhibition of Na^+/H^+ antiporter induced by EIPA treatment, we confirmed this result by using NHE1 knockdown cell lines. The following siRNA sequence was used to silence NHE1 gene: NHE1 siRNA-1 sense: CCCUGUUAAUCAUUCCGUCACUGAU **(**RNA Sequence 5' to 3'); NHE1 siRNA-1 antisense: AUCAGUGACGGAAUGAUUAACAGGG **(**RNA Sequence 5' to 3'). Cells transfected with siRNA targeting Luciferase serve as negative control for comparison. Transient knockdown was performed as mentioned in Methods section 2.2.4. As expected, NHE1 knockdown cells show defects in spindle orientation, as characterized by an increase in the spindle angle relative to substratum (Figure 4.6 H).

Taken together, these findings suggest ion channels play an essential role in regulating the orientation of the spindle during metaphase.

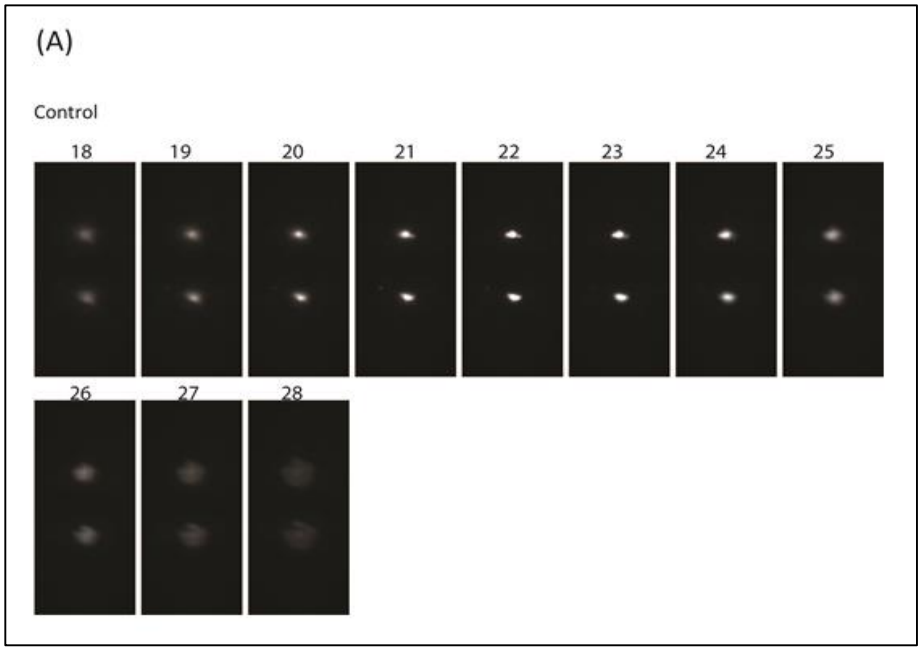
(A)
Control
18
19
20
21
22
23
24
25
26
27
28

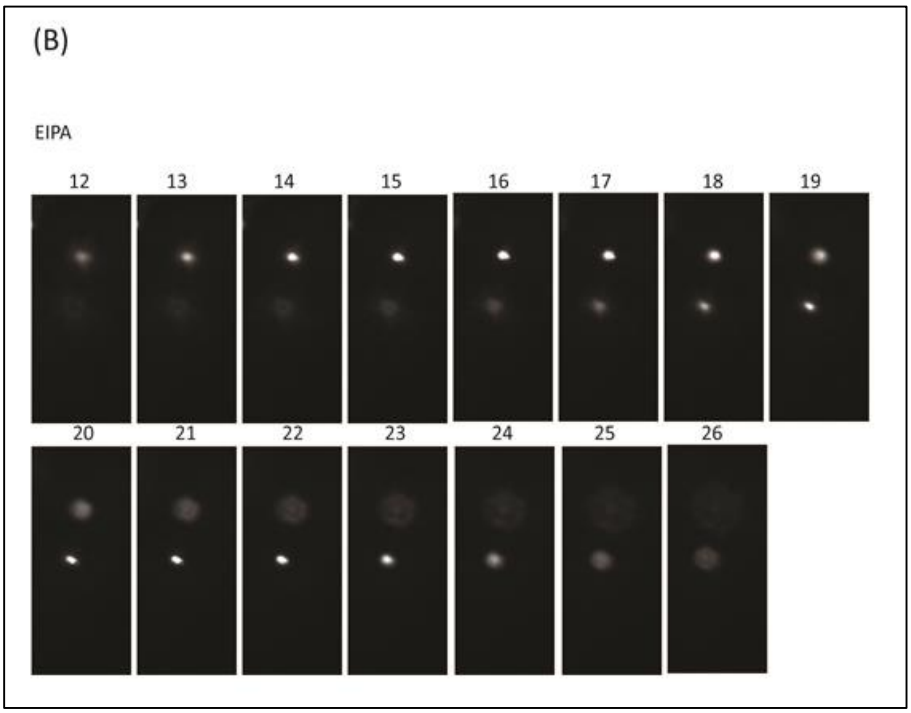
(B)
EIPA
12
13
14
15
16
17
18
19
20
21
22
23
24
25
26

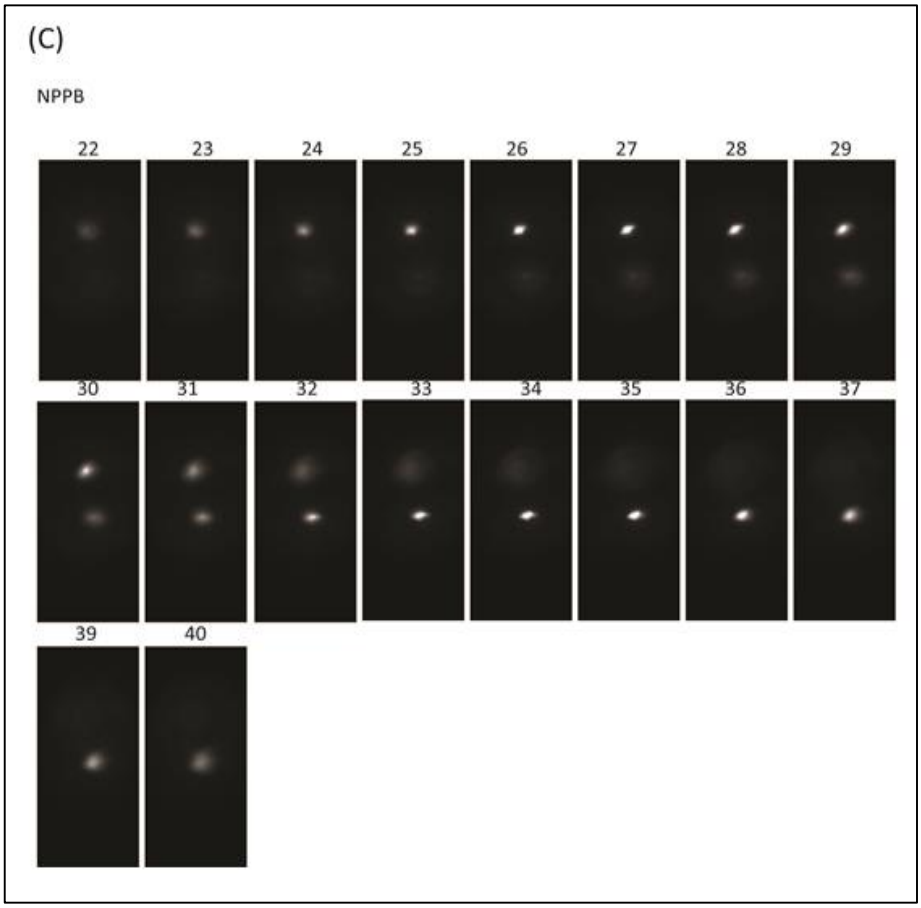
(C)
NPPB
22
23
24
25
26
27
28
29
30
31
32
33
34
35
36
37
39
40

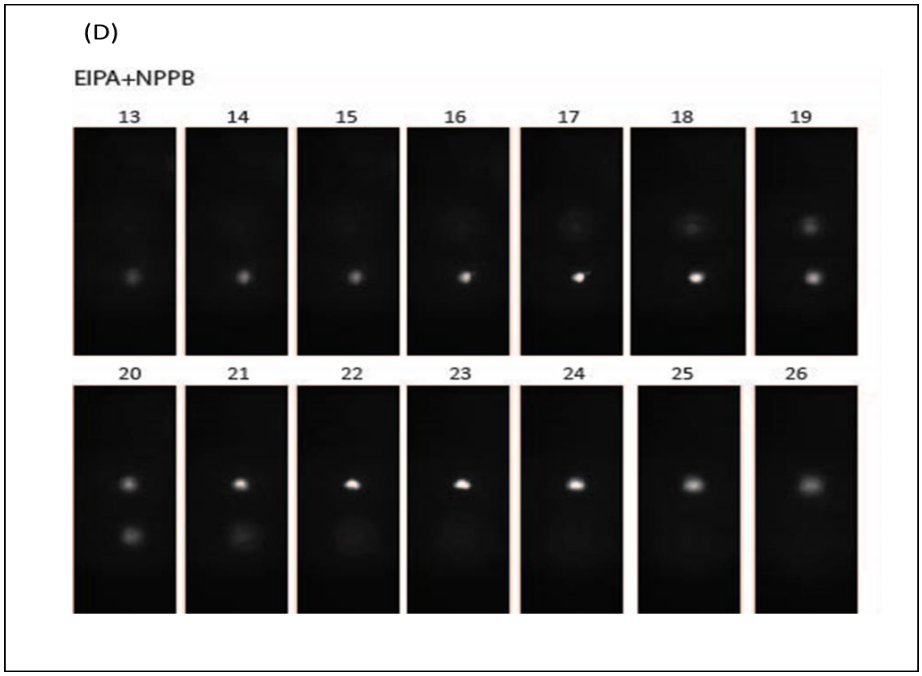
(D)
EIPA+NPPB
13
14
15
16
17
18
19
20
21
22
23
24
25
26

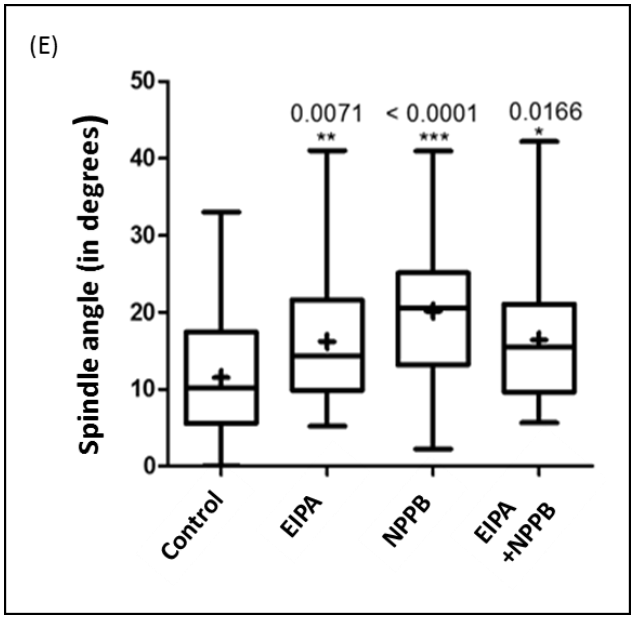
(E)
Spindle angle (in degrees)
50
40
30
20
10
0
0.0071
**
< 0.0001
***
0.0166
*
Control
EIPA
NPPB
EIPA +NPPB

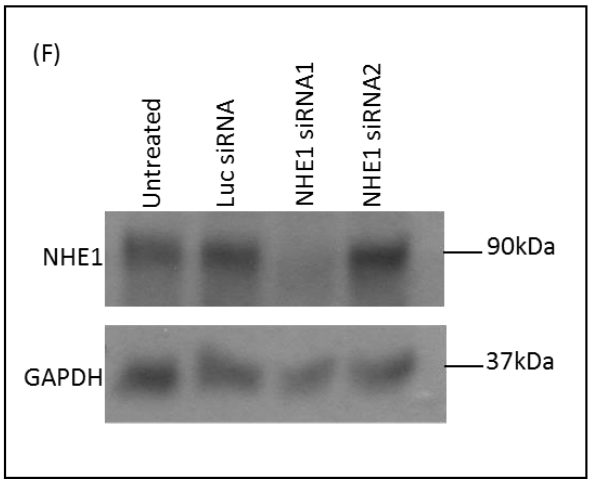
(F)
Untreated
Luc siRNA
NHE1 siRNA1
NHE1 siRNA2
NHE1
90kDa
GAPDH
37kDa

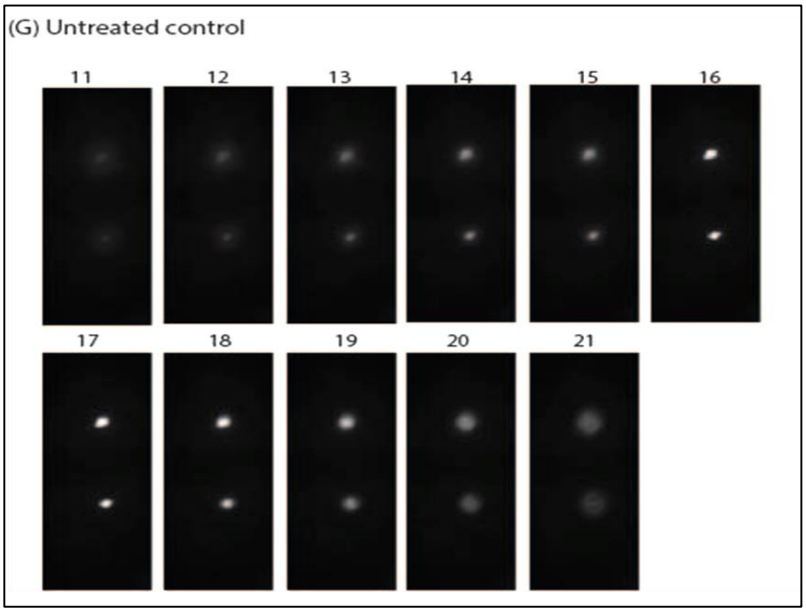
(G) Untreated control
11
12
13
14
15
16
17
18
19
20
21

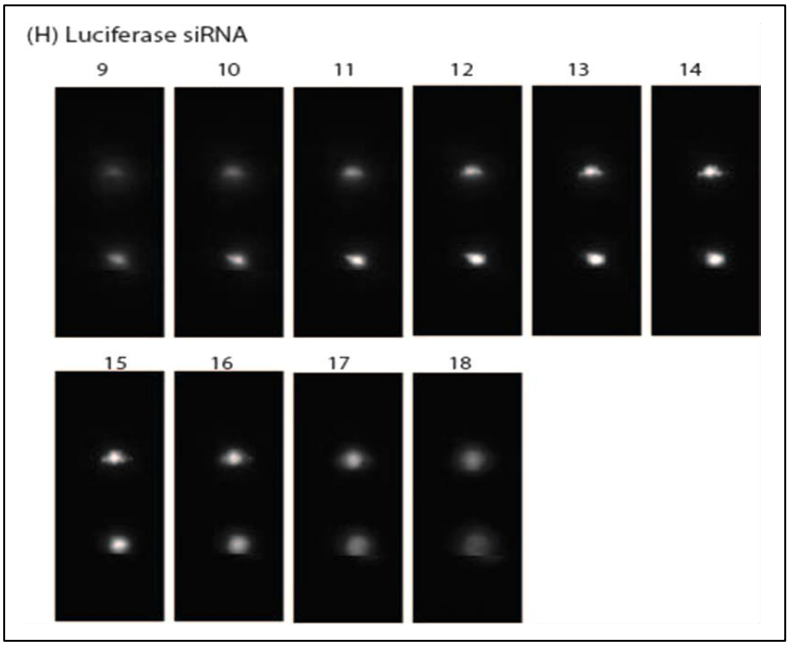
(H) Luciferase siRNA
9
10
11
12
13
14
15
16
17
18

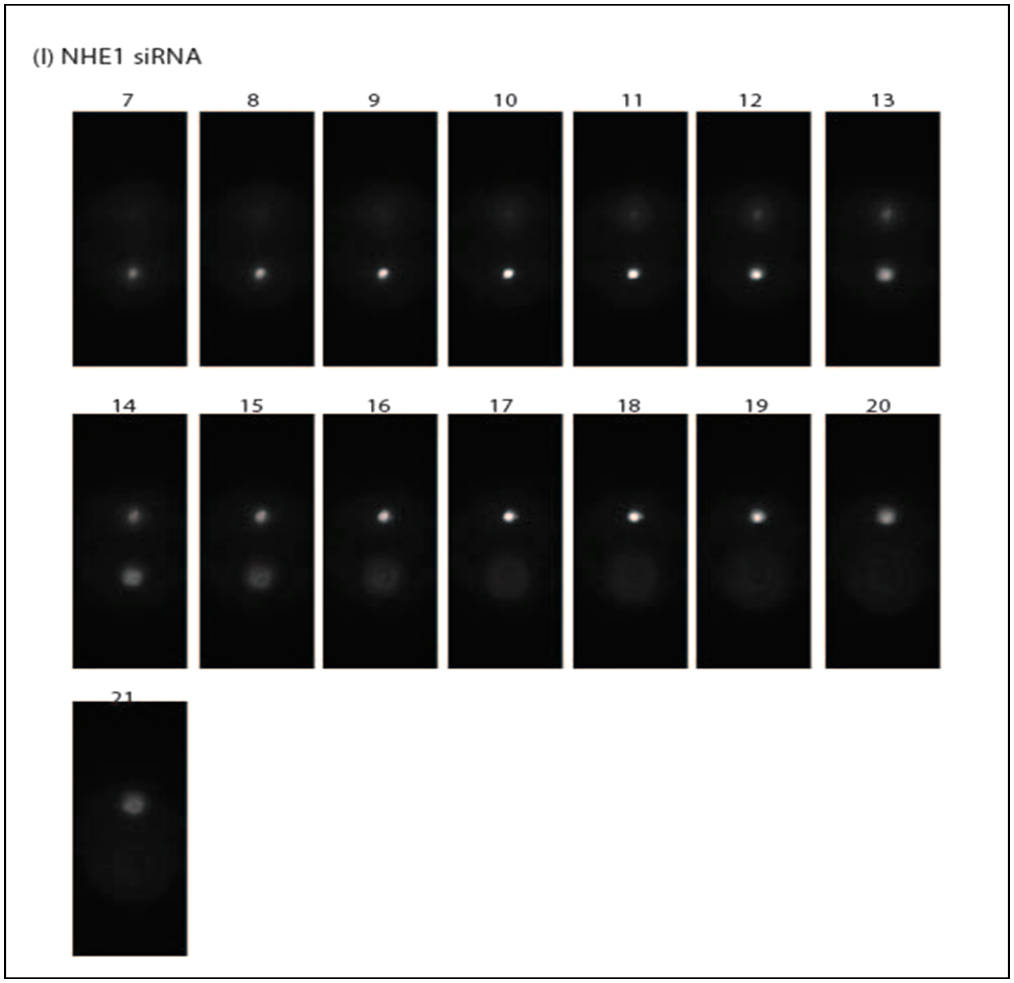
(I) NHE1 siRNA
7
8
9
10
11
12
13
14
15
16
17
18
19
20
21

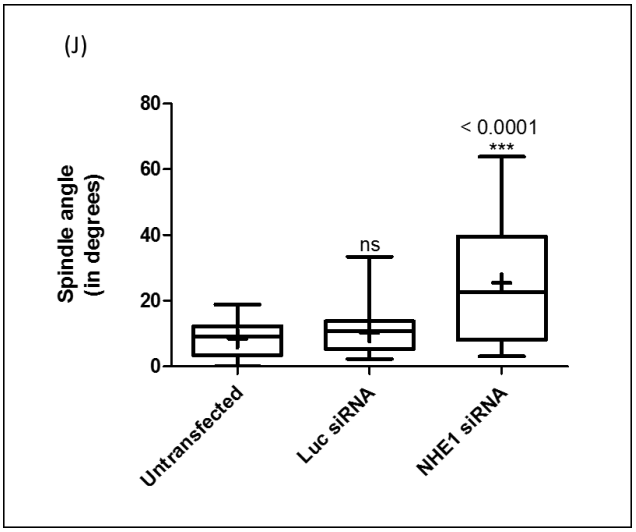

Figure 4.6 Inhibition of Na^+/H^+antiporter and Cl^- exchanger resulted in spindle misorientation. **(**A), (B), (C), (D) HeLa cells seeded on Fibronectin coated glass coverslips and subjected to isotonic and media containing EIPA or/and NPPB. Treated cells were then immuno-stained with pericentrin to visualize centrosomes. DAPI staining was carried out to visualize mitotic chromosomes. Numbers above the images indicate the Z-plane of the respective image. (E) The spindle angle was calculated as described in the Methods section. 180 cells from four independent biological repeats were imaged, analyzed using ImageJ software and plotted with Graphpad Prism software. Box-and-whiskers diagram; box lines represent upper quartile, median and lower quartile; whiskers represent 5-95 percentile, + represents the mean spindle angle. Unpaired student's t-test was used for statistical analysis. Error bars represent mean (±SEM). *** represents $p < 0.0001$, ** denotes $p=0.0071$, * represents $p= 0.0166$. (F) HeLa cells were transfected with 200 picomole Luciferase (Luc) siRNA, NHE1 siRNA1 and NHE1 siRNA2 for 48 hours and subjected to Western Blotting using NHE1 antibody. Cells transfected with siRNA targeting Luciferase (Luc siRNA) serve as negative control. Untransfected cells were also included as control for comparison. GAPDH was used as a loading control. (G), (H), (I) HeLa cells seeded on fibronectin coated glass coverslips were transfected with the respective siRNAs for 48 hours and then immuno-stained with pericentrin to visualize centrosomes. DAPI staining was carried out to visualize mitotic chromosomes. Numbers above the images indicate the Z-plane of the respective image. (J) Graph showing increased spindle angle upon NHE1 knockdown. 100 cells from three independent biological repeats were imaged and analyzed using ImageJ software. Unpaired student's t-test was used for statistical analysis. Error bars represent mean (±SEM). *** represents $p < 0.0001$.

4.1.7 Hypertonic stress results in the activation of ERM proteins and cortical rigidity in mitotic cells

In order to establish a connecting link between the observed defects in astral microtubule arrangement, spindle misorientation and the modulation of the osmotic pressure, we proceeded to study the involvement of ERM proteins. The ERM proteins have been reported to act as cross-linkers between the plasma membrane and the underlying actin cortex. As mentioned earlier, the ERM proteins are activated upon phosphorylation.

Studies in *Drosophila*, where a single protein moesin, is present have shown that the active form of moesin is redistributed to the cell cortex, thereby promoting the rearrangement of actin filaments [268]. This organization triggers an increase in cortical rigidity and favors mitotic cell rounding [269]. In order to investigate the role of hypertonic stress in the activation of ERM proteins, the effect of the changes in the hydrostatic pressure on the phosphorylation status of the ERM proteins was investigated.

HeLa cells were subjected to the hypertonic media for different times from 3 minutes to 15 minutes (Figure 4.7 A). Different time points were chosen for our study initially since the effect of the osmotic stress is rapid and transient. Since, we observe changes in astral microtubule arrangement when cells are exposed to hypertonic stress for a duration of 30 minutes, we examined the phospho ERM levels at this time point also (Figure 4.7 B).Total cell protein lysates were harvested and subjected to Western Blotting. We found that hypertonic media induced phosphorylation and hence, activation of the ERM proteins (Figure 4.7 A, B). Densitometric analysis of normalized phospho ERM protein levels show an increase in ERM protein phosphorylation upon hypertonic stimulation (Figure 4.7 C).

Since the active form of moesin contributes to cortical rigidity [54] and cell rounding in *Drosophila* S2 cells during mitosis, we next assessed whether the hypertonic environment affected rigidity. HeLa cells exposed to 0.15M NaCl and xylose containing media were assayed for cortical rigidity with the help of the micropipette aspiration assay. Mitotic cells were collected by mechanical shake-off, resuspended in different osmotic media and subjected to micropipette aspiration (Figure 4.7 D). As expected, the treated cells showed a significant increase in the cortical rigidity as compared to control cells (Figure 4.5 E).

Taken together, our results imply that hypertonic stress upregulated phospho-ERM protein levels and exhibit an increased cortical rigidity in mitotic cells.

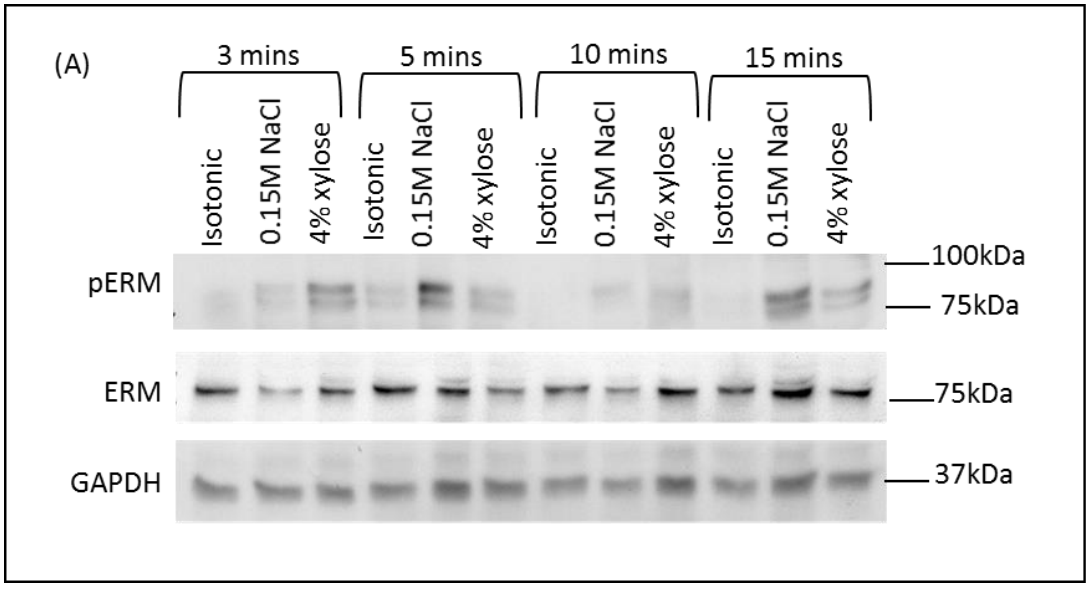
(A)
3 mins
5 mins
10 mins
15 mins
Isotonic
0.15M NaCl
4% xylose
pERM
ERM
GAPDH
100kDa
75kDa
75kDa
37kDa

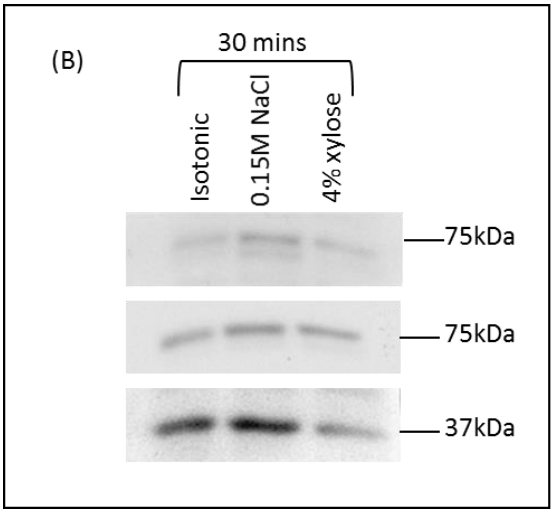
(B)
30 mins
Isotonic
0.15M NaCl
4% xylose
75kDa
75kDa
37kDa

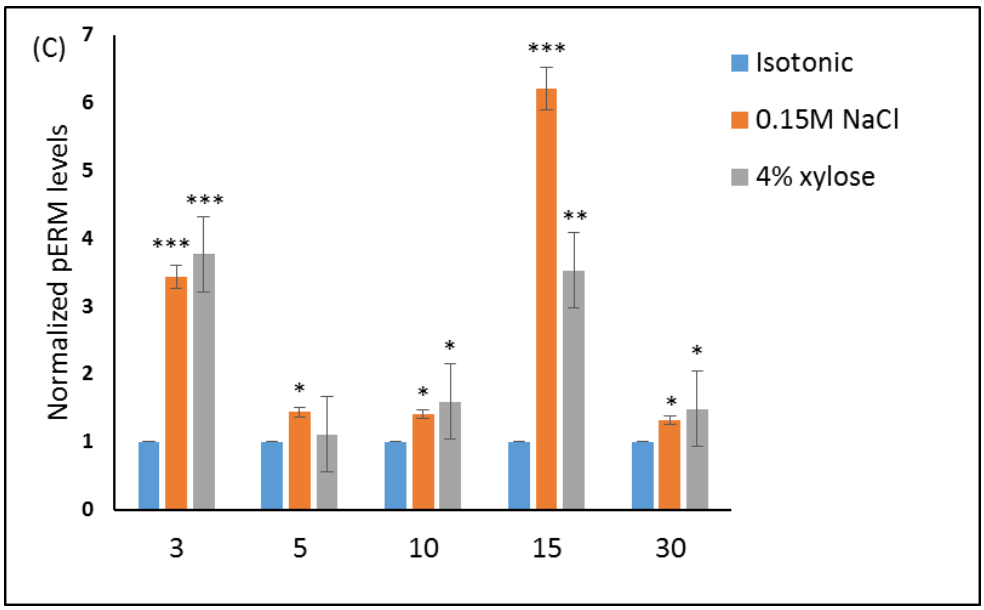
(C)
Normalized pERM levels
Isotonic
0.15M NaCl
4% xylose
3
5
10
15
30

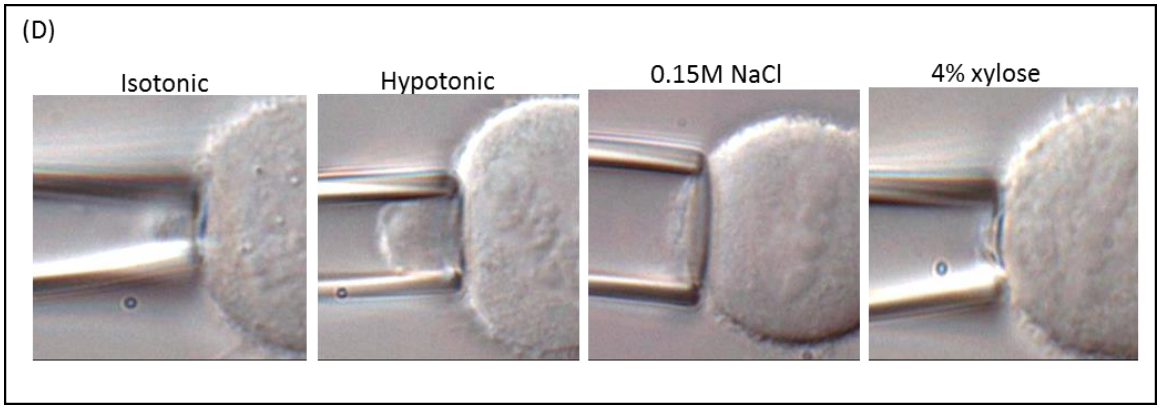

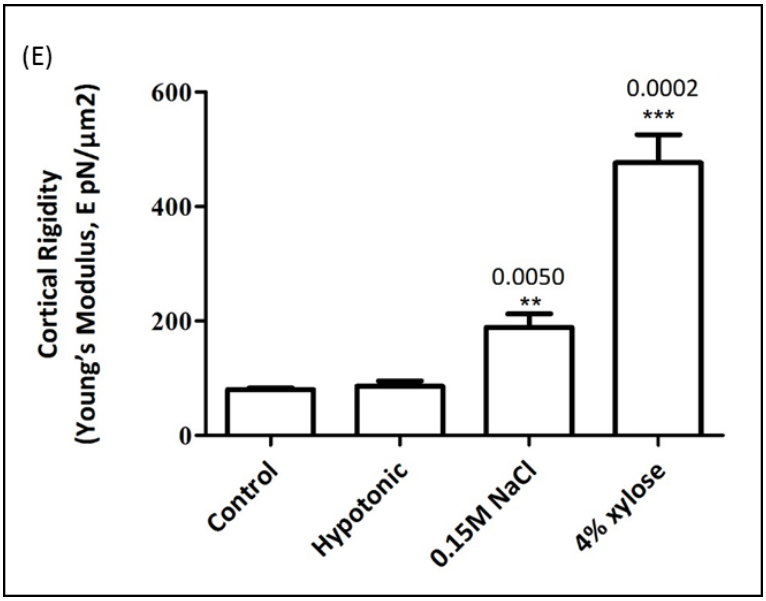

Figure 4.7 Hypertonic stress leads to activation of pERM proteins with a concomitant increase in cortical rigidity of mitotic cells. HeLa cells were subjected to hypertonic media containing 0.15M NaCl for (A) 3 minutes, 5 minutes, 10 minutes, 15 minutes and (B) 30 minutes and harvested for Western Blotting to detect phosphor ERM levels. GAPDH was used as the loading control. (C) Densitometric analysis of phospho ERM levels was performed using ImageJ software. Phospho ERM and ERM levels were normalized to the GAPDH levels and the adjusted phospho ERM was then normalized to adjusted ERM levels. Values are expressed as mean (±SEM) of three independent experiments. *** $p<0.0001$. (D) Mitotic HeLa cells were collected by mechanical shake off and resuspended in different osmotic media followed by aspiration by the micropipette. (E) Graph of the Young's modulus of treated cells shows a significant decrease upon perturbation of osmotic balance. Error bars represent Mean (±SEM). **$p=0.007$.

4.1.8 Moesin phosphorylation is responsible for the regulation of astral microtubules during metaphase.

As hypertonic milieu induced activation of ERM proteins, which are directly linked to a higher cortical rigidity, we next investigated the effect of moesin phosphorylation on the organization of metaphase astral microtubules. To achieve this, we constructed phospho-

mimic (T558D) and phospho-dead (T558A) form of moesin, which denote a constitutively active and a dominant negative form of the protein respectively. HeLa cells were transfected with the vector control, wild type moesin and the both the inactive and active moesin mutants, followed by immunostaining with anti-α-tubulin and staining with Alexa 546 secondary antibody to visualize the microtubules. Only the cells expressing GFP were selected and analyzed. The transfection efficiency was close to 80%. The cells showed very strong GFP signal upon transient transfection, which masked the signal from Alexa 546 channel, which stained tubulin. Hence, only DAPI and tubulin panel was shown as a representative image (Figure 4.8 A).

HeLa cells expressing the phopho-mimic and phospho-dead form of moesin exhibited an impaired arrangement of astral microtubules.

Thus, we conclude that moesin phosphorylation induced by osmotic stress (Figure 4.7 A, B, C) could be a possible reason for the observed defects in astral microtubule arrangement (Figure 4.1).

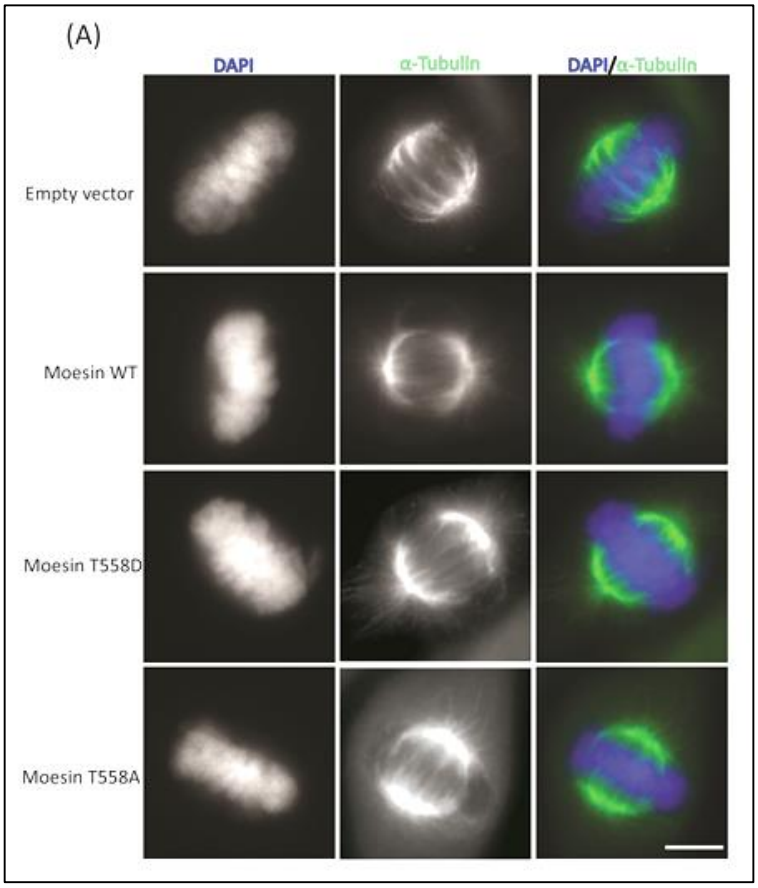

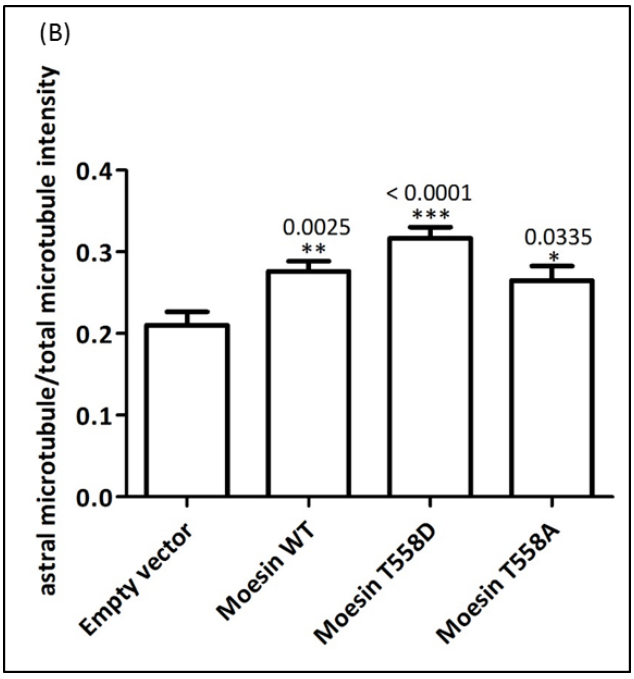

Figure 4.8 Moesin phosphorylation may control astral microtubules during metaphase. (A) HeLa cells were transfected with the vector control, Moesin wild type (WT), phopsho-mimic (T558D) and phospho-dead (T558A) and stained with anti-α-tubulin (green) and DAPI (blue). (B) The mean background-corrected integrated astral microtubule intensity from (A) was calculated using ImageJ software and plotted with Graphpad Prism software. Unpaired student's t-test was performed for statistical analysis. Graph shows significant increase ion astral microtubule intensity upon moesin

phosphorylation. Experiment was performed in triplicate; n=100. Error bars represent mean (±SEM). ***p=0.0002, *=0.0357, **=0.0100.

4.1.9 Moesin phosphorylation triggered by hypertonic stress results in the misorientation of the mitotic spindle

As mentioned earlier, the astral microtubules emanating from the spindle poles form a connecting bridge between the spindle and cell cortex. This subset of microtubules assists the spindle to orient itself correctly and also controls the plane of division [270]. Since we observed impaired astral microtubule organization in cells expressing the phospho-mimic form of moesin, we next proceeded to check if the spindle orientation is compromised under these conditions.

We transfected HeLa cells with the vector control, wild type, inactive and active mutants of moesin and performed immuno-staining with pericentrin. Z-stack images were recorded for the measurement of the spindle angle relative to the substratum. As expected, our results show defects in the spindle orientation in cells transfected with the phospho mimic form of moesin (T558D). Cells expressing the vector control have spindle angles close to zero. In contrast, cells transfected with the active moesin construct (T558D) exhibit higher spindle angles. As stated above, only the cells expressing GFP were selected and analyzed. The transfection efficiency was close to 80%. The cells showed very strong GFP signal upon transient transfection, which masked the signal from Alexa 546 channel which stained pericentrin. Hence, only DAPI and pericentrin panel was shown as a representative image

Taken together, we propose that the defects in spindle orientation when cells are under hypertonic stress could be due to the hyper-activation of moesin.

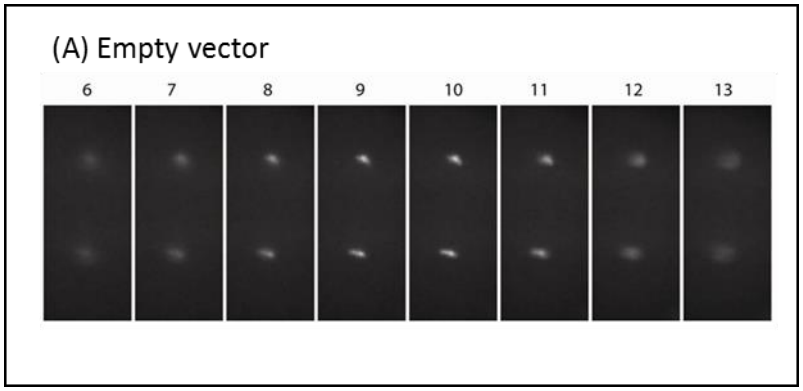
(A) Empty vector
6
7
8
9
10
11
12
13

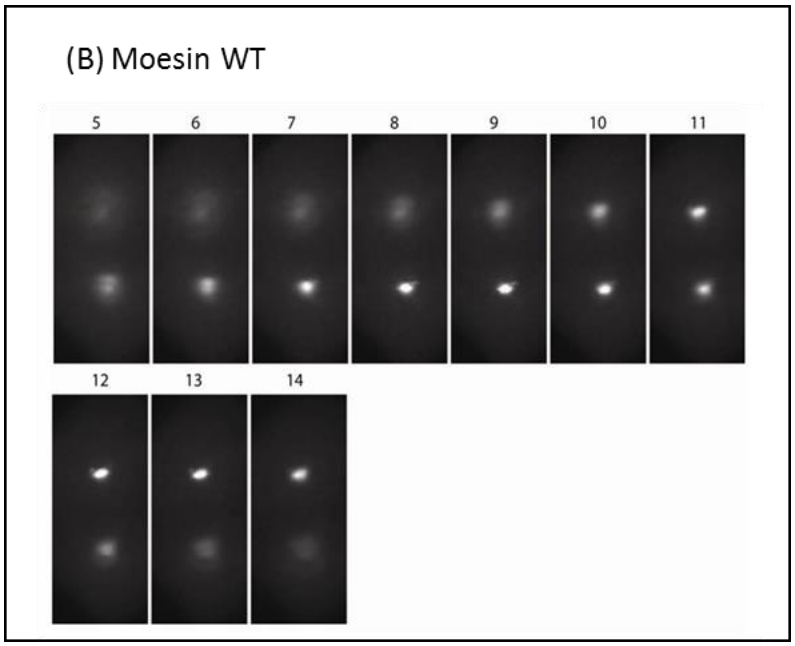
(B) Moesin WT
5
6
7
8
9
10
11
12
13
14

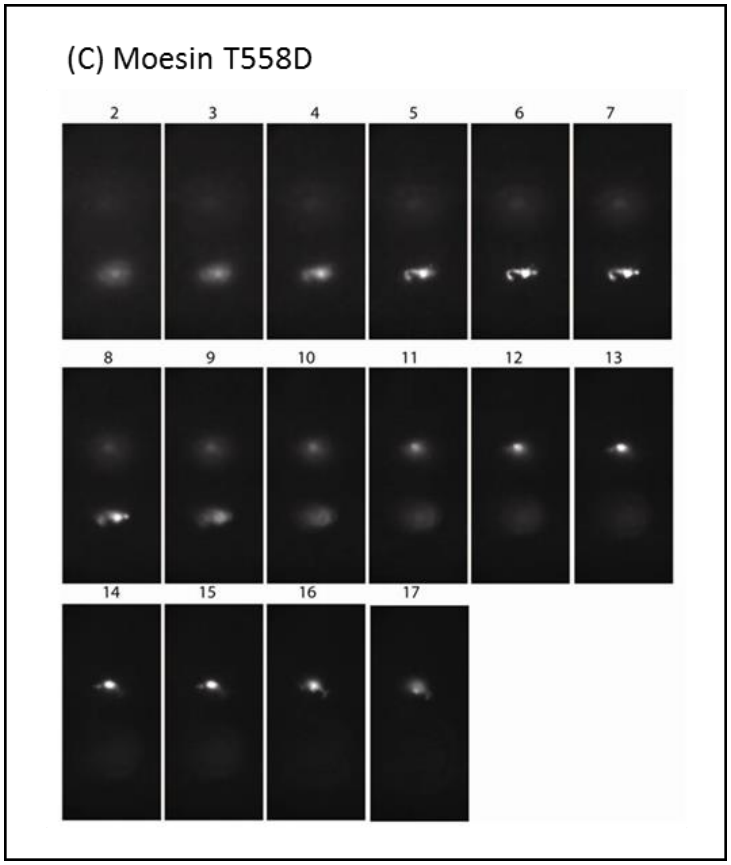
(C) Moesin T558D
2
3
4
5
6
7
8
9
10
11
12
13
14
15
16
17

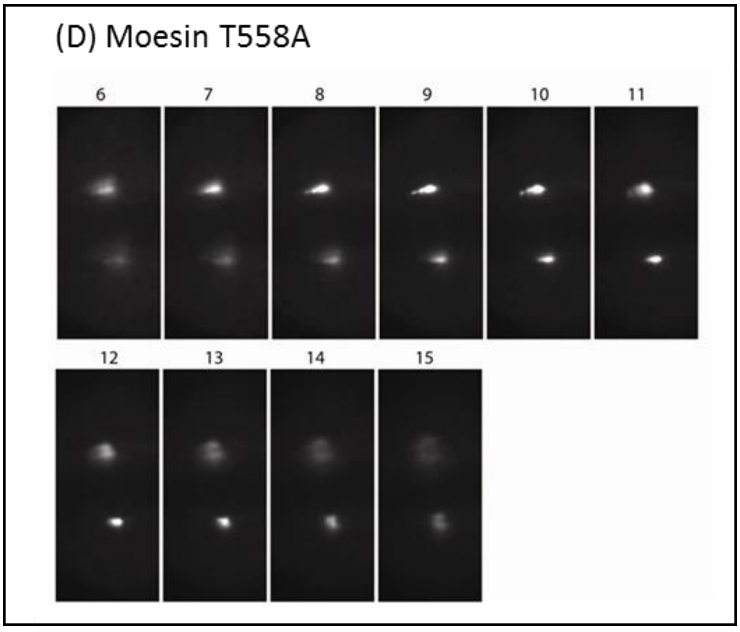
(D) Moesin T558A
6
7
8
9
10
11
12
13
14
15

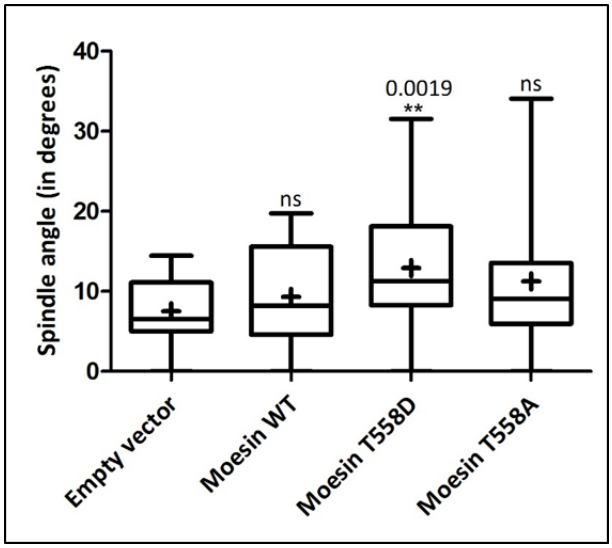

Figure 4.9 Activation of Moesin results in a misorientation of the metaphase spindle. HeLa cells seeded on fibronectin-coated coverslips were transfected with HeLa cells were transfected with the (A) vector control, (B) Moesin wild type (WT), (C) phopsho-mimic (T558D) and (D) phospho-dead (T558A and stained with anti-pericentrin and DAPI. Numbers above the images indicate the Z-plane of the respective image. (E) Graph displaying the spindle angles under different moesin mutants. The spindle angle was calculated as described in the Methods section. 150 cells from three independent biological repeats were imaged, analyzed using ImageJ software and plotted with Graphpad Prism software. Box-and-whiskers diagram; box lines represent upper quartile, median and lower quartile; whiskers represent 5-95 percentile, + represents the mean spindle angle. Unpaired student's t-test was used for statistical analysis. Error bars represent mean (±SEM). ** denotes p=0.0069.

So far, our findings have identified that hypertonic stress induces activation of ERM proteins, which are directly linked to the cortical rigidity of cells. Further, activated form of moesin was shown to cause aberrant astral microtubule arrangement and spindle misorienation. Therefore, we examined the possible factors that might contribute to the hypertonicity-induced ERM protein phosphorylation. Since earlier studies have reported that phosphorylation of ERM is dependent on Rho activity and independent of ROCK activity [226], we then went on to check whether RhoA is involved in the hypertonicity-mediated upregulation of phosphorylated ERM protein levels.

To accomplish this, cells were treated with C3 transferase, a specific inhibitor of Rho, followed by exposure to media containing 2 parts water (hypotonic), 0.15M NaCl or 4% xylose and harvested for Western blotting. Inhibition of Rho abrogated the phosphorylation of ERM proteins, induced under osmotic stress.

The results obtained therefore suggest that Rho might function collectively with osmotic stress in regulating the activity of ERM proteins.

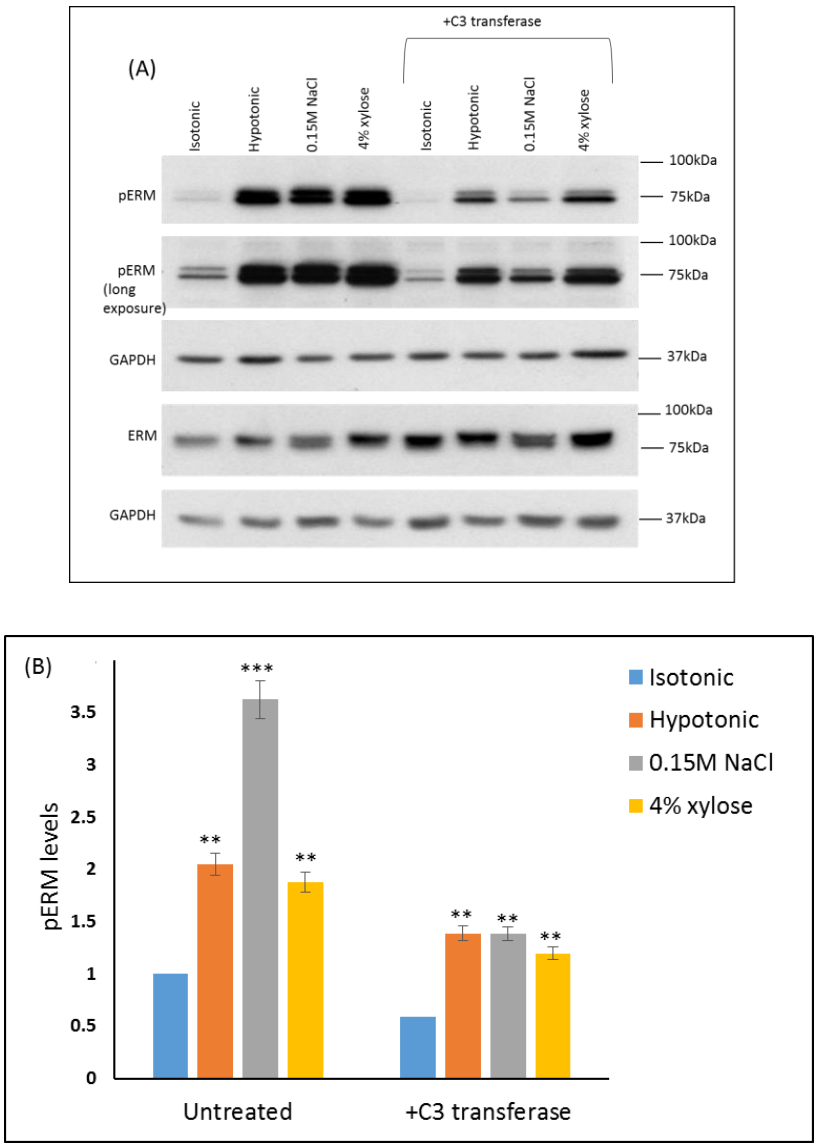

Figure 4.10 Rho plays a role in the hypertonicity-induced ERM activation. (A) HeLa cells were treated with C3 transferase for 3 hours, followed by treatment with different osmotic media. Cells were harvested for Western Blotting to detect p-ERM protein levels. GAPDH serve as the loading control. (B) Densitometric analysis of phospho ERM levels was performed using ImageJ software. Phospho ERM and ERM protein levels were normalized to their respective GAPDH levels and the adjusted phospho ERM was then normalized to adjusted ERM levels. Values are expressed as mean (±SEM) of three independent experiments. *** $p<0.0001$, **$p<0.001$.

4.1.10 Hypertonic stress results in an impaired cortical localizationof spindle assembly proteins at the cortex, which might contribute to defects in spindle orientation.

In order to further elucidate the mechanism underlying the observed defects in spindle angle upon hypertonic stimulation, we designed a model in collaboration with Koon Yen Ling and Chiam Kheng Hwee of the Bioinformatics Institute, A*STAR, Singapore.

The small guanosine triphosphatase, Ran has previously been implicated in coordinating the spindle assembly. Two forms of Ran exist in the cell: the active RanGTP form found around the chromosomes and the inactive RanGDP, which is abundant in the cytoplasm. By tethering to other cytoplasmic proteins such as importin-β, long-range gradients dependent on Ran can be created. Such long-range gradients serve physiological relevant purposes such as dictating the sites of microtubule nucleation and stabilization [215]. In addition, various papers have also implicated Ran in mediating astral microtubule attachment [215, 271]. Chromosome-derived RanGTP gradient was observed to limit the regions of LGN localization thus specifying the spindle orientation axis. Diffusion is of paramount importance to the creation of such gradients. Nonetheless, no papers have discussed the role of diffusion and its significance in ensuring proper spindle assembly. In earlier studies, fluorescent dextran tagged with Texas Red was dissolved in hypertonic media containing NaCl and ejected from a micropipette into the brain slices of rat cells. An image was captured for reference before ejection and after each ejection; ten images at an interval of ten seconds were captured. The intensity profile of the diffusing molecules was measured and was used to calculate the apparent diffusion coefficient (ADC). A 15% increase in the diffusion coefficient was observed under hypertonic condition [272], thereby suggesting that hypertonic environment results in higher rate of diffusion.

It is well documented that the Ras-related GTPase Ran is implicated in mitotic spindle assembly RanGTP is present at a higher concentration in the vicinity of the chromosomes as compared to the cell periphery. During mitosis, a diffusion-limited RanGTP gradient surrounds the chromosomes [273]. This RanGTP gradient is important to drive the recruitment of various proteins functioning as spindle assembly factors (SAFs) at the cell cortex. It has been shown that the RanGTP gradient enables the localization of LGN and NuMA to the lateral cell cortex in order to maintain the axis of spindle orientation [215]. Additionally, G_{α} facilitates recruitment of LGN (Leucine-Glycine-Asparagine repeats), also known as GPSM2 (G-protein signaling modulator 2) to the cortex, which in turn recruits NuMA (Nuclear mitotic apparatus protein) and dynein. The interaction of the astral microtubules with the cell cortex mediates the release of the G_{α}/LGN/dynein/NuMA complex to the poles. Upon reaching the poles, this complex is recycled back to the cortex. The cortical transport and recycling of this complex is essential for generating pulling forces on astral microtubules, which eventually control spindle orientation [274].

We seek to develop a mathematical model that attempts to reproduce the main experimental finding showing an aberrant increase in astral microtubule and spindle angle upon hypertonic stress and to delineate the underlying mechanism.

In this model, high osmolarity of the external media is assumed to result in an increase in the diffusion coefficient of Ran. Such a phenomenon has been observed where the diffusion coefficient of dextran was increased in rat neocortex under increased osmotic stress [272]. We speculate that under conditions of hyperosmolarity, the Ran dependent gradient is perturbed resulting in mislocalization of LGN on the cortex, ultimately leading to spindle misalignment.

To test the hypothesis, we first built a reaction-diffusion system to investigate the effects of increased diffusion rates on the Ran gradient in the cell. The reaction-diffusion system constitutes the first tier of the modeling approach. In the model, the cell is assumed to have a typical radius of 15μm with the chromosomes occupying an elliptical space in the middle. The reaction-diffusion model uses a series of partial differentiation equations to model how each species vary in space and time. For example, the equation for RanGTP is as follows.

$$\frac{\partial \text{RanGTP}}{\partial t} = D\Delta\text{RanGTP} + R(\text{RanGDP})$$

The equation above describes the rate of change of RanGTP where the first term on the right denotes Fick's laws of diffusion while the second term describes the generation of active RanGTP from RanGDP at the chromosomes. The equations for other Ran related compounds take a similar form.

Using the reaction-diffusion model, we elucidated the concentrations of RanGTP as well as its associated compounds in the cell under two different diffusion constants at steady state. A lower diffusion constant represents a cell placed in hypotonic solution (Figure 4.11 A) while a higher diffusion constant represents a cell placed in hypertonic solution (Figure 4.11 B). In the following figure (Figure 4.11 A-B), the RanGTP concentrations in the cell at steady state are shown for different conditions. The concentrations are colour coded where red represents high concentration of RanGTP and dark blue represents low concentration of RanGTP.

The concentration of the proteins recruited by Ran along the cell periphery obtained from the first tier of modeling is fed into the second tier to obtain the spindle angles. Since the RanGTP gradient restricts LGN localization to the lateral cell cortex where LGN is a known mediator for astral microtubule attachment to the membrane, the second tier of

modeling essentially calculates the spatial distribution of LGN based on different Ran gradients. Locations along the membrane with high concentrations of LGN are more likely to have microtubule attached. A Poisson process is used to model microtubule attachments. Based on the mean position of microtubule attachment, the spindle angle can be derived by calculating the deviation of the mean position from the horizontal.

In the second tier of the mathematical model, astral microtubule formation is modeled as a Poisson process with nucleation times governed by the amount of free tubulin in the cytoplasm and the density of LGN on the cortex.

A couple of assumptions are made in order to simplify the working of the model:

(1) Microtubule nucleation on the membrane is dependent on the fraction of available tubulin available in the cytoplasm and the density of LGN on the membrane.

This assumption is reminiscent of the law of mass action, which states that the rate of any chemical reaction is proportional to the product of the masses of the reacting substances.

(2) Microtubule forms rapidly upon nucleation and detachment of the microtubule may occur.

(3) Microtubules deliver LGN to the membrane at a rate proportional to the amount of available LGN.

A brief description of the model is as follows:

The cell membrane is modeled as a circle with 100 partitions, n. Total number of LGN particles simulated is 1000. At each time interval, t, the density of LGN at each partition, n defined by $f(n,t)$ is monitored, so is the fraction of LGN not bound to the membrane defined by $F(t)$. Since each partition can either have a microtubule attached or not attached, an indicator function denoted by $a(n,t)$ describes the state of attachment where $a(n,t) = 0$ denotes no microtubule attached and $a(n,t) = 1$ denotes attachment of microtubule. Similarly, the fraction of partitions still allowed to nucleate at time, t is designated as $A(t)$. With this, we can calculated the probability of a microtubule

nucleating at partition, *n* in the time interval, *dt* where the probability is assumed to be directly proportional to the partitions still allowed to nucleate and the amount of tubulin present at the partition (Figure 4.11 C).

$$P(n, dt) = A(t) * f(n, t) * dt$$

If a nucleation event has occurred, the microtubule may detach from the membrane with an arbitrary probability. LGN concentrations along the membrane can then be calculated as follows with the following ordinary differential equation:

$$\frac{d}{dt} f(n,t) \; = \; v * F(t) * a(n,t) \; + \; D * I(\text{RanGTP}) * F(t) - \; d * f(n,t)$$

The first term on the right denotes the rate of attachment of LGN when it is being delivered via microtubules where *v* refers to the transport rate constant. The second term on the right denotes the attachment of LGN based on free diffusion with diffusion constant, *D*. *I(*RanGTP*)* describes the effect of RanGTP on LGN localization along the membrane. In this model, a monotonic decreasing function of RanGTP on LGN localization was chosen to describe the inhibitory interaction between RanGTP and LGN. The third term on the right denotes the dissociation of LGN with decay constant, *d*.

A total number of 100 simulations are conducted for each diffusion constant and in each simulation, the position of the microtubule attachment along the membrane after 10000 time intervals were recorded. The spindle angle was calculated by taking the deviation of the mean position of microtubule attachment from the horizontal (Figure 4.11 D). Preliminary computational results reveal that as the variance of RanGTP gradient is increased, a greater proportion of cells exhibit misalignment of the spindles. As variance increases, the number of cells with higher spindle angles increases. For example, at a variance of 1, the proportion of cells with spindle angle of 20° is 0 while increasing the variance from 5 to 10 causes the proportion of cells to increase from 0.01 to 0.07 (Figure 4.11D).

This can be interpreted by the following:

(1) When diffusion is slow which results in a steep RanGTP gradient, less spindles are inappropriately aligned. (2) However, as the RanGTP gradient becomes gentler at high diffusion constant, more spindles become misaligned.

Since diffusion rate is presumed to be faster in the presence of hypertonicity, one can conjecture that under hypertonic stress, a greater proportion of cells will exhibit large spindle angles as compared to the hypertonic condition. This is further confirmed by experimental results plotted below which shows that under hypertonic solutions, the proportion of cells exhibiting large spindle angles of 20° increases from 0.056 in cells placed in normal control media to 0.080 when cells are placed in NaCl solution (Figure 4.11 E).

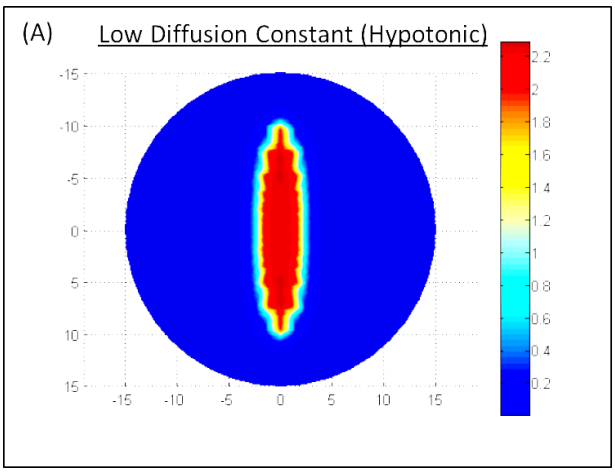

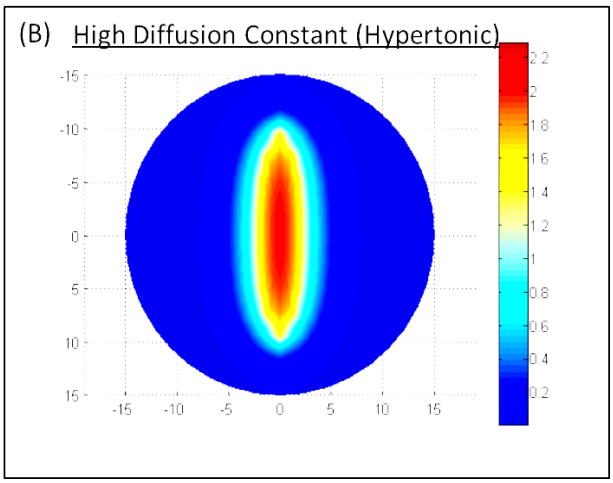

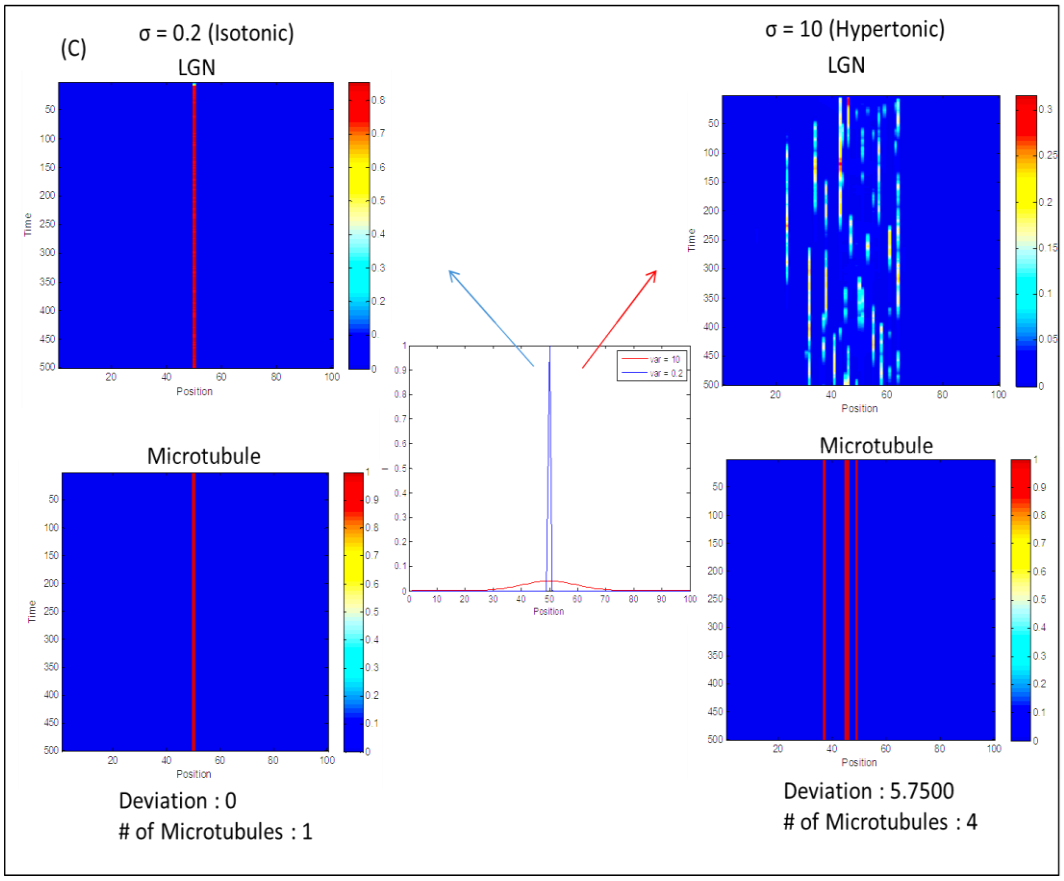
(C)
σ = 0.2 (Isotonic)
LGN
Microtubule
Time
Position
var = 10
var = 0.2
σ = 10 (Hypertonic)
LGN
Microtubule
Deviation : 0
# of Microtubules : 1
Deviation : 5.7500
# of Microtubules : 4

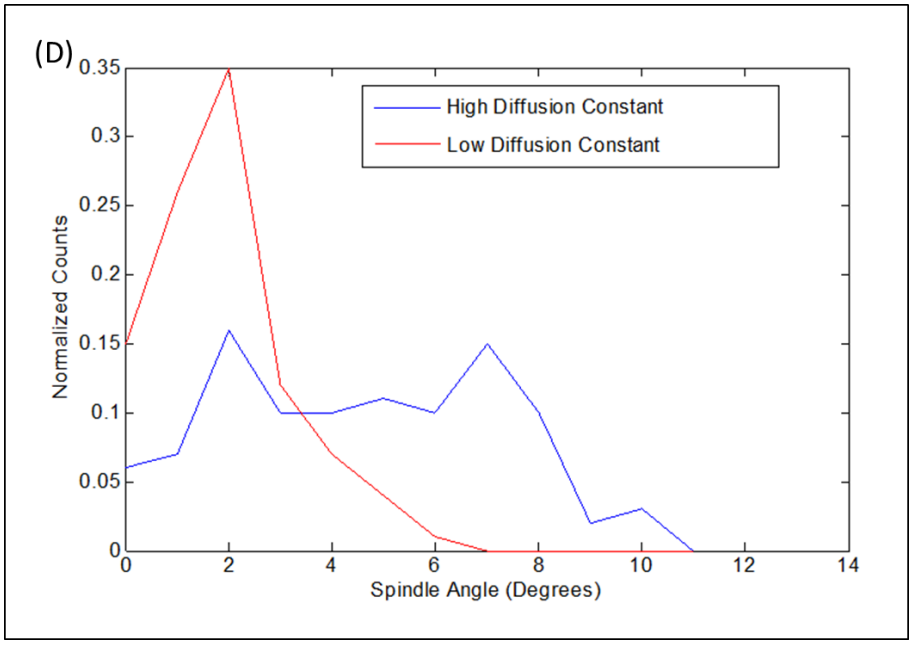
(D)
High Diffusion Constant
Low Diffusion Constant
Normalized Counts
Spindle Angle (Degrees)

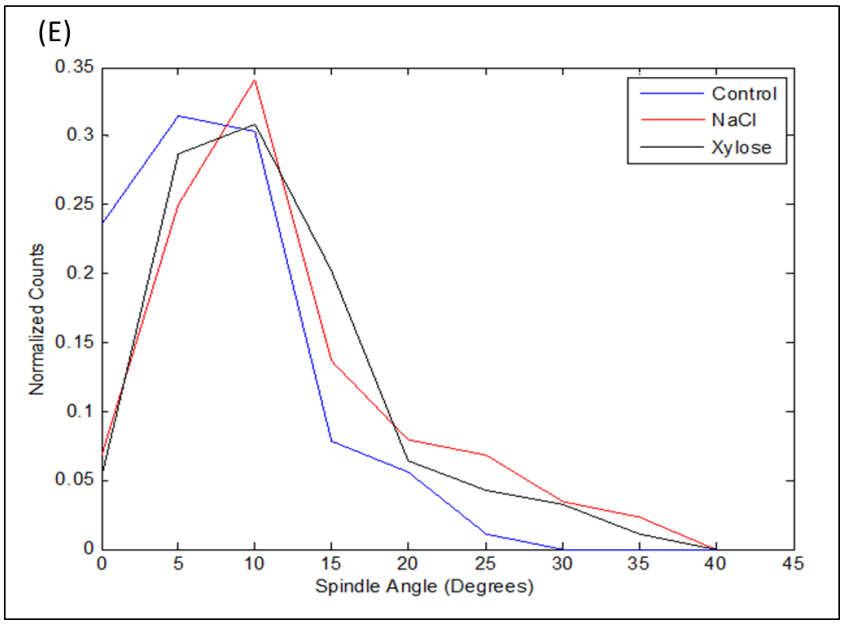

Figure 4.11 Modelling studies validated the increase in astral microtubules and spindle angle upon hypertonic stress and predicted this defect might be attributed to defective cortical localization of G_{α}//LGN/NuMA/dynein. (A) Concentration of RanGTP around the cell at low diffusion constant (A) and at high diffusion constant (B). As observed in the figure, at a higher diffusion constant, the RanGTP is able to "reach further" into the cytoplasm as observed by a thicker bright blue band that is visible in Panel B which is absent in the corresponding location in Panel A. Hence, changes in diffusion rates can bring about differences in localization of RanGTP within the cell. The dark red elliptical area in both Panels A and B represent the high concentration of RanGTP at the chromosomes. (C) Model showing an aberrant localization of LGN at the cortex during conditions of high osmolality (high variance) which leads to improper recruitment of astral microtubules. (D) Plot of normalized counts against spindle angle for high diffusion constant (blue line) and low diffusion constant (red line). Preliminary computational results reveal that as the diffusion constant is increased, a greater proportion of cells exhibit misalignment of the spindles. This is illustrated in the following histogram plot where the percentage of runs observed for each spindle angle deviation range is shown. At higher diffusion constant, the simulations run tend to be dominated by larger spindle angles while at smaller diffusion constants, a larger proportion of the runs have small spindle angles. (E) Proportion of cells placed in different osmotic media plotted against the spindle angle.

4.1.11 Hypertonic stress caused defective cortical localization of G_{α}, NuMA and dynactin during metaphase.

The primary cause of the misalignment in the model is due to aberrant cortical localization of proteins required for spindle assembly, which leads to improper recruitment of astral microtubules along the cortex. Dynactin is a plus end tracking protein that binds and activates the motor protein cytoplasmic dynein and associates with the microtubules with the help of its largest dimeric subunit $p150^{Glued}$ [275-277]. $p150^{Glued}$ plays a critical role in the functioning of the dynein/dynactin complex. During

mitosis, the stable attachment of the astral microtubules at the lateral cell cortex is mediated by the dynein/dynactin complex [262, 278]. During metaphase, $p150^{Glued}$ is localized at the centrosomes, along spindle and astral microtubules and at the cell cortex, where it appears as cortical spots [279]. The cortical accumulation of $p150^{Glued}$ is essential for bipolar spindle orientation. We proceeded to examine the effects of osmotic perturbation on the cortical distribution of the proteins involved in spindle assembly, namely G_{α}, NuMA, LGN, and dynactin subunit in order to verify the model.

To achieve this, HeLa cells treated with hypertonic media containing 0.15 M NaCl and 4% xylose were stained with antibodies against the proteins mentioned above. However, we failed to obtain a distinct cortical localization of these proteins during metaphase. In order to obtain proper cortical staining, we pre-extracted the cells in a buffer containing 25 mM HEPES, 60 mM 1,4-piperazinediethanesulfonic acid, 10 mM ethylene glycol tetraacetic acid, 2 mM $MgCl_2$, pH 6.9 containing 0.2% Triton X-100 and fixed in 4% PFA, followed by immuno-staining. We could observe faint cortical staining in isotonic control cells stained with anti- G_{α}, (Figure 4.12 A) anti-NuMA (Figure 4.12 B and anti-$p150^{Glued}$ (Figure 4.12 C). However, we could only observe cytoplasmic localization of LGN and were not successful in visualizing LGN at the cortex. Our results indeed showed an impaired cortical localization of G_{α} (Figure 4.12 A), NuMA (Figure 4.12 B) and $p150^{Glued}$ (Figure 4.12 C) around the cortex under hypertonic conditions in comparison to a more localized cortical distribution in isotonic cells.

Defective localization of the G_{α}, NuMA and dynactin subunit around the cell cortex under hypertonic stimulation might be responsible for the observed wider distribution of spindle angle.

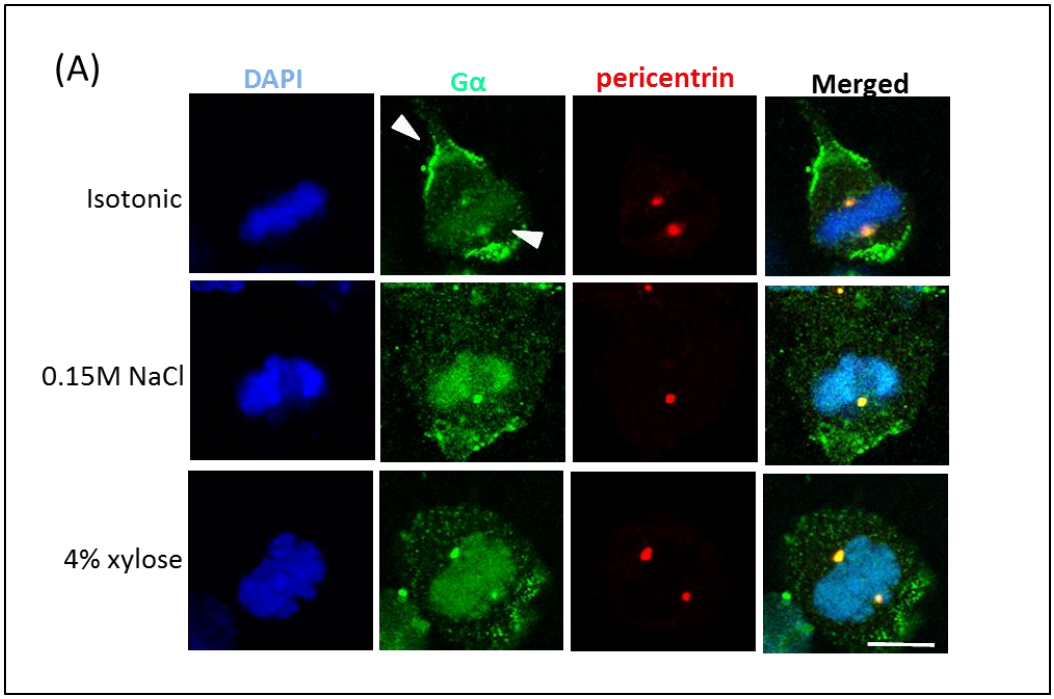
(A)
DAPI
Gα
pericentrin
Merged
Isotonic
0.15M NaCl
4% xylose

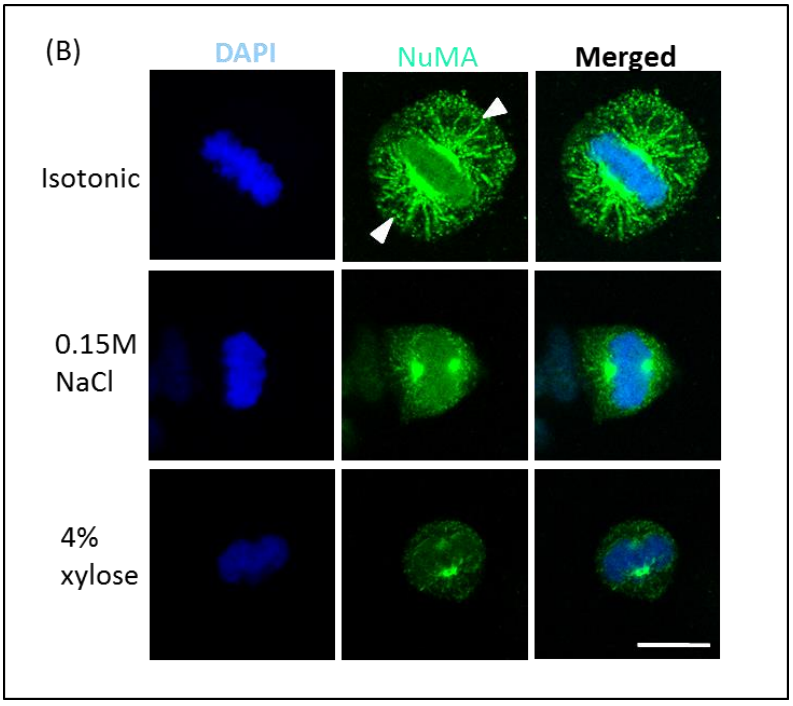
(B)
DAPI
NuMA
Merged
Isotonic
0.15M NaCl
4% xylose

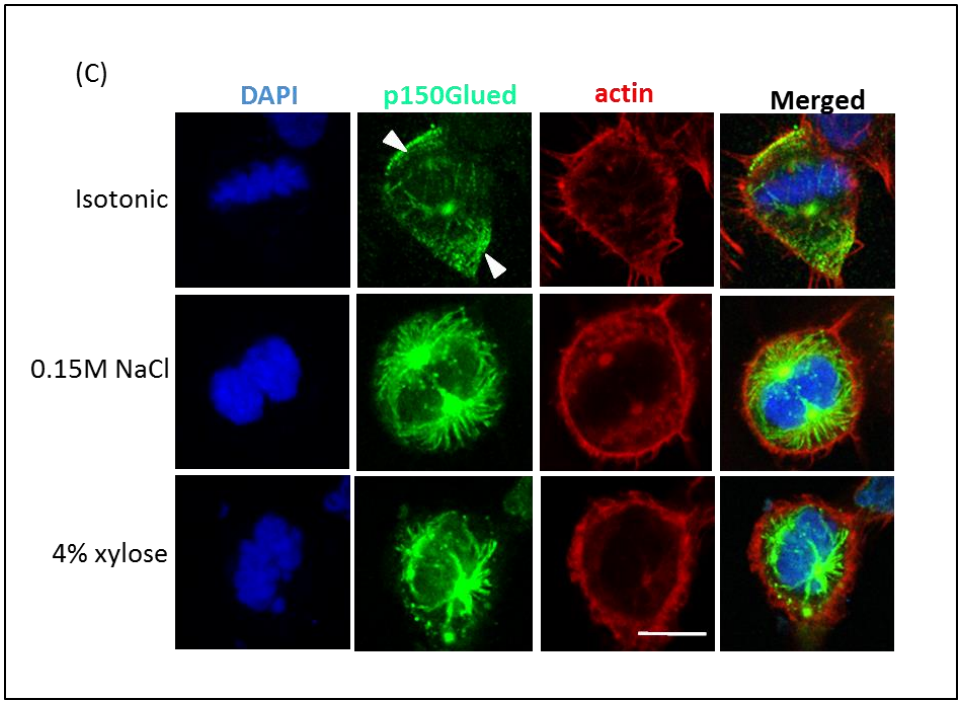

Figure 4.12 Hypertonic stress showed impaired cortical staining of G_{α}, NuMA and dynactin subunit p150^{Glued}. HeLa cells treated with media containing 0.15M NaCl or 4% xylose were pre-extracted using PHEM buffer and immuno-stained with (A) Gα (green), (B) NuMA (green) and (C) p150Glued (green) and DAPI (blue). Confocal images of 120 cells from three independent biological experiments were captured. Representative image is shown above. Scale bar 10µm.

In conclusion, in this chapter we have uncovered the effects of osmotic stress on the mitotic spindle assembly, in particular astral microtubule formation and spindle orientation. Our results show that perturbation of the osmotic gradient leads to an increase in astral microtubules and spindle misorientation. As ion channels are implicated in the recovery of the cells subjected to osmotic challenge, we examined their role in the proper assembly of the mitotic spindle apparatus. Similar to the hypertonic challenge, our experimental results show that when mitotic cells are treated with EIPA and NPPB (Na^+/H^+ antiporter and Cl^- exchanger inhibitors, respectively), it leads to an increase in astral microtubule number as well misorientation of the spindle.

One possible reason behind these phenotypic defects might be the hyper activation of ERM proteins since hypertonicity-induced moesin phosphorylation is implicated in the defects observed in mitotic spindle apparatus [280]. In addition, we hypothesize a second

model involving the RanGTP-mediated cortical localization of several proteins associated with spindle orientation to explain the observed impairment in astral microtubules and spindle assembly induced by hypertonic stress.

4.2 Discussion

The mitotic progression of adherent cultured cells is associated with a profound change in the organization of the actin cytoskeleton and cell shape. The initiation of cell rounding during mitosis is characterized by de-adhesion from the substrate, followed by extensive remodeling of the cytoskeleton, which terminates with cell elongation and division into two daughter cells upon mitotic exit [47, 281]. As mentioned earlier, a rigid, well-defined actomyosin cytoskeleton and osmotic pressure primarily stimulate mitotic cell rounding. The involvement of the actomyosin contractility in mitosis has been well documented. Several regulators of the actin cytoskleleton, namely moesin, adducin, cofilin have been shown to mediate cortical rigidity and cell rounding. However, the role of the hydrostatic pressure in this aspect still remains elusive.

4.2.1 Hydrostatic pressure during mitosis

Cells have been reported to experience an increase in the intracellular hydrostatic pressure during mitotic entry [53]. As the cells enter mitosis, they experience an increase in the surface tension and consequently the internal hydrostatic pressure also rises in accordance with the Laplace law. Owing to the rise in hydrostatic pressure, the chemical potential of water within the cell exceeds that of the medium and water flows out of the cell, thereby increasing the concentration of osmolytes in the cytosol. This efflux continues till the osmotic pressure difference equals the increased hydrostatic difference within the cell [282]. This rise in the internal hydrostatic pressure governs mitotic cell rounding.

Earlier it was believed that only kidney cells are affected by hypertonic stress. However recent reports have provided increasing evidence showing hypertonic stress modulates the functions of non-kidney cell types as well [113]. Exposure to hypertonic stress causes cytoskeletal rearrangement, DNA damage and cell cycle arrest. In the first part of the thesis, we reported that cells showed defects in mitotic progression under hypertonic stress. Since we observe a prolonged metaphase arrest upon hypertonic stimulation, we investigated whether osmotic imbalance results in defects in the assembly of the bipolar metaphase spindle. Aberrant spindle morphogenesis and orientation are associated with aneuploidy and cancer. Therefore, studying the effects of hypertonic stress and the roles of ion transporters on mitotic spindle assembly will throw light on possible therapeutic strategies and targets, thus augmenting our knowledge of measures against cancer.

4.2.2 Activation of ERM proteins by hypertonic stress

Phosphorylation and activation of moesin has been shown to be essential in cell rounding and cortical stability in *Drosophila* [54, 105]. The upstream kinase known to phosphorylate moesin in *Drosophila* S2 cells is Slik, however it was not clear whether the phosphorylation is direct or an intermediate protein is involved [54, 105, 109, 280]. Recent studies have reported that mammalian ERMs are activated by the human orthologue Ste20-like kinase (SLK). An *in vitro* kinase assay revealed that SLK is able to phosphorylate ERM proteins directly and this phosphorylation was affected when SLK was mutated [280]. Alternatively, SLK may have additional substrates that resulted in ERM activation. Previous data from our lab have shown lower levels of phospho-ERM upon treatment with C3 transferase but not downstream of ROK and mDia [226], suggesting the involvement of RhoA but not its well-known effectors, ROK and mDia (Diaphanous related formin). Treatment of NIH3T3 cells with lyophosphatidic acid (LPA) facilitates the phosphorylation of ERM proteins and the opposite effect was

observed upon C3 transferase treatment, validating that the contribution of RhoA is necessary for ERM protein phosphorylation [283]. Phosphatidylinositol 4,5-bisphosphate (PIP_2) has been identified as a primary mediator of ERM protein activation [284]. ERM proteins exist in an auto-inhibited, closed conformation, whereby the N-terminal FERM domain and C-terminal domain associate with each other [100, 285]. Many *in vitro* and *in vivo* studies suggest that the activation of the ERM proteins occurs in two distinct steps [268, 286-288]. Firstly, the N-terminal FERM domain binds to the PIP_2 –rich regions of the plasma membrane. PIP_2 binding results in a conformational change and partial activation of the proteins [102, 289]. The conformational change renders moesin more accessible to phosphorylation at the C-terminal conserved Threonine 558 residue [104]. ERM proteins are active upon phosphorylation [99, 101]. Overexpression of phosphatidylinositol 4-phosphate 5-kinase (PIP5-kinase), which is a direct effector of RhoA results in elevated levels of PIP_2; which eventually leads to upregulated phospho ERM levels [290]. However, there are contradictory reports stating that PIP_2 alone can directly activate ERM proteins in A431 cells [291], independent of Rho activity.

Further both RhoA and PIP_2 levels have been shown to be stimulated by hypertonic stress in kidney tubular epithelial cells and HeLa cells respectively [159, 163]. In order to check whether RhoA mediates the hypertonicity-induced upregulation of phospho-ERM, we treated the cells with RhoA inhibitor, followed by hypertonic shock. C3 transferase inhibited the hypertonicity-induced increase in phospho-ERM (Figure 4.10), suggesting that RhoA might act cooperatively with osmotic stress to activate ERM proteins. However, we cannot conclude whether RhoA is acting directly upstream or the hypertonic stress induced response is mediated by PIP_2.

Previous work from our lab suggests that phospho-mimic and phopho-dead mutants of moesin were able to increase and decrease the cortical rigidity of mitotic cells

respectively [226]. Alteration in the cortical rigidity of cells could explain the observed increase in astral microtubules (Figure 4.8) and spindle misorientation (Figure 4.9) when cells were transfected with active forms of moesin since astral microtubules function in anchoring the spindle at the cortex, thereby regulating positioning of the spindle.

4.2.3 Spindle misorientation under hypertonic stress

The maintenance of accurate position and orientation of the mitotic spindle is pivotal for several cellular responses, such as cell fate determination and tissue organization during development [292]. Several reports indicate that proper orientation of the spindle is essential for determining cell fate during development. Asymmetric cell division takes place during embryonic development to give rise to two daughter cells with distinct cellular contents. The different cellular content found in the daughter cells caused by the asymmetric cell division eventually directs the developmental fate of the cell. This asymmetric cell division relies on the orientation and position of the mitotic spindle [292]. Studies in *Drosophila* neuroblast cells have shown that the mitotic spindle is oriented along the apical-basal axis to give rise to a self-renewing neuroblast and another daughter cell directed towards neuronal cell differentiation [293, 294]. Since the spindle apparatus determines the orientation of the cleavage furrow, it is likely to contribute to the asymmetric distribution of cellular contents during embryonic development [295]. Besides its role in development, the proper orientation of the mitotic spindle is also important in tissue organization. Improper orientation of the mitotic spindle exhibits adverse effects in a variety of cell types. For example, the organization of the airways in the lungs is dependent on changes in spindle orientation and positioning [296]. The arrangement of epithelial cells of lungs and blood vessels into tubes that form a complex network is controlled by mitotic spindle orientation. The mitotic spindle is aligned with respect to the longitudinal axis of the epithelial tube in epithelial cells. This aids in the

longitudinal extension of tube with a consistent diameter. Abrogating the orientation of the mitotic spindle perturbs the organization of the kidney epithelium by increasing the diameter of the kidney tubule [297]. In addition to embryonic development and tissue organization, positioning of the mitotic spindle apparatus also contributes to tumor progression. A major contributing factor in many tumors has been attributed to abnormal chromosome number, termed as aneuploidy [298]. Several microtubule plus-end tracking proteins known to affect spindle orientation also hamper proper chromosome segregation [299, 300]. Defects in mitotic chromosome segregation can contribute towards aneuploidy [301, 302]. Furthermore, defects in spindle orientation cause cytokinesis failure, leading to tetraploidy [303]. Since tumor cells have a rapid rate of cell proliferation, the mitotic index is higher and time available for correcting the errors during mitosis is low. Moreover, many tumor suppressor signaling pathways like PTEN-PI3K, Hippo and Wnt signaling pathways are implicated in the regulation of spindle positioning [304]. These findings highlight the importance of proper maintenance of spindle orientation.

RhoGTPase proteins and their downstream effectors have been reported to contribute towards spindle orientation. Studies have suggested that Cdc42 regulates spindle alignment and controls cell migration, polarity and morphogenesis [305, 306]. In Caco-2 cells, when Cdc42 was depleted, the spindle orientation was compromised which eventually led to defective tissue organization [307]. Cdc42 knockdown increased the number of cells with defective mitotic spindles [308]. Cdc42 regulates spindle orientation via Cdc42-PAK2-βPIX signaling and the phosphatidyl 3,4,5 triphosphate (PIP_3) pathways [309]. The Cdc42-PAK2-βPIX pathway drives the arrangement of the cortical actin network, which is essential for establishing the connection between the astral microtubules and the cortex [309]. The interaction between the astral microtubules

emanating from the spindle poles and the cortical actin is essential for proper orientation of the mitotic spindle apparatus.

RhoA has also been known to influence spindle orientation. Dominant-negative form of RhoA induced spindle misorientation in chick neuroepithelium cells [310]. Inhibition of RhoA by addition of C3 transferase also exhibited similar defects in spindle positioning [226]. RhoA-ROCK signaling pathway may function cooperatively with moesin to control spindle positioning. ERM proteins are the primary regulators of cortical F-actin filaments [103, 280]. Studies in *Drosophila* and mammalian cells have suggested that moesin is required to maintain cortical stability and spindle orientation during mitosis [67, 105, 311-313]. Ste20-like kinase (SLK) dependent activation of ERM proteins is crucial for proper alignment of the mitotic spindle [280]. Both depletion of ERM-activating Slk kinase and constitutive activation of Ezrin perturbed spindle orientation [280]. It has been proposed that phospho-ERM proteins enable the cortical recruitment of LGN-NuMA complex. The activation of ERM proteins facilitates the organization of cortical actin filaments and the recruitment of LGN-NuMA [280]. LGN is recruited to the cell cortex by a membrane-associated protein named Gα, which subsequently recruits NuMA and dynein. The Gα/LGN/NuMA/dynein complex is stabilized by actin filaments and is required for the maintenance of spindle orientation [215, 274, 314]. Depletion of Slik and ERM proteins impaired the localization of LGN-NuMA and this correlated with spindle misorientaion. Hyperactivation of Ezrin also disrupted the polarized NuMA localization at the cortex. During prometaphase and during metaphase, NuMA was present at the cortex facing the poles of the mis-oriented spindles [280]. Our results also show that exposure to hypertonic stress during metaphase activates ERM proteins as indicated by the increase in phospho-ERM levels. Because constitutive activation of moesin leads to spindle misorientation, hypertonicity-induced phosphorylation of ERM

could be an explanation of the observed defects in spindle orientation. Since earlier studies have suggested that hypertonic stress stimulates RhoA, thereby leading to myosin light chain (MLC) phosphorylation in kidney proximal tubule cells [163], we examined the involvement of RhoA in the hypertonicity-induced phosphorylation of ERM proteins. Earlier studies have shown a reduction in the phospho-ERM levels upon RhoA inhibition. However, no effect was observed when ROCK was inhibited [226]. When cells treated with C3 transferase were subjected to hypertonic shock, we observed a down regulation in the hypertonicity-induced phosphorylation of ERM proteins, suggesting that both RhoA and osmotic stress might act cooperatively to ensure proper activation of ERM proteins. Our results suggest that hyper-activation of ERM proteins induced by hypertonic stress might contribute to the observed spindle misorientation.

As an alternative approach to understand the underlying mechanism behind the observed spindle misorientation, we designed a model based on the finding that hypertonic stress results in an increase in the diffusion rate. The small GTPase, Ran has been implicated in spindle assembly by negatively regulating LGN localization [215, 271]. In this model, high osmolarity of the external media is assumed to result in a change in the diffusion coefficient of Ran. This results in a defective localization of spindle assembly factors like NuMA-LGN on the cortex, which ultimately leads to spindle misalignment.

Osmolarity has been known to alter diffusion rates. Dextran was observed to diffuse more quickly in rat neocortex cells under conditions of hypertonic stress while the reverse occurs in hypotonic stress [272]. The RanGTP gradient was shown using FRET microscopy [215] to vary spatially within the cell whereupon its spatial localization is dependent on diffusion. Furthermore, the authors also provide evidence showing that a chromosome derived RanGTP gradient restricts LGN localization to the lateral cell cortex. Since LGN is a mediator for astral microtubule attachment to the membrane, it is not

surprising that altering the Ran gradient by changing the osmolarity of the external media might lead to spindle misalignment. Since LGN-NuMA complex is recruited by Gα at the cell cortex, the localization of these proteins would also be affected under hypertonic stress. Our immnuno-fluorescence cell staining results obtained indeed show impaired cortical staining of Gα and NuMA under conditions of hypertonic stress (Figure 4.12 A, B). However, the antibodies used for LGN staining failed to show a defined cortical localization (data not shown here) after several attempts of trouble shooting. This could be because the antibody was not sensitive and specific for immunofluorescence. Future studies to investigate the localization of LGN will be done using GFP-tagged with LGN. As mentioned above, the RanGTP gradient from the mitotic chromosome, as well as PLK1 at the centrosomes regulates cortical localization of Gα-LGN-NuMA complex [215, 314], which in turn recruits dynein-dynactin complex at the cell cortex. The minus-end directed movement of the cortical dynein generates pulling forces on the spindle by capturing astral microtubules and helps positioning the spindle at the centre of cells [315]. Since our results show impaired astral microtubule arrangement and spindle misorientation, we examined if the localization of dynein and dynactin were perturbed under osmotic imbalance. In agreement with the model, when cells were subjected to hypertonic stimulation, $p150^{Glued}$, which is a subunit of the dynactin complex, showed aberrant localization at the cortex (Figure 4.12 C).

In conclusion, based on the results obtained, we propose that alteration of the osmolarity of the medium affects the cortical distribution of the proteins required for spindle orientation, which explains the observed wider distribution of spindle angle (Figure 4.13).

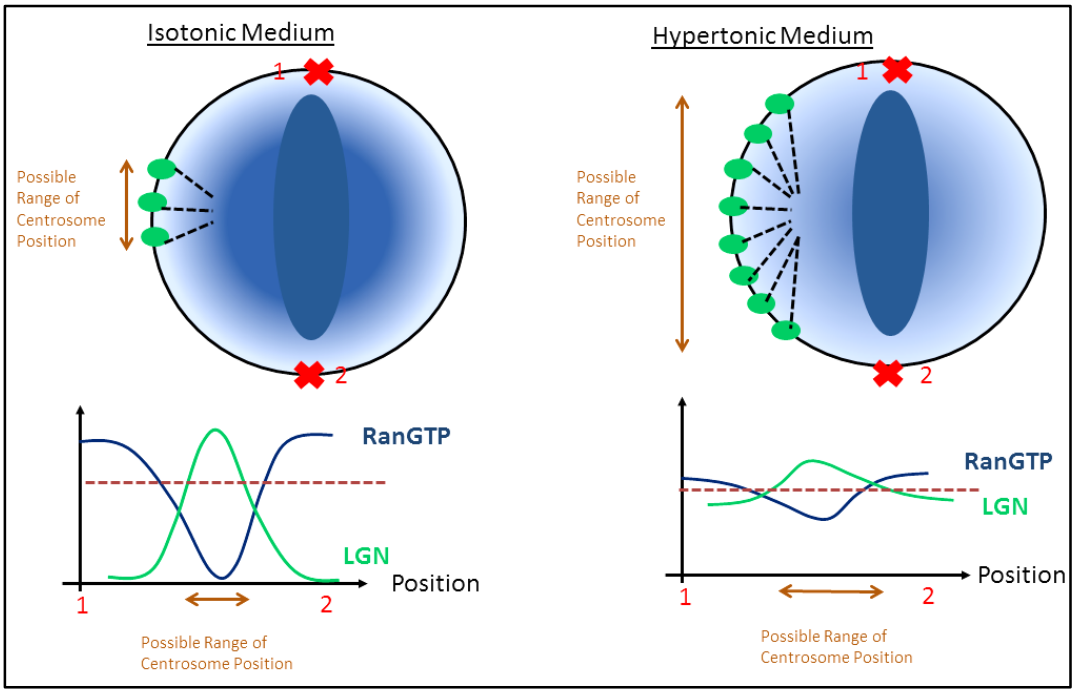

Figure 4.13 Model for how osmolarity affects diffusion. A higher concentration of RanGTP (blue) is present around the chromosomes along the metaphase plate (position 1 and 2) and the concentration decreases towards the spindle poles, thereby establishing a gradient. This is essential for the establishment of a proper bipolar spindle assembly. RanGTP gradient is perturbed and due to diffusion under conditions of hypertonic stress. RanGTP and LGN-NuMA levels are inversely related with respect to the distance from the metaphase plate towards the poles as shown in the graph. Under isotonic conditions, RanGTP gradient results in a narrow distribution of LGN-NuMA (green) around the cortex (left). Osmolarity has been shown to affect diffusion rates. Therefore, when cells are placed in hypertonic media, the RanGTP gradient is perturbed due to which spindle assembly proteins are distributed more widely around the cortex (right). The aberrant localization of spindle assembly proteins at the cortex results in an impaired astral microtubule arrangement and spindle misorientation.

Chapter 5

SUMMARY

This study emphasizes the role of osmotic stress in cell cycle control. Prolonged exposure to hypertonic conditions is known to result in DNA damage [242] and apoptosis [243, 244]. The cells accumulate osmolytes as a compensatory response, thereby restoring the intracellular osmotic balance and cell volume. Hypertonic stress has been shown to affect gene transcription and cell proliferation. Apart from kidney cells, retinal pigmented epithelial cells exposed to hypertonic shock causes cell cycle arrest at G_1/S and G_2/M phases of the cell [113]. The delay in cell cycle progression is an early osmoadaptive response, allowing the cells to adapt to the increased tonicity. Besides kidney cells of the inner medulla, cancer cells may also be affected by hypertonicity. For example, it is shown that increased osmolarity during colonic water absorption activates colon cancer cells and promotes expression of vascular endothelial growth factor (VEGF), which correlates with enhanced metastatic potential [232]. Thus, we aimed to examine the effects of hypertonic stress on a non-kidney-type cancer cell, such as HeLa. Our preliminary results show an increase in the percentage of cells in G_2/M phase (Figure 3.1) and a subsequent delay in cell cycle progression when hypertonicity is induced. The sequential activation of cyclin-dependent kinases (CDKs) and their association with cyclins drives progression through cell cycle [20]. Since cyclin D/CDK4 and cyclinB/CDK1complex drives progression through G_1 and G_2/M respectively, our results showed that arrest at the G_1 and G_2/M correlated with the downregulation of cyclin D1 and cyclin B1 protein levels (Figure 3.4A) under hyperosmotic conditions.

After establishing a delay in cell progression, primarily due to mitotic deceleration, we next intended to check the progression timings of each mitotic stage. Our results show

that when cells were released in hypertonic media from nocodazole arrest, they were unable to recover and stuck at metaphase (Figure 3.6). This observation was further confirmed by time-lapse live cell imaging of HeLa cells (Figure 3.7). It has been shown that a balance between an intracellular hydrostatic pressure and an outward directed osmotic pressure is instrumental for mitotic cell rounding [53]. Failure of the cells to round up is associated with defects in mitotic spindle architecture. As the cells begin deadhering from their substrate during mitotic entry to assume a spherical shape, they increase their intracellular hydrostatic pressure to facilitate this process. Exposure to hypertonic conditions results in a decrease in rounding pressure and volume of metaphase HeLa cells [53]. Additionally, earlier work from our lab has shown that an intact actin cytoskeleton is required for proper spindle assembly at the early stage of mitosis. Perturbation of the actin cytoskeleton resulted in a less-defined mitotic spindle with an aberrant increase in astral microtubules emanating from the spindle pole towards the cortex. Cells treated with inhibitors of Rho GTPase pathway to perturb the actin cytoskeleton showed centrosome defocusing and spindle misorientation, thereby suggesting that actin cytoskeleton plays an essential role in mitotic spindle assembly [226]. However, not much has been explored about the role of osmotic pressure in the assembly and maintenance of a bipolar mitotic spindle. Since reduction of the osmotic pressure is associated with decrease in rounding pressure and volume and defects in cell rounding, we hypothesized that hypertonic stress could have adverse effects on the establishment of a bipolar spindle. Thus, we examined the effects of hypertonic stress on the assembly of the mitotic spindle and observed that exposure to hypertonic environment indeed led to defects in spindle assembly, characterized by a dramatic increase in astral microtubules (Figure 4.1) and misorientation of the bipolar spindle (Figure 4.4).

Under physiological conditions, ion transporters are activated in response to hypertonic stress to increase the intracellular osmotic pressure and restore normal cell volume by

compensatory regulatory volume increase. Since ion channels are responsible for the rescue of cells following an osmotic shock, we speculated that they might be involved in the organization of the cortical cytoskeleton and spindle assembly. As expected, HeLa cells treated with inhibitors of Na^+/H^+ antiporter and Cl^- exchanger showed an aberrant increase in astral microtubules (Figure 4.5) and misorientation of the mitotic spindle (Figure 4.6).

In order to provide a nexus between the observed phenotypic defects in the spindle assembly and regulation of the osmotic pressure, we proposed two possible underlying mechanisms. In the first approach, we studied the involvement of ERM (ezrin, radixin, moesin) proteins. ERM proteins are activated upon phosphorylation and are redistributed to the cortex, where it mediates rearrangement of actin filaments and favors a rounded morphology during mitosis [269, 316]. Our studies show a rapid (within 3 minutes) and prolonged (30 minutes) upregulation in phospho-ERM levels upon hypertonic challenge (Figure 4.7). Since the active form of moesin directly contributes to cortical rigidity [55] and our results show an increase in phopsho-ERM levels upon hypertonic induction, we examined the role of osmotic imbalance on the cortical rigidity of mitotic cells. Micropipette aspiration assay results showed lesser deformation and hence, higher cortical rigidity under hyperosmotic conditions (Figure 4.7). Since hypertonic milieu induced ERM protein activation by phosphorylation and increase in cortical rigidity, we then studied the effect of moesin phosphorylation on the organization of the mitotic spindle. Our results show that metaphase cells expressing the phospho-mimic form (T558D) of moesin showed impairment in the astral microtubule arrangement (Figure 4.8) and an increase in spindle angle relative to the substratum (Figure 4.9). Thus, we suggest that the hypertonicity-defects in spindle orientation could be due to hyperactivation of moesin. Since, earlier studies have identified RhoA to be an upstream regulator of ERM protein phosphorylation [283], we proceeded to check whether Rho

plays a role in the hypertonicity-mediated upregulation of phosphorylated ERM protein levels. Cells treated with C3 transferase, a specific inhibitor of Rho, followed by hypertonic challenge inhibited the phosphorylation of ERM proteins, induced by osmotic stress (Figure 4.10). Thus, these data collectively imply that Rho may act collectively with osmotic stress to regulate the phosphorylation of ERM proteins. Hyperactivation of ERM proteins by increased tonicity might result in impaired metaphase astral microtubule organization and defects in bipolar spindle orientation.

As an alternative approach to delineate the mechanism underlying the observed defects in spindle assembly induced by hypertonic stress, we designed a model based on the observation that hypertonic environment affects the rate of diffusion. Earlier study shows that when fluorescent dextran tagged with Texas red dissolved in hypertonic media containing NaCl was injected into the brain slices of rat cells and the intensity profile of the diffusing molecules was measured, there was a 15% increase in the diffusion coefficient under hypertonic conditions [272]. During mitosis, a diffusion-limited RanGTP gradient surrounds the chromosomes [273], which helps in the cortical recruitment of several proteins required for spindle assembly. Gα and the RanGTP gradient enable the recruitment of LGN to the cortex, which recruits NuMA and dynein/dynactin complex. The interaction of the astral microtubules with the cell cortex results in the release of the ternary complex Gα/LGN/NuMA/dynein from the cortex to the poles. Upon reaching the poles, this complex is recycled back to the cortex. This movement of the ternary complex is required for generating cortical pulling forces on astral microtubules, thus leading to the stabilization of the bipolar spindle [274]. The model predicted that since hypertonic stress affects diffusion, RanGTP gradient will be disrupted and consequently, the cortical recruitment of the above-mentioned proteins will likely be impaired. The defects in the cortical localization of Gα, LGN, NuMA or dynein may, in turn, be responsible for the aberrant organization of metaphase astral

microtubules and spindle angle defect. A total of 100 simulations were carried out for each osmotic condition and the results obtained were fitted with the experimental results which shows that under hypertonic solutions, the proportion of cells exhibiting large spindle angles of 20° increases from 0.056 in cells placed in normal control media to 0.080 when cells are placed in NaCl solution (Figure 4.11 C). We then we proceeded to investigate the effects of osmotic perturbation on the cortical distribution of the proteins involved in spindle assembly, namely G_{α}, LGN, NuMA, and dynactin subunit, $p150^{Glued}$ which binds dynein. In accordance with the model, our experimental results also showed defective cortical localization of these proteins upon induction of hyperosmotic stress (Figure 4.12).

In conclusion, our study shows that osmotic balance is required for timely progression through the cell cycle and disruption of the osmotic gradient is responsible for delay in mitotic progression due to defects in the bipolar metaphase spindle assembly, characterized by an aberrant increase in astral microtubules and defects in spindle orientation. One possible reason behind these phenotypic defects might be the hyper activation of ERM proteins since hypertonicity-induced moesin phosphorylation is implicated in the defects observed in mitotic spindle apparatus. Besides, we hypothesize a second model involving the RanGTP-mediated cortical localization of several proteins associated with spindle orientation to explain the observed impairment in astral microtubules and spindle assembly induced by hypertonic stress.

Chapter 6

FUTURE DIRECTIONS

Although we have delineated two possible pathways to explain the observed defects in spindle misorientation when cells are subjected to osmotic stress, further studies are needed obtain a more holistic picture.

6.1 Upstream effectors of ERM activation

Our results show an upregulation in phospho-ERM levels upon induction of hypertonic stress (Figure 4.7). However, we have yet to identify the upstream effectors governing this phosphorylation. Studies from our lab have reported a decrease in phospho-ERM levels upon Rho inhibition, suggesting that Rho plays a role in ERM protein activation [226]. Our results show that Rho and hypertonic stress exhibits a synergistic effect on the phosphorylation of ERM proteins as Rho inhibition reduced hypertonicity-induced increase in phospho-ERM levels (Figure 4.10). However, Rho is not indispensable for ERM activation under hypertonic conditions. It would therefore be worthwhile to assess the involvement of Rho in this process. One possible method would be to examine Rho activity under conditions of hypertonic stress. Rho alters between an active, GTP-bound form and an inactive GDP-bound form. The underlying principle of this assay is that the Rho family effector proteins will recognize the active GTP bound of Rho. The Rho binding domain (RBD) of the effector protein Rhotekin has a high affinity for the GTP bound form of RhoA and can be effectively used for affinity purification of active RhoA from cell lysates [167, 317]. We will use a RBD-GST fusion protein and this fusion protein is then coupled to Glutathione beads and cell lysates are incubated with this complex to pull down active, GTP-bound of Rho. Rho activity assay performed with cell

lysates subjected to hypertonic treatment will help us in understanding how the activity of Rho is affected under these conditions.

Moreover, as mentioned above, since PIP_2 activated by PIP5-kinase results in higher phospho-ERM levels, it would be interesting to study if the phosphorylation of ERM proteins by hypertonic stress in directly controlled by RhoA or mediated by PIP_2.

6.2 Microtubule dynamics under osmotic stress

Secondly, our observations suggest that hypertonic stress affects astral microtubule arrangement during metaphase (Figure 4.1 A). EB1 specifically localizes to the growing microtubule distal tips and our EB1 immuno-staining further confirmed the increase in the astral microtubules during hypertonic stress (Figure 4.1 D). Kif18B is a plus-tip-tracking protein that interacts directly with EB1 and controls length of astral microtubules during mitosis. Kif18B possesses microtubule-depolymerizing activity and is found to localize to the plus ends of the astral microtubule population, thereby affecting the dynamics and stability of this subset of microtubules [318]. Depletion of Kif18B results in an increase in the astral microtubule length and spindle misorientation [319]. Since hypertonic stimulation shows an aberrant increase in astral microtubules and spindle misorientation, it would be worthwhile to study if the association of Kif18B and EB1 is affected by hypertonic stress.

Although our studies show hypertonic stress exerts an effect on astral microtubules, we have yet to elucidate how it affects microtubule dynamics. In order to accomplish this, we aim to visualize microtubules using a mCherry tagged-CLIP-170 construct and track the net elongation rate of microtubules by visualizing fluorescent of CLIP-170 fluorescence by time-lapse microscopy. Under conditions of hypertonic stress, if the microtubule elongation rate is higher compared to the control, these finding might indicate that the

osmotic stress results in an increased microtubule polymerization, thus explaining the increase in astral microtubules during metaphase.

6.3 Effects of hypertonic stress on spindle misorientation

Our results show an increase in the spindle angle relative to the substratum under conditions of hypertonic stress (Figure 4.4) and increased phosphorylation of moesin (Figure 4.9). Our data suggest that the hyper tonicity- induced ERM phosphorylation might be responsible for the observed spindle defects. However, we have not determined whether this effect is direct or mediated by any upstream regulators. The immediate upstream kinase phosphorylating moesin is SLK. Future studies can be performed to establish if SLK levels or activities are acting downstream of osmotic stress to regulate spindle assembly in during mitosis.

Our proposed model describes that hypertonic stress affects the diffusion rate in cells, which disrupts the RanGTP gradient in the cells, leading to a wide cortical distribution of proteins essential for spindle orientation (Figure 4.13). Our immuno-staining results are in agreement with the model. We will next validate if the RanGTP gradient is altered under osmotic stress as predicted by the model. We are currently optimizing conditions for performing a fluorescence resonance energy transfer (FRET) assay to measure RanGTP gradient around the metaphase chromosomes using the Rango (Ran-regulated importin-β cargo) probe [224] This biosensor named Rango contains importin-β binding domain flanked by yellow fluorescent protein at the amino terminal and CFP at the carboxy terminus. RanGTP competes for binding with importin-β, thereby freeing the Rango probe and allowing the Rango probe to undergo FRET. In mitotic HeLa cells, Rango is dispersed throughout the cytoplasm. Photobleaching results showed that in mitotic cells, a gradient was recorded, a region with high FRET was observed around the chromatin and the signal decreased towards the cell periphery. However, we could not obtain a high

number of mitotic cells during our experiments for analysis. We are in the process of optimizing this assay in order to obtain more conclusive results.

Finally, the model predicts defective cortical localization of Gα/LGN/NuMA/dynein-dynactin, which we have confirmed by immuno-staining. Although our results indicate an impaired distribution of NuMA and Gα, we failed to observe cortical localization of LGN. One possible reason might be the antibody used to detect the cortical LGN was not suitable. In order to visualize cortical LGN, we propose to use a GFP-LGN construct to study its localization during mitosis under different conditions of osmotic stress.

These findings, taken together, will then provide substantial evidence to validate our model and explain the underlying mechanisms governing orientation of the mitotic spindle apparatus under hyperosmotic milieu.

Chapter 7

REFERENCES

1. Sanger, J.W., *Changing patterns of actin localization during cell division.* Proc Natl Acad Sci U S A, 1975. **72**(5): p. 1913-6.
2. Varmark, H., *Functional role of centrosomes in spindle assembly and organization.* J Cell Biochem, 2004. **91**(5): p. 904-14.
3. Heald, R., *Motor function in the mitotic spindle.* Cell, 2000. **102**(4): p. 399-402.
4. Sawin, K.E. and J.M. Scholey, *Motor proteins in cell division.* Trends Cell Biol, 1991. **1**(5): p. 122-9.
5. Wordeman, L., *How kinesin motor proteins drive mitotic spindle function: Lessons from molecular assays.* Semin Cell Dev Biol, 2010. **21**(3): p. 260-8.
6. Hornick, J.E., et al., *Kinesins to the core: The role of microtubule-based motor proteins in building the mitotic spindle midzone.* Seminars in Cell & Developmental Biology, 2010. **21**(3): p. 290-299.
7. Gorbsky, G.J., *Kinetochores, microtubules and the metaphase checkpoint.* Trends Cell Biol, 1995. **5**(4): p. 143-8.
8. Zhou, J., J. Yao, and H.C. Joshi, *Attachment and tension in the spindle assembly checkpoint.* J Cell Sci, 2002. **115**(Pt 18): p. 3547-55.
9. Draviam, V.M., S. Xie, and P.K. Sorger, *Chromosome segregation and genomic stability.* Curr Opin Genet Dev, 2004. **14**(2): p. 120-5.
10. Walczak, C.E., S. Cai, and A. Khodjakov, *Mechanisms of chromosome behaviour during mitosis.* Nat Rev Mol Cell Biol, 2010. **11**(2): p. 91-102.
11. Green, R.A., E. Paluch, and K. Oegema, *Cytokinesis in animal cells.* Annu Rev Cell Dev Biol, 2012. **28**: p. 29-58.
12. Pelham, R.J. and F. Chang, *Actin dynamics in the contractile ring during cytokinesis in fission yeast.* Nature, 2002. **419**(6902): p. 82-6.
13. Kinoshita, M., et al., *Self- and actin-templated assembly of Mammalian septins.* Dev Cell, 2002. **3**(6): p. 791-802.
14. Barr, F.A. and U. Gruneberg, *Cytokinesis: placing and making the final cut.* Cell, 2007. **131**(5): p. 847-60.
15. Jahn, R. and R.H. Scheller, *SNAREs--engines for membrane fusion.* Nat Rev Mol Cell Biol, 2006. **7**(9): p. 631-43.
16. Glotzer, M., *The molecular requirements for cytokinesis.* Science, 2005. **307**(5716): p. 1735-9.
17. Morgan, D.O., *Principles of CDK regulation.* Nature, 1995. **374**(6518): p. 131-4.
18. Vermeulen, K., D.R. Van Bockstaele, and Z.N. Berneman, *The cell cycle: a review of regulation, deregulation and therapeutic targets in cancer.* Cell Prolif, 2003. **36**(3): p. 131-49.
19. Evans, T., et al., *Cyclin: a protein specified by maternal mRNA in sea urchin eggs that is destroyed at each cleavage division.* Cell, 1983. **33**(2): p. 389-96.
20. Pines, J., *Cyclins: wheels within wheels.* Cell Growth Differ, 1991. **2**(6): p. 305-10.
21. Sherr, C.J., *G1 phase progression: cycling on cue.* Cell, 1994. **79**(4): p. 551-5.
22. Ekholm, S.V. and S.I. Reed, *Regulation of G(1) cyclin-dependent kinases in the mammalian cell cycle.* Curr Opin Cell Biol, 2000. **12**(6): p. 676-84.
23. Ohtsubo, M., et al., *Human cyclin E, a nuclear protein essential for the G1-to-S phase transition.* Mol Cell Biol, 1995. **15**(5): p. 2612-24.
24. Chen, E. and C.C. Li, *Association of Cdk2/cyclin E and NF-kappa B complexes at G1/S phase.* Biochem Biophys Res Commun, 1998. **249**(3): p. 728-34.

25. Girard, F., et al., *Cyclin A is required for the onset of DNA replication in mammalian fibroblasts.* Cell, 1991. **67**(6): p. 1169-79.
26. Walker, D.H. and J.L. Maller, *Role for cyclin A in the dependence of mitosis on completion of DNA replication.* Nature, 1991. **354**(6351): p. 314-7.
27. King, R.W., P.K. Jackson, and M.W. Kirschner, *Mitosis in transition.* Cell, 1994. **79**(4): p. 563-71.
28. Arellano, M. and S. Moreno, *Regulation of CDK/cyclin complexes during the cell cycle.* Int J Biochem Cell Biol, 1997. **29**(4): p. 559-73.
29. Fisher, R.P. and D.O. Morgan, *A novel cyclin associates with MO15/CDK7 to form the CDK-activating kinase.* Cell, 1994. **78**(4): p. 713-24.
30. Rechsteiner, M. and S.W. Rogers, *PEST sequences and regulation by proteolysis.* Trends Biochem Sci, 1996. **21**(7): p. 267-71.
31. Jeffrey, P.D., et al., *Mechanism of CDK activation revealed by the structure of a cyclinA-CDK2 complex.* Nature, 1995. **376**(6538): p. 313-20.
32. Lew, D.J. and S. Kornbluth, *Regulatory roles of cyclin dependent kinase phosphorylation in cell cycle control.* Curr Opin Cell Biol, 1996. **8**(6): p. 795-804.
33. Ducommun, B., et al., *cdc2 phosphorylation is required for its interaction with cyclin.* EMBO J, 1991. **10**(11): p. 3311-9.
34. Hayles, J., et al., *Temporal order of S phase and mitosis in fission yeast is determined by the state of the p34cdc2-mitotic B cyclin complex.* Cell, 1994. **78**(5): p. 813-22.
35. Sherr, C.J. and J.M. Roberts, *Inhibitors of mammalian G1 cyclin-dependent kinases.* Genes Dev, 1995. **9**(10): p. 1149-63.
36. Carnero, A. and G.J. Hannon, *The INK4 family of CDK inhibitors.* Curr Top Microbiol Immunol, 1998. **227**: p. 43-55.
37. Hengst, L. and S.I. Reed, *Inhibitors of the Cip/Kip family.* Curr Top Microbiol Immunol, 1998. **227**: p. 25-41.
38. Harper, J.W., et al., *Inhibition of cyclin-dependent kinases by p21.* Mol Biol Cell, 1995. **6**(4): p. 387-400.
39. Lee, M.H., I. Reynisdottir, and J. Massague, *Cloning of p57KIP2, a cyclin-dependent kinase inhibitor with unique domain structure and tissue distribution.* Genes Dev, 1995. **9**(6): p. 639-49.
40. Hagting, A., et al., *MPF localization is controlled by nuclear export.* EMBO J, 1998. **17**(14): p. 4127-38.
41. Toyoshima, F., et al., *Nuclear export of cyclin B1 and its possible role in the DNA damage-induced G2 checkpoint.* EMBO J, 1998. **17**(10): p. 2728-35.
42. Heald, R., M. McLoughlin, and F. McKeon, *Human wee1 maintains mitotic timing by protecting the nucleus from cytoplasmically activated Cdc2 kinase.* Cell, 1993. **74**(3): p. 463-74.
43. Liu, F., et al., *The human Myt1 kinase preferentially phosphorylates Cdc2 on threonine 14 and localizes to the endoplasmic reticulum and Golgi complex.* Mol Cell Biol, 1997. **17**(2): p. 571-83.
44. Peng, C.Y., et al., *Mitotic and G2 checkpoint control: regulation of 14-3-3 protein binding by phosphorylation of Cdc25C on serine-216.* Science, 1997. **277**(5331): p. 1501-5.
45. Yang, J., et al., *Maintenance of G2 arrest in the Xenopus oocyte: a role for 14-3-3-mediated inhibition of Cdc25 nuclear import.* EMBO J, 1999. **18**(8): p. 2174-83.
46. Aubin, J.E., K. Weber, and M. Osborn, *Analysis of actin and microfilament-associated proteins in the mitotic spindle and cleavage furrow of PtK2 cells by immunofluorescence microscopy. A critical note.* Exp Cell Res, 1979. **124**(1): p. 93-109.

47. Cramer, L.P. and T.J. Mitchison, *Investigation of the mechanism of retraction of the cell margin and rearward flow of nodules during mitotic cell rounding.* Mol Biol Cell, 1997. **8**(1): p. 109-19.
48. Lecuit, T. and P.F. Lenne, *Cell surface mechanics and the control of cell shape, tissue patterns and morphogenesis.* Nature Reviews Molecular Cell Biology, 2007. **8**(8): p. 633-644.
49. Dao, V.T., et al., *Dynamic changes in Rap1 activity are required for cell retraction and spreading during mitosis.* Journal of Cell Science, 2009. **122**(16): p. 2996-3004.
50. Britch, M. and T.D. Allen, *The modulation of cellular contractility and adhesion by trypsin and EGTA.* Exp Cell Res, 1980. **125**(1): p. 221-31.
51. Suzuki, K. and K. Takahashi, *Reduced cell adhesion during mitosis by threonine phosphorylation of beta1 integrin.* J Cell Physiol, 2003. **197**(2): p. 297-305.
52. Mitchison, T.J., *Actin based motility on retraction fibers in mitotic PtK2 cells.* Cell Motil Cytoskeleton, 1992. **22**(2): p. 135-51.
53. Stewart, M.P., et al., *Hydrostatic pressure and the actomyosin cortex drive mitotic cell rounding.* Nature, 2011. **469**(7329): p. 226-30.
54. Kunda, P., et al., *Moesin controls cortical rigidity, cell rounding, and spindle morphogenesis during mitosis.* Curr Biol, 2008. **18**(2): p. 91-101.
55. Kunda, P. and B. Baum, *The actin cytoskeleton in spindle assembly and positioning.* Trends in Cell Biology, 2009. **19**(4): p. 174-179.
56. Lancaster, O.M., et al., *Mitotic rounding alters cell geometry to ensure efficient bipolar spindle formation.* Dev Cell, 2013. **25**(3): p. 270-83.
57. Foley, E.A. and T.M. Kapoor, *Microtubule attachment and spindle assembly checkpoint signalling at the kinetochore.* Nat Rev Mol Cell Biol, 2013. **14**(1): p. 25-37.
58. Collins, E.S., et al., *Cell cycle-regulated cortical dynein/dynactin promotes symmetric cell division by differential pole motion in anaphase.* Mol Biol Cell, 2012. **23**(17): p. 3380-90.
59. Tse, H.T., W.M. Weaver, and D. Di Carlo, *Increased asymmetric and multi-daughter cell division in mechanically confined microenvironments.* PLoS One, 2012. **7**(6): p. e38986.
60. Horvitz, H.R. and I. Herskowitz, *Mechanisms of asymmetric cell division: two Bs or not two Bs, that is the question.* Cell, 1992. **68**(2): p. 237-55.
61. Fabritius, A.S., M.L. Ellefson, and F.J. McNally, *Nuclear and spindle positioning during oocyte meiosis.* Curr Opin Cell Biol, 2011. **23**(1): p. 78-84.
62. Li, R. and D.F. Albertini, *The road to maturation: somatic cell interaction and self-organization of the mammalian oocyte.* Nat Rev Mol Cell Biol, 2013. **14**(3): p. 141-52.
63. Gonczy, P., *Mechanisms of asymmetric cell division: flies and worms pave the way.* Nat Rev Mol Cell Biol, 2008. **9**(5): p. 355-66.
64. Siller, K.H. and C.Q. Doe, *Spindle orientation during asymmetric cell division.* Nat Cell Biol, 2009. **11**(4): p. 365-74.
65. Dinarina, A., et al., *Chromatin shapes the mitotic spindle.* Cell, 2009. **138**(3): p. 502-13.
66. Basto, R., et al., *Centrosome amplification can initiate tumorigenesis in flies.* Cell, 2008. **133**(6): p. 1032-42.
67. Thery, M. and M. Bornens, *Get round and stiff for mitosis.* HFSP J, 2008. **2**(2): p. 65-71.
68. Gachet, Y., et al., *A MAP kinase-dependent actin checkpoint ensures proper spindle orientation in fission yeast.* Nature, 2001. **412**(6844): p. 352-5.

69. Lee, K. and K. Song, *Actin dysfunction activates ERK1/2 and delays entry into mitosis in mammalian cells.* Cell Cycle, 2007. **6**(12): p. 1487-95.
70. Bohmer, R.M., E. Scharf, and R.K. Assoian, *Cytoskeletal integrity is required throughout the mitogen stimulation phase of the cell cycle and mediates the anchorage-dependent expression of cyclin D1.* Mol Biol Cell, 1996. **7**(1): p. 101-111.
71. Bottazzi, M.E., et al., *Distinct effects of mitogens and the actin cytoskeleton on CREB and pocket protein phosphorylation control the extent and timing of cyclin A promoter activity.* Mol Cell Biol, 2001. **21**(22): p. 7607-16.
72. Fasshauer, M., M. Iwig, and D. Glaesser, *Synthesis of proto-oncogene proteins and cyclins depends on intact microfilaments.* Eur J Cell Biol, 1998. **77**(3): p. 188-95.
73. Huang, S., C.S. Chen, and D.E. Ingber, *Control of cyclin D1, p27(Kip1), and cell cycle progression in human capillary endothelial cells by cell shape and cytoskeletal tension.* Mol Biol Cell, 1998. **9**(11): p. 3179-93.
74. Iwig, M., et al., *Growth regulation by cell shape alteration and organization of the cytoskeleton.* Eur J Cell Biol, 1995. **67**(2): p. 145-57.
75. Maness, P.F. and R.C. Walsh, Jr., *Dihydrocytochalasin B disorganizes actin cytoarchitecture and inhibits initiation of DNA synthesis in 3T3 cells.* Cell, 1982. **30**(1): p. 253-62.
76. Ohta, T., et al., *Cytochalasin D inhibits the progression from the Go to S phase at the mid-prereplicative stage in GC-7 cells stimulated with serum.* Cell Struct Funct, 1985. **10**(1): p. 37-46.
77. Reshetnikova, G., et al., *Disruption of the actin cytoskeleton leads to inhibition of mitogen-induced cyclin E expression, Cdk2 phosphorylation, and nuclear accumulation of the retinoblastoma protein-related p107 protein.* Exp Cell Res, 2000. **259**(1): p. 35-53.
78. Rubtsova, S.N., et al., *Disruption of actin microfilaments by cytochalasin D leads to activation of p53.* FEBS Lett, 1998. **430**(3): p. 353-7.
79. Takasuka, T., S. Ishibashi, and T. Ide, *Expression of cell-cycle-dependent genes in serum stimulated cells whose entry into S phase is blocked by cytochalasin D.* Biochim Biophys Acta, 1987. **909**(2): p. 161-4.
80. Tsakiridis, T., et al., *Actin filaments facilitate insulin activation of the src and collagen homologous/mitogen-activated protein kinase pathway leading to DNA synthesis and c-fos expression.* J Biol Chem, 1998. **273**(43): p. 28322-31.
81. Moulding, D.A., et al., *Unregulated actin polymerization by WASp causes defects of mitosis and cytokinesis in X-linked neutropenia.* J Exp Med, 2007. **204**(9): p. 2213-24.
82. Hall, A., *Rho GTPases and the actin cytoskeleton.* Science, 1998. **279**(5350): p. 509-14.
83. Jaffe, A.B. and A. Hall, *Rho GTPases: biochemistry and biology.* Annu Rev Cell Dev Biol, 2005. **21**: p. 247-69.
84. Maddox, A.S. and K. Burridge, *RhoA is required for cortical retraction and rigidity during mitotic cell rounding.* Journal of Cell Biology, 2003. **160**(2): p. 255-265.
85. Amano, M., et al., *Phosphorylation and activation of myosin by Rho-associated kinase (Rho-kinase).* Journal of Biological Chemistry, 1996. **271**(34): p. 20246-20249.
86. Kimura, K., et al., *Regulation of myosin phosphatase by Rho and Rho-Associated kinase (Rho-kinase).* Science, 1996. **273**(5272): p. 245-248.

87. Rosenblatt, J., et al., *Myosin II-dependent cortical movement is required for centrosome separation and positioning during mitotic spindle assembly.* Molecular Biology of the Cell, 2004. **15**: p. 378A-378A.
88. Maekawa, M., et al., *Signaling from rho to the actin cytoskeleton through protein kinases ROCK and LIM-kinase.* Science, 1999. **285**(5429): p. 895-898.
89. Amano, T., et al., *Mitosis-specific activation of LIM motif-containing protein kinase and roles of cofilin phosphorylation and dephosphorylation in mitosis.* Journal of Biological Chemistry, 2002. **277**(24): p. 22093-22102.
90. Kimura, K., et al., *Regulation of the association of adducin with actin filaments by Rho-associated kinase (Rho-kinase) and myosin phosphatase.* Journal of Biological Chemistry, 1998. **273**(10): p. 5542-5548.
91. Fukata, Y., et al., *Phosphorylation of adducin by rho-kinase plays a crucial role in cell motility.* Journal of Cell Biology, 1999. **145**(2): p. 347-361.
92. Bretscher, P. and N. Peters, *Two signal models of lymphocyte activation incorporate a mechanism of peripheral tolerance, and have implications for achieving immunological unresponsiveness and effective transplantation.* Vox Sanguinis, 2002. **83**: p. 155-158.
93. Hirao, M., et al., *Regulation mechanism of ERM (ezrin/radixin/moesin) protein/plasma membrane association: possible involvement of phosphatidylinositol turnover and Rho-dependent signaling pathway.* J Cell Biol, 1996. **135**(1): p. 37-51.
94. Takahashi, K., et al., *Direct interaction of the Rho GDP dissociation inhibitor with ezrin/radixin/moesin initiates the activation of the Rho small G protein.* J Biol Chem, 1997. **272**(37): p. 23371-5.
95. Trofatter, J.A., et al., *A novel moesin-, ezrin-, radixin-like gene is a candidate for the neurofibromatosis 2 tumor suppressor.* Cell, 1993. **75**(4): p. 826.
96. Hanzel, D., et al., *The secretion-stimulated 80K phosphoprotein of parietal cells is ezrin, and has properties of a membrane cytoskeletal linker in the induced apical microvilli.* EMBO J, 1991. **10**(9): p. 2363-73.
97. Helander, T.S., et al., *ICAM-2 redistributed by ezrin as a target for killer cells.* Nature, 1996. **382**(6588): p. 265-8.
98. Serrador, J.M., et al., *Moesin interacts with the cytoplasmic region of intercellular adhesion molecule-3 and is redistributed to the uropod of T lymphocytes during cell polarization.* J Cell Biol, 1997. **138**(6): p. 1409-23.
99. Matsui, T., et al., *Rho-kinase phosphorylates COOH-terminal threonines of ezrin/radixin/moesin (ERM) proteins and regulates their head-to-tail association.* J Cell Biol, 1998. **140**(3): p. 647-57.
100. Pearson, M.A., et al., *Structure of the ERM protein moesin reveals the FERM domain fold masked by an extended actin binding tail domain.* Cell, 2000. **101**(3): p. 259-70.
101. Nakamura, F., M.R. Amieva, and H. Furthmayr, *Phosphorylation of threonine 558 in the carboxyl-terminal actin-binding domain of moesin by thrombin activation of human platelets.* Journal of Biological Chemistry, 1995. **270**(52): p. 31377-31385.
102. Yonemura, S., et al., *Rho-dependent and -independent activation mechanisms of ezrin/radixin/moesin proteins: an essential role for polyphosphoinositides in vivo.* Journal of Cell Science, 2002. **115**(12): p. 2569-2580.
103. Fehon, R.G., A.I. McClatchey, and A. Bretscher, *Organizing the cell cortex: the role of ERM proteins.* Nature Reviews Molecular Cell Biology, 2010. **11**(4): p. 276-287.
104. Fievet, B.T., et al., *Phosphoinositide binding and phosphorylation act sequentially in the activation mechanism of ezrin.* Journal of Cell Biology, 2004. **164**(5): p. 653-659.

105. Carreno, S., et al., *Moesin and its activating kinase Slik are required for cortical stability and microtubule organization in mitotic cells.* Journal of Cell Biology, 2008. **180**(4): p. 739-746.
106. Simons, P.C., et al., *C-terminal threonine phosphorylation activates ERM proteins to link the cell's cortical lipid bilayer to the cytoskeleton.* Biochemical and Biophysical Research Communications, 1998. **253**(3): p. 561-565.
107. Polesello, C., et al., *Dmoesin controls actin-based cell shape and polarity during Drosophila melanogaster oogenesis.* Nat Cell Biol, 2002. **4**(10): p. 782-9.
108. Speck, O., et al., *Moesin functions antagonistically to the Rho pathway to maintain epithelial integrity.* Nature, 2003. **421**(6918): p. 83-87.
109. Hipfner, D.R., N. Keller, and S.M. Cohen, *Slik Sterile-20 kinase regulates Moesin activity to promote epithelial integrity during tissue growth.* Genes & Development, 2004. **18**(18): p. 2243-2248.
110. Burg, M.B., J.D. Ferraris, and N.I. Dmitrieva, *Cellular response to hyperosmotic stresses.* Physiol Rev, 2007. **87**(4): p. 1441-74.
111. Beck, F.X., et al., *Heat shock proteins and the cellular response to osmotic stress.* Cell Physiol Biochem, 2000. **10**(5-6): p. 303-6.
112. Hoffert, J.D., et al., *Hypertonic induction of aquaporin-5 expression through an ERK-dependent pathway.* J Biol Chem, 2000. **275**(12): p. 9070-7.
113. Arsenijevic, T., et al., *Hyperosmotic stress induces cell cycle arrest in retinal pigmented epithelial cells.* Cell Death Dis, 2013. **4**: p. e662.
114. Cai, Q., et al., *Rate of increase of osmolality determines osmotic tolerance of mouse inner medullary epithelial cells.* Am J Physiol Renal Physiol, 2002. **283**(4): p. F792-8.
115. Krarup, T., et al., *Na+-K+-2Cl- cotransport in Ehrlich cells: regulation by protein phosphatases and kinases.* Am J Physiol, 1998. **275**(1 Pt 1): p. C239-50.
116. Cai, Q., et al., *Effects of expression of p53 and Gadd45 on osmotic tolerance of renal inner medullary cells.* Am J Physiol Renal Physiol, 2006. **291**(2): p. F341-9.
117. Arima, H., et al., *Hyperosmolar mannitol stimulates expression of aquaporins 4 and 9 through a p38 mitogen-activated protein kinase-dependent pathway in rat astrocytes.* Journal of Biological Chemistry, 2003. **278**(45): p. 44525-44534.
118. Dmitrieva, N., L. Michea, and M. Burg, *p53 tumor suppressor protein protects renal inner medullary cells from hypertonic stress by restricting DNA replication.* Faseb Journal, 2001. **15**(5): p. A850-A850.
119. Dmitrieva, N.I., et al., *Rapid activation of G2/M checkpoint after hypertonic stress in renal inner medullary epithelial (IME) cells is protective and requires p38 kinase.* Proc Natl Acad Sci U S A, 2002. **99**(1): p. 184-9.
120. Sheikh-Hamad, D. and M.C. Gustin, *MAP kinases and the adaptive response to hypertonicity: functional preservation from yeast to mammals.* Am J Physiol Renal Physiol, 2004. **287**(6): p. F1102-10.
121. Galcheva-Gargova, Z., et al., *An osmosensing signal transduction pathway in mammalian cells.* Science, 1994. **265**(5173): p. 806-8.
122. Kyriakis, J.M., et al., *The stress-activated protein kinase subfamily of c-Jun kinases.* Nature, 1994. **369**(6476): p. 156-60.
123. Rosette, C. and M. Karin, *Ultraviolet light and osmotic stress: activation of the JNK cascade through multiple growth factor and cytokine receptors.* Science, 1996. **274**(5290): p. 1194-7.
124. Wang, L., W. Dai, and L. Lu, *Stress-induced c-Jun activation mediated by Polo-like kinase 3 in corneal epithelial cells.* J Biol Chem, 2007. **282**(44): p. 32121-7.
125. Wang, L., W. Dai, and L. Lu, *Osmotic stress-induced phosphorylation of H2AX by polo-like kinase 3 affects cell cycle progression in human corneal epithelial cells.* J Biol Chem, 2014. **289**(43): p. 29827-35.

126. Thatcher, T.H. and M.A. Gorovsky, *Phylogenetic analysis of the core histones H2A, H2B, H3, and H4.* Nucleic Acids Res, 1994. **22**(2): p. 174-9.
127. Pilch, D.R., et al., *Characteristics of gamma-H2AX foci at DNA double-strand breaks sites.* Biochem Cell Biol, 2003. **81**(3): p. 123-9.
128. Burg, M.B., E.D. Kwon, and D. Kultz, *Regulation of gene expression by hypertonicity.* Annu Rev Physiol, 1997. **59**: p. 437-55.
129. Xie, S., et al., *Plk3 functionally links DNA damage to cell cycle arrest and apoptosis at least in part via the p53 pathway.* J Biol Chem, 2001. **276**(46): p. 43305-12.
130. Michea, L., et al., *Mitochondrial dysfunction is an early event in high-NaCl-induced apoptosis of mIMCD3 cells.* Am J Physiol Renal Physiol, 2002. **282**(6): p. F981-90.
131. Lang, K.S., et al., *Stimulation of TNF alpha expression by hyperosmotic stress.* Pflugers Arch, 2002. **443**(5-6): p. 798-803.
132. Robbins, E., T. Pederson, and P. Klein, *Comparison of Mitotic Phenomena and Effects Induced by Hypertonic Solutions in Hela Cells.* Journal of Cell Biology, 1970. **44**(2): p. 400-&.
133. Saborio, J.L., S.S. Pong, and G. Koch, *Selective and Reversible Inhibition of Initiation of Protein-Synthesis in Mammalian-Cells.* Journal of Molecular Biology, 1974. **85**(2): p. 195-211.
134. Dmitrieva, N.I., et al., *Cell cycle delay and apoptosis in response to osmotic stress.* Comp Biochem Physiol A Mol Integr Physiol, 2001. **130**(3): p. 411-20.
135. Brigotti, M., et al., *Effects of osmolarity, ions and compatible osmolytes on cell-free protein synthesis.* Biochemical Journal, 2003. **369**: p. 369-374.
136. Greenberg, M.M., *In vitro and in vivo effects of oxidative damage to deoxyguanosine.* Biochemical Society Transactions, 2004. **32**: p. 46-50.
137. Stadtman, E.R. and R.L. Levine, *Protein oxidation.* Reactive Oxygen Species: From Radiation to Molecular Biology, 2000. **899**: p. 191-208.
138. Zhang, Z., et al., *High urea and NaCl carbonylate proteins in renal cells in culture and in vivo, and high urea causes 8-oxoguanine lesions in their DNA.* Proceedings of the National Academy of Sciences of the United States of America, 2004. **101**(25): p. 9491-9496.
139. Zhang, Z., X.Y. Yang, and D.M. Cohen, *Urea-associated oxidative stress and Gadd153/CHOP induction.* American Journal of Physiology-Renal Physiology, 1999. **276**(5): p. F786-F793.
140. Yang, T.X., et al., *Hypertonic induction of COX-2 in collecting duct cells by reactive oxygen species of mitochondrial origin.* Journal of Biological Chemistry, 2005. **280**(41): p. 34966-34973.
141. Lang, F., et al., *Functional significance of cell volume regulatory mechanisms.* Physiological Reviews, 1998. **78**(1): p. 247-306.
142. Alfieri, R.R., et al., *Creatine as a compatible osmolyte in muscle cells exposed to hypertonic stress.* Journal of Physiology-London, 2006. **576**(2): p. 391-401.
143. Umenishi, F. and R.W. Schrier, *Hypertonicity-induced aquaporin-1 (AQP1) expression is mediated by the activation of MAPK pathways and hypertonicity-responsive element in the AQP1 gene.* Journal of Biological Chemistry, 2003. **278**(18): p. 15765-15770.
144. Maruyama, T., et al., *CHIP-dependent termination of MEKK2 regulates temporal ERK activation required for proper hyperosmotic response.* Embo Journal, 2010. **29**(15): p. 2501-2514.
145. Zhang, M.Z., et al., *Cyclooxygenase-2 in rat nephron development.* American Journal of Physiology-Renal Physiology, 1997. **273**(6): p. F994-F1002.

146. Lim, W., et al., *Hypertonic sodium chloride and mannitol induces COX-2 via different signaling pathways in mouse cortical collecting duct M-1 cells.* Life Sci, 2007. **80**(22): p. 2085-92.
147. Bourque, C.W., *Central mechanisms of osmosensation and systemic osmoregulation.* Nat Rev Neurosci, 2008. **9**(7): p. 519-31.
148. Yang, T., et al., *MAPK mediation of hypertonicity-stimulated cyclooxygenase-2 expression in renal medullary collecting duct cells.* J Biol Chem, 2000. **275**(30): p. 23281-6.
149. Christoph, K., F.X. Beck, and W. Neuhofer, *Osmoadaptation of Mammalian cells - an orchestrated network of protective genes.* Curr Genomics, 2007. **8**(4): p. 209-18.
150. Tian, W., et al., *Urea and hypertonicity increase expression of heme oxygenase-1 in murine renal medullary cells.* Am J Physiol Renal Physiol, 2001. **281**(5): p. F983-91.
151. Gabert, B.J. and D. Kultz, *Osmoprotective proteome adjustments in mouse kidney papilla.* Biochim Biophys Acta, 2011. **1814**(3): p. 435-48.
152. Arroyo, J.A., et al., *Determination of the NFAT5/TonEBP transcription factor in the human and ovine placenta.* Syst Biol Reprod Med, 2009. **55**(4): p. 164-70.
153. Cheung, C.Y. and B.C. Ko, *NFAT5 in cellular adaptation to hypertonic stress - regulations and functional significance.* J Mol Signal, 2013. **8**(1): p. 5.
154. Xu, S., et al., *Phosphorylation by casein kinase 1 regulates tonicity-induced osmotic response element-binding protein/tonicity enhancer-binding protein nucleocytoplasmic trafficking.* J Biol Chem, 2008. **283**(25): p. 17624-34.
155. Gallazzini, M., et al., *High NaCl-induced activation of CDK5 increases phosphorylation of the osmoprotective transcription factor TonEBP/OREBP at threonine 135, which contributes to its rapid nuclear localization.* Mol Biol Cell, 2011. **22**(5): p. 703-14.
156. Gao, Y., et al., *Heat shock protein 70 together with its co-chaperone CHIP inhibits TNF-alpha induced apoptosis by promoting proteasomal degradation of apoptosis signal-regulating kinase1.* Apoptosis, 2010. **15**(7): p. 822-33.
157. Olazabal, I.M. and L.M. Machesky, *Abp1p and cortactin, new "hand-holds" for actin.* J Cell Biol, 2001. **154**(4): p. 679-82.
158. Weaver, A.M., et al., *Cortactin promotes and stabilizes Arp2/3-induced actin filament network formation.* Curr Biol, 2001. **11**(5): p. 370-4.
159. Yamamoto, M., et al., *Hypertonic stress increases phosphatidylinositol 4,5-bisphosphate levels by activating PIP5KIbeta.* J Biol Chem, 2006. **281**(43): p. 32630-8.
160. Sumi, T., et al., *Cofilin phosphorylation and actin cytoskeletal dynamics regulated by rho- and Cdc42-activated LIM-kinase 2.* J Cell Biol, 1999. **147**(7): p. 1519-32.
161. Bernard, O., *Lim kinases, regulators of actin dynamics.* Int J Biochem Cell Biol, 2007. **39**(6): p. 1071-6.
162. Thirone, A.C., et al., *Hyperosmotic stress induces Rho/Rho kinase/LIM kinase-mediated cofilin phosphorylation in tubular cells: key role in the osmotically triggered F-actin response.* Am J Physiol Cell Physiol, 2009. **296**(3): p. C463-75.
163. Di Ciano-Oliveira, C., et al., *Hyperosmotic stress activates Rho: differential involvement in Rho kinase-dependent MLC phosphorylation and NKCC activation.* Am J Physiol Cell Physiol, 2003. **285**(3): p. C555-66.
164. Rasmussen, M., et al., *Osmotic cell shrinkage activates ezrin/radixin/moesin (ERM) proteins: activation mechanisms and physiological implications.* Am J Physiol Cell Physiol, 2008. **294**(1): p. C197-212.
165. Okada, Y., *Ion channels and transporters involved in cell volume regulation and sensor mechanisms.* Cell Biochem Biophys, 2004. **41**(2): p. 233-58.

166. Hoffmann, E.K. and L.O. Simonsen, *Membrane mechanisms in volume and pH regulation in vertebrate cells.* Physiol Rev, 1989. **69**(2): p. 315-82.
167. Okada, Y., *Volume expansion-sensing outward-rectifier Cl- channel: fresh start to the molecular identity and volume sensor.* Am J Physiol, 1997. **273**(3 Pt 1): p. C755-89.
168. Grinstein, S. and J.K. Foskett, *Ionic mechanisms of cell volume regulation in leukocytes.* Annu Rev Physiol, 1990. **52**: p. 399-414.
169. Xu, J.C., et al., *Molecular cloning and functional expression of the bumetanide-sensitive Na-K-Cl cotransporter.* Proc Natl Acad Sci U S A, 1994. **91**(6): p. 2201-5.
170. Klein, J.D. and W.C. O'Neill, *Volume-sensitive myosin phosphorylation in vascular endothelial cells: correlation with Na-K-2Cl cotransport.* Am J Physiol, 1995. **269**(6 Pt 1): p. C1524-31.
171. Koliakos, G., K. Paletas, and M. Kaloyianni, *NHE-1: a molecular target for signalling and cell matrix interactions.* Connect Tissue Res, 2008. **49**(3): p. 157-61.
172. Bianchini, L., G. L'Allemain, and J. Pouyssegur, *The p42/p44 mitogen-activated protein kinase cascade is determinant in mediating activation of the Na+/H+ exchanger (NHE1 isoform) in response to growth factors.* J Biol Chem, 1997. **272**(1): p. 271-9.
173. Voyno-Yasenetskaya, T., et al., *G alpha 13 stimulates Na-H exchange.* J Biol Chem, 1994. **269**(7): p. 4721-4.
174. Kitamura, K., et al., *G alpha q and G alpha 13 regulate NHE-1 and intracellular calcium in epithelial cells.* Am J Physiol, 1995. **268**(1 Pt 1): p. C101-10.
175. Dhanasekaran, N., et al., *Protein kinase C-dependent and -independent activation of Na+/H+ exchanger by G alpha 12 class of G proteins.* J Biol Chem, 1994. **269**(16): p. 11802-6.
176. Hooley, R., et al., *G alpha 13 stimulates Na+-H+ exchange through distinct Cdc42-dependent and RhoA-dependent pathways.* J Biol Chem, 1996. **271**(11): p. 6152-8.
177. Tominaga, T. and D.L. Barber, *Na-H exchange acts downstream of RhoA to regulate integrin-induced cell adhesion and spreading.* Mol Biol Cell, 1998. **9**(8): p. 2287-303.
178. Tominaga, T., et al., *p160ROCK mediates RhoA activation of Na-H exchange.* EMBO J, 1998. **17**(16): p. 4712-22.
179. Moor, A.N. and L. Fliegel, *Protein kinase-mediated regulation of the Na(+)/H(+) exchanger in the rat myocardium by mitogen-activated protein kinase-dependent pathways.* J Biol Chem, 1999. **274**(33): p. 22985-92.
180. Denker, S.P., et al., *Direct binding of the Na--H exchanger NHE1 to ERM proteins regulates the cortical cytoskeleton and cell shape independently of H(+) translocation.* Mol Cell, 2000. **6**(6): p. 1425-36.
181. Watson, A.J., et al., *Serum regulates Na+/H+ exchange in Caco-2 cells by a mechanism which is dependent on F-actin.* J Biol Chem, 1992. **267**(2): p. 956-62.
182. Shrode, L.D., et al., *Shrinkage-induced activation of Na+/H+ exchange in primary rat astrocytes: role of myosin light-chain kinase.* Am J Physiol, 1995. **269**(1 Pt 1): p. C257-66.
183. Putney, L.K., S.P. Denker, and D.L. Barber, *The changing face of the Na+/H+ exchanger, NHE1: structure, regulation, and cellular actions.* Annu Rev Pharmacol Toxicol, 2002. **42**: p. 527-52.
184. Coelho, C.M. and S.J. Leevers, *Do growth and cell division rates determine cell size in multicellular organisms?* J Cell Sci, 2000. **113 (Pt 17)**: p. 2927-34.

185. Lang, F., et al., *Cell volume in the regulation of cell proliferation and apoptotic cell death.* Cell Physiol Biochem, 2000. **10**(5-6): p. 417-28.
186. Denker, S.P. and D.L. Barber, *Cell migration requires both ion translocation and cytoskeletal anchoring by the Na-H exchanger NHE1.* Journal of Cell Biology, 2002. **159**(6): p. 1087-1096.
187. Schwab, A., *Function and spatial distribution of ion channels and transporters in cell migration.* Am J Physiol Renal Physiol, 2001. **280**(5): p. F739-47.
188. Bussolino, F., et al., *Stimulation of the Na+/H+ exchanger in human endothelial cells activated by granulocyte- and granulocyte-macrophage-colony-stimulating factor. Evidence for a role in proliferation and migration.* J Biol Chem, 1989. **264**(31): p. 18284-7.
189. Lagana, A., et al., *Regulation of the formation of tumor cell pseudopodia by the Na(+)/H(+) exchanger NHE1.* J Cell Sci, 2000. **113 (Pt 20)**: p. 3649-62.
190. Borisy, G.G. and T.M. Svitkina, *Actin machinery: pushing the envelope.* Curr Opin Cell Biol, 2000. **12**(1): p. 104-12.
191. Carlier, M.F., F. Ressad, and D. Pantaloni, *Control of actin dynamics in cell motility. Role of ADF/cofilin.* J Biol Chem, 1999. **274**(48): p. 33827-30.
192. Oster, G.F. and A.S. Perelson, *The physics of cell motility.* J Cell Sci Suppl, 1987. **8**: p. 35-54.
193. Weaver, B.A. and D.W. Cleveland, *Does aneuploidy cause cancer?* Curr Opin Cell Biol, 2006. **18**(6): p. 658-67.
194. Desai, A. and T.J. Mitchison, *Microtubule polymerization dynamics.* Annu Rev Cell Dev Biol, 1997. **13**: p. 83-117.
195. Saxton, W.M., et al., *Tubulin dynamics in cultured mammalian cells.* J Cell Biol, 1984. **99**(6): p. 2175-86.
196. Belmont, L.D., et al., *Real-time visualization of cell cycle-dependent changes in microtubule dynamics in cytoplasmic extracts.* Cell, 1990. **62**(3): p. 579-89.
197. Rusan, N.M., et al., *Cell cycle-dependent changes in microtubule dynamics in living cells expressing green fluorescent protein-alpha tubulin.* Mol Biol Cell, 2001. **12**(4): p. 971-80.
198. Hyman, A. and E. Karsenti, *The role of nucleation in patterning microtubule networks.* J Cell Sci, 1998. **111 (Pt 15)**: p. 2077-83.
199. Kirschner, M. and T. Mitchison, *Beyond self-assembly: from microtubules to morphogenesis.* Cell, 1986. **45**(3): p. 329-42.
200. Urbani, L. and T. Stearns, *The centrosome.* Curr Biol, 1999. **9**(9): p. R315-7.
201. Zheng, Y., et al., *Nucleation of microtubule assembly by a gamma-tubulin-containing ring complex.* Nature, 1995. **378**(6557): p. 578-83.
202. Khodjakov, A. and C.L. Rieder, *The sudden recruitment of gamma-tubulin to the centrosome at the onset of mitosis and its dynamic exchange throughout the cell cycle, do not require microtubules.* J Cell Biol, 1999. **146**(3): p. 585-96.
203. Piehl, M., et al., *Centrosome maturation: measurement of microtubule nucleation throughout the cell cycle by using GFP-tagged EB1.* Proc Natl Acad Sci U S A, 2004. **101**(6): p. 1584-8.
204. Kotwaliwale, C. and S. Biggins, *Microtubule capture: a concerted effort.* Cell, 2006. **127**(6): p. 1105-8.
205. Chan, G.K., S.T. Liu, and T.J. Yen, *Kinetochore structure and function.* Trends Cell Biol, 2005. **15**(11): p. 589-98.
206. Schroer, T.A., *Microtubules don and doff their caps: dynamic attachments at plus and minus ends.* Curr Opin Cell Biol, 2001. **13**(1): p. 92-6.
207. Holzbaur, E.L. and R.B. Vallee, *DYNEINS: molecular structure and cellular function.* Annu Rev Cell Biol, 1994. **10**: p. 339-72.

208. Robinson, J.T., et al., *Cytoplasmic dynein is required for the nuclear attachment and migration of centrosomes during mitosis in Drosophila.* J Cell Biol, 1999. **146**(3): p. 597-608.
209. Walczak, C.E., et al., *A model for the proposed roles of different microtubule-based motor proteins in establishing spindle bipolarity.* Curr Biol, 1998. **8**(16): p. 903-13.
210. Gaglio, T., M.A. Dionne, and D.A. Compton, *Mitotic spindle poles are organized by structural and motor proteins in addition to centrosomes.* J Cell Biol, 1997. **138**(5): p. 1055-66.
211. Gaglio, T., et al., *Opposing motor activities are required for the organization of the mammalian mitotic spindle pole.* J Cell Biol, 1996. **135**(2): p. 399-414.
212. Harborth, J., K. Weber, and M. Osborn, *Epitope mapping and direct visualization of the parallel, in-register arrangement of the double-stranded coiled-coil in the NuMA protein.* EMBO J, 1995. **14**(11): p. 2447-60.
213. Du, Q. and I.G. Macara, *Mammalian Pins is a conformational switch that links NuMA to heterotrimeric G proteins.* Cell, 2004. **119**(4): p. 503-16.
214. Woodard, G.E., et al., *Ric-8A and Gi alpha recruit LGN, NuMA, and dynein to the cell cortex to help orient the mitotic spindle.* Mol Cell Biol, 2010. **30**(14): p. 3519-30.
215. Kiyomitsu, T. and I.M. Cheeseman, *Chromosome- and spindle-pole-derived signals generate an intrinsic code for spindle position and orientation.* Nat Cell Biol, 2012. **14**(3): p. 311-7.
216. Kotak, S., C. Busso, and P. Gonczy, *NuMA phosphorylation by CDK1 couples mitotic progression with cortical dynein function.* EMBO J, 2013. **32**(18): p. 2517-29.
217. Holy, T.E. and S. Leibler, *Dynamic instability of microtubules as an efficient way to search in space.* Proc Natl Acad Sci U S A, 1994. **91**(12): p. 5682-5.
218. Brittle, A.L. and H. Ohkura, *Centrosome maturation: Aurora lights the way to the poles.* Curr Biol, 2005. **15**(21): p. R880-2.
219. Stoppin, V., et al., *Isolated Plant Nuclei Nucleate Microtubule Assembly: The Nuclear Surface in Higher Plants Has Centrosome-like Activity.* Plant Cell, 1994. **6**(8): p. 1099-1106.
220. Gorlich, D. and U. Kutay, *Transport between the cell nucleus and the cytoplasm.* Annu Rev Cell Dev Biol, 1999. **15**: p. 607-60.
221. Weis, K., *Importins and exportins: how to get in and out of the nucleus.* Trends Biochem Sci, 1998. **23**(5): p. 185-9.
222. Caudron, M., et al., *Spatial coordination of spindle assembly by chromosome-mediated signaling gradients.* Science, 2005. **309**(5739): p. 1373-6.
223. Kalab, P., K. Weis, and R. Heald, *Visualization of a RanGTP gradient in interphase and mitotic Xenopus egg extracts.* Science, 2002. **295**(5564): p. 2452-6.
224. Kalab, P., et al., *Analysis of a RanGTP-regulated gradient in mitotic somatic cells.* Nature, 2006. **440**(7084): p. 697-701.
225. Gruss, O.J., et al., *Ran induces spindle assembly by reversing the inhibitory effect of importin alpha on TPX2 activity.* Cell, 2001. **104**(1): p. 83-93.
226. Heng, Y.W., et al., *TPPP acts downstream of RhoA-ROCK-LIMK2 to regulate astral microtubule organization and spindle orientation.* J Cell Sci, 2012. **125**(Pt 6): p. 1579-90.
227. Marsh, D.J. and S.P. Azen, *Mechanism of NaCl reabsorption by hamster thin ascending limbs of Henle's loop.* Am J Physiol, 1975. **228**(1): p. 71-9.
228. Wu, S.G., et al., *Red blood cell osmotic fragility in chronically hemodialyzed patients.* Nephron, 1998. **78**(1): p. 28-32.

229. Mitono, H., et al., *Acute hypoosmolality attenuates the suppression of cutaneous vasodilation with increased exercise intensity.* J Appl Physiol (1985), 2005. **99**(3): p. 902-8.
230. Ito, T., et al., *Plasma hyperosmolality augments peripheral vascular response to baroreceptor unloading during heat stress.* Am J Physiol Regul Integr Comp Physiol, 2005. **289**(2): p. R432-R440.
231. Holtfreter, B., et al., *Serum osmolality and outcome in intensive care unit patients.* Acta Anaesthesiol Scand, 2006. **50**(8): p. 970-7.
232. Gentile, L.B., B. Piva, and B.L. Diaz, *Hypertonic stress induces VEGF production in human colon cancer cell line Caco-2: inhibitory role of autocrine PGE(2).* PLoS One, 2011. **6**(9): p. e25193.
233. Januschke, J. and C. Gonzalez, *Drosophila asymmetric division, polarity and cancer.* Oncogene, 2008. **27**(55): p. 6994-7002.
234. Thery, M. and M. Bornens, *Get round and stiff for mitosis.* Hfsp Journal, 2008. **2**(2): p. 65-71.
235. Maeno, E., N. Takahashi, and Y. Okada, *Dysfunction of regulatory volume increase is a key component of apoptosis.* FEBS Lett, 2006. **580**(27): p. 6513-7.
236. Xiong, Y., et al., *Human D-type cyclin.* Cell, 1991. **65**(4): p. 691-9.
237. Pearce, A.K. and T.C. Humphrey, *Integrating stress-response and cell-cycle checkpoint pathways.* Trends Cell Biol, 2001. **11**(10): p. 426-33.
238. de Nadal, E., P.M. Alepuz, and F. Posas, *Dealing with osmostress through MAP kinase activation.* EMBO Rep, 2002. **3**(8): p. 735-40.
239. Cuenda, A. and S. Rousseau, *p38 MAP-kinases pathway regulation, function and role in human diseases.* Biochim Biophys Acta, 2007. **1773**(8): p. 1358-75.
240. Kultz, D., *Phylogenetic and functional classification of mitogen- and stress-activated protein kinases.* J Mol Evol, 1998. **46**(5): p. 571-88.
241. Zieve, L., *The mechanism of hepatic coma.* Hepatology, 1981. **1**(4): p. 360-5.
242. Kultz, D. and D. Chakravarty, *Hyperosmolality in the form of elevated NaCl but not urea causes DNA damage in murine kidney cells.* Proc Natl Acad Sci U S A, 2001. **98**(4): p. 1999-2004.
243. Santos, B.C., et al., *A combination of NaCl and urea enhances survival of IMCD cells to hyperosmolality.* Am J Physiol, 1998. **274**(6 Pt 2): p. F1167-73.
244. Michea, L., et al., *Cell cycle delay and apoptosis are induced by high salt and urea in renal medullary cells.* Am J Physiol Renal Physiol, 2000. **278**(2): p. F209-18.
245. Kultz, D. and M.B. Burg, *Intracellular signaling in response to osmotic stress.* Contrib Nephrol, 1998. **123**: p. 94-109.
246. Kyriakis, J.M. and J. Avruch, *Mammalian mitogen-activated protein kinase signal transduction pathways activated by stress and inflammation.* Physiol Rev, 2001. **81**(2): p. 807-69.
247. Ono, K. and J. Han, *The p38 signal transduction pathway: activation and function.* Cell Signal, 2000. **12**(1): p. 1-13.
248. Brocker, C., D.C. Thompson, and V. Vasiliou, *The role of hyperosmotic stress in inflammation and disease.* Biomol Concepts, 2012. **3**(4): p. 345-364.
249. Lin, L.R., et al., *The effect of hypertonicity on aldose reductase, alpha B-crystallin, and organic osmolytes in the retinal pigment epithelium.* Invest Ophthalmol Vis Sci, 1993. **34**(7): p. 2352-9.
250. Sherr, C.J., *Mammalian G1 cyclins and cell cycle progression.* Proc Assoc Am Physicians, 1995. **107**(2): p. 181-6.
251. Strzalka, W. and A. Ziemienowicz, *Proliferating cell nuclear antigen (PCNA): a key factor in DNA replication and cell cycle regulation.* Ann Bot, 2011. **107**(7): p. 1127-40.

252. Maga, G. and U. Hubscher, *Proliferating cell nuclear antigen (PCNA): a dancer with many partners.* J Cell Sci, 2003. **116**(Pt 15): p. 3051-60.
253. Pedeux, R., et al., *Thymidine dinucleotides induce S phase cell cycle arrest in addition to increased melanogenesis in human melanocytes.* J Invest Dermatol, 1998. **111**(3): p. 472-7.
254. Bement, W.M., H.A. Benink, and G. von Dassow, *A microtubule-dependent zone of active RhoA during cleavage plane specification.* J Cell Biol, 2005. **170**(1): p. 91-101.
255. Yuce, O., A. Piekny, and M. Glotzer, *An ECT2-centralspindlin complex regulates the localization and function of RhoA.* J Cell Biol, 2005. **170**(4): p. 571-82.
256. Goshima, G. and J.M. Scholey, *Control of mitotic spindle length.* Annu Rev Cell Dev Biol, 2010. **26**: p. 21-57.
257. Wuhr, M., et al., *Evidence for an upper limit to mitotic spindle length.* Curr Biol, 2008. **18**(16): p. 1256-61.
258. Bringmann, H., et al., *LET-99, GOA-1/GPA-16, and GPR-1/2 are required for aster-positioned cytokinesis.* Curr Biol, 2007. **17**(2): p. 185-91.
259. Dumont, S. and T.J. Mitchison, *Force and length in the mitotic spindle.* Curr Biol, 2009. **19**(17): p. R749-61.
260. Jiang, H., *Cell size modulates oscillation, positioning and length of mitotic spindles.* Sci Rep, 2015. **5**: p. 10504.
261. Zhu, J., et al., *Finding the cell center by a balance of dynein and myosin pulling and microtubule pushing: a computational study.* Mol Biol Cell, 2010. **21**(24): p. 4418-27.
262. Laan, L., et al., *Cortical dynein controls microtubule dynamics to generate pulling forces that position microtubule asters.* Cell, 2012. **148**(3): p. 502-14.
263. Salmon, E.D., *Pressure-induced depolymerization of spindle microtubules. II. Thermodynamics of in vivo spindle assembly.* J Cell Biol, 1975. **66**(1): p. 114-27.
264. Palmer, R.E., et al., *Role of astral microtubules and actin in spindle orientation and migration in the budding yeast, Saccharomyces cerevisiae.* J Cell Biol, 1992. **119**(3): p. 583-93.
265. Lim, C.T., E.H. Zhou, and S.T. Quek, *Mechanical models for living cells--a review.* J Biomech, 2006. **39**(2): p. 195-216.
266. Kemp, G., H. Young, and L. Fliegel, *Structure and function of the human Na+/H+ exchanger isoform 1.* Channels (Austin), 2008. **2**(5): p. 329-36.
267. Slepkov, E.R., et al., *Structural and functional analysis of the Na+/H+ exchanger.* Biochem J, 2007. **401**(3): p. 623-33.
268. Bretscher, A., K. Edwards, and R.G. Fehon, *ERM proteins and merlin: Integrators at the cell cortex.* Nature Reviews Molecular Cell Biology, 2002. **3**(8): p. 586-599.
269. Pollard, T.D. and G.G. Borisy, *Cellular motility driven by assembly and disassembly of actin filaments.* Cell, 2003. **112**(4): p. 453-65.
270. Mora-Bermudez, F., F. Matsuzaki, and W.B. Huttner, *Specific polar subpopulations of astral microtubules control spindle orientation and symmetric neural stem cell division.* Elife, 2014. **3**.
271. Bird, S.L., R. Heald, and K. Weis, *RanGTP and CLASP1 cooperate to position the mitotic spindle.* Mol Biol Cell, 2013. **24**(16): p. 2506-14.
272. Tao, L., *Effects of osmotic stress on dextran diffusion in rat neocortex studied with integrative optical imaging.* J Neurophysiol, 1999. **81**(5): p. 2501-7.
273. Hetzer, M., O.J. Gruss, and I.W. Mattaj, *The Ran GTPase as a marker of chromosome position in spindle formation and nuclear envelope assembly.* Nat Cell Biol, 2002. **4**(7): p. E177-84.

274. Zheng, Z., et al., *Evidence for dynein and astral microtubule-mediated cortical release and transport of Galphai/LGN/NuMA complex in mitotic cells.* Mol Biol Cell, 2013. **24**(7): p. 901-13.
275. Karki, S. and E.L. Holzbaur, *Affinity chromatography demonstrates a direct binding between cytoplasmic dynein and the dynactin complex.* J Biol Chem, 1995. **270**(48): p. 28806-11.
276. King, S.J., et al., *Analysis of the dynein-dynactin interaction in vitro and in vivo.* Mol Biol Cell, 2003. **14**(12): p. 5089-97.
277. Vaughan, K.T. and R.B. Vallee, *Cytoplasmic dynein binds dynactin through a direct interaction between the intermediate chains and p150Glued.* J Cell Biol, 1995. **131**(6 Pt 1): p. 1507-16.
278. Hendricks, A.G., et al., *Dynein tethers and stabilizes dynamic microtubule plus ends.* Curr Biol, 2012. **22**(7): p. 632-7.
279. Tuncay, H., et al., *JAM-A regulates cortical dynein localization through Cdc42 to control planar spindle orientation during mitosis.* Nat Commun, 2015. **6**: p. 8128.
280. Machicoane, M., et al., *SLK-dependent activation of ERMs controls LGN-NuMA localization and spindle orientation.* J Cell Biol, 2014. **205**(6): p. 791-9.
281. Carreno, S., et al., *Moesin and its activating kinase Slik are required for cortical stability and microtubule organization in mitotic cells.* J Cell Biol, 2008. **180**(4): p. 739-46.
282. Kleszczynski, K., et al., *Melatonin prevents ultraviolet radiation-induced alterations in plasma membrane potential and intracellular pH in human keratinocytes.* J Pineal Res, 2013. **54**(1): p. 89-99.
283. Shaw, R.J., et al., *RhoA-dependent phosphorylation and relocalization of ERM proteins into apical membrane/actin protrusions in fibroblasts.* Mol Biol Cell, 1998. **9**(2): p. 403-19.
284. Hao, J.J., et al., *Phospholipase C-mediated hydrolysis of PIP2 releases ERM proteins from lymphocyte membrane.* J Cell Biol, 2009. **184**(3): p. 451-62.
285. Li, Y., et al., *Phosphorylated ERM is responsible for increased T cell polarization, adhesion, and migration in patients with systemic lupus erythematosus.* J Immunol, 2007. **178**(3): p. 1938-47.
286. Fievet, B., D. Louvard, and M. Arpin, *ERM proteins in epithelial cell organization and functions.* Biochim Biophys Acta, 2007. **1773**(5): p. 653-60.
287. Hughes, S.C. and R.G. Fehon, *Understanding ERM proteins--the awesome power of genetics finally brought to bear.* Curr Opin Cell Biol, 2007. **19**(1): p. 51-6.
288. Niggli, V. and J. Rossy, *Ezrin/radixin/moesin: versatile controllers of signaling molecules and of the cortical cytoskeleton.* Int J Biochem Cell Biol, 2008. **40**(3): p. 344-9.
289. Barret, C., et al., *Mutagenesis of the phosphatidylinositol 4,5-bisphosphate (PIP(2)) binding site in the NH(2)-terminal domain of ezrin correlates with its altered cellular distribution.* J Cell Biol, 2000. **151**(5): p. 1067-80.
290. Ben-Aissa, K., et al., *Activation of moesin, a protein that links actin cytoskeleton to the plasma membrane, occurs by phosphatidylinositol 4,5-bisphosphate (PIP2) binding sequentially to two sites and releasing an autoinhibitory linker.* J Biol Chem, 2012. **287**(20): p. 16311-23.
291. Yonemura, S., et al., *Rho-dependent and -independent activation mechanisms of ezrin/radixin/moesin proteins: an essential role for polyphosphoinositides in vivo.* J Cell Sci, 2002. **115**(Pt 12): p. 2569-80.
292. Tang, N. and W.F. Marshall, *Centrosome positioning in vertebrate development.* J Cell Sci, 2012. **125**(Pt 21): p. 4951-61.
293. Doe, C.Q., *Neural stem cells: balancing self-renewal with differentiation.* Development, 2008. **135**(9): p. 1575-87.

294. Chang, K.C., C. Wang, and H. Wang, *Balancing self-renewal and differentiation by asymmetric division: insights from brain tumor suppressors in Drosophila neural stem cells.* Bioessays, 2012. **34**(4): p. 301-10.
295. Oliferenko, S., T.G. Chew, and M.K. Balasubramanian, *Positioning cytokinesis.* Genes Dev, 2009. **23**(6): p. 660-74.
296. Tang, N., et al., *Control of mitotic spindle angle by the RAS-regulated ERK1/2 pathway determines lung tube shape.* Science, 2011. **333**(6040): p. 342-5.
297. Fischer, E. and M. Pontoglio, *[Planar cell polarity and polycystic kidney disease]*. Med Sci (Paris), 2006. **22**(6-7): p. 576-8.
298. Chandhok, N.S. and D. Pellman, *A little CIN may cost a lot: revisiting aneuploidy and cancer.* Curr Opin Genet Dev, 2009. **19**(1): p. 74-81.
299. Green, R.A., R. Wollman, and K.B. Kaplan, *APC and EB1 function together in mitosis to regulate spindle dynamics and chromosome alignment.* Mol Biol Cell, 2005. **16**(10): p. 4609-22.
300. Palazzo, A.F., et al., *Cdc42, dynein, and dynactin regulate MTOC reorientation independent of Rho-regulated microtubule stabilization.* Curr Biol, 2001. **11**(19): p. 1536-41.
301. Lengauer, C., K.W. Kinzler, and B. Vogelstein, *Genetic instabilities in human cancers.* Nature, 1998. **396**(6712): p. 643-9.
302. Pihan, G.A. and S.J. Doxsey, *The mitotic machinery as a source of genetic instability in cancer.* Semin Cancer Biol, 1999. **9**(4): p. 289-302.
303. Caldwell, C.M., R.A. Green, and K.B. Kaplan, *APC mutations lead to cytokinetic failures in vitro and tetraploid genotypes in Min mice.* J Cell Biol, 2007. **178**(7): p. 1109-20.
304. Dachsel, J.C., et al., *The Rho guanine nucleotide exchange factor Syx regulates the balance of dia and ROCK activities to promote polarized-cancer-cell migration.* Mol Cell Biol, 2013. **33**(24): p. 4909-18.
305. Gotta, M., M.C. Abraham, and J. Ahringer, *CDC-42 controls early cell polarity and spindle orientation in C. elegans.* Curr Biol, 2001. **11**(7): p. 482-8.
306. Na, J. and M. Zernicka-Goetz, *Asymmetric positioning and organization of the meiotic spindle of mouse oocytes requires CDC42 function.* Curr Biol, 2006. **16**(12): p. 1249-54.
307. Jaffe, A.B., et al., *Cdc42 controls spindle orientation to position the apical surface during epithelial morphogenesis.* J Cell Biol, 2008. **183**(4): p. 625-33.
308. Yasuda, S. and S. Narumiya, *Analysis of a mitotic role of Cdc42.* Methods Enzymol, 2006. **406**: p. 656-65.
309. Mitsushima, M., F. Toyoshima, and E. Nishida, *Dual role of Cdc42 in spindle orientation control of adherent cells.* Mol Cell Biol, 2009. **29**(10): p. 2816-27.
310. Roszko, I., et al., *Key role played by RhoA in the balance between planar and apico-basal cell divisions in the chick neuroepithelium.* Dev Biol, 2006. **298**(1): p. 212-24.
311. Kunda, P., et al., *Moesin controls cortical rigidity, cell rounding, and spindle morphogenesis during mitosis.* Current Biology, 2008. **18**(2): p. 91-101.
312. Luxenburg, C., et al., *Developmental roles for Srf, cortical cytoskeleton and cell shape in epidermal spindle orientation.* Nat Cell Biol, 2011. **13**(3): p. 203-14.
313. Nakajima, Y., et al., *Epithelial junctions maintain tissue architecture by directing planar spindle orientation.* Nature, 2013. **500**(7462): p. 359-62.
314. Kotak, S., C. Busso, and P. Gonczy, *Cortical dynein is critical for proper spindle positioning in human cells.* J Cell Biol, 2012. **199**(1): p. 97-110.
315. McNally, F.J., *Mechanisms of spindle positioning.* J Cell Biol, 2013. **200**(2): p. 131-40.

316. Bretscher, A., K. Edwards, and R.G. Fehon, *ERM proteins and merlin: integrators at the cell cortex.* Nat Rev Mol Cell Biol, 2002. **3**(8): p. 586-99.
317. Wei, L., et al., *beta(1)-integrin and PI 3-kinase regulate RhoA-dependent activation of skeletal alpha-actin promoter in myoblasts.* Am J Physiol Heart Circ Physiol, 2000. **278**(6): p. H1736-43.
318. Tame, M.A., et al., *Astral microtubules control redistribution of dynein at the cell cortex to facilitate spindle positioning.* Cell Cycle, 2014. **13**(7): p. 1162-70.
319. Stout, J.R., et al., *Kif18B interacts with EB1 and controls astral microtubule length during mitosis.* Mol Biol Cell, 2011. **22**(17): p. 3070-80.